Applied Bionics and Biomechanics

Application of Biomedical Information in Sports and Health Care

Lead Guest Editor: Yaodong Gu
Guest Editors: Julien S. Baker and Justin Fernandez

Application of Biomedical Information in Sports and Health Care

Applied Bionics and Biomechanics

Application of Biomedical Information in Sports and Health Care

Lead Guest Editor: Yaodong Gu
Guest Editors: Julien S. Baker and Justin Fernandez

Contents

Hindawi
Applied Bionics and Biomechanics
Volume 2022, Article ID 1666792, 11 pages
https://doi.org/10.1155/2022/1666792

Research Article

The Risk Correlation between N7-Methylguanosine Modification-Related lncRNAs and Survival Prognosis of Oral Squamous Cell Carcinoma Based on Comprehensive Bioinformatics Analysis

Yanglong Xu,[1] Xue Zou,[2] and Jie Mei[3]

[1]*Department of General Dentistry, Stomatological Hospital Affiliated to Zunyi Medical University, China*
[2]*Department of Periodontics, Stomatological Hospital Affiliated to Zunyi Medical University, China*
[3]*Stomatological Hospital, Southern Medical University, China*

Correspondence should be addressed to Jie Mei; meijie@smu.edu.cn

Received 5 June 2022; Revised 23 June 2022; Accepted 2 July 2022; Published 24 August 2022

Academic Editor: Yaodong Gu

Objective. N7-methylguanosine modification-related lncRNAs (m7G-related lncRNAs) are involved in progression of many diseases. This study was aimed at revealing the risk correlation between N7-methylguanosine modification-related lncRNAs and survival prognosis of oral squamous cell carcinoma. *Methods*. In the present study, coexpression network analysis and univariate Cox analysis were used to obtained 31 m7G-related mRNAs and 399 m7G-related lncRNAs. And the prognostic risk score model of OSCC patients was evaluated and optimized through cross-validation. *Results*. Through the coexpression analysis and risk assessment analysis of m7G-related prognostic mRNAs and lncRNAs, it was found that six m7G-related prognostic lncRNAs (AC005332.6, AC010894.1, AC068831.5, AL035446.1, AL513550.1, and HHLA3) were high-risk lncRNAs. Three m7G-related prognostic lncRNAs (AC007114.1, HEIH, and LINC02541) were protective lncRNAs. Then, survival curves were drawn by comparing the survival differences between patients with high and low expression of each m7G-related prognostic lncRNA in the prognostic risk score model. Further, risk curves, scatter plots, and heat maps were drawn by comparing the survival differences between high-risk and low-risk OSCC patients in the prognostic model. Finally, forest maps and the ROC curve were generated to verify the predictive power of the prognostic risk score model. Our results will help to find early and accurate prognostic risk markers for OSCC, which could be used for early prediction and early clinical intervention of survival, prognosis, and disease risk of OSCC patients in the future.

1. Introduction

Oral squamous cell carcinoma (OSCC) is a malignant tumor occurring in oral cavity with squamous cell as the main cell. Cancer cells can occur in gingival, hard palate, tongue, buccal mucosa, lips, and other organs [1]. It is the most malignant and harmful tumor of the head and neck, accounting for about 50% of the incidence of the head and neck squamous cell carcinoma [2]. Due to the rich blood flow and complex anatomical structure of oral and maxillofacial region, OSCC surgery often cannot completely remove the tumor [3]. At the same time, OSCC is prone to lymph node metastasis and postoperative recurrence, so its prognosis is poor [4]. Therefore, it is particularly urgent to identify new prognostic genes to accurately predict the prognosis of OSCC patients at an early stage.

Long noncoding RNAs (lncRNAs) are noncoding RNAs with a length of more than 200 nucleotides. They are functional RNA molecules that cannot be translated into proteins, but they are involved in a variety of biological regulation processes in cells of the body, such as epigenetic regulation, cell cycle regulation, and cell differentiation regulation [5, 6]. N7-methylguanine (m7G) is a metabolite of RNA methylation, which can be produced by methylation agents and is used as probes for protein-RNA interactions and as a key component of RNA sequencing methods [7, 8].

Some studies have shown that N7-methylguanosine modification-related lncRNAs (m7G-related lncRNAs) are

involved in maintaining RNA stability, processing, nucleation, translation, and other functions, affecting the occurrence and progression of many diseases [9–13]. However, as far as we know, no studies on m7G-related lncRNAs have been reported in OSCC. This study was aimed at revealing the risk correlation between N7-methylguanosine modification-related lncRNAs and survival prognosis of oral squamous cell carcinoma.

In this study, we constructed a prognostic risk score model for OSCC based on the new m7G-related lncRNAs; conducted risk assessment, survival analysis, and risk analysis for OSCC patients; and finally verified the accuracy and independent predictive ability of the prognostic risk model. The purpose of this study was to find early and accurate prognostic risk markers for OSCC, which could be used for early prediction and early clinical intervention of survival, prognosis, and disease risk of OSCC patients in the future.

2. Materials and Methods

2.1. Acquisition and Cleaning of Gene Matrix and Clinical Data. The transcriptome expression matrix of all OSCC samples and clinical data of patients were obtained from The Cancer Genome Atlas (TCGA) database (https://tcga-data.nci.nih.gov/tcga), which provides clinical information and genome variation, mRNA expression, miRNA expression, methylation, and other data on various human cancers, making it an important data source for cancer researchers [14, 15]. A total of 83 samples were collected, including 70 OSCC tissue samples and 13 normal tissue samples. In addition, we used custom Perl scripts to clean and organize all the data for further bioinformatics analysis and statistical analysis.

2.2. Identification of m7G-Related mRNAs and lncRNAs. Firstly, the transcriptome expression matrix of all OSCC samples was divided into mRNA and lncRNA expression profiles using customized Perl scripts and human gene profiles. Then from MSigDB database (http://www.gsea-msigdb.org/gsea/login.jsp) [16] to arrange m7G-related mRNAs list, then extracted each relative expression of m7G-related mRNAs via R package limma [17] from OSCC gene matrix. Finally, the lncRNA expression matrix and the list of m7G-related mRNAs were read respectively; the expression values of repeated genes and normal samples were removed; the coexpression of lncRNAs with m7G-related mRNAs was identified through the cyclic calculation of correlation test, named as m7G-related lncRNAs; and the expression matrix was obtained [18]. The cutoff criterion was Pearson correlation coefficient > 0.4 and P value < 0.001.

2.3. Identification of m7G-Related Prognostic lncRNAs. First, the survival data of all patients (including survival time and survival status) were collated, and the m7G-related lncRNA expression matrix was combined with the survival data of patients (only patients with complete information were included). Then, Kaplan-Meier (KM) analysis and univariate Cox analysis methods [19, 20] were used to test the correlation between m7G-related lncRNA expression levels and survival time and status of patients via R package survival [21], so as to identify the m7G-related prognostic lncRNAs. Only P values less than 0.05 for the two analysis methods were considered statistically significant.

2.4. Construction of Prognostic Risk Score Model for OSCC. We used the m7G-related prognostic lncRNA expression matrix with survival information as input file to construct Cox model through R package survival and optimized the model by calculating AIC value, so as to obtain the formula of prognostic risk score model [22, 23]. We then calculated each OSCC patient's risk scores based on this formula and compared the risk scores with the median risk score to predict whether each patient was a high- or low-risk patient.

2.5. Analysis of Prognostic Gene Coexpression Network. First, we extracted the list of m7G-related prognostic lncRNAs involved in prognostic model construction and the table of coexpression relationship between m7G-related prognostic mRNAs and lncRNAs. Then, by customizing Perl scripts, we sorted out and obtained coexpression relations and node attributes of m7G-related prognostic mRNAs and lncRNAs, which were used as input files to build coexpression networks [24]. Finally, we visualized the prognostic gene coexpression network using Cytoscape software [25]. In the gene coexpression network, hub genes represent a small proportion of nodes with maximal information exchange with other nodes. Cytoscape is an open source software for visualizing complex networks and integrating these with any type of attribute data.

2.6. Risk Assessment of m7G-Related Prognostic lncRNAs. In order to identify which m7G-related prognostic lncRNAs in the prognostic model are high-risk lncRNAs (hazard ratio, HR > 1) and which are protective lncRNAs (HR < 1), we analyzed the association between m7G-related prognostic lncRNAs and mRNAs [26] and conducted a risk assessment for these lncRNAs via packages ggalluvial, ggplot2, and dplyr [27, 28]. The result was represented by a Sankey diagram [29].

2.7. Survival Analyses of m7G-Related Prognostic lncRNAs. Through R package survival, survival analyses were performed on all m7G-related prognostic lncRNAs involved in the establishment of the prognostic risk score model to explore the relationship between m7G-related prognostic lncRNA expression and survival prognosis of OSCC patients [30]. Prognostic models or risk scores are frequently used to aid individualize risk assessment for diseases with multiple, complex risk factors and diagnostic challenges. According to the median m7G-related prognostic lncRNA expression value, all OSCC patients were divided into high m7G-related prognostic lncRNA expression group and low m7G-related prognostic lncRNA expression group, and then, survival analysis function was defined to compare whether there was statistical difference in survival rate between the two groups [31]. Results were visualized by survival curves [32].

Table 1: Identification of m7G-related prognostic lncRNAs.

lncRNAs	HR	HR.95L	HR.95H	KM_*P* value	Cox_*P* value
TMEM99	1.177014456	1.094434527	1.265825407	0.000111836	$1.13E-05$
HHLA3	1.167767969	1.075729404	1.267681281	0.007342318	0.000213266
AC010894.1	2.447756883	1.687562963	3.5503942	0.007956686	$2.38E-06$
AL513550.1	2.097224234	1.463206544	3.005966249	0.002772334	$5.52E-05$
LINC02541	0.576058399	0.524831944	0.632284835	0.009523161	0.002882225
AL035446.1	1.270188027	1.072263941	1.504645976	0.001398622	0.005652859
MAPKAPK5-AS1	1.517938814	1.224317121	1.881978292	0.006793084	0.000141708
CASC9	1.15835462	1.074073357	1.249249334	0.001601384	0.000136753
FLJ20021	1.062598463	1.019889443	1.107095972	$7.95E-05$	0.00372095
AC007114.1	0.560783838	0.386005302	0.814699982	0.000430497	0.006336202
AC010326.3	1.374941078	1.101926411	1.715598201	0.005999112	0.004811556
PCCA-DT	1.191786502	1.071410431	1.325687174	0.002625784	0.001239526
AP001505.1	1.124910675	1.037735455	1.21940907	0.000367312	0.004236502
AC068831.5	2.156967923	1.40121821	3.320332685	0.00403799	0.000478102
AC005332.6	1.342011378	1.076790983	1.672557225	0.008783854	0.008830636
HEIH	0.414925538	0.247038478	0.696908446	0.005205462	0.005809747

2.8. Risk Analysis of the Prognostic Risk Score Model for OSCC. To further elucidate the relationship between patient survival time, survival status, m7G-related prognostic lncRNA expression levels, and risk scores, we conducted a comprehensive risk analysis for OSCC patients with high- and low-risk groups. Results were displayed by a risk curve, a survival scatter plot, and a risk gene heat map [33, 34].

2.9. Independent Prognostic Analysis of the Prognostic Risk Score Model for OSCC. We performed independent prognostic analyses of the prognostic risk score model to verify whether risk score could be an independent prognostic factor for OSCC patients [35]. Univariate and multivariate independent prognostic analyses were performed using the R package survival by extracting and combining risk information (including survival time, survival status, risk score, and m7G-related prognostic lncRNA expression matrix) and clinical trait lists (including patients' age, gender, cancer grade, and stage) of all patients. The results were shown in forest maps [36].

2.10. ROC Curve Analyses of Several Clinical Traits in the Prognostic Model. Receiver operating characteristic (ROC) curve, also known as sensitivity curve, is a comprehensive index reflecting the continuous variables of sensitivity and specificity [37]. Generally, the relationship between the two is revealed by using the composition method. The larger the area under ROC curve (AUC), the higher the diagnostic accuracy of the test [38]. To test the predictive performance of OSCC prognostic risk score model, R package survival ROC was used to perform KM analysis on patients' survival time, survival status, risk score, and clinical characteristics (age, gender, tumor stage, and grade), and ROC curves of risk score and clinical traits were plotted [39, 40].

Table 2: Coefficient profiles of the nine m7G-related prognostic lncRNAs.

lncRNAs (Expβ)	Coef (β)	HR value
HHLA3	0.177050205	1.19369102
AC010894.1	1.226938632	3.410771908
AL513550.1	1.011070188	2.748540896
LINC02541	-0.319316881	0.726645252
AL035446.1	0.301815135	1.352311208
AC007114.1	-0.737018334	0.478538633
AC068831.5	0.793005914	2.210029611
AC005332.6	0.539498029	1.715145692
HEIH	-0.800902563	0.448923599

Calculation formula: Risk score = Exp$\beta 1 \times \beta 1$ + Exp$\beta 2 \times \beta 2$ + Exp$\beta 3 \times \beta 3$ + Exp$\beta i \times \beta i$.

Table 3: Coefficient profiles of the nine m7G-related prognostic lncRNAs.

lncRNAs (Expβ)	Coef (β)	HR value
HHLA3	0.177050205	1.19369102
AC010894.1	1.226938632	3.410771908
AL513550.1	1.011070188	2.748540896
LINC02541	-0.319316881	0.726645252
AL035446.1	0.301815135	1.352311208
AC007114.1	-0.737018334	0.478538633
AC068831.5	0.793005914	2.210029611
AC005332.6	0.539498029	1.715145692
HEIH	-0.800902563	0.448923599

Calculation formula: Risk score = Exp$\beta 1 \times \beta 1$ + Exp$\beta 2 \times \beta 2$ + Exp$\beta 3 \times \beta 3$ + Exp$\beta i \times \beta i$.

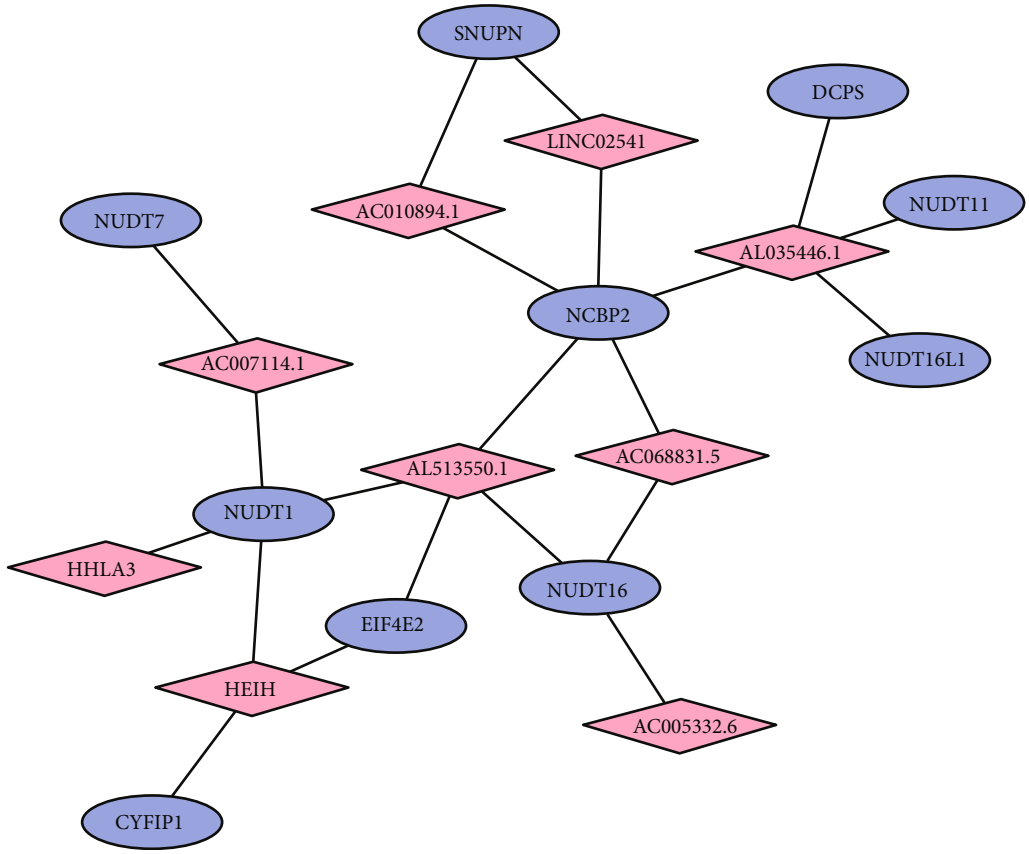

Figure 1: The coexpression network of m7G-related prognostic lncRNAs and mRNA. Pink diamonds represent lncRNAs, and blue ellipses represent mRNAs. Black solid lines represent the coexpression relationships between the mRNAs and lncRNAs.

3. Results

3.1. Identification of m7G-Related lncRNAs. We downloaded 60,660 gene transcription expression matrices from TCGA database, including 16,798 lncRNAs and 19,926 mRNAs. According to MSigDB database and OSCC mRNA matrix, 31 m7G-related mRNAs were obtained. Then, 399 m7G-related lncRNAs were identified through coexpression network analysis. For the expression matrix and coexpression relationship of m7G-related lncRNAs, see Supplementary Files (m7G-lncRNAs_exp.xls and co-exp_rel.xls).

3.2. Identification of m7G-Related Prognostic lncRNAs. Combined with KM analysis and univariate Cox analysis, we identified 16 m7G-related prognostic lncRNAs (as shown in Table 1). Three lncRNAs, LINC02541, AC007114.1, and HEIH, were low-risk lncRNAs (HR values < 1), and the rest were high-risk lncRNAs (HR values > 1). The P values of lncRNAs identified by the two methods were all less than 0.05.

3.3. The Prognostic Risk Score Model for OSCC. We performed univariate Cox analysis on 16 m7G-related prognostic lncRNAs and optimized 9 m7G-related prognostic lncRNAs, among which LINC02541, AC007114.1, and HEIH were low-risk lncRNAs (HR value < 1) and HHLA3, AC010894.1, AL513550.1, AL035446.1, AC068831.5, and AC005332.6 were high-risk lncRNAs (HR value > 1). The prognostic risk score model of OSCC patients was evaluated and optimized through cross-validation. lncRNAs and prognostic model formula that comprised the prognostic risk score model are shown in Tables 2 and 3. The raw data related to the prognostic model are detailed in Supplementary Files (risk.xls and uniSigExp.xls).

3.4. The Coexpression Network of m7G-Related Prognostic lncRNAs and mRNAs. A total of 10 m7G-related prognostic mRNAs and 9 m7G-related prognostic lncRNAs were identified through coexpression network analysis. For details about the coexpression relationship between the m7G-related prognostic lncRNAs and mRNAs, see Supplementary Files (coexp_network.xls). Coexpression network was used to visualize the correlation between the 10 m7G-related prognostic mRNAs and 9 m7G-related prognostic lncRNAs (Figure 1).

3.5. Risk Identification of m7G-Related Prognostic lncRNAs. Through the coexpression analysis and risk assessment analysis of m7G-related prognostic mRNAs and lncRNAs, it was found that six m7G-related prognostic lncRNAs (AC005332.6, AC010894.1, AC068831.5, AL035446.1, AL513550.1, and HHLA3) were high-risk lncRNAs. Three

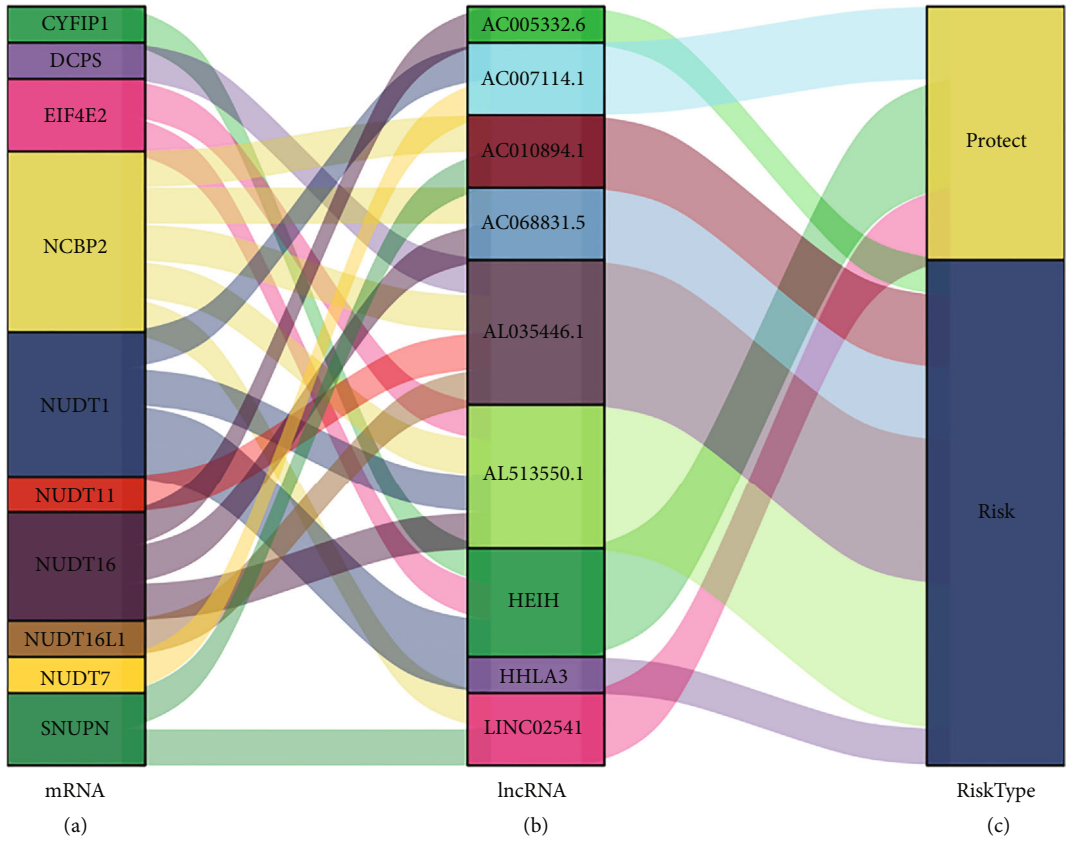

Figure 2: The Sankey diagram showed the risk profile of nine m7G-related prognostic lncRNAs. The blocks represent (a) the m7G-related prognostic mRNAs, (b) the m7G-related prognostic lncRNAs, and (c) the risk types of lncRNAs.

m7G-related prognostic lncRNAs (AC007114.1, HEIH, and LINC02541) were protective lncRNAs. The Sankey diagram showed the risk profile of all m7G-related prognostic lncRNAs (Figure 2).

3.6. Survival Curves of m7G-Related Prognostic lncRNAs. Survival curves were drawn by comparing the survival differences between patients with high and low expression of each m7G-related prognostic lncRNA in the prognostic risk score model. As shown in Figure 3, the survival of six m7G-related prognostic lncRNAs (AC005332.6, AC010894.1, AC068831.5, AL035446.1, AL513550.1, and HHLA3) with the high expression group was significantly lower than that with the low expression group ($P < 0.05$), while the survival of the other three m7G-related prognostic lncRNAs (AC007114.1, HEIH, and LINC02541) with the high expression group was significantly higher than that with the low expression group ($P < 0.05$).

3.7. Risk Assessment of the Prognostic Risk Score Model for OSCC. Risk curves, scatter plots, and heat maps were drawn by comparing the survival differences between high-risk and low-risk OSCC patients in the prognostic risk score model. As shown in Figure 4(a), the risk score of OSCC patients in the high-risk group was significantly higher than that in the low-risk group ($P < 0.05$). As shown in Figure 4(b), there were significantly more deaths in the high-risk group than in the low-risk group. In addition, Figure 4(c) shows that AC005332.6, AC010894.1, AC068831.5, AL035446.1, AL513550.1, and HHLA3 were highly expressed in the high-risk OSCC group, while AC007114.1, HEIH, and LINC02541 were highly expressed in the low-risk OSCC group. These results suggested that this prognostic risk score model could accurately predict the prognostic risk outcomes of both groups of OSCC patients.

3.8. Validation of the Predictive Power of the Prognostic Risk Score Model. Forest maps and the ROC curve were generated to verify the predictive power of the prognostic risk score model. According to Figures 5(a) and 5(b), P values of risk score were less than 0.05 and HR values were greater than 1 in both univariate and multivariate independent prognostic analyses, suggesting that risk score in the prognostic risk score model may be a reliable clinical independent prognostic factor. As shown in Figure 5(c), the risk score had the highest AUC value (0.931) compared to other clinical trait parameters. These results suggested that the prognostic risk score model has the ability to predict the prognosis of OSCC patients accurately and independently.

4. Discussion

Factors that influence the recurrence of OSCC have been extensively explored in recent years. Cai et al. [40] have

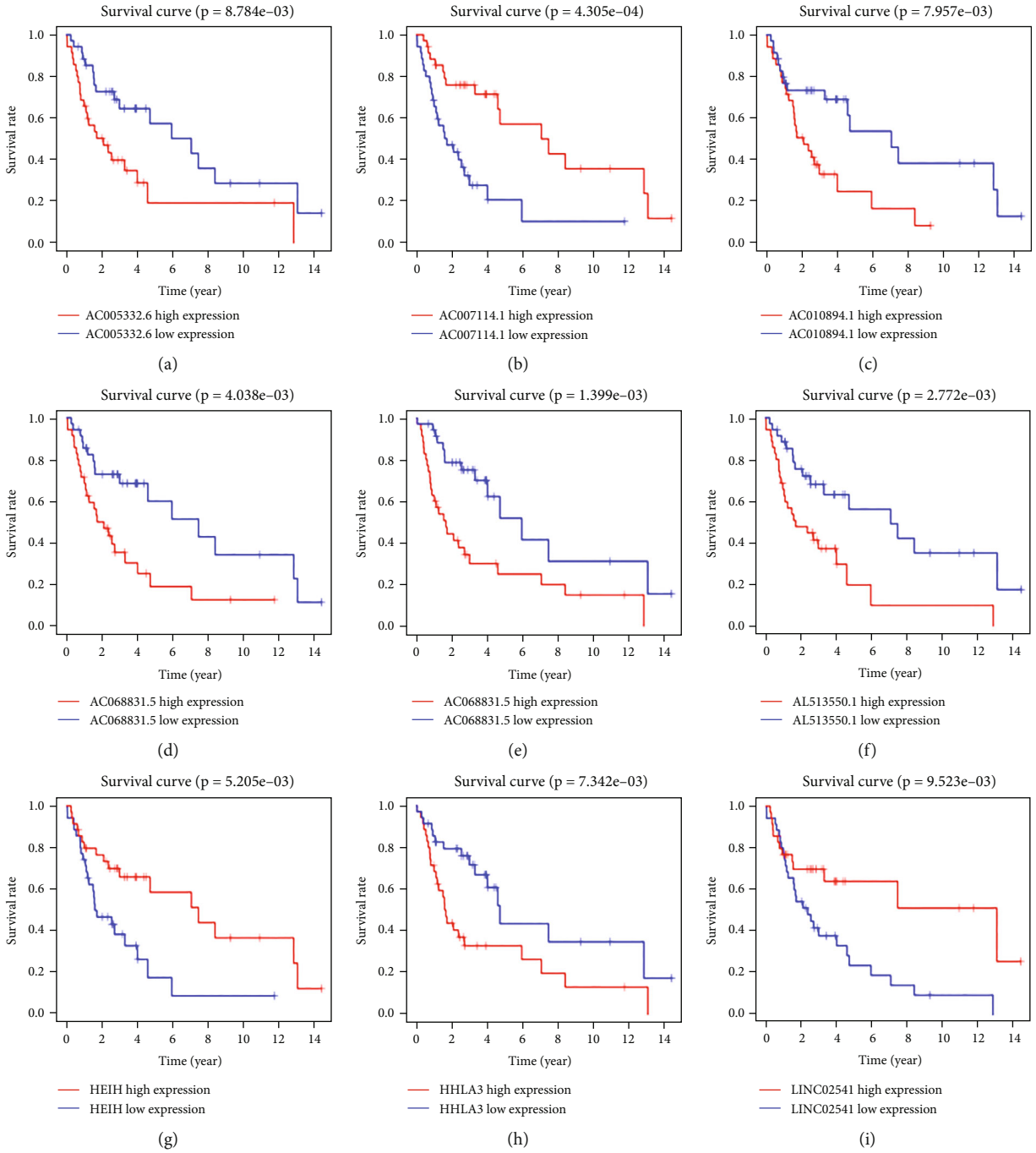

Figure 3: The survival curve of high (red) and low (blue) expression groups of m7G-related prognostic lncRNAs. Abscissa: survival years of patients; ordinate: survival rate of patients.

analyzed the patient clinicopathologic data, including tumor sites, clinical and pathologic stage, histological grade, invasion mode, and perineural invasion. They have concluded that tongue cancer and poor differentiation contributed to OSCC recurrence after surgery. Xia et al. [41] have reported that the recurrence rate was 44.9% in 118 patients with OSCC. Statistical analysis showed that comorbidities, degree of tumor differentiation, and tumor stage were important prognostic factors for recurrence. In this paper, 31 m7G-related mRNAs and 399 m7G-related lncRNAs were obtained through coexpression network analysis. Afterwards, we performed univariate Cox analysis on 16 m7G-related prognostic lncRNAs and optimized 9 m7G-related prognostic lncRNAs, and the prognostic risk score model of OSCC patients was evaluated and optimized through cross-validation. Further, through the coexpression analysis and risk assessment analysis of m7G-related prognostic mRNAs and lncRNAs, it was found that six m7G-related prognostic lncRNAs (AC005332.6, AC010894.1, AC068831.5, AL035446.1, AL513550.1, and HHLA3) were

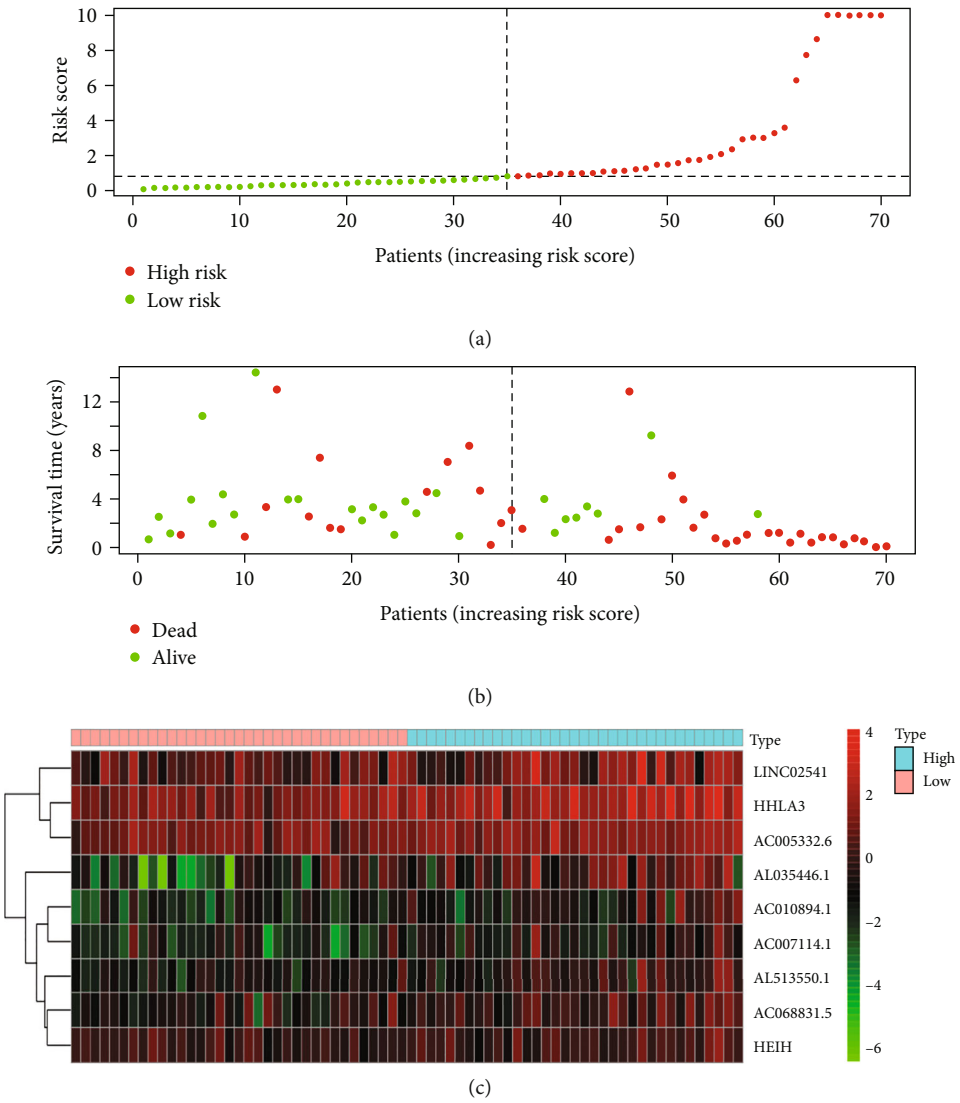

Figure 4: (a) The risk curves of OSCC patients. Abscissa: patients' risk scores ranked from low to high; ordinate: risk score. Red dots: high-risk group; green dots: low-risk group. (b) The risk scatter plots of OSCC patients. Ordinate: survival time. Red dots: dead patients; green dots: alive patients. (c) The risk heat maps of nine m7G-related prognostic lncRNAs of OSCC patients. Red squares: high-expression lncRNAs; green squares: low-expression lncRNAs.

high-risk lncRNAs. Three m7G-related prognostic lncRNAs (AC007114.1, HEIH, and LINC02541) were protective lncRNAs. Then, survival curves were drawn by comparing the survival differences between patients with high and low expression of each m7G-related prognostic lncRNA in the prognostic risk score model. Further, risk curves, scatter plots, and heat maps were drawn by comparing the survival differences between high-risk and low-risk OSCC patients in the prognostic model. Finally, forest maps and the ROC curve were generated to verify the predictive power of the prognostic risk score model.

So far, no study has reported the risk correlation between m7G-related lncRNAs and survival prognosis of OSCC based on bioinformatics analysis. However, in other areas of cancer, a few studies have found that m7G-modification is involved in gene regulation of tumor cell biology. Chen et al. [10] conducted tRNA modification and expression profile, mRNA translation profile, and rescue analysis in a conditional gene knockout mouse model and found that abnormal translation regulated by METTL1/WDR4-mediated tRNA m7G-modification drives the development and progression of squamous cell carcinoma of the head and neck. Xia et al. [41] verified the high expression of WD repeat Domain 4 (WDR4) in hepatocellular carcinoma (HCC) by cell culture and functional experiments and observed that upregulated WDR4 expression increased m7G-methylation level in HCC. And HCC cell proliferation was promoted by inducing G2/M cell cycle conversion and inhibiting apoptosis. Liu et al. [42] confirmed that methyltransferase-like 1 (METTL1) acts as a tumor suppressor in colon cancer by activating m7G-regulated let-7e miRNA/HMGA2 axis through quantitative PCR, Western

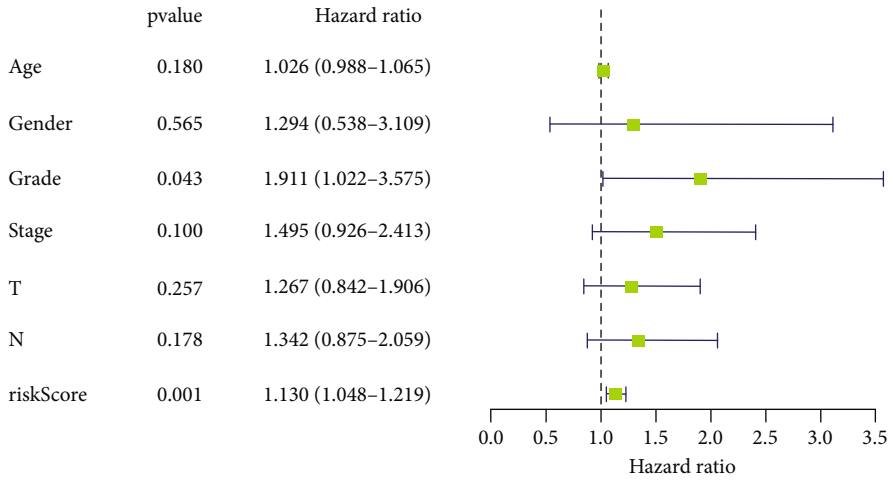

(a)

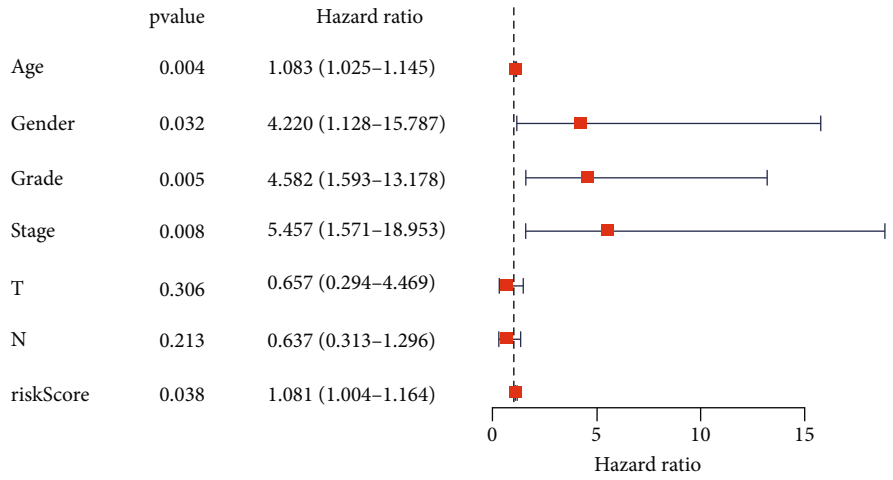

(b)

Figure 5: Continued.

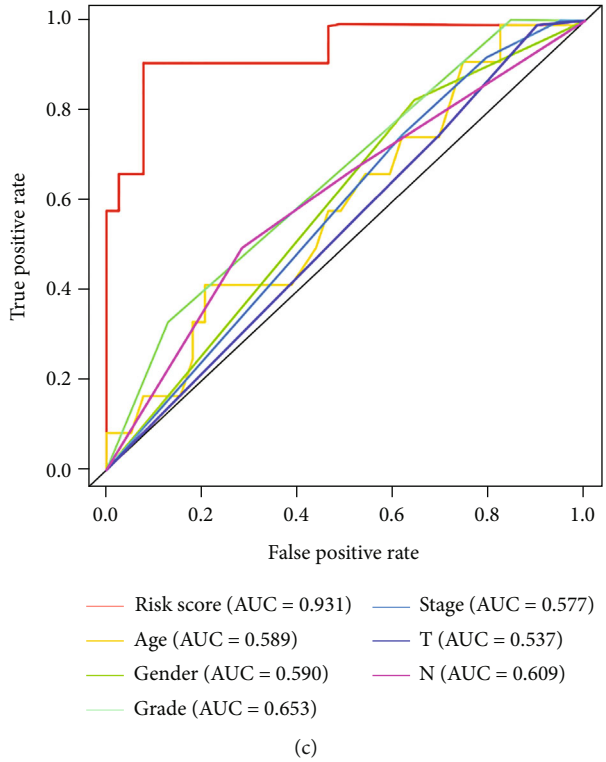

Figure 5: Forest plots of univariate (a) and multivariate (b) independent prognostic analyses of clinical trait parameters in OSCC patients. Green or red squares represent hazard ratio (HR) value, and blue solid lines represent 95% confidence intervals. (c) A ROC curve of the prognostic risk score model. The different colored curves represent different clinical trait parameters. AUC: area under the ROC curve. Abscissa: false positive rate (1 − specificity); ordinate: true positive rate (sensitivity).

blot, CCK-8 assay, transwell assay, and dual-luciferase reporter gene system. To our knowledge, this study has manifested the risk correlation between N7-methylguanosine modification-related lncRNAs and survival prognosis of oral squamous cell carcinoma for the first time. Our data has identified m7G-related lncRNAs through coexpression analysis and the m7G-related prognostic lncRNAs by KM analysis and univariate Cox analysis methods. Then, a prognostic risk score model for OSCC were constructed and obtained the formula of the model. Next, coexpression network analysis, risk assessment, and survival analysis of m7G-related prognostic lncRNAs were carried out. In addition, we conducted a comprehensive risk analysis for OSCC patients with high- and low-risk groups and performed independent prognostic analyses and ROC curve analyses to verify the predictive performance of OSCC prognostic risk score model.

However, there are still some limitations in this study, such as the lack of further studies on the important functions and key pathways of different pathological subtypes of OSCC and m7G-related gene [43]. More experimental validation of tissue samples from patients is needed in the future to further validate our new findings.

Data Availability

The dataset used and/or analyzed during this study may be granted by contacting the corresponding author.

Conflicts of Interest

The authors declare that they have no competing interests.

Authors' Contributions

Yanglong Xu and Xue Zou contributed equally to this study.

Acknowledgments

The authors thank the TCGA database for providing the valuable gene expression matrix and clinical information of OSCC.

Supplementary Materials

Supplementary Materials. File m7G-lncRNAs_exp.xls shows the expression matrix of 399 m7G-related lncRNAs. Rows represent m7G-related lncRNA names, and columns represent samples. File co-exp_rel.xls shows the coexpression relationship of m7G-related lncRNAs and m7G-realated mRNAs. The first column represents m7G-realated mRNAs, the second column represents m7G-realated lncRNAs, the third column represents coexpression correlation coefficients, and the fourth column represents the *P* value of the correlation test. File risk.xls presents univariate Cox regression analysis for 16 significant m7G-related prognostic lncRNAs. The first column represents samples, the second column represents the survival time of patients, the third

column represents their survival status, and columns 4 to 19 represent m7G-related prognostic lncRNAs. File risk.xls presents the risk scores of nine m7G-related prognostic lncRNAs that constitute the prognostic model. The first column represents samples, the second column represents the survival time of patients, the third column represents their survival status, columns 4 to 12 represent m7G-related prognostic lncRNAs, and columns 13 and 14 represent the risk score and risk grouping for each patient. File coexp_network.xls shows the coexpression relationship between the m7G-related prognostic lncRNAs and mRNAs. The first column represents prognostic m7G-realated mRNAs, the second column represents prognostic m7G-realated lncRNAs, and the third column represents the correlation type. *(Supplementary Materials)*

References

[1] Q. Duan, M. Xu, M. Wu, X. Zhang, M. Gan, and H. Jiang, "Long noncoding RNA UCA1 promotes cell growth, migration, and invasion by targeting miR-143-3p in oral squamous cell carcinoma," *Cancer Medicine*, vol. 9, no. 9, pp. 3115–3129, 2020.

[2] R. Siegel, K. Miller, H. Fuchs, and A. Jemal, "Cancer statistics, 2022," *CA: a Cancer Journal for Clinicians*, vol. 72, no. 1, pp. 7–33, 2022.

[3] H. Suenaga, H. Hoang Tran, H. Liao et al., "Real-time in situ three-dimensional integral videography and surgical navigation using augmented reality: a pilot study," *International Journal of Oral Science*, vol. 5, no. 2, pp. 98–102, 2013.

[4] T. Ishida, H. Hijioka, K. Kume, A. Miyawaki, and N. Nakamura, "Notch signaling induces EMT in OSCC cell lines in a hypoxic environment," *Oncology Letters*, vol. 6, no. 5, pp. 1201–1206, 2013.

[5] J. Xiao, H. Lai, S. Wei, Z. Ye, F. Gong, and L. Chen, "lncRNA HOTAIR promotes gastric cancer proliferation and metastasis via targeting miR-126 to active CXCR4 and RhoA signaling pathway," *Cancer Medicine*, vol. 8, no. 15, pp. 6768–6779, 2019.

[6] Q. Yang, J. Wang, P. Zhong et al., "The clinical prognostic value of lncRNA FAM83H-AS1 in cancer patients: a meta-analysis," *Cancer Cell International*, vol. 20, no. 1, p. 72, 2020.

[7] S.-Y. Zhang, S.-W. Zhang, T. Zhang, X.-N. Fan, and J. Meng, "Recent advances in functional annotation and prediction of the epitranscriptome," *Computational and Structural Biotechnology Journal*, vol. 19, pp. 3015–3326, 2021.

[8] V. H. Cowling, "Regulation of mRNA cap methylation," *The Biochemical Journal*, vol. 425, no. 2, pp. 295–302, 2009.

[9] X. Ying, B. Liu, Z. Yuan et al., "METTL1-m7G-EGFR/EFEMP1 axis promotes the bladder cancer development," *Clinical and Translational Medicine*, vol. 11, no. 12, p. e675, 2021.

[10] J. Chen, K. Li, J. Chen et al., "Aberrant translation regulated by METTL1/WDR4-mediated tRNA N7-methylguanosine modification drives head and neck squamous cell carcinoma progression," *Cancer Communications (London, England)*, vol. 42, no. 3, pp. 223–244, 2022.

[11] O. Katsara and R. J. Schneider, "m^7G tRNA modification reveals new secrets in the translational regulation of cancer development," *Molecular Cell*, vol. 81, no. 16, pp. 3243–3245, 2021.

[12] Z. Chen, W. Zhu, S. Zhu et al., "METTL1 promotes hepatocarcinogenesis via m7G tRNA modification-dependent translation control," *Clinical and Translational Medicine*, vol. 11, no. 12, p. e661, 2021.

[13] Z. Dai, H. Liu, J. Liao et al., "N^7-methylguanosine tRNA modification enhances oncogenic mRNA translation and promotes intrahepatic cholangiocarcinoma progression," *Molecular Cell*, vol. 81, no. 16, pp. 3339–3355.e8, 2021.

[14] C. Ganini, I. Amelio, R. Bertolo et al., "Global mapping of cancers: The Cancer Genome Atlas and beyond," *Molecular Oncology*, vol. 15, no. 11, pp. 2823–2840, 2021.

[15] J. Lee, "Exploring cancer genomic data from the cancer genome atlas project," *BMB Reports*, vol. 49, no. 11, pp. 607–611, 2016.

[16] A. Liberzon, A. Subramanian, R. Pinchback, H. Thorvaldsdóttir, P. Tamayo, and J. Mesirov, "Molecular Signatures Database (MSigDB)," *Bioinformatics (Oxford, England)*, vol. 27, no. 12, pp. 1739-1740, 2011.

[17] M. Ritchie, B. Phipson, D. Wu et al., "limma powers differential expression analyses for RNA-sequencing and microarray studies," *Nucleic Acids Research*, vol. 43, no. 7, article e47, 2015.

[18] Z. Wang, Z. Guo, J. Li et al., "Genome-wide search for competing endogenous RNAs responsible for the effects induced by Ebola virus replication and transcription using a trVLP system," *Frontiers in Cellular and Infection Microbiology*, vol. 7, p. 479, 2017.

[19] S. Qin, Y. Liao, Q. Du et al., "DSG2 expression is correlated with poor prognosis and promotes early-stage cervical cancer," *Cancer Cell International*, vol. 20, no. 1, p. 206, 2020.

[20] M. Wu, Y. Xia, Y. Wang et al., "Development and validation of an immune-related gene prognostic model for stomach adenocarcinoma," *Bioscience Reports*, vol. 40, no. 10, 2020.

[21] Z. Hu, D. Yang, Y. Tang et al., "Five-long non-coding RNA risk score system for the effective prediction of gastric cancer patient survival," *Oncology Letters*, vol. 17, no. 5, pp. 4474–4486, 2019.

[22] S. Li, L. Wang, Q. Zhao et al., "Genome-wide analysis of cell-free DNA methylation profiling for the early diagnosis of pancreatic cancer," *Frontiers in Genetics*, vol. 11, p. 596078, 2020.

[23] Y. Zhang, X. Zhang, X. Lv et al., "Development and validation of a seven-gene signature for predicting the prognosis of lung adenocarcinoma," *BioMed Research International*, vol. 2020, Article ID 1836542, 10 pages, 2020.

[24] R. Dobrin, J. Zhu, C. Molony et al., "Multi-tissue coexpression networks reveal unexpected subnetworks associated with disease," *Genome Biology*, vol. 10, no. 5, p. R55, 2009.

[25] P. Shannon, A. Markiel, O. Ozier et al., "Cytoscape: a software environment for integrated models of biomolecular interaction networks," *Genome Research*, vol. 13, no. 11, pp. 2498–2504, 2003.

[26] B. P. Turnwald, J. P. Goyer, D. Z. Boles, A. Silder, S. L. Delp, and A. J. Crum, "Learning one's genetic risk changes physiology independent of actual genetic risk," *Nature Human Behaviour*, vol. 3, no. 1, pp. 48–56, 2019.

[27] K. Shameer, Y. Zhang, A. Prokop et al., "OSPred tool: a digital health aid for rapid predictive analysis of correlations between early end points and overall survival in non-small-cell lung cancer clinical trials," *JCO Clinical Cancer Informatics*, vol. 6, no. 6, p. e2100173, 2022.

[28] S. Mangiola, M. Doyle, and A. Papenfuss, "Interfacing Seurat with the R Tidy Universe," *Bioinformatics (Oxford, England)*, vol. 37, no. 22, pp. 4100–4107, 2021.

[29] G. Chen, G. Yang, J. Long et al., "Comprehensive analysis of autophagy-associated lncRNAs reveal potential prognostic prediction in pancreatic cancer," *Frontiers in Oncology*, vol. 11, p. 596573, 2021.

[30] B. George, S. Seals, and I. Aban, "Survival analysis and regression models," *Journal of Nuclear Cardiology*, vol. 21, no. 4, pp. 686–694, 2014.

[31] M. Wang, T. Xie, Y. Wu et al., "Identification of RFC5 as a novel potential prognostic biomarker in lung cancer through bioinformatics analysis," *Oncology Letters*, vol. 16, no. 4, pp. 4201–4210, 2018.

[32] G. D'Arrigo, D. Leonardis, S. Abd ElHafeez, M. Fusaro, G. Tripepi, and S. Roumeliotis, "Methods to analyse time-to-event data: the Kaplan-Meier survival curve," *Oxidative Medicine and Cellular Longevity*, vol. 2021, Article ID 2290120, 7 pages, 2021.

[33] P. Zhang, X. Tan, D. Zhang, Q. Gong, and X. Zhang, "Development and validation of a set of novel and robust 4-lncRNA-based nomogram predicting prostate cancer survival by bioinformatics analysis," *PLoS One*, vol. 16, no. 5, p. e0249951, 2021.

[34] R. Huang, J. Guo, P. Yan et al., "The construction of bone metastasis-specific prognostic model and co-expressed network of alternative splicing in breast cancer," *Frontiers in Cell and Development Biology*, vol. 8, p. 790, 2020.

[35] X. Qi, Z. Liu, Q. Zhang et al., "Systematic analysis of the function and prognostic value of RNA binding proteins in colon adenocarcinoma," *Journal of Cancer*, vol. 12, no. 9, pp. 2537–2549, 2021.

[36] Q. Zhang, G. Guan, P. Cheng, W. Cheng, L. Yang, and A. Wu, "Characterization of an endoplasmic reticulum stress-related signature to evaluate immune features and predict prognosis in glioma," *Journal of Cellular and Molecular Medicine*, vol. 25, no. 8, pp. 3870–3884, 2021.

[37] Y. Yue, K. Astvatsaturyan, X. Cui, X. Zhang, B. Fraass, and S. Bose, "Stratification of prognosis of triple-negative breast cancer patients using combinatorial biomarkers," *PLoS One*, vol. 11, no. 3, p. e0149661, 2016.

[38] K.-H. Pan, L. Jian, W.-J. Chen et al., "Diagnostic performance of contrast-enhanced ultrasound in renal cancer: a meta-analysis," *Frontiers in Oncology*, vol. 10, p. 586949, 2020.

[39] Y. Zheng, Y. Wen, H. Cao et al., "Global characterization of immune infiltration in clear cell renal cell carcinoma," *Oncotargets and Therapy*, vol. 14, pp. 2085–2100, 2021.

[40] S. Cai, X. Hu, R. Chen, and Y. Zhang, "Identification and validation of an immune-related eRNA prognostic signature for hepatocellular carcinoma," *Frontiers in Genetics*, vol. 12, p. 657051, 2021.

[41] P. Xia, H. Zhang, K. Xu et al., "MYC-targeted WDR4 promotes proliferation, metastasis, and sorafenib resistance by inducing CCNB1 translation in hepatocellular carcinoma," *Cell Death & Disease*, vol. 12, no. 7, p. 691, 2021.

[42] Y. Liu, Y. Zhang, Q. Chi, Z. Wang, and B. Sun, "RETRACTED: Methyltransferase-like 1 (METTL1) served as a tumor suppressor in colon cancer by activating 7-methyguanosine (m7G) regulated let-7e miRNA/HMGA2 axis," *Life Sciences*, vol. 249, p. 117480, 2020.

[43] Z. Chen, Z. Zhang, W. Ding et al., "Expression and potential biomarkers of regulators for M7G RNA modification in gliomas," *Frontiers in Neurology*, vol. 13, no. 13, p. 886246, 2022.

Hindawi
Applied Bionics and Biomechanics
Volume 2022, Article ID 7135040, 10 pages
https://doi.org/10.1155/2022/7135040

Research Article

Effect of Different Ankle-Foot Immobility on Lateral Gait Stability in the Stance Phase

Wen Fan[1] **and Yasuhiko Hatanaka**[1,2]

[1]*Graduate School of Health Science, Suzuka University of Medical Science, 5100293 Mie, Japan*
[2]*Department of Rehabilitation Physical Therapy Course, Faculty of Health Science, Suzuka University of Medical Science, 5100293 Mie, Japan*

Correspondence should be addressed to Yasuhiko Hatanaka; hatanaka@suzuka-u.ac.jp

Received 15 June 2022; Revised 15 July 2022; Accepted 21 July 2022; Published 3 August 2022

Academic Editor: Yaodong Gu

Background. This study aimed to investigate the effect of limited foot and ankle mobility on the lateral stability of gait through the observation of the mediolateral margin of stability and related kinematic parameters. *Methods*. Thirty young, healthy participants walked at a fixed gait velocity on a level surface. Participants achieved different degrees of restricted mobility by wearing soft-soled shoes (S), an ankle-foot orthosis with unrestricted dorsiflexion-plantarflexion activity only (A), and an ankle-foot orthosis with unrestricted dorsiflexion-plantarflexion and adjustable horizontal rotation of the foot (OU/OR). Furthermore, the spatiotemporal parameters, mediolateral margin of stability, center of pressure, angle of the fore and hind foot relative to the tibia, and correlation coefficients of the factors were analyzed. Regression analysis was also performed. *Results*. At right heel strike, group A had a significantly lower mediolateral margin of stability than group S and group OU. Meanwhile, forefoot adduction ($0.2 < |r| < 0.4$) and plantarflexion ($0.2 < |r| < 0.4$), as well as hindfoot internal rotation ($0.2 < |r| < 0.6$) and inversion ($0.2 < |r| < 0.4$), correlated negatively with lateral stability. Regression analysis revealed forefoot dorsiflexion and supination were the main independent variables for group A. At right heel off, groups OU and OR had a significantly lower mediolateral margin of stability than those in groups A and S. Forefoot adduction ($0.2 < |r| < 0.4$) and dorsiflexion ($0.4 < |r| < 0.6$) were correlated with lateral stability, as were hindfoot dorsiflexion ($0.2 < |r| < 0.4$) and inversion ($0.2 < |r| < 0.4$). Regression analysis revealed forefoot abduction and plantarflexion were the main independent variables for groups OU and OR. *Conclusions*. The present study verified from gait data that forefoot dorsiflexion and supination at the initial contact of the stance phase were relevant factors for the differences in lateral gait stability, whereas abduction and plantar flexion of the forefoot at the terminal stance phase were the main influencing factors of lateral gait stability.

1. Introduction

The frequently occurring traffic accidents, cardiovascular and cerebrovascular events, and the increasing aging of the population in our society have led to the presence of large numbers of potentially or apparently unstable gait holders. Moreover, in the available studies, cases of decreased gait stability or abnormal gait due to disease [1–3] and surgery [4, 5] have been reported. Falls and their secondary injuries caused by instability of gait often have serious consequences. Meanwhile, such consequences also result in significant financial, time, and labor costs associated with care and rehabilitation [6, 7]. Clinical diagnostic and treatment criteria for normal and abnormal gait characteristics allow for timely detection and intervention of gait health conditions in patients with unstable gait, thereby reducing the serious consequences of unstable gait [7].

Gait stability is affected by many factors [8], such as age, walking speed, weight shift, and center of pressure (COP) trajectory. Walking in the living environment is often performed while experiencing complex road conditions, multidirectional disturbances, multitask walking, sound and light stimulation, and other situations that are more complex than those in the laboratory environment [9]. Due to the

structure of the human lower limb musculoskeletal system, gait adjustment ability in the sagittal direction is greater than lateral adjustment ability [10]. However, at the same time, lateral adjustment is also considered to be a critical influence on lateral stability.

The scale scores of traditional evaluation methods are subjective, and the static evaluation results cannot fully reflect dynamic stability [11, 12]. Therefore, by using motion capture and other technologies, objective and detailed data are obtained, and gait stability analysis that can distinguish gait events and vector directions can be performed. This is helpful for a simple, unified, and quantitative assessment of the gait stability of people [12]. Biomechanical measurements are relevant for both quantitative assessments of fall risk and gait characteristics in different age populations [13]. Most of the time, in a gait cycle, the projection of the center of mass (CoM) onto the ground is outside the base of support (BoS), but the stability of walking can still be satisfied [14]. The margin of stability (MoS) as one of the gait stability assessment metrics has the advantages of efficiency and simplicity of operation over the local dynamic stability, foot placement estimator, global dynamic stability, and other metrics or methods [15]. Therefore, it is more convenient to be widely used for gait analysis of straight walking and turning. However, due to the variability in the application of MoS, the development of a standard process for the use of the method and the availability of a larger amount of data are needed [16].

Moreover, due to the basic kinematic theories such as inverse dynamics [17] and closed kinetic chain, we can determine the importance of foot and ankle joint action for gait stability. Ankle kinematic parameters have different characteristics in different periods of the stance phase [18]. Therefore, biomechanical gait analysis is of great significance for disease assessment and more targeted treatment plan development. The widespread use of ankle-foot orthoses (AFOs) has provided mobility and stability gains not only for patients with conditions such as cerebral palsy and stroke. In a review of prior studies, there is also a tendency for AFO categories [19] to cause limited joint motion or for AFO stiffness [20] to cause abnormal joint motion in different phases of the walking cycle.

Therefore, in the present study, we observed the changes in biomechanical characteristics and stability of different gait cycles in the stance phase using the limitations and effects that different AFOs possess on the normal joint range of motion and joint movement trends in walking, respectively. The objective was to fill the gap in the observation of the effect of limited foot and ankle mobility on lateral gait stability in prior studies, as well as to provide data on kinematic parameters with MoS as the main factor.

2. Method

2.1. Participants. Thirty (16 male and 14 female) healthy volunteers participated in the experiment. They were all from Suzuka University of Medical Sciences with a mean age of 20.6 ± 0.8 years and mean height and weight of 1.65 ± 0.02 m and 58.2 ± 2.04 kg. All participants met the following criteria: (1) no psychiatric or neurological disorders or orthopedic disorders that interfere with walking, (2) no cerebellar lesions or bilateral motor deficits, and (3) no dance or gymnastic training for more than three months at any time in their lives.

2.2. Ethical Approval. All participants were fully informed and understood the content of this study. All participants confirmed their willingness to participate in the experiment. This study was approved by the Ethics Committee of Suzuka University of Medical Sciences (approval number: 437). This study was conducted following the Helsinki Declaration.

2.3. Instruments. The equipment in the laboratory used to obtain kinematic data in the trial included a Motion Capture System (Vicon: Nexus 2.11 and 14 at 100 Hz; Vero v2.2∗12, Vantage 5∗2; Vicon Motion Systems Ltd., Oxford, UK); and five force measurement platforms were used to record three components of ground reaction forces: vector, COP, and the timing of the gait events of heel strike and toe off the ground (AMTI: OR 6-6-OP -2000 force platform; Advanced Mechanical Technology, Inc., Watertown, MA, USA). The following shoes (Figure 1(a)) and ankle-foot orthosis were worn on the participant's right foot: Agilium-freestep orthosis (Ottobock KGaA, Duderstadt, Germany) (Figure 1(b)) and Matsumoto custom orthosis for the right foot (Matsumoto Gishi Co. Ltd., Hayashi Komaki, Japan) (Figure 2(a)). The Agilium-freestep orthosis allows only dorsiflexion and plantarflexion of the foot. The Matsumoto custom orthosis also allows for free dorsiflexion and plantarflexion. And there is a locking hole next to the bottom horizontal rotation axis, which can be adjusted by a locking screw to determine whether to restrict the horizontal rotation (Figure 2(b)).

2.4. Experimental Protocol and Data Collection. Participants received instructions before the day of the experiment and practiced at a specific cadence on a 10-m-long linear walking path. Based on the average cadence value of healthy adults in Japan [21], the pace tempo of this experiment was set at 112 steps/min. Participants' weight, height, leg length, knee width, and ankle width were measured and recorded on the day of the experiment. The Oxford Foot Model (OFM), which can provide multisegmental kinematic and kinetic data with accuracy for the study [22], was used based on the need for data on the restricted mobility of the foot and ankle. Therefore, the reflex markers were applied to the skin at the location marked by the OFM method. To prevent high inter-subject variability, an experienced laboratory technician determined the final location of the markers.

Each participant was asked to wear shoes or orthosis on their right foot as follows: S, data while wearing soft-soled shoes; A, gait measurement and recording completed while wearing Agilium-freestep orthosis; S, data collected while wearing soft-soled shoes; OU: gait data with the Matsumoto orthosis but no horizontal rotational restriction holes locked; OR: gait data with the Matsumoto orthosis but the bottom horizontal rotation restriction hole locked. A soft-soled shoe of the same thickness was worn on the left foot. Each

(a) (b)

Figure 1: Soft-soled shoes (a) and Agilium-freestep orthosis (b). The soft-soled shoes have no restrictions on the foot and ankle joints, and the bottom surface is soft and has the same thickness as the orthosis. The bottom surface of the Agilium-freestep orthosis forefoot is soft.

(a) (b)

Figure 2: Matsumoto custom orthosis (a) and bottom view of the Matsumoto orthosis (b). The bottom surface is hard, which limits the rotation of the forefoot and midfoot to a certain extent. The screw marked by the red circle is the horizontal rotation limiter.

participant wore the shoes or AFOs in turn and completed the measurement of gait data for each group of 5 tracks. After one foot and ankle condition was fixed, static modeling was first performed, followed by dynamic data measurements and recording. After data recording for one condition was completed, static modeling and dynamic data measurement and recording for the next foot and ankle condition were performed after an interval of ten minutes.

The Vicon Nexus motion capture data was exported to three-dimensional geometric calculation software (Visual 3D: C-motion), which applied a second-order Butterworth filter with a cut-off frequency of 6 Hz and defined a local coordinate system for each body part. Also, information on spatiotemporal parameters and their normalized means and standard deviations was obtained through Vicon Nexus. FFTBA is the angle between the forefoot segment and the tibial segment, while HFTBA is the angle between the hindfoot segment and the tibial segment. All angles were recorded in the sagittal, frontal, and coronal planes. At least three markers are used to locate each segment. Each gait event was defined and modified to obtain the 3D position coordinate information of the BoS in each gait event and to calculate the MoS. Sincethe CoM trajectory is extrapolated along its velocity direction, theextrapolated center of mass (XcoM) is used for the calculation of MoS. The differencebetween XcoM and the boundary ofBoS is MoS. In this study, the definition of BoS by Ohtsu et al. [23] was followed, and the front boundary and inner boundary of the BoS were defined. The formula for MoS is shown below as Equation (1) and Equation (2). The x in the formula is the coordinate of CoM, and l is the distance from CoM to the axis of rotation. And v is the velocity of CoM. The MoS obtained by this calculation was used as the stability of gait is described by the change in the MoS value. We analyzed the ML MoS of the average of five walking routes for each group for each gait event.

$$\mathrm{MoS} = \mathrm{BoS} - \mathrm{XcoM}, \tag{1}$$

$$\mathrm{XcoM} = x + \frac{v}{\omega} = x + \frac{v}{\sqrt{g/l}}. \tag{2}$$

2.5. Statistical Analysis. The Shapiro-Wilk test was used to examine the distribution and variance of the ML MoS in each group for each walking event, followed by a one-way ANOVA. A post hoc Bonferroni test was then performed to test for significant differences in spatiotemporal parameters, foot and ankle kinematics, ML MoS, and COP based on different ankle-foot mobility limitations. The gait events used for statistical analysis were defined as follows: The time points of right heel strike (RHS), left toe off (LTO), left heel strike (LHS), and right toe off (RTO) were automatically labeled by Vicon Nexus based on data from the force measurement platform. The RTOE at the midpoint of the base

Table 1: The result of spatiotemporal parameters (n =30).

Variables	A	S	OU	OR
Walking speed (m/s)	1.39 (0.13)	1.41 (0.13)	1.40 (0.13)	1.41 (0.14)
Cadence (steps/min)				
Left	118.75 (4.37)	116.40** (3.50)	116.48** (3.91)	116.20** (4.67)
Right	113.53 (3.92)	116.08** (4.24)	116.79** (4.85)	116.71** (4.27)
Stride length (m)	1.47 (0.12)	1.46 (0.13)	1.46 (0.14)	1.46 (0.14)
Stride width (m)	0.18 (0.02)	0.16 (0.02)**	0.17 (0.03)	0.16 (0.02)**

Note:* indicates that the value is significantly different from the value in group A (**$p < 0.01$); mean (standard deviation).

of the 1st and 5th metatarsal in the anterior part of the right foot was used to construct the forefoot segment for the calculation of the FFTBA. The vertical coordinates of the RTOE were also used to define the gait event RFF as well as the RHO gait event based on the RFF. The time point at which the velocity of the RTOE is below 100 mm/s was defined as right foot flat (RFF). The right heel off (RHO) was defined when the vertical coordinate of the heel mark is 10 mm or greater than that of the RFF. The moment of immediately coming to LHS was defined as pre-LHS. Significance levels were determined at a 5% risk rate ($p < 0.05$). Statistical analyses were performed using IBM SPSS Statistics 21 statistical software (IBM, Armonk, NY, USA).

3. Results

3.1. Spatiotemporal Parameters. The results of the spatiotemporal parameter analysis based on one gait cycle are shown in Table 1. The results of the one-way ANOVA and post hoc multiple comparisons showed no significant differences between the results of walking speed and stride length for the following variables. The results of the left foot cadence showed that the values of group A were significantly higher than those of the groups S, OU, and OR ($p < 0.01$). The results of the right foot cadence showed that the values of group A were significantly lower than those of groups S, OU, and OR ($p < 0.01$). In addition, the stride width of group A was also significantly wider than that of groups S and OR ($p < 0.01$).

3.2. ML MoS (Mediolateral Margin of Stability). The results of the analysis of ML MoS in this study showed a significant difference in ML MoS outcomes during the RHS and RHO gait events (Figure 3). The ML MoS values of group A at RHS were significantly smaller than those of groups S and OU ($p < 0.05$). The ML MoS values in groups OU and OR were significantly smaller than those in groups A and S ($p < 0.01$) at RHO.

3.3. COP (Center of Pressure). According to the normal distribution test results of the Shapiro-Wilk method ($p < 0.05$), the COP results of groups A, S, OU, and OR are all non-normally distributed, so the Kruskal-Wallis (K-W) test was selected. The significant differences in COP were as follows (Figure 4): the values of group A at RHS were significantly greater than those of groups S ($p < 0.01$) and OR ($p < 0.05$); the values of group A at pre-LHS and LHS were significantly smaller than those of group OU ($p < 0.01$) and OR ($p < 0.05$); and the values of group A at RTO were significantly smaller than those of group S ($p < 0.05$).

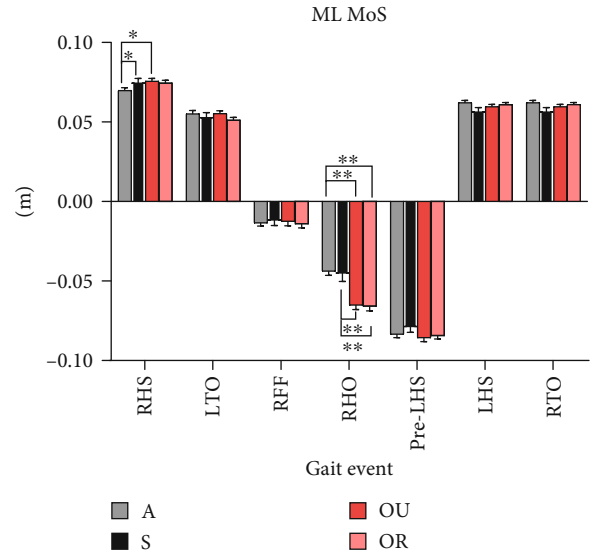

Figure 3: The mediolateral margin of stability (ML MoS) during the stance phase. The ML MoS of each gait event during the stance phase. The results in the figure are the mean values of the ML MoS of each group at different gait events ($*p < 0.05$), ($**p < 0.01$). A:gray column with stripes; S: black column; OU: red column; OR: red column with lattice.

3.4. Forefoot Tibia Angle (FFTBA) and Hindfoot Tibia Angle (HFTBA). The foot tibial angle in a gait cycle is shown below (Figure 5). According to the results of FFTBA and HFTBA, the forefoot adduction angle in group S was greater than in the other three groups during the whole gait cycle, and the forefoot abduction angle in group A was significantly greater than in the other three groups at the end of the stance phase (60%). The forefoot plantarflexion angle of the groups OU and OR in the mid-stance phase was smaller than that of group S, while group A had a greater dorsiflexion angle than the other groups during the whole phase. Moreover, group A showed an opposite dorsiflexion tendency to the other groups at the end of the stance phase. The group OU with unlimited horizontal rotation had greater pronation in the initial contact period, while the range of pronation and supination of the group OR with restricted horizontal rotation was the smallest. The external rotation angle of the hindfoot

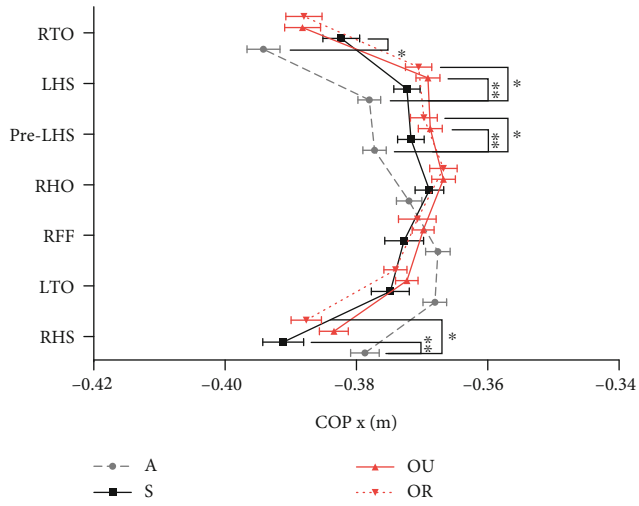

FIGURE 4: Center of pressure (COP) x at each gait event. The figure shows the mean values with SD of the COP x of each group in the different gait events ($^{*}p < 0.05$, $^{**}p < 0.01$). A: gray interrupted lines with dots; S: solid black line with squares; OU: solid red line with triangles; OR: red dotted line with inverted triangles.

in group A was smallest in the initial contact phase (0–10%), while its internal rotation angle was smallest in the preswing phase (30–60%) than in the other groups. Group S had the greatest hindfoot plantarflexion, while groups OU and OR had the greatest hindfoot dorsiflexion during the whole gait cycle. Group A had the smallest range of inversion and eversion in the standing phase, followed by group OR, which also had no limitation in dorsiflexion and plantarflexion only.

The peaks of the angles of the FFTBA and HFTBA based on the Oxford foot model are shown in Table 2. The groups A, OU, and OR with AFOs exhibited common characteristics of greater forefoot abduction with less adduction, less forefoot plantarflexion, less forefoot pronation, and greater hindfoot dorsiflexion with less plantarflexion than group S. This included the largest forefoot abduction and smallest forefoot plantarflexion in group A, the largest hindfoot dorsiflexion in groups OU and OR, and the smallest hindfoot plantarflexion in group OU. In addition, some disparate features included greater forefoot dorsiflexion and smaller hindfoot internal rotation in group A, smaller hindfoot eversion in groups OU and OR, and greater forefoot pronation in group OU than in group A and OR.

3.5. Correlation Analysis and Stepwise Regression Analysis. Since the significant difference in ML MoS appeared at the time of both RHS and RHO gait events, the correlation analysis and stepwise multiple regression analysis of FFTBA and HFTBA relative to ML MoS at these two time points were performed. The values of FFTBA, HFTBA, and ML MOS at RHS and RHO were obtained by Visual 3D. The results of the Pearson correlation coefficient analysis are shown in Table 3.

Stepwise multiple regression analysis of FFTBA and HFTBA concerning ML MoS was implemented. Figure 6 presents the results of the analysis at RHS, and Figure 7 shows the results of the analysis at RHO.

Each motion angle of the FFTBA and HFTBA at RHS was used as the independent variable (D-W values between 0-4), while ML MoS was used as the dependent variable for stepwise multiple regression analysis. And after automatic model identification, the best-fit equations obtained from stepwise multiple regression analysis can be found in Figure 6.

After automatic model identification, each motion angle of the FFTBA and HFTBA at RHO was used as the independent variable (D-W values between 0-4), while ML MoS was used as the dependent variable for stepwise multiple regression analysis. The best-fit equations obtained from stepwise multiple regression analysis can be found in Figure 7.

4. Discussion

The present study showed that different ankle mobility limitations led to differences in lateral stability in different periods of the stance phase. The results showed that participants with limited ankle mobility differed in the spatiotemporal parameters, mainly in terms of changes in cadence and step width. The differences in lateral stability were found at the RHS and RHO. And the COP differences appeared at the RHS, pre-LHS, LHS, and RTO of the stance phase. During the initial contact of the stance phase, the angles of restricted ankle movements mainly associated with poorer lateral stability were forefoot dorsiflexion and pronation, whereas, at the end of the stance phase, the angles of restricted ankle movement mainly associated with poorer lateral stability were forefoot abduction and plantarflexion.

Based on the spatiotemporal parameters, a significant influence of the kinematic parameters received by the foot and ankle in immobilized healthy adults can be found. Parameters such as walking speed and stride length did not differ significantly for participants. However, significant differences were found in parameters such as step width and the cadence of left and right foot. The participant's cadence was significantly lower in the right foot with limited mobility, while the cadence of the contralateral foot was significantly higher. According to prior studies, the step width was also significantly altered, and according to prior studies, this may have occurred as compensation for the limited mobility of the ankle joint [25].

The increase in ML MoS is also considered related to the increase in cadence [26]. As an assessment tool for lateral stability in this study, ML MoS showed significant differences at the RHS and RHO during the stance phase of walking. The difference in ML MoS at the RHS was mainly attributed to the difference in ML BoS. And the difference in ML MoS at RHO was mainly due to the difference in the velocity of lateral movement of the CoM. Therefore, dynamic stability analysis by direction is necessary to improve the sensitivity of fall risk assessment [15, 22].

In comparison with the results of ML MoS, the gait events and groups that showed significant differences in COP were different. The trajectory of COP x in group A showed a greater difference compared to the other three

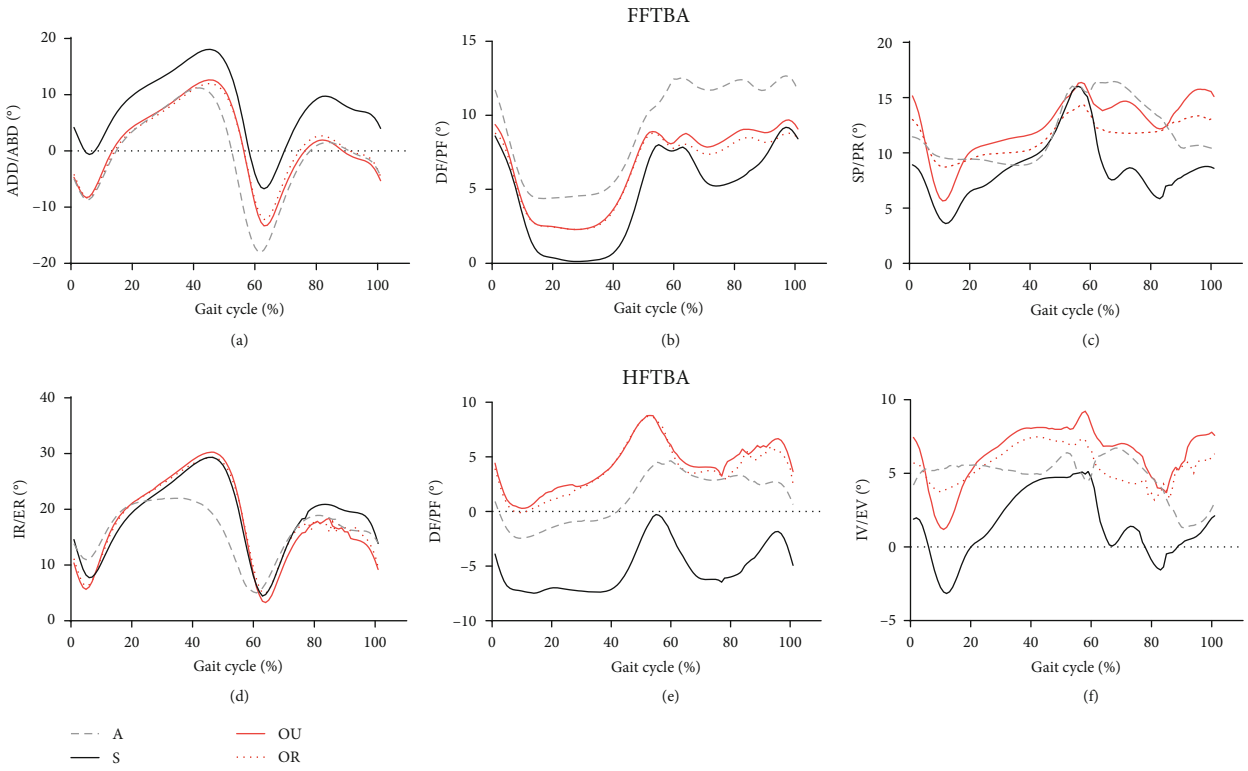

Figure 5: FFTBA and HFTBA during the gait cycle. (a)–(c) are the results of adduction (ADD) (+)/abduction (ABD) (-), dorsiflexion (DF) (+)/plantarflexion (PF) (-), supination (SP) (+)/pronation (PR) (-) of the FFTBA. (d)–(f) are the results of internal rotation (IR) (+)/external rotation (ER) (-), dorsiflexion (DF) (+)/plantarflexion (PF) (-), inversion (IV) (+)/eversion (EV) (-) [24] of HFTBA. A: black interrupted line, S: black realized, OU: red solid line, OR: red dotted line.

Table 2: Foot kinematic parameters based on the Oxford foot model (unit: °).

	A	S	OU	OR
FFTBA				
ADD	11.2 (6.61) $^{\#\#}$	18.07 (8.17)	12.65 (6.79) $^{\#\#}$	11.97 (6.51) $^{\#\#}$
ABD	-18.05 (7.49)$^{\#\#}$	-6.72 (8.47) **	-13.33 (7.43) $^{**,\#\#}$	-12.2 (6.97) $^{**,\#\#}$
DF	12.67 (5.41)	9.19 (8.25) **	9.69 (5.5) **	8.81 (5.89) **
PF	4.39 (4.3)	0.13 (5.58) **	2.29 (4.42) $^{**,\#\#}$	2.29 (4.99) $^{**,\#\#}$
SP	16.46 (8.28)	16.03 (7.24)	16.38 (7.26)	14.45 (6.8)
PR	8.88 (6.35)	3.61 (5.39) **	5.56 (8.44) **	8.72 (7.72) $^{\#\#,\$\$}$
HFTBA				
IR	21.98 (8.37)	29.34 (11.87) **	30.28 (6.07) **	29.34 (5.54) **
ER	5.02 (8.94)	4.46 (8.35)	3.28 (7.76)	4.94 (7.34)
DF	4.65 (8.35)	-4.88 (7.29) **	8.8 (8.78) $^{**,\#\#}$	8.72 (7.97) $^{**,\#\#}$
PF	-2.44 (7.97)	-7.48 (7.66) **	0.29 (7.73) $^{*,\#\#}$	-0.12 (7.14) $^{\#\#}$
IV	6.72 (10.84)	5.13 (9.0)	9.22 (8.67) $^{\#}$	7.44 (7.81)
EV	1.28 (14.01)	-3.16 (7.97) *	1.2 (8.68) $^{\#}$	3.09 (16.53) $^{\#\#}$

Note: $^{*,\#,\$}$ indicate significant differences from group A, group S, and group OU, respectively. $^{*,\#,\$}$: $p < 0.05$, $^{**,\#\#,\$\$}$: $p < 0.01$.

groups. Limited ankle mobility at initial contact can lead to differences in COP and can have an impact on COP during the subsequent stance phase. Mark A et al. [27] assessed the outcomes of treatment for gait deficits using the COP indicator, and the possibility that the change occurred may be based on the improvement of neurofeedback by rehabilitation. In patients with limited ankle mobility, attention can be focused on COP during gait events such as RHS, pre-LHS, LHS, and RTO at the initial and terminal phases of the stance phase.

Based on the contents of Figure 5 and Table 2, the characteristics of FFTBA and HFTBA of each group can be

Table 3: Analysis of the correlation coefficient between FFTBA and HFTBA relative to ML MoS at RHS and RHO.

		FFTBA				HFTBA	
		ADD/ABD	DF/PF	SP/PR	IR/ER	DF/PF	IV/EV
RHS	S	-0.14	0.22**	-0.23**	-0.35**	0.11	-0.31**
	A	-0.13	0.30**	0.15	-0.09	0.19*	0.05
	OU	-0.16	0.06	0.30**	-0.35**	0.01	-0.06
	OR	-0.28**	0.24**	0.14	-0.41**	-0.11	-0.31**
RHO	S	-0.09	-0.14	0.07	-0.02	0.04	0.07
	A	-0.23**	0.01	-0.13	0.13	-0.04	-0.22**
	OU	-0.02	-0.56**	-0.02	-0.16	-0.22*	0.14
	OR	0.12	-0.65**	-0.10	0.16	-0.06	-0.23*

Note: * Indicates that the value is significantly correlated with the ML MoS at a given gait event, $^{*}p < 0.05$, $^{**}p < 0.01$.

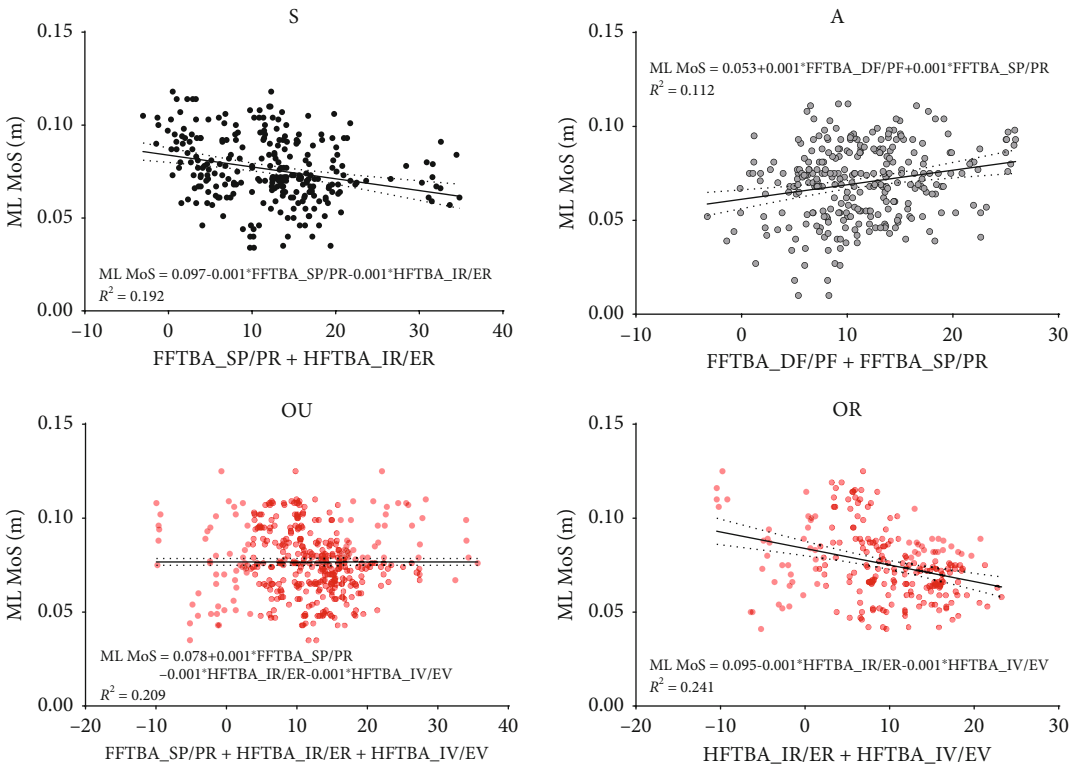

Figure 6: Scatter plots of the FFTBA and HFTBA with significant effects on ML MoS and corresponding ML MoS values at RHS. The solid black line is the reference line of the best-fit equation obtained from the stepwise multiple regression analysis.

found. The groups (A, OU, OR) with AFOs had the characteristics of small forefoot adduction and large forefoot abduction, which should be attributed to the neutral position design of the AFO. Another characteristic that was widespread across the groups wearing AFOs was a smaller forefoot plantarflexion. This characteristic might well be caused by the AFO's axis of sagittal plane movement deviating from the ankle joint's own axis of dorsiflexion and plantarflexion. Group A's greater dorsiflexion was caused by the AFO's forefoot's lower rigidity. In contrast, the OR group, which allowed only dorsiflexion-plantarflexion and had higher forefoot rigidity, had a significantly smaller range of forefoot pronation and pronation than the other groups. Combined with the results of ML MoS, it is evident that the effect of AFO in preventing sports injuries and proper joint angulation may also create a reduction in lateral gait stability due to joint stiffness [28]. These changes occurred significantly in the initial contact phase and the pre-swing phase when the joint angle changed rapidly.

Correlation coefficient analysis can provide a reference for simplifying the number of observed indicators for stability assessment in the clinical setting. For normal human gait, forefoot dorsiflexion and plantarflexion, and forefoot supination and pronation, as well as hindfoot internal and external rotation at RHS, can be used as the main kinematic parameters to assess the lateral stability of gait. In individuals with no forefoot stiffness but limited pronation-supination and adduction-abduction, forefoot dorsiflexion

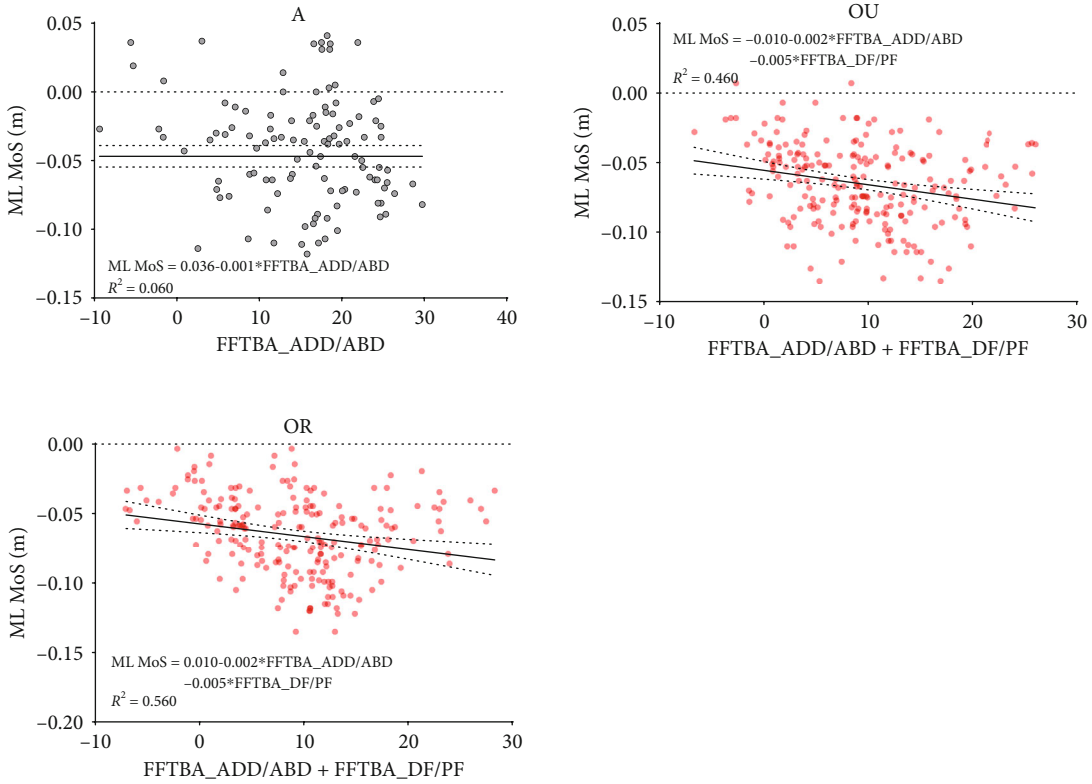

Figure 7: Scatter plots of the joint motion angles with significant effects on ML MoS and corresponding ML MoS values at RHO. The solid black line is the reference line of the best-fit equation obtained from the stepwise multiple regression analysis.

and plantarflexion at RHS, as well as forefoot abduction-adduction and hindfoot inversion-eversion at RHO, are the main kinematic parameters associated with lateral stability. In individuals with foot stiffness and limited inversion-eversion, pronation-supination at RHS and hindfoot internal and external rotation, as well as dorsiflexion and plantarflexion at RHO, are the kinematic parameters associated with lateral stability. In individuals with foot stiffness with limited adduction-abduction and inversion-eversion, forefoot adduction-abduction, forefoot dorsiflexion-plantarflexion, hindfoot internal and external rotation, and hindfoot inversion-eversion at RHS, as well as forefoot dorsiflexion-plantarflexion and hindfoot inversion-eversion at RHO, are kinematic parameters associated with lateral stability.

The stepwise multiple regression analysis of joint mobility to ML MoS at RHS and RHO provided clues to finding kinetic-related gait stability. At RHS, forefoot supination and forefoot dorsiflexion had a significant positive effect on ML MoS, while hindfoot internal rotation and inversion had a significant negative effect. While at RHO, forefoot adduction and dorsiflexion had a significant negative effect on ML MoS. Based on the R^2 values of the stepwise multiple regression analysis, it can be observed that the variability of the effect of joint mobility on ML MoS was higher in the groups S and A with lower rigidity. In contrast, the variability of the effects of joint mobility on ML MoS was lower in the groups OU and OR, and the optimal regression equation could reflect the true situation with greater probability. Likewise, the stepwise multiple regression analysis of variance was smaller in the single-limb supported phase than in the double-limb supported phase, and the effect of joint mobility on ML MoS was greater.

The inadequate foot pronation and plantar flexion result in inadequate supination of the supporting foot, making the MTP joint tension lower and reducing the rigidity of the Agilium orthosis forefoot support. During this phase, the contralateral limb swings forward over the support foot, generating external rotational forces. This external rotation generates lateral shear forces in the foot that promote rotation back [29]. However, passive supination is accompanied by limited foot mobility; the position of the foot bones that constitute the rigid lever; and the muscles that provide tension for the rigid lever are synergistically poor, resulting in the windlass effect not being fully exploited. Consequently, the stability of the levers, such as the first MTP joint push-off of the foot, is reduced and cannot provide sufficient support height and anterior lateral thrust for the anterior lateral swing of the contralateral swing foot. This disruption of the kinetic chain may be responsible for the lack of antagonistic effects on the control of the CoM transfer velocity. In turn, it affects lateral stability. The deficit in plantar flexion at the end of the stance phase in patients with limited plantar flexion function or the elderly may lead to weak plantar rigidity. This leads to kinetic and kinematic abnormalities, which can affect lateral stability.

For patients with inadequate forefoot control, exercises corresponding to forefoot adduction and abduction, eversion, and plantar flexion [30] should be recommended, or the use of an orthosis that can provide sufficient support for the forefoot to improve the rigidity of the forefoot. Where possible, the functional training of lower limb abductors or extensors and plantar flexors should be strengthened in the neutral position of the hip joint and the hip joint extension position to be closer to the supporting foot function at the vital moments of the stance phase [31]. Therefore, at the end of the stance and before the contralateral heel strike, the forefoot of the supporting foot can be fully internally rotated and vagus, so that the stability of the midfoot joint and the first ray is improved [32], thus providing sufficient support for foot height and joint torque. Consequently, the swinging foot can be fully swung into place to obtain a sufficient BoS; at the same time, so that the CoM shift velocity can be better controlled. In this way, lateral gait stability can be improved [33].

Lateral stability requires active adjustment. And longitudinal stability passive adjustment through the conversion of energy absorbed by the stride and loading response to gradually eliminate external disturbances reduces the impact [4]. In contrast to previous research, this study carried out a correlation analysis of the dynamic indicators in the stance phase as well as an analysis of the differences between the groups according to gait events. In the study of other active factors, the research subjects will adopt an adapted pace, changing their stride length, cadence, etc. based on their exercise ability under specific physiological and pathological conditions, walking tasks, and psychological factors (e.g., fear of falling). Because lateral stability has more active regulation than longitudinal stability, and the frontal control of the foot has a more sensitive influence on lateral stability [34], lateral stability control is of greater significance in dealing with sudden lateral disturbances and preventing the resulting falls [35].

As a widely used rehabilitation treatment for patients, AFO has the effect of improving postural control of the foot and ankle in the swing and loading response phases, which has a significant positive effect on improving gait [36]. However, the restriction of the foot and ankle caused by the AFO can also obstruct the normal degree of movement of the foot and ankle joints. It has been suggested that AFO may impede the advancement of the tibia over the foot during the stance phase and prevent normal gait from occurring [37]. Combined with the results of this study, we suggest that better plantar rigidity combined with a foot adduction-abduction angle appropriate for the wearer may provide better lateral gait stability for the orthotic wearer.

During the transition, gait stability changes, such as loading response and terminal stance phase. This study reveals that the foot responds to loading acceptance primarily with supination and pronation. There is a link between the increase in tendon strain and the ability of the subtalar joint to absorb, and the total pronation [38]. Foot supination can assist in pushing off the ground steadily at the end of the stance phase [30]. In clinical patients with low gait stability or a high incidence of falls, attention should be paid to the patient's ability to perform adduction and abduction of the foot and whether their plantar flexion and supination ability can provide sufficient forefoot rigidity and structural stability of the first ray.

A limitation exists in this study. The model of foot and ankle mobility limitation used in this study was based on normal individuals wearing ankle-foot orthoses. The results of gait characteristics may differ from the effects of joint mobility limitations caused by disease or deformity. Studies based on patients or physically impaired individuals may further validate the reliability of this study.

5. Conclusion

This study reveals that lateral gait stability showed significant differences at RHS in initial contact and at RHO in terminal stance under different conditions of limited foot and ankle mobility. The analysis of the groups with significantly low stability during these two gait events indicates that low lateral stability at RHS was positively correlated with forefoot and hindfoot dorsiflexion in the group with transverse and coronal plane restriction as well as low forefoot rigidity. The main positive influence factors of lateral stability were its forefoot dorsiflexion and supination. Low lateral stability at RHO was negatively correlated with forefoot and hindfoot dorsiflexion as well as hindfoot inversion in the group with coronal plane restriction and foot stiffness. The main positive influence factors of lateral stability were forefoot abduction and plantarflexion.

Data Availability

All data used during the study are available from the corresponding author by request "hatanaka@suzuka-u.ac.jp".

Conflicts of Interest

The authors declare that there is no conflict of interest regarding the publication of this paper.

References

[1] S. Ghai and I. Ghai, "Effects of (music-based) rhythmic auditory cueing training on gait and posture post-stroke: a systematic review & dose-response meta-analysis," *Scientific Reports*, vol. 9, no. 1, p. 2183, 2019.

[2] F. G. Krause and L. D. Iselin, "Hindfoot varus and neurologic disorders," *Foot and Ankle Clinics*, vol. 17, no. 1, pp. 39–56, 2012.

[3] Y.-S. Cheng, R. Reisdorf, A. Vrieze et al., "Kinetic analysis of canine gait on the effect of failure tendon repair and tendon graft," *Journal of Biomechanics*, vol. 66, pp. 63–69, 2018.

[4] A. Farouk, A. Ibrahim, M. M. Abd-Ella, and S. El Ghazali, "Effect of subtalar fusion and calcaneal osteotomy on function, pain, and gait mechanics for calcaneal malunion," *Foot & Ankle International*, vol. 40, no. 9, pp. 1094–1103, 2019.

[5] A. F. Ambrose, L. Cruz, and G. Paul, "Falls and fractures: a systematic approach to screening and prevention," *Maturitas*, vol. 82, no. 1, pp. 85–93, 2015.

[6] C. S. Florence, G. Bergen, A. Atherly, E. Burns, J. Stevens, and C. Drake, "Medical costs of fatal and nonfatal falls in older

adults," *Journal of the American Geriatrics Society*, vol. 66, no. 4, pp. 693–698, 2018.

[7] L. D. Gillespie, M. C. Robertson, W. J. Gillespie et al., "Interventions for preventing falls in older people living in the community," *Cochrane Database of Systematic Reviews*, vol. 9, 2012.

[8] M. Tramontano, G. Morone, A. Curcio et al., "Maintaining gait stability during dual walking task: effects of age and neurological disorders," *European Journal of Physical and Rehabilitation Medicine*, vol. 53, no. 1, 2017.

[9] P. Tamburini, F. Storm, C. Buckley, M. C. Bisi, R. Stagni, and C. Mazzà, "Moving from laboratory to real life conditions: influence on the assessment of variability and stability of gait," *Gait & Posture*, vol. 59, pp. 248–252, 2018.

[10] A. L. Hof and J. Duysens, "Responses of human ankle muscles to mediolateral balance perturbations during walking," *Human Movement Science*, vol. 57, pp. 69–82, 2018.

[11] R. L. Cromwell and R. A. Newton, "Relationship between balance and gait stability in healthy older adults," *Journal of Aging and Physical Activity*, vol. 12, no. 1, pp. 90–100, 2004.

[12] K. Bower, S. Thilarajah, Y. H. Pua et al., "Dynamic balance and instrumented gait variables are independent predictors of falls following stroke," *Journal of Neuroengineering and Rehabilitation*, vol. 16, no. 1, p. 3, 2019.

[13] D. Hamacher, N. B. Singh, J. H. Van Dieën, M. O. Heller, and W. R. Taylor, "Kinematic measures for assessing gait stability in elderly individuals: a systematic review," *Journal of The Royal Society Interface*, vol. 8, no. 65, pp. 1682–1698, 2011.

[14] A. L. Hof, M. G. J. Gazendam, and W. E. Sinke, "The condition for dynamic stability," *Journal of Biomechanics*, vol. 38, pp. 1–8, 2005.

[15] C. He, R. Xu, M. Zhao et al., "Dynamic stability and spatiotemporal parameters during turning in healthy young adults," *Biomedical Engineering Online*, vol. 17, no. 1, p. 127, 2018.

[16] F. Watson, P. C. Fino, M. Thornton, C. Heracleous, R. Loureiro, and J. J. H. Leong, "Use of the margin of stability to quantify stability in pathologic gait – a qualitative systematic review," *BMC Musculoskeletal Disorders*, vol. 22, no. 1, p. 597, 2021.

[17] K. E. Zelik and E. C. Honert, "Ankle and foot power in gait analysis: implications for science, technology and clinical assessment," *Journal of Biomechanics*, vol. 75, pp. 1–12, 2018.

[18] P. Yu, Q. Mei, L. Xiang, J. Fernandez, and Y. Gu, "Differences in the locomotion biomechanics and dynamic postural control between individuals with chronic ankle instability and copers: a systematic review," *Sports Biomechanics*, vol. 21, no. 4, pp. 531–549, 2022.

[19] Y. Feng and Y. Song, "The Categories of AFO and its effect on patients with foot impair: a systemic review," *Physical Activity and Health*, vol. 1, no. 1, 2017.

[20] D. Totah, M. Menon, C. Jones-Hershinow, K. Barton, and D. H. Gates, "The impact of ankle-foot orthosis stiffness on gait: a systematic literature review," *Gait & Posture*, vol. 69, pp. 101–111, 2019.

[21] R. Nakamura, H. Saito, and H. Nagasaki, *Fundamental Kinesiology Sixth Edition*, Ishiyaku publishers Inc, 2003.

[22] S. Hoeve, J. de Vos, P. Weijers, J. Verbruggen, and P. Willems, "Repeatability of the Oxford foot model for kinematic gait analysis of the foot and ankle," *Clinical Research on Foot & Ankle*, vol. 3, no. 2, 2015.

[23] H. Ohtsu, S. Yoshida, T. Minamisawa, T. Takahashi, S. Yomogida, and H. Kanzaki, "Investigation of balance strategy over gait cycle based on margin of stability," *Journal of Biomechanics*, vol. 95, article 109319, 2019.

[24] D. Sun, G. Fekete, Q. Mei, and Y. Gu, "The effect of walking speed on the foot inter-segment kinematics, ground reaction forces and lower limb joint moments," *PeerJ*, vol. 6, article e5517, 2018.

[25] A. K. Blanchette, M. Noël, C. L. Richards, S. Nadeau, and L. J. Bouyer, "Modifications in ankle dorsiflexor activation by applying a torque perturbation during walking in persons post-stroke: a case series," *Journal of Neuroengineering and Rehabilitation*, vol. 11, no. 1, p. 98, 2014.

[26] "Journal of Rehabilitation Medicine-Stride frequency and length adjustment in post-stroke individuals: Influence on the margins of stability," June, 2022, https://www.medicaljournals.se/jrm/content/html/.

[27] M. A. Feger, J. M. Hart, S. Saliba, M. F. Abel, and J. Hertel, "Gait training for chronic ankle instability improves neuromechanics during walking," *Journal of Orthopaedic Research*, vol. 36, no. 1, pp. 515–524, 2017.

[28] P. Meyns, Y. L. Kerkum, M. A. Brehm, J. G. Becher, A. I. Buizer, and J. Harlaar, "Ankle foot orthoses in cerebral palsy: effects of ankle stiffness on trunk kinematics, gait stability and energy cost of walking," *European Journal of Paediatric Neurology*, vol. 26, pp. 68–74, 2020.

[29] M. P. Kadaba, H. K. Ramakrishnan, M. E. Wootten, J. Gainey, G. Gorton, and G. V. Cochran, "Repeatability of kinematic, kinetic, and electromyographic data in normal adult gait," *Journal of Orthopaedic Research*, vol. 7, no. 6, pp. 849–860, 1989.

[30] R. Donatelli, "Normal biomechanics of the foot and ankle," *The Journal of Orthopaedic and Sports Physical Therapy*, vol. 7, no. 3, pp. 91–95, 1985.

[31] R. Mohammadi and C. P. Phadke, "Effects of treadmill incline and speed on peroneus longus muscle activity in persons with chronic stroke and healthy subjects," *Gait & Posture*, vol. 54, pp. 221–228, 2017.

[32] L. Gill, A. H. Huntley, and A. Mansfield, "Does the margin of stability measure predict medio-lateral stability of gait with a constrained-width base of support?," *Journal of Biomechanics*, vol. 95, article 109317, 2019.

[33] H. A. C. Jacob, "Forces acting in the forefoot during normal gait – an estimate," *Clinical Biomechanics*, vol. 16, no. 9, pp. 783–792, 2001.

[34] B. W. Schulz, "A new measure of trip risk integrating minimum foot clearance and dynamic stability across the swing phase of gait," *Journal of Biomechanics*, vol. 55, pp. 107–112, 2017.

[35] M. Ernst, B. Altenburg, and T. Schmalz, "Characterizing adaptations of prosthetic feet in the frontal plane," *Prosthetics and Orthotics International*, vol. 44, no. 4, pp. 225–233, 2020.

[36] C. Neville, M. Bucklin, N. Ordway, and F. Lemley, "An ankle-foot orthosis with a lateral extension reduces forefoot abduction in subjects with stage II posterior tibial tendon dysfunction," *Journal of Orthopaedic & Sports Physical Therapy*, vol. 46, 2018.

[37] P. Dedieu, C. Drigeard, L. Gjini, F. Dal Maso, and P.-G. Zanone, "Effects of foot orthoses on the temporal pattern of muscular activity during walking," *Clinical Biomechanics*, vol. 28, no. 7, pp. 820–824, 2013.

[38] M. Wenning, D. Gehring, M. Mauch, H. Schmal, R. Ritzmann, and J. Paul, "Functional deficits in chronic mechanical ankle instability," *Journal of Orthopaedic Surgery*, vol. 15, no. 1, p. 304, 2020.

Hindawi
Applied Bionics and Biomechanics
Volume 2022, Article ID 8132402, 11 pages
https://doi.org/10.1155/2022/8132402

Research Article

The Effect of Standing Mats on Biomechanical Characteristics of Lower Limbs and Perceived Exertion for Healthy Individuals during Prolonged Standing

Yan Zhang[1,2] **Yining Xu**[2] **Zixiang Gao**[3] **Hongjun Yan**[4] **Jianshe Li**[1,2] **and Yichen Lu**[5]

[1]*Research Academy of Grand Health, Ningbo University, Ningbo 315211, China*
[2]*Faculty of Sports Science, Ningbo University, Ningbo 315211, China*
[3]*Faculty of Engineering, University of Pannonia, Veszprém 8200, Hungary*
[4]*Ningbo Bohan Crafts Co., Ltd., Ningbo 315336, China*
[5]*Department of Sport and Physical Education, Zhejiang Pharmaceutical College, Ningbo 315100, China*

Correspondence should be addressed to Yichen Lu; luyc@mail.zjpc.net.cn

Received 27 February 2022; Revised 30 March 2022; Accepted 13 July 2022; Published 30 July 2022

Academic Editor: Fuhao Mo

Objective. To identify the effect of standing mats on biomechanical characteristics of lower limbs and perceived exertion for healthy adult individuals during a prolonged standing task. *Methods*. 32 healthy college students were recruited in the randomized and cross-over designed trial according to the effect size and statistical power. After collecting the anthropometric data, each participant was asked to finish 2 sessions of 4-hour prolonged standing tasks on standing mats (MS) and hard ground (GS) in a random order and with a 72-hour interval rest. The plantar pressure distribution, foot morphology, and scores of the BESS (balance error scoring system) would be recorded pre- and posteach task. The Borg Rating of Perceived Exertion (RPE) would be collected during the whole task. Paired-samples t test was adopted to analyse the before and after difference within group and independent-samples t test was adopted to analyse the difference between groups separately. *Results*. (1) A prolonged standing task on both MS and GS have a negative effect on RPE and balance performance. (2) The negative effect on RPE and balance performance induced by MS is significantly smaller than that induced by GS. (3) Compared to GS, prolonged standing on MS has a lower peak plantar pressure and an implicit decrease in navicular drop and AHI (arch index). *Conclusion*. Standing mat tends to alleviate the fatigue induced by prolonged standing in lower limbs, optimize the distribution of plantar pressure, and maintain the stability.

1. Introduction

Standing is one of the basic human postures, in which an individual's trunk keeps straight with his or her bodyweight loaded by feet. During standing, the ankles should play the role of anchor points, by this way, the center of body weight would slightly swing in the sagittal plane in a motion pattern similar to an inverted pendulum and keep relatively still with the space static references [1]. Standing, which could be learned during 8 to 12 months old, is an easy to learn task [2]. Generally, standing causes few healthy threatens; however, there would be a risk of falling if someone cannot keep balance while standing. Besides, the posture of standing is also associated with some pathological symptoms. For example, a sudden change from a low center of gravity to a standing posture might be associated with postural hypotension, and prolonged standing could induce foot pain [3], leg stiffness [4, 5], low back pain [6, 7], and other complications [8].

Prolonged standing is common in many occupations such as workers in assembly lines, equipment operators, cashiers, teachers, greeters, and soldiers. Although the numbers are limited, previous studies have shown that prolonged standing

would increase the risk of musculoskeletal disorders and cardiovascular diseases [9–12]. However, most of these previous studies were conducted in the working circumstances [13] and have not reached a consensus about the duration threshold of prolonged standing. Some previous studies claimed that a standing task for just 30 minutes could affect postural control and proprioception of the human body [14]. Moreover, a systematic review included 25 relative studies that explored the relationship between prolonged standing, and the symptoms in the low back and lower limbs showed that there was consistent evidence verifying the correlation between prolonged standing and low back symptoms, trunk flexion, and lumbar curvature, indicating that after a 71-minute prolonged standing task, lower back symptoms would reach clinically relevant levels, and for individuals who already had low back pain, the threshold was reduced to 42 minutes. This review recommended not standing for longer than 40 minutes to avoid musculoskeletal symptoms [15].

Previous studies mostly focused on the physical discomfort and physiological changes in the cardiovascular and musculoskeletal systems during prolonged standing [12, 16–20], and limited studies have explored the effects of prolonged standing on the biomechanics characteristics. The study attempted to investigate the mediating effect of joint mobility on the effect of prolonged standing on venous function suggesting that excessive joint mobility might be a risk factor for venous insufficiency, suggesting that it was necessary to assess joint mobility in individuals who should stand for a long-time during work [21]. Nelson-Wong and Callaghan explored the effect of prolonged standing from biomechanical perspectives that included the activation of trunk muscles, joint stiffness, and kinetic parameters, finding that subjects would develop low back pain during exposure to prolonged standing and show a decrease in rotational stiffness at lateral flexion, as well as an increase in center of pressure (COP) offset during the unilateral standing test after the exposure of prolonged standing. Moreover, the study also found that prolonged standing might result in a reduction in balance response and the ability to resist lateral loads on the trunk effectively [22]. The result was consistent with that of the study conducted by Duarte which demonstrated that there were three COP migration patterns during a task of unconstrained standing more than 30 minutes: (a) shifting, a fast-displacement of the average position of COP from one region to another; (b) fidgeting, a fast and large displacement and returning of COP to approximately the same position; and (c) drifting, a slow continuous displacement of the average position of COP [23].

According to the negative effect induced by prolonged standing, some countries have identified prolonged standing as a major ergonomic problem and have been seeking interventions [24]. At present, some interventions come from several different perspectives, for example, a previous study that compared the biomechanical and subjective response induced by prolonged standing on inclined surfaces of ±16°, stating that inclined standing surfaces could reduce subjective pain in individuals with lower back pain and should be recommended for use in occupational settings where prolonged standing was required [25]. Recently, a study compared the effects of wearing regular socks, compression socks which could create a pressure of 15 to 20 mmHg, and compression socks which could create a pressure of 20 to 30 mmHg on fatigue of calf muscles, edema of body segments, and discomfort in prolonged standing from a wearing-point perspective. This study found that compression socks appeared to be effective in reducing fatigue of calf muscles induced by prolonged standing, and the effect of 15-20 mmHg compression socks and 20-30 mmHg compression socks was similar [26]. Some researchers claimed that standing on a soft surface could reduce muscle fibre recruitment and tension and improve blood circulation, thus reducing musculoskeletal system discomfort and fatigue [27]. Madeleine's team examined the difference of physiological and biomechanical responses between prolonged standing in polyurethane pad surface (soft) and aluminum casting surface (hard), and the results showed, compared with prolonged standing on the soft surface, prolonged standing on a hard surface would make the calf sore and numb and increase the electromyographic signal of the soleus muscle and the displacement of the COP in the frontal plane. The study suggested that prolonged standing on a soft surface would be more comfortable and prevent the leg from feeling sore and numb [28].

After taking the cost-effectiveness in practical applications into consideration, there is limitation in offering adapts inclined standing surfaces for workers who are in exposure to prolonged standing. The limitation is not only from the heterogeneity of anthropometry and anatomy of human beings but also from that the quantification protocol of the best incline angle for different individuals has not been determined yet by the academy. Besides, considering the user's retention, it would be difficult to ask workers who should prolongedly stand to maintain uniform footwear in every workday.

Therefore, it seems that providing a soft standing surface for this kind of population has health promotion potential. At present, it is more common to provide special standing mats or insoles. Standing mats and insoles designed for prolonged standing individuals have the same mechanism, which is to achieve the purpose of optimizing the distribution of body mass by changing the material properties of the contact interface between the standing area and the plantar [29]. The properties of the standing surface material are important factors affecting the discomfort of prolonged standing [30]. The previous studies showed that absorption and transmission of ground reaction force during standing would be optimized, and the subjective comfort during prolonged standing would be improved when the material of the standing surface has greater elasticity, stiffness, and thickness [27]. A systematic review that published in 2018 demonstrated that there was moderate level of evidence supporting the use of cushioning materials for the reduction of perceived musculoskeletal discomfort of the lower limb and the lower back while standing at work, calling for larger, good quality prospective RCT intervention trials [31]. Most studies of the intervention for the adverse reactions caused by prolonged standing are aimed at the clinical population and workers of specific occupations, making it difficult to generalize their results to other populations. There are not enough studies on surface interventions on the change of biomechanical parameters and the subjective proprioception induced by fatigue after prolonged standing to provide guidelines or suggestions with a high level of evidence.

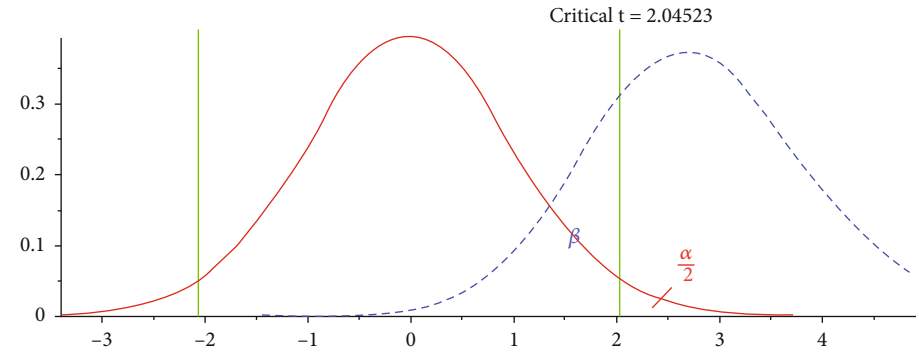

Figure 1: Schematic diagram of the sampling distribution.

Additionally, considering that since most workers, who are exposed in prolonged standing, have fixed workstations, it would be not only feasible but also convenient to provide standing mats at their workstations. Lastly, previous studies have not reached consensus on the significant positive effect of standing mat application on subjective fatigue, plantar pressure distribution, and individual's physical balance ability. The reason might come from the heterogeneity between study protocols such as the time of prolonged standing. This study was designed and conducted to explore the effects of a new-type polyurethane foamed standing mat on biomechanics characteristics of lower limbs and perceived exertion for young healthy individuals during a 4-hour prolonged standing task.

2. Materials and Methods

2.1. Participant Recruitment and Ethics. The recruitment information of volunteers would be published online by one of the researchers, and the volunteers would register their names and contact information. Necessary personal information such as name, age, gender, and basic health condition was collected and was screened according to inclusion and exclusion criteria for the trial by another researcher. In this period, all volunteers would not know anything about the trial. They would just know there was a prolonged standing task. Volunteers who met the inclusion criteria (participants) were randomly allocated by the second research group. In this period, all participants still did not know details about the trial. The inclusion criteria of participants were as follows: (1) from 18 to 60 years old; (2) free from endocrine, metabolic, neuromuscular, and musculoskeletal disorders; (3) BMI from 18.5 to 23.9 [32]; (4) without any diseases that are not clinically recommended for physical activity; (5) not engaged in any physical activity with moderate or above intensity for at least 6 months. The exclusion criteria of participants were as follows: (1) under 18 years old or over 60 years old; (2) with endocrine, metabolic, neuromuscular, or musculoskeletal disorders; (3) be clinically required not to participate in any physical exercise; (4) be asked to participate in the trial involuntarily; (5) participated in physical activity with moderate or above intensity within the last 6 months.

The software G∗Power (Version 3.1.9.3, Heinrich Heine University, German, https://www.psychologie.hhu.de/arbeitsgruppen/allgemeine-psychologie-und-arbeitspsychologie/gpower) was used to calculate the sample size. The two-tailed paired t test whose α error probability was set at 0.05, the effect size (d_z) was set at 0.5, and the statistical power ($1-\beta$) was set at 0.75. The β would be calculated by Equation (1), and the schematic diagram of the sampling distribution when the hypothesis is true and false was provided in Figure 1.

$$Z_\beta = \frac{(d - d_\mu)}{\sigma/\sqrt{n}} = \sqrt{n}\frac{d}{\sigma} - Z_\alpha. \quad (1)$$

All participants had written informed consent, and the study was approved by the Institutional Ethics Committee of Ningbo University (ARGH20210804).

2.2. Study Protocol. The trial was randomized and cross-over controlled. Each participant was asked to finish two sessions of prolonged standing tasks, one of which was standing on a standing mat (MS, density: 200 D, hardness: 65-75, size: 1080 mm × 508 mm × 19 mm, Bohan Craft Co., LTD, Ningbo, China), and the other was standing on the hard ground surface (GS), which was a wooden floor. In both standing tasks, the participants were asked to stand barefoot.

Considering that previous studies discovered that significant subjective and physiological changes were not observed until a minimum of 3-hour exposure to standing and suggested longer testing durations [9, 31, 33] and the eight-hour system of labor in China society (usually 8 : 00 to 12 : 00 in the morning and 13 : 00 to 17 : 00 in the afternoon), in this trial, each prolonged standing task lasted 240 minutes. During the task, participants were asked to stand in front of a height-adjustable table (size: 1.0 m × 1.5 m) for daily office activities and were required not to use the table to support any body part except the forearm during the task. The participants were allowed to adjust the table to a comfortable height to support their forearms.

Each participant would have a 10 min rest after standing for 110 minutes and be allowed to walk or sit then perform the rest of the task which lasted 120 minutes. The participants were kept barefoot during the whole trial, and each participant was supervised by a researcher who was allowed to give verbal cues to ensure that every participant could complete the whole task according to the trial requirements. The schematic diagram of the trial and the photo of the testing site was presented in Figures 2 and 3. Since the aim of this study is to explore the effects of prolonged standing on standing mat and hard ground

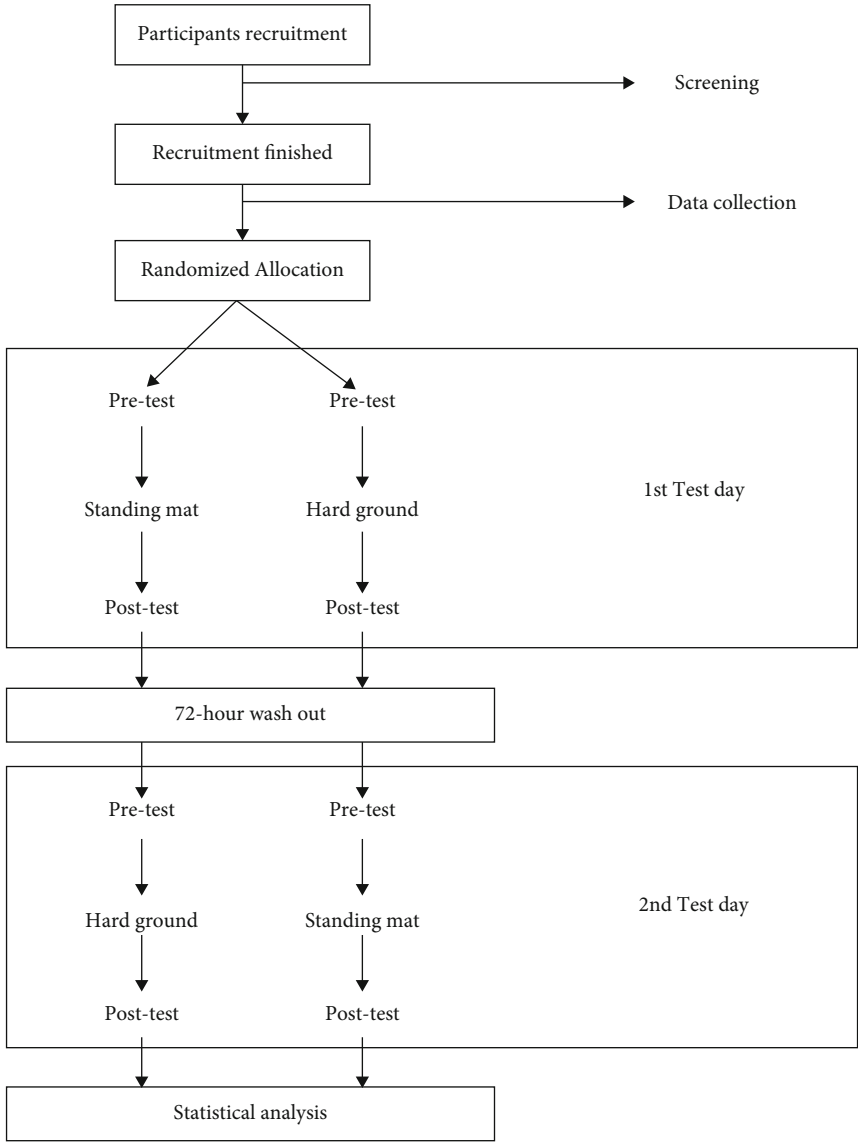

Figure 2: The schematic diagram of the trial.

on biomechanical parameters and the physical balance ability of each participant, the difference within each group between pre and post a prolonged standing and the mean differences between groups would be calculated. To eliminate the interference of the learning effect, all the outcome measures would be taken pre and post each prolonged standing task.

2.3. Data Collection

2.3.1. Perceived Exertion. The Borg Rating of Perceived Exertion (RPE), whose range of score was 6 to 15, was used to evaluate the perceived physical fatigue from the musculoskeletal system, of each participant. Each participant was asked to subjectively rate the overall physical fatigue of legs, the perceived standing surface hardness, and the discomfort of specific body areas (upper back, low back, hips, thighs, knees, calves, ankles, and planters) before and after prolonged standing on the hard ground and standing mat.

2.3.2. Plantar Pressure Distribution. The Novel® Plantar Pressure Collecting System (Version PEDAR X, Novel, German) with 99 sensors was used to collect the plantar pressure distribution, the shift of COP, and the pressure between the touch-down area and different anatomical regions of the plantar. The calculation of the peak pressure in different anatomical regions of the plantar, arch index (AI), and the amplitude of COP was based on the zoning in the system according to the average geometric center offset of the area in which the plantar pressure reached the maximum value.

According to the zoning in the system, the whole touch-down area could be divided into hallux (BH), other toes (OT), medial foot (MF), lateral foot (LF), midfoot (M), and heel (H). The schematic diagram of the plantar zone divisions was provided in Figure 4. All sensors were individually calibrated before each test to reduce measurement system error.

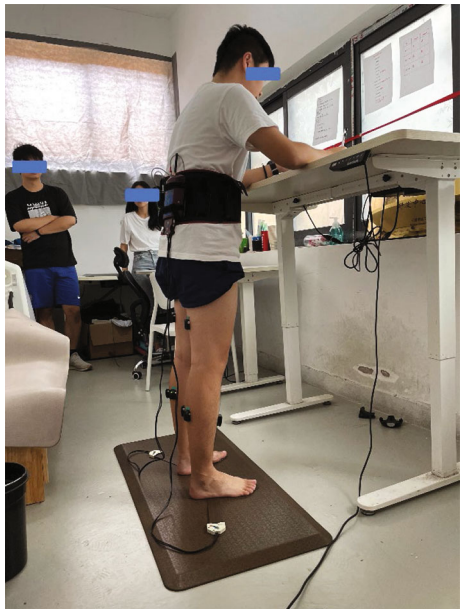

Figure 3: The photo of the testing site.

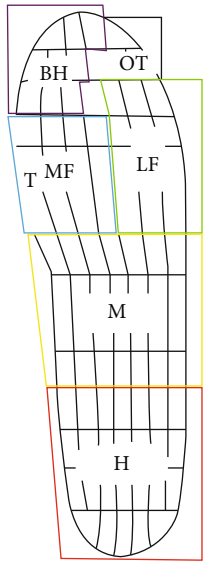

Figure 4: The schematic diagram of the plantar zones division (BH: hallux; OT: other toes; MF: medial foot; LF: lateral foot; M: midfoot; H: heel).

2.3.3. Balance Error Scoring System (BESS). The BESS test was used to assess the physical stability of participants before and after prolonged standing on hard ground and a standing mat.

Each participant was asked to (1) stand on both feet: stand side by side on the test surface with the inside of the feet in contact, hands-on the anterior superior iliac ridge, eyes closed; (2) stand by single-foot: Stand on the test surface on the nondominant foot with hip flexion at about 30 degrees and knee flexion at about 45 degrees. Place both hands on the anterior superior iliac ridge with eyes closed; (3) stand on lunge posture: both feet should be placed on the test surface, the nondominant foot should be placed in the back, toes should be fully followed before contact, hands should be placed on the anterior superior iliac ridge, and eyes closed [34]. It should be emphasized that the BESS test is a wide-used standard physical balance test that could only represent an individual's physical ability to keep balance in different postures and could not represent the body's balance condition during the 4-hour prolonged standing task in this study.

Each test lasted 20 seconds, and the researchers recorded the number of turnovers. "Turnover" in the test was defined as (1) hands leaving the anterior superior iliac ridge, (2) open either eye, (3) tripping or falling, (4) abduction or flexion of the hip exceeds 30 degrees, (5) leave the test surface with either foot, and (6) leave the test surface for more than 5 seconds [35].

The final score was the total deduction score which was calculated after the BESS test was repeated 3 times.

2.3.4. Plantar Morphology Assessment. AutoCAD software (Version 2018, Autodesk, USA) was used to assess the plantar morphological structure which included the instep height and ball of the foot length and calculate the arch height index (AHI), which equaled the ratio of the instep height and ball of the foot length.

2.4. Quality Control. The order of the two tests was randomized, and the SPSS Software 17.0 (SPSS, Inc., Chicago, IL, USA) was used for the allocation of the participants and generation of the randomized order. Moreover, to reduce the effect of biological circadian rhythm and the fatigue induced by the previous task, each task was arranged at the same time on the same day with a rest interval of 72 hours. Moreover, the assessment blinding was adopted in this trial, the researchers who supervised the participants during the task and those who collect the data were different, and the researchers responsible for collecting the data were not informed of the participants' allocation.

2.5. Statistical Analysis. The SPSS Software 17.0 (SPSS, Inc., Chicago, IL, USA) was used for statistical analyses. Paired-samples t test and independent-samples t test were adopted for within-group and between groups separately. Data would be presented as means and standard deviations except if otherwise specified and considered statistically significant at $P < 0.05$.

3. Results and Discussion

3.1. Sample Size and Participant Recruitment. The plot of the sample size and statistical power made by the G∗power software was presented in Figure 5. According to the plot and the calculated results, the trial should recruit at least 30 participants to guarantee a statistical power of more than 0.75. After considering the participants lost to follow-up and invalid data, the trial planned to recruit 36 subjects. Eventually, 36 students from Ningbo University were recruited, and after eliminating the invalid data, 32 participants completed the test. The anthropometric information of participants is shown in Table 1.

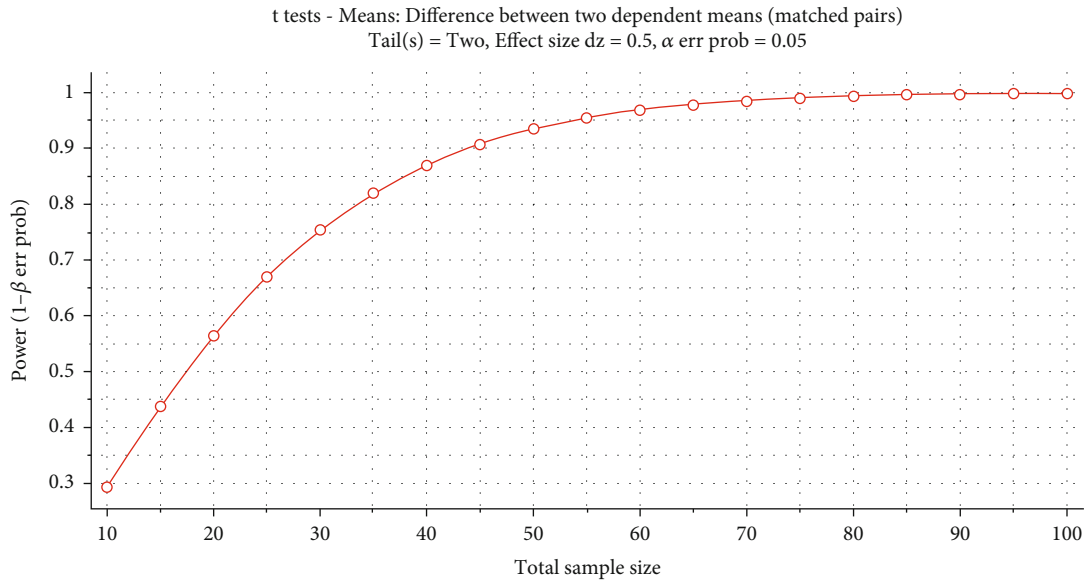

Figure 5: The plot of the sample size and statistical power.

Table 1: Information of the eligible participants.

	Male	Female
Number	16	16
Age (year)	24.2 ± 1.8	23.6 ± 1.6
Height (cm)	178.6 ± 5.4	163.4 ± 4.2
Body weight (kg)	73.6 ± 5.2	57.3 ± 4.8
BMI (kg/m^2)	22.9 ± 1.4	21.6 ± 1.7

BMI: body mass index.

3.2. Perceived Exertion and Biomechanical Parameters. As shown in Figure 6(a) and Table 2, the Rating of Perceived Exertion (RPE) of feet, calves, knees, thighs, and lumbar was significantly increased after a prolonged standing task in both MS and GS. However, the RPE increase in MS was significantly smaller than that in GS ($P < 0.05$), especially around the lumbar area ($P < 0.01$), indicating that the intervention of a standing mat might effectively relieve the individual's fatigue caused by prolonged standing task and the fatigue in the low back area. Besides, it can be seen from Figure 6(b) and Table 2 that the amplitude of COP on the x-axis ($P < 0.05$) and y-axis ($P < 0.05$) in MS is significantly smaller than that of GS, indicating that the use of standing mat intervention might be able to maintain COP stability during prolonged standing. As was shown in Figure 6(c) and Table 2, the difference in peak plantar pressure was mainly concentrated in MF ($P < 0.05$), M ($P < 0.05$), and H ($P < 0.05$) areas, and those in MF, LF, M, and H in MS were all significantly smaller than GS. Moreover, the peak plantar pressure in the LF area decreased after prolonged standing tasks on both GS and MS whereas those in other plantar areas increased. These results showed that the standing mat might be able to reduce the pressure on the forefoot and heel effectively. In terms of AI, as shown in Table 2, in MS condition, AI increased and reached statistical significance, while that in GS almost did not change, indicating that the intervention of a standing mat might be able to support the arch of the foot and increase the touch-down area of the midfoot.

3.3. Balance Error Scoring System (BESS). The results of the BESS balance test were shown in Figure 6(d) and Table 3. According to the results, the error score of the BESS test increased in both MS and GS after a prolonged standing task, suggesting that the body stability of participants decreases. However, in MS, the decreased instability of all test postures was significantly smaller than that in GS, indicating that the intervention of a standing mat might be able to reduce the degree or slow the rate of body stability decline.

3.4. Plantar Morphological Change. Morphological results of the foot scan were shown in Table 4. Regardless of prolonged standing in MS or GS, both the instep height and ball of the foot length were significantly decreased after a prolonged standing task ($P < 0.05$). In addition, the AHI was significantly decreased in GS ($P < 0.05$) but did not change significantly in MS ($P > 0.05$). Meanwhile, both in MS and GS, there was no statistically significant difference between groups in the instep height and ball of the foot length.

4. Discussion

The purpose of this study was to explore the effects of a new-type polyurethane foamed standing mat on biomechanics characteristics of lower limbs and perceived exertion for young healthy individuals during a prolonged standing task. The main findings were that prolonged standing, despite surface, standing mat, and hard ground lead to an increase in rating of perceived exertion and induce a negative effect on the individual's balance ability. However, the standing mat seemed to delay or reduce the increase of subjective discomfort in the lower limbs with a

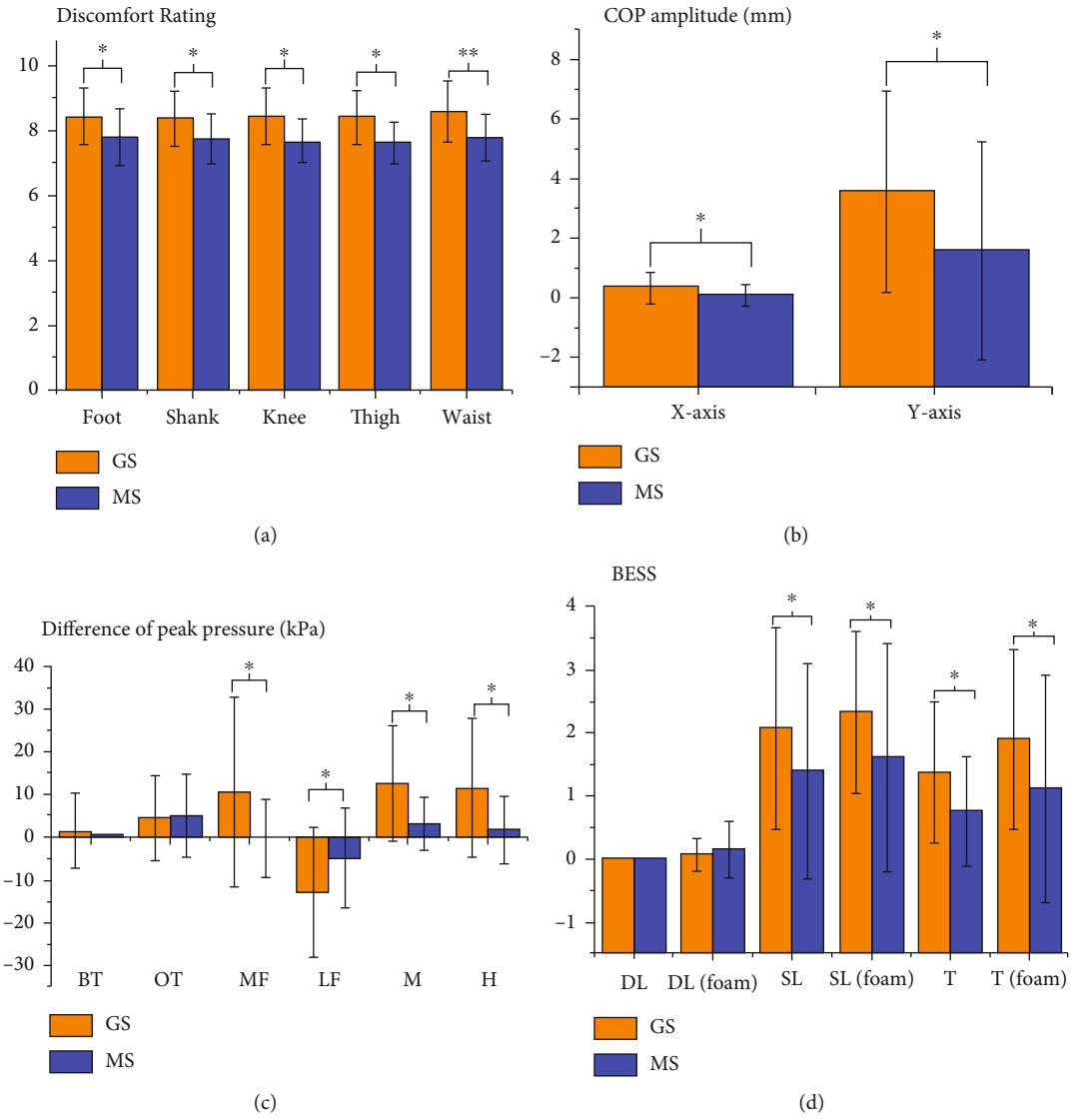

Figure 6: Comparisons of perceived exertion and foot biomechanical parameters. (a) Perceived exertion. (b) COP amplitude. (c) Peak plantar pressure. (d) balance error scoring.

less negative effect on balance which reached a statistically significant difference between groups. Compared with prolonged standing on the hard ground, the COP amplitude, and the peak plantar pressure of the median foot, midfoot, and heel were lower during standing on a standing mat, and the instep height and ball of the foot length decreased less, and the AI changed less, which also reached statistical significance.

The increased RPE was consistent with the results of some previous studies. For example, a cross-sectional study published in 2012 found that prolonged standing was one of the major causes of psychological and muscle fatigue in production workers. In the study, participants who were exposed to prolonged standing for more than 5 hours every day were asked to fill out questionnaires that were used to assess psychological fatigue. Moreover, surface electromyography (sEMG) was used to assess muscle fatigue. Eventually, a moderate and positive correlation with a statistical significance between the changes in sEMG of erector spinae muscle and psychological fatigue was found according to the study's result [36]. Although the subjects in this study were all male, its result was consistent with this study, which might imply that there would be no gender difference in physical fatigue induced by prolonged standing and that it should be confirmed by further studies with female subjects. In terms of body balance ability, this study is the first to evaluate the effects of prolonged standing tasks on body balance ability on different standing surfaces in a young and healthy population. Previous studies have shown that prolonged standing tasks would reduce the adaptability of the posture control system in patients with Parkinson's disease or obesity [37], increasing the risk of falling [38]. This study also shows that prolonged standing tasks could also have a negative influence on the balance ability of young and healthy individuals with a potential mechanism that might be related to muscle fatigue. In addition, adults who are exposed to prolonged standing working circumstances would be at a higher clinical risk of low back pain and hip abductor muscle fatigue that include hip muscle and tensor fascia in daily life [39]. Furthermore, a study conducted by Marshall et al. in 2011 showed that a prolonged

Table 2: Comparison of perceived exertion and foot biomechanical parameters change within and between groups.

Items	Subitems	Group	Paired t test				Student's t-test	
			Before	After	Mean difference	P value	T	P value
RPE (point)	Foot	GS	0.96 ± 0.75	9.40 ± 0.71	8.43 ± 0.88	<0.05	2.60	<0.05
		MS	0.40 ± 0.49	8.20 ± 0.83	7.80 ± 0.87	<0.05		
	Shank	GS	0.90 ± 0.75	9.30 ± 0.74	8.40 ± 0.84	<0.05	2.95	<0.05
		MS	0.40 ± 0.49	8.13 ± 0.81	7.77 ± 0.76	<0.05		
	Knee	GS	0.97 ± 0.84	9.40 ± 0.71	8.43 ± 0.88	<0.05	2.95	<0.05
		MS	0.40 ± 0.49	8.10 ± 0.79	7.70 ± 0.69	<0.05		
	Thigh	GS	0.87 ± 0.85	9.30 ± 0.69	8.43 ± 0.84	<0.05	2.95	<0.05
		MS	0.33 ± 0.47	7.97 ± 0.71	7.63 ± 0.66	<0.05		
	Waist	GS	0.73 ± 0.73	9.33 ± 0.70	8.60 ± 0.10	<0.05	3.54	<0.01
		MS	0.33 ± 0.47	8.13 ± 0.72	7.80 ± 0.70	<0.05		
COP amplitude (mm)	X-axis	GS	1.51 ± 0.52	1.83 ± 0.48	0.32 ± 0.52	0.08	2.45	<0.05
		MS	1.77 ± 0.31	1.87 ± 0.32	0.10 ± 0.34	0.07		
	Y-axis	GS	11.58 ± 3.24	15.13 ± 4.56	3.55 ± 4.36	0.10	2.14	<0.05
		MS	12.90 ± 3.16	14.49 ± 3.67	1.59 ± 3.67	<0.05		
Peak plantar pressure (kPa)	BH	GS	5.95 ± 12.55	7.49 ± 13.71	1.55 ± 8.71	<0.05	0.56	0.581
		MS	9.20 ± 15.00	9.68 ± 13.64	0.48 ± 10.09	0.21		
	OT	GS	5.89 ± 11.65	10.49 ± 11.48	4.60 ± 9.95	<0.05	0.16	0.874
		MS	6.21 ± 9.73	11.29 ± 13.79	5.09 ± 9.55	<0.05		
	MF	GS	42.50 ± 18.80	53.16 ± 19.90	10.66 ± 22.26	<0.05	2.35	<0.05
		MS	35.50 ± 10.34	35.24 ± 11.97	−0.26 ± 9.05	0.46		
	LF	GS	70.11 ± 19.29	57.22 ± 18.53	−12.89 ± 15.24	<0.05	2.63	<0.05
		MS	47.78 ± 14.82	43.02 ± 10.36	−4.76 ± 11.68	0.14		
	M	GS	17.25 ± 12.81	29.90 ± 11.63	12.65 ± 13.70	0.25	2.60	<0.05
		MS	26.55 ± 9.27	29.76 ± 7.02	3.20 ± 6.14	0.30		
	H	GS	136.22 ± 22.46	147.77 ± 22.12	11.55 ± 16.32	0.44	2.95	<0.05
		MS	109.73 ± 29.20	111.48 ± 26.91	1.75 ± 7.78	0.55		
AI	AI	GS	0.15 ± 0.07	0.16 ± 0.06	0.06 ± 0.05	0.67	2.68	<0.05
		MS	0.15 ± 0.05	0.17 ± 0.04	0.02 ± 0.03	0.85		

GS: hard ground surface; MS: standing mat surface; BH: hallux; OT: other toes; MF: median foot; LF: lateral foot; M: midfoot; H heal; AI: arch index.

Table 3: Comparison of BESS score between groups.

Standing task	Difference between groups		P value
	GS	MS	
Standing on both feet (GS)	0.00 ± 0.00	0.00 ± 0.00	1.000
Standing on both feet (MS)	0.07 ± 0.26	0.14 ± 0.44	0.161
Standing on a single foot (GS)	2.07 ± 1.60	1.39 ± 1.70	0.011
Standing on single foot (MS)	2.32 ± 1.28	1.61 ± 1.78	0.014
Standing by lunge posture (GS)	1.36 ± 1.11	0.75 ± 0.87	0.048
Standing by lunge posture (MS)	1.89 ± 1.42	1.11 ± 1.80	0.023

GS: hard ground surface; MS: standing mat surface.

standing task of just 2 hours could make the gluteus medius muscle, which was one of the hip abductor muscle groups and plays an important role to maintain the stability of the pelvis and trunk, become fatigued, leading to a significant decrease in muscle strength and endurance [40]. However, the performance of balance is multifaceted and multidimensional, leading to the diversity and specificity of its assessment methods. Therefore, future research should explore the effects of prolonged standing tasks on various static and dynamic balance abilities and determine the specific influencing mechanism.

The results of the RPE assessment showed that the standing mat seemed to delay or reduce the increase of the subjective fatigue and discomfort of the lower limbs and reached a statistically significant difference between groups. The findings are consistent with those of some previous explorations that researched the effect of different contact surfaces on the prolonged standing subjective, physiological, and biomechanical

Table 4: Comparison of foot morphological change within and between groups.

Item	Group	Paired t-test within the group			Student's t-test between groups	
		Before	After	Mean difference	T	P value
Instep height(mm)	GS	74.70 ± 5.53	72.96 ± 4.70	−1.11 ± 7.23*	0.004	0.997
	MS	74.50 ± 3.91	73.39 ± 3.76	−1.11 ± 6.16*		
Ball of the foot length (mm)	GS	42.22 ± 8.04	41.02 ± 6.99	-1.02 ± 10.65*	0.704	0.492
	MS	42.88 ± 4.65	41.54 ± 7.44	−1.34 ± 8.77*		
AHI (%)	GS	30.00 ± 0.02	29.00 ± 0.01	−1.00 ± 0.02*	3.540	0.003**
	MS	32.00 ± 0.02	32.00 ± 0.02	0.00 ± 0.03		

GS: hard ground surface; MS: standing mat surface; **: $P < 0.01$; *: $P < 0.05$.

parameters. Madeleine's team published a study in 1998, pointing out that, compared with a hard surface (aluminum casting surface), a soft surface (polyurethane surface) could decrease subjective discomfort of the lower body, alleviate leg swelling, weaker electrical signals in the calf triceps, and induce less fatigue after a prolonged standing task. Meanwhile, similar to this study, Madeleine's study also measured the amplitude and displacement of the COP in the sagittal plane and frontal plane and found that the amplitude and total angular displacement of the COP were larger in the process of standing on the hard surface for a long time, which was consistent with the results of this study [28]. At the same time, this study also found that the use of a standing mat had a less negative effect on balance which reached a statistically significant difference when compared with prolonged standing on hard ground. The possible mechanism of the positive effect induced by using a standing mat on RPE might come from the optimization of plantar pressure distribution. According to the change of peak plantar pressure in different foot areas, the peak plantar pressure changed less in all foot areas after prolonged standing tasks on a standing mat than on the hard ground, meaning that the functioning of the foot was maintained more. This phenomenon might be interpreted by the difference in muscle activation when standing on different surfaces. A similar phenomenon has been identified in a study conducted in 2021 with healthy computer workers as participants. This study found that standing mats were associated with reduced discomfort in lower-body and increased physical performance compared to the concrete floor after a 2-hour standing task and concluded that the use of standing mats showed potential to improve the ergonomic experience and lessen discomfort as well as accumulated musculoskeletal strain during prolonged standing [41].

In terms of intervention protocols that use a standing mat, Wiggermann's team compared the effects of 4 different types of standing mats and hard ground surfaces in 4-hour standing on ontological discomfort and bipedal center of COP deviation in 2013, finding that 3 of these 4 types of standing mats could reduce the discomfort after 4-hour standing with no significant difference compared with the control group. However, there were significant differences in the frequency of COP deviation within the three types of standing mats, and the COP deviation frequency was positively correlated with the degree of discomfort. Also, the study believed that the subjective report might be less sensitive for the intervention of standing mats, and the biomechanical parameters might have higher sensitivity and be a better choice of outcome measures [42]. In 2004, a study by Orlando's team investigated the fatigue and discomfort perceived by assembly line workers in different body segments after standing for 8 hours under three different standing conditions: ordinary floor, soft standing mat, and soft insole. It was found that general physical fatigue, leg fatigue, and discomfort were reduced by standing conditions with a standing mat and insole. Orlando's team found that there was a moderate positive correlation between the effect and variables such as age, height, body weight, and years of work. Their conclusion might be inferred according to the fact that older subjects and those with longer working lives reported less discomfort after standing with insoles, while subjects with less body height reported less discomfort when standing on ordinary floors and soft mats. At the same time, no statistically significant differences were found between RPE or discomfort in various parts of the body while standing on the ordinary floor. The results of Orlando's study could be considered consistent with those of this study since insole and standing mats have softer surfaces compared to the ordinary floor [27].

When it comes to intervention protocols that use a wearable device, Tarrade's team published a study that assessed the positive effect of custom foot orthoses for prolonged standing workers in 2019. The study assessed the participants' static balance and static and dynamic plantar pressure after a 3-week intervention protocol of using 3D printing custom foot orthoses and finally found that the subjects' subjective pain, discomfort, and leg stiffness were significantly reduced and the mean peak plantar pressure in static and dynamic posterior plantar area was significantly decreased after the intervention. Meanwhile, the mean peak plantar pressure in midfoot was significantly increased, and the balance between medial and lateral parts of the body was significantly improved. Therefore, the study suggested that custom foot orthotics could help the body balance the distribution of plantar pressure and provide better support and stimulation to the arch of the foot. The underlying mechanism might be that the orthotics transfer plantar pressure from the heel to the midfoot successfully [43]. Future studies should compare the effects of different intervention protocols on different populations with different standing duration.

Previous studies have not explored the morphological changes of the foot. This study is the first to assess the effects of prolonged standing on foot morphology using foot morphology scans with a result showed that after prolonged standing on a standing mat, there was less decline in the instep height and ball of the foot length, and less change in AHI, all of which were statistically significant. However, there was no statistically significant difference between the instep height and ball of the foot length, and there may be different hypotheses about the underlying mechanisms leading to this result, such as acute changes in the mechanical properties of plantar fascia or fatigue of the plantar intrinsic muscles, and the decrease of the ball of foot length might not mean a change on anatomical structure, since it seems that only long-term intervention has an effect on anatomical structure. Additionally, it cannot be ruled out that the precision of the assessment equipment or the sample size was insufficient, which leads to the inability to carry out statistical analysis of the results on a smaller spatial scale, which is also one of the limitations of this study. Moreover, as has been mentioned above, from the perspective of practical application, the use of pedals and external-used devices has some obvious limitations; therefore, the effect of pedals or external-used devices has not been taken into comparison in this study. It cannot be ruled out that the application of pedals and other devices would have better effects on RPE and biomechanical parameters during the prolonged standing task than a standing mat. Last but not the least, the standard deviation is greater than the mean value in some parameters, making the reliability of the results should be considered. Future studies should attempt to use more precise methods to monitor changes in foot morphology and musculoskeletal anatomy.

There are some limitations from a statistical perspective. On one hand, the hardness of the wooden floor (GS) was not tested before the trial, inducing the analysis of the difference between GS and MS partially qualitative, and the quantitative difference between standing grounds of different hardness is still unclear. On the other hand, the gender difference was not analyzed in this study. Considering that the stamina of prolonged standing within males and females might be different, further studies should balance the baseline difference in stamina.

5. Conclusions

In conclusion, the results of this study support the fact that the utilization of a standing mat alleviates perceived exertion of lower limbs during prolonged standing, optimizes plantar pressure distribution, and maintains body stability. Future studies should use a more precise duration threshold of prolonged standing, better measurement of health outcomes, and more rigorous trial designs to develop a higher level of evidence to provide evidence-based recommendations and guidelines for reducing the health risks induced by prolonged standing.

Data Availability

Link: https://1drv.ms/u/s!Aqz2bCok6hp–y-ZM4Cg4E6fJB16?e=WoXoGJ.

Conflicts of Interest

The authors declare that there is no conflicts of interest regarding the publication of this paper.

Acknowledgments

This study was supported by the Natural Science Foundation of Zhejiang Province (LQ21H060003).

References

[1] W. H. Gage, D. A. Winter, J. S. Frank, and A. L. Adkin, "Kinematic and kinetic validity of the inverted pendulum model in quiet standing," *Gait & Posture*, vol. 19, no. 2, pp. 124–132, 2004.

[2] M. Hanada, "Behavioral studies in the newborn infant–from the stand point of neuro-psychiatric development," *Seishin Shinkeigaku Zasshi*, vol. 72, no. 1, pp. 61–80, 1970.

[3] N. E. Wiggermann, R. A. Werner, and W. M. Keyserling, "The effect of prolonged standing on touch sensitivity threshold of the foot: a pilot study," *PM & R : The Journal of Injury, Function, and Rehabilitation*, vol. 4, no. 2, pp. 117–122, 2012.

[4] Z. Karimi, T. Allahyari, M. R. Azghani, and H. Khalkhali, "Influence of unstable footwear on lower leg muscle activity, volume change and subjective discomfort during prolonged standing," *Applied Ergonomics*, vol. 53, no. Part A, pp. 95–102, 2016.

[5] M. Y. Liaw and M. K. Wong, "The effects of leg elevation to reduce leg edema resulting from prolonged standing," *Taiwan Yi Xue Hui Za Zhi. Journal of the Formosan Medical Association*, vol. 88, no. 6, pp. 630–634, 1989.

[6] J. H. Park and D. Srinivasan, "The effects of prolonged sitting, standing, and an alternating sit-stand pattern on trunk mechanical stiffness, trunk muscle activation and low back discomfort," *Ergonomics*, vol. 64, no. 8, pp. 983–994, 2021.

[7] K. M. Fewster, K. M. Gallagher, S. H. Howarth, and J. P. Callaghan, "Low back pain development differentially influences centre of pressure regularity following prolonged standing," *Gait & Posture*, vol. 78, pp. e1–e6, 2020.

[8] W. Blattler, H. J. Thomae, and F. Amsler, "Venous leg symptoms in healthy subjects assessed during prolonged standing," *Journal of Vascular Surgery. Venous and Lymphatic Disorders*, vol. 4, no. 4, pp. 455–462, 2016.

[9] T. R. Waters and R. B. Dick, "Evidence of health risks associated with prolonged standing at work and intervention effectiveness," *Rehabilitation Nursing*, vol. 40, no. 3, pp. 148–165, 2015.

[10] P. Smith, H. Ma, R. H. Glazier, M. Gilbert-Ouimet, and C. Mustard, "The relationship between occupational standing and sitting and incident heart disease over a 12-year period in Ontario, Canada," *American Journal of Epidemiology*, vol. 187, no. 1, pp. 27–33, 2018.

[11] N. Krause, J. W. Lynch, G. A. Kaplan, R. D. Cohen, R. Salonen, and J. T. Salonen, "Standing at work and progression of carotid atherosclerosis," *Scandinavian Journal of Work, Environment & Health*, vol. 26, no. 3, pp. 227–236, 2000.

[12] D. M. Antle, N. Vézina, K. Messing, and J. N. Côté, "Development of discomfort and vascular and muscular changes during a prolonged standing task," *Occupational Ergonomics*, vol. 11, no. 1, pp. 21–33, 2013.

[13] A. Biswas, P. M. Smith, and D. A. Alter, "Is promoting six hours of standing an appropriate public health message?," *European Journal of Preventive Cardiology*, vol. 25, no. 7, pp. 751-752, 2018.

[14] M. Duarte and D. Sternad, "Complexity of human postural control in young and older adults during prolonged standing," *Experimental Brain Research*, vol. 191, no. 3, pp. 265–276, 2008.

[15] P. Coenen, S. Parry, L. Willenberg et al., "Associations of prolonged standing with musculoskeletal symptoms–a systematic review of laboratory studies," *Gait & Posture*, vol. 58, pp. 310–318, 2017.

[16] M. C. Peddie, C. Kessell, T. Bergen et al., "The effects of prolonged sitting, prolonged standing, and activity breaks on vascular function, and postprandial glucose and insulin responses: a randomised crossover trial," *PLoS One*, vol. 16, no. 1, article e0244841, 2021.

[17] P. M. L. Miguelote, L. H. Carneiro, M. Oliveira, F. M. Costa, and D. G. Corrêa, "Test yourself question: right knee pain following prolonged standing," *Skeletal Radiology*, vol. 50, no. 12, pp. 2549–2551, 2021.

[18] H. Jo, O. B. Lim, Y. S. Ahn, S. J. Chang, and S. B. Koh, "Negative impacts of prolonged standing at work on musculoskeletal symptoms and physical fatigue: the fifth Korean working conditions survey," *Yonsei Medical Journal*, vol. 62, no. 6, pp. 510–519, 2021.

[19] T. Yates, C. L. Edwardson, C. Celis-Morales et al., "Metabolic effects of breaking prolonged sitting with standing or light walking in older south Asians and White Europeans: a randomized acute study," *The Journals of Gerontology. Series A, Biological Sciences and Medical Sciences*, vol. 75, no. 1, pp. 139–146, 2020.

[20] R. Wall, G. Garcia, T. Läubli et al., "Physiological changes during prolonged standing and walking considering age, gender and standing work experience," *Ergonomics*, vol. 63, no. 5, pp. 579–592, 2020.

[21] K. Azma, P. Mottaghi, A. Hosseini, S. Salek, and R. Bina, "Venous insufficiency after prolonged standing: is joint hypermobility an important risk factor?," *Advanced Biomedical Research*, vol. 4, p. 98, 2015.

[22] E. Nelson-Wong and J. P. Callaghan, "The impact of a sloped surface on low back pain during prolonged standing work: a biomechanical analysis," *Applied Ergonomics*, vol. 41, no. 6, pp. 787–795, 2010.

[23] M. Duarte and V. M. Zatsiorsky, "Patterns of center of presure migration during prolonged unconstrained standing," *Motor Control*, vol. 3, no. 1, pp. 12–27, 1999.

[24] P. M. King, "A comparison of the effects of floor mats and shoe in-soles on standing fatigue," *Applied Ergonomics*, vol. 33, no. 5, pp. 477–484, 2002.

[25] E. Nelson-Wong, S. J. Howarth, and J. P. Callaghan, "Acute biomechanical responses to a prolonged standing exposure in a simulated occupational setting," *Ergonomics*, vol. 53, no. 9, pp. 1117–1128, 2010.

[26] M. G. Garcia, M. G. Roman, A. Davila, and B. J. Martin, "Comparison of physiological effects induced by two compression stockings and regular socks during prolonged standing work," *Human Factors*, 2021.

[27] A. R. Orlando and P. M. King, "Relationship of demographic variables on perception of fatigue and discomfort following prolonged standing under various flooring conditions," *Journal of Occupational Rehabilitation*, vol. 14, no. 1, pp. 63–76, 2004.

[28] P. Madeleine, M. Voigt, and L. Arendt-Nielsen, "Subjective, physiological and biomechanical responses to prolonged manual work performed standing on hard and soft surfaces," *European Journal of Applied Physiology and Occupational Physiology*, vol. 77, no. 1-2, pp. 1–9, 1998.

[29] H. White, "Flooring & matting. Where the feet hit the floor," *Occupational Health & Safety*, vol. 71, no. 9, pp. 164–167, 2002.

[30] N. Wiggermann, *The Effect of Flooring Surface Compliance on Plantar Pressures and Discomfort during Prolonged Standing*, University of Michigan, 2011.

[31] G. Speed, K. Harris, and T. Keegel, "The effect of cushioning materials on musculoskeletal discomfort and fatigue during prolonged standing at work: a systematic review," *Applied Ergonomics*, vol. 70, pp. 300–314, 2018.

[32] J. Xue, S. Li, Y. Zhang, and P. Hong, "Accuracy of predictive resting-metabolic-rate equations in Chinese mainland adults," *International Journal of Environmental Research and Public Health*, vol. 16, no. 15, p. 2747, 2019.

[33] I. Halim, A. R. Omar, A. M. Saman, and I. Othman, "A review on health effects associated with prolonged standing in the industrial workplaces," *International Journal of Research and Reviews in Applied Sciences*, vol. 8, no. 1, pp. 14–21, 2011.

[34] D. R. Bell, K. M. Guskiewicz, M. A. Clark, and D. A. Padua, "Systematic review of the balance error scoring system," *Sports Health*, vol. 3, no. 3, pp. 287–295, 2011.

[35] D. Formenti, A. Trecroci, M. Duca et al., "Differences in inhibitory control and motor fitness in children practicing open and closed skill sports," *Scientific Reports*, vol. 11, no. 1, p. 4033, 2021.

[36] I. Halim, A. R. Omar, A. M. Saman, and I. Othman, "Assessment of muscle fatigue associated with prolonged standing in the workplace," *Safety and Health at Work*, vol. 3, no. 1, pp. 31–42, 2012.

[37] D. Singh, W. Park, M. S. Levy, and E. S. Jung, "The effects of obesity and standing time on postural sway during prolonged quiet standing," *Ergonomics*, vol. 52, no. 8, pp. 977–986, 2009.

[38] G. F. Moretto, F. B. Santinelli, T. Penedo, L. Mochizuki, N. M. Rinaldi, and F. A. Barbieri, "Prolonged standing task affects adaptability of postural control in people with Parkinson's disease," *Neurorehabilitation and Neural Repair*, vol. 35, no. 1, pp. 58–67, 2021.

[39] D. Viggiani and J. P. Callaghan, "Hip abductor fatigability and recovery are related to the development of low back pain during prolonged standing," *Journal of Applied Biomechanics*, vol. 34, no. 1, pp. 39–46, 2018.

[40] P. W. Marshall, H. Patel, and J. P. Callaghan, "Gluteus medius strength, endurance, and co-activation in the development of low back pain during prolonged standing," *Human Movement Science*, vol. 30, no. 1, pp. 63–73, 2011.

[41] M. B. Lin, Y. T. Yen, and C. H. Chang, "Use of an inflatable mat to reduce body discomfort development when performing computer work at a standing desk," *Ergonomics*, vol. 65, no. 7, pp. 1015–1034, 2022.

[42] N. Wiggermann and W. M. Keyserling, "Effects of anti-fatigue mats on perceived discomfort and weight-shifting during prolonged standing," *Human Factors*, vol. 55, no. 4, pp. 764–775, 2013.

[43] T. Tarrade, F. Doucet, N. Saint-Lô, M. Llari, and M. Behr, "Are custom-made foot orthoses of any interest on the treatment of foot pain for prolonged standing workers?," *Applied Ergonomics*, vol. 80, pp. 130–135, 2019.

Hindawi
Applied Bionics and Biomechanics
Volume 2022, Article ID 4498161, 12 pages
https://doi.org/10.1155/2022/4498161

Research Article

Analysis of the Prognostic Impact of Staged Nursing Interventions on the Treatment of Patients with COPD Combined with Type II Respiratory Failure

Yun Zheng[1] **and Haihua Wu**[2]

[1]*Pulmonary and Critical Care Medicine, TongDe Hospital, Zhejiang Province, China*
[2]*Emergency Department, Tongde Hospital, Zhejiang Province, China*

Correspondence should be addressed to Haihua Wu; 13588452659@163.com

Received 16 May 2022; Revised 27 June 2022; Accepted 6 July 2022; Published 19 July 2022

Academic Editor: Justin Fernandez

Objective. To analyze the prognostic impact of staged nursing interventions on the treatment of patients with chronic obstructive pulmonary diseases (COPD) combined with type II respiratory failure. *Methods*. 120 patients with COPD combined with type II respiratory failure admitted to our hospital between January 2021 and January 2022 were divided into a control group and a study group, with 60 patients in each group. The control group received conventional strategy interventions, and the study group received staged nursing interventions. Pulmonary function, blood gases, health impairment, knowledge, mood, hope level, and quality of survival were evaluated before and after patient care, and satisfaction and the impact on patient prognosis were assessed. *Results*. The improvement of pulmonary function and blood gas in the study group was better than that in the control group aftercare, and the difference was statistically significant ($P < 0.05$). Health impairment and mood scores were lower in the study group compared to the control group aftercare, and the difference was statistically significant ($P < 0.05$). Knowledge awareness, hope, and quality of survival scores were higher in the study group compared to the control group aftercare, with statistically significant differences ($P < 0.05$). The rate of excellent prognosis and satisfaction was higher in the study group compared with the control group, and the difference was statistically significant ($P < 0.05$). *Conclusion*. The implementation of staged nursing interventions during the treatment of patients with COPD combined with type II respiratory failure can significantly improve patient prognosis and has a high application value.

1. Introduction

Chronic obstructive pulmonary disease (COPD) is a chronic respiratory disease with high mortality and recurrence rates, which is characterized by decreased lung function and incomplete reversible airflow obstruction. Studies have concluded [1] that the aggravation of airway obstruction in patients affects the ventilation function and eventually leads to the development of type II respiratory failure, which has a certain impact on the life safety of patients. Currently, the treatment of COPD combined with type II respiratory failure is mainly based on noninvasive ventilation therapy, which can not only effectively relieve airway obstruction but also inhibit further aggravation of respiratory failure, with significant clinical efficacy [2]. However, it has been reported [3] that in order to effectively improve the efficacy of mechanical ventilation therapy in patients, reasonable and effective nursing interventions are needed to maximize the effect of ventilation and improve the prognosis.

The main contents of staged nursing intervention include admission education and management, operation period nursing, early postoperative rehabilitation nursing, and continuous rehabilitation nursing guidance. According to different surgical approaches and repair methods, targeted care, especially

Table 1: Comparison of general information between the two groups [$\bar{x} \pm s$, n(%)].

General information	Control group ($n = 60$)	Study group ($n = 60$)	χ^2/t	P
Gender				
Male	24(40.00)	28(46.67)	0.543	0.461
Female	36(60.00)	32(53.33)		
Average age (years)	58.06 ± 4.56	58.11 ± 4.32	0.062	0.951
Average BMI (kg/m^2)	23.54 ± 2.31	23.67 ± 2.43	0.300	0.764
Duration of COPD (years)	5.12 ± 0.78	5.17 ± 0.80	0.347	0.729
Duration of respiratory failure (d)	8.93 ± 1.12	9.11 ± 1.16	0.865	0.389
Degree of dyspnea				
Moderate	45(75.00)	41(68.33)	0.657	0.418
Severe	15(25.00)	19(31.67)		
Educational level				
Junior high school and below	17(28.33)	16(26.67)		
Secondary and high school	21(35.00)	26(43.33)	0.962	0.618
College and above	22(36.67)	18(30.00)		
Combined diabetes	6(10.00)	7(11.67)	0.086	0.769
Combined hypertension	8(13.33)	7(11.67)	0.076	0.783
Combined hyperlipidemia	10(16.67)	9(15.00)	0.062	0.802
APACHE II score (points)	20.71 ± 2.31	20.89 ± 2.34	0.424	0.672

Table 2: Specific care measures.

Implementation phase	Measures
Initial stage	At the initial stage of noninvasive ventilation, the nurse should give the patient a brief education about the necessity and safety of noninvasive ventilation to avoid emotional fluctuations. The mask should be selected according to the patient's face shape to avoid mask leakage, the appropriate tightness should be adjusted, and the sponge or gauze should be placed on the patient's frontal bone and nasal bridge.
Medium stage	This stage is 2 h after the patient's noninvasive ventilation until the disease is stable. At this time, observe the patient's adaptation to noninvasive ventilation, in order to avoid the patient's agitation, divert the patient's attention during this process, and elevate the head of the bed according to the patient's acceptance, and keep the patient's head and neck and airway vertical. Pay attention to whether there is sputum in the patient's airway, and if there is sputum, remove it in time to avoid the airway being obstructed.
Late stage	This stage is from the patient's disease stabilization to the ventilator withdrawal stage. (i) Withdrawal care: before withdrawing the ventilator, comprehensively assess whether the patient meets the withdrawal criteria, explain to the patient in detail the reasons and precautions for withdrawal, monitor the vital signs in real-time during the withdrawal process, and be prepared to get on the ventilator again at any time. (ii) Psychological guidance: pay close attention to the psychological and emotional changes of the patients, use visual simulation scoring to rate the patients' psychological state, and grade the care according to the score. <2 points for level 1 psychological care, use common psychological care, focus on the establishment of a sense of security when caring for the patients, focus on the current problems that the patients have, and understand the underlying causes of the patients' psychological problems. Use comfort, communication, and explanation to give patients psychological support and improve their sense of security. 2 points ≤ score < 4 points for level 2 psychological care, use mental relaxation method to improve patients' psychology and use light music in a quiet environment to allow patients to achieve a state of general relaxation to relieve mental tension and improve psychology. ≥4 points of level 3 psychological care to give patients family support, build confidence, and relieve negative emotions. During the implementation process, patients were made aware of the adverse psychological effects on recovery after treatment to establish a correct positive mindset.
Later consolidation care	In the later stage, we did the consolidation nursing intervention of respiratory function exercise, recorded the patient's respiratory function exercise daily, actively guided and helped the patient in the process of exercise, did about 0.5 h of exercise each time, and performed 3-5 times of exercise daily. During the exercise process, patients were encouraged appropriately according to their positive degree of exercise, so as to improve their compliance with exercise and promote rapid recovery from disease.

Table 3: Comparison of lung function between the two groups ($\bar{x} \pm s$).

Group	FEV_1(L)		FVC(L)		FEV_1/FVC(%)	
	Before nursing	After nursing	Before nursing	After nursing	Before nursing	After nursing
Control group ($n = 60$)	1.32 ± 0.24	1.72 ± 0.25	1.97 ± 0.22	2.32 ± 0.25	66.14 ± 5.62	72.61 ± 4.91
Study group ($n = 60$)	1.33 ± 0.21	2.46 ± 0.16	1.99 ± 0.19	2.85 ± 0.31	66.21 ± 5.49	76.84 ± 5.04
t	0.243	19.310	0.533	10.310	0.069	4.657
P	0.809	0.001	0.595	0.001	0.945	0.001

postoperative rehabilitation care and functional exercise, can greatly promote the recovery of patients' functions and shorten the patient's hospital stay. In contrast, routine care mainly reffered to admission guidance, simple health education, regular physical examination, prevention of complications, and guidance of patients on the use of COPD medication, which was demonstrated to be less efficient than staged nursing intervention [4]. As shown in a study of nursing intervention on self-efficacy among elderly patients with acute coronary syndrome after percutaneous coronary intervention, the nursing intervention effect of the 2 groups after intervention was improved before intervention ($P < 0.05$), and the hospital anxiety and depression scale (HADS) was lower than that of the control group after psychological intervention. The general self-efficacy scale scores of experimental group were obviously improved after receiving the intervention, and the scores in the experimental group were much higher than the control group after receiving the intervention, namely $P < 0.05$ [1]. Inspired by these data of the prognostic effect of nursing interventions, this study is aimed at investigating the effectiveness of its application by adding staged nursing interventions during patient treatment, which is reported as below.

2. Objects and Methods

2.1. Object of the Study. 120 patients with COPD combined with type II respiratory failure who met the inclusion and exclusion criteria and were admitted to our hospital between January 2021 and January 2022 were selected and divided into a control group and a study group of 60 cases each according to the random number table method. The general information of the two groups is shown in Table 1, and the two groups were balanced and comparable ($P > 0.05$). The inclusion criteria are as follows: meeting the clinical diagnostic criteria for COPD and type II respiratory failure, complete information, voluntary participation, and all treated with the same treatment protocol. The exclusion criteria are as follows: having other pulmonary pathologies such as pulmonary embolism; lung cancer; aberrant cardiogenic pulmonary edema; liver, kidney, and another important organ insufficiency; blurred consciousness; and no communication ability.

2.2. Methods

2.2.1. Treatment Method. Both groups were treated with conventional interventions, including nutritional support and water-electrolyte balance, and were treated with a dual-level noninvasive ventilator, with 12 breaths/min to 20 breaths/min, 6 cm H_2O to 8 cm H_2O as the initial inspiratory pressure, and 2 cm H_2O to 3 cm H_2O as the initial inspiratory pressure, and the patients were closely monitored for changes in their condition during treatment, and the parameters were adjusted in time. The maximum inspiratory air pressure was 5 cm H_2O~6 cm H_2O, and when the patient's condition was in a

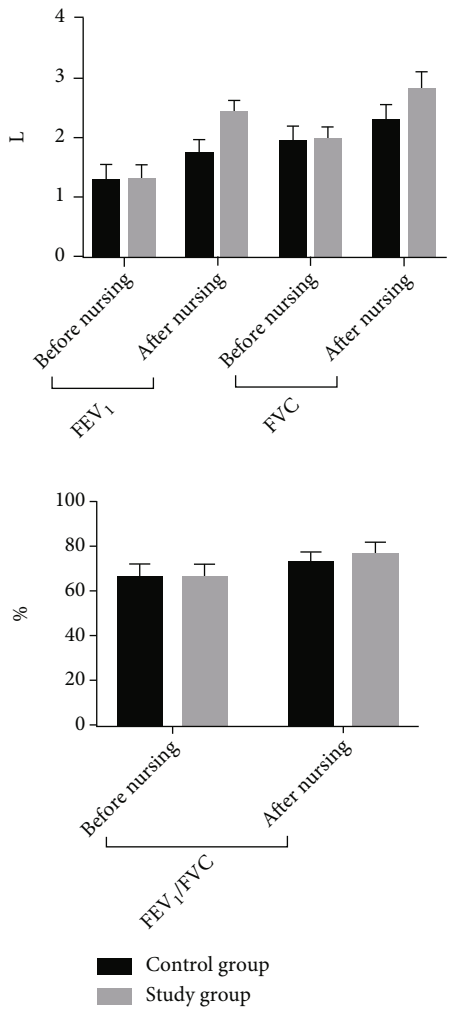

Figure 1: Histogram comparing pulmonary function before and after patient care in the two groups.

Table 4: Comparison of blood gas indicators between the two groups ($\bar{x} \pm s$).

Group	$PaCO_2$ (mmHg)		PaO_2 (mmHg)		SaO_2 (%)		PH	
	Before nursing	After nursing	Before nursing	After nursing	Before nursing	After nursing	Before nursing	After nursing
Control group ($n = 60$)	72.38 ± 7.26	62.82 ± 6.04	52.62 ± 5.49	67.03 ± 6.56	74.39 ± 4.85	82.31 ± 4.91	7.18 ± 0.05	7.34 ± 0.03
Study group ($n = 60$)	73.09 ± 7.14	51.96 ± 4.31	52.93 ± 5.52	81.14 ± 7.06	73.76 ± 4.32	94.82 ± 4.71	7.19 ± 0.04	7.48 ± 0.06
t	0.540	11.340	0.308	11.340	0.747	14.240	1.210	16.170
P	0.590	0.001	0.758	0.001	0.457	0.001	0.229	0.001

stable state, the inspiratory air pressure and suction pressure were adjusted down, and the inspiratory oxygen level was 40% during this process, and the flow rate was 4 L/min~6 L/min, and ventilation was performed for 4 h ~6 h each time.

2.2.2. Nursing Method. In the control group, the general routine strategy interventions such as disease monitoring and complication prevention were performed, disease monitoring was done according to medical prescriptions, and patients were closely monitored for the presence of sputum in the respiratory tract and cleared in time to reduce the occurrence of adverse events.

The study group applied the stage nursing strategy intervention and formed a stage nursing team, which consisted of a department physician, a department nurse manager, and 5 nurses with more than 5 years of experience in respiratory medicine and excellent service attitude. The nurse manager, as the team leader, discussed the nursing interventions with the team members and formulated the stage nursing measures, which were specifically implemented by the nurses. The specific measures are shown in Table 2.

2.3. Indicator Observation

2.3.1. Pulmonary Function, Blood Gas Analysis. Pulmonary function and arterial blood gas stability were measured using a pulmonary function and fully automated blood gas analyzer (GEM Premier 4000) before the patients were admitted to the group (before care) and before they were discharged from the hospital (aftercare). Pulmonary function was evaluated based on FEV1, FVC, and FEV1/FVC, and arterial blood gas stability was evaluated based on PaO_2, SaO_2, and $PaCO_2$ levels.

2.3.2. St. George's Respiratory Questionnaire (SGRQ) Evaluation. The health impairment of patients before and after patient care was evaluated based on the St. George's Respiratory Questionnaire (SGRQ) [5], which includes dimensions such as disease impact on life, activity limitation, and respiratory condition. The entire scale consists of 50 questions, where the lowest and highest scores on the scale are 0 and 100, respectively, with lower scores indicating less health damage to the patient from the disease.

2.3.3. Evaluation of Knowledge of Pulmonary Rehabilitation. Before and after the patients' care, the patients' knowledge was evaluated based on the scores of our self-made pulmonary rehabilitation knowledge questionnaire, which consisted of 5 items: diet, medication, disease, exercise, and oxygen therapy.

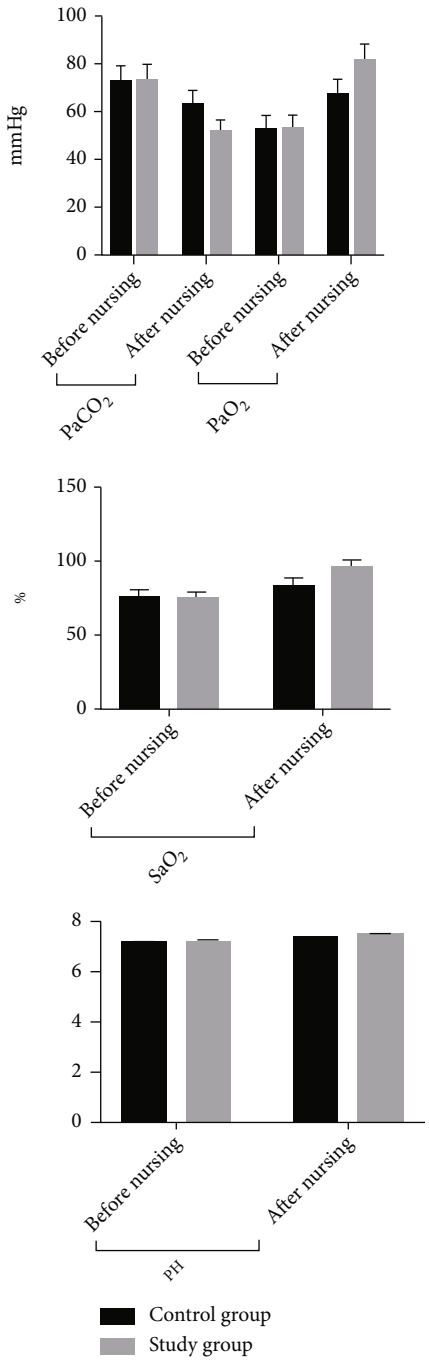

Figure 2: Histogram of blood gas comparison between two groups before and after patient care.

Table 5: Comparison of SGRQ scores for health impairment between the two groups [($\bar{x} \pm s$), points].

Group	Breathing conditions		Restricted activities		Disease impact on life		Total score	
	Before nursing	After nursing	Before nursing	After nursing	Before nursing	After nursing	Before nursing	After nursing
Control group ($n = 60$)	64.82 ± 7.45	48.39 ± 6.98	69.31 ± 8.14	57.08 ± 7.43	61.41 ± 8.04	49.32 ± 6.53	67.09 ± 9.15	54.51 ± 7.11
Study group ($n = 60$)	65.12 ± 8.07	44.52 ± 6.21	71.12 ± 8.21	51.42 ± 7.22	61.52 ± 8.11	43.15 ± 6.41	66.35 ± 9.26	46.41 ± 6.26
t	0.212	3.209	1.213	4.232	0.075	5.223	0.440	6.623
P	0.833	0.002	0.228	0.001	0.941	0.001	0.661	0.001

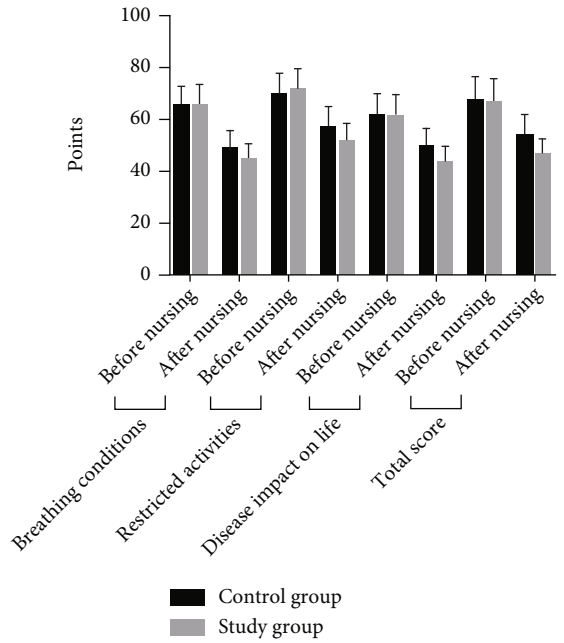

Figure 3: Histogram comparing SGRQ scores of health impairment in the two groups.

The entire scale consisted of 24 questions, where the lowest and highest scores of the scale were 0 and 24, respectively, with lower scores indicating more desirable patient perceptions of the disease.

2.3.4. Emotion, Hope Level Evaluation. The patient's mood and hope level were evaluated before and after patient care using the Self-Rating Scale for Depression (SDS), Self-Assessment Scale for Anxiety (SAS), and Herth Hope Scale developed by Zung, respectively; SDS and SAS both contain 20 questions and are rated on a 4-point scale, with lower scores indicating weaker depression and anxiety. The Herth Hope Scale consists of 12 questions, with scores of 12-23 being low, 24-35 being moderate, and 36-48 being high, with higher scores indicating a higher level of hope.

2.3.5. Survival Quality Evaluation. The quality of survival was evaluated on the Quality of Survival Scale before and after patient care, with a total of 26 questions on a 5-point scale, with each question scoring 0-5, with higher scores indicating better quality of survival.

2.3.6. Prognostic Evaluation. The occurrence of adverse events such as multiple organ failure, cardiovascular disease, and death that occurred before the patient was admitted to the hospital for treatment until discharge was used as a prognostic evaluation criterion, and the occurrence was considered a poor prognosis, and the opposite was considered an excellent prognosis.

2.3.7. Nursing Satisfaction Evaluation. Patients in both groups were assessed for nursing satisfaction by our questionnaire, which included 4 items, namely, very satisfied, satisfied, dissatisfied, and very dissatisfied, and (very satisfied + satisfied)/the total number of cases ×100% = total satisfaction.

2.4. Statistical Analysis. SPSS22.0 statistical software was used for analysis and processing. The Kolmogorov-Smirnov test was applied to test whether the data conformed to a normal distribution, and the measurement data conforming to normal distribution were described by the mean ± standard deviation ($\bar{x} \pm s$), and the independent samples t-test was used for comparison between groups, and the paired t-test was used for

Table 6: Comparison of pulmonary rehabilitation knowledge scores between the two groups [($\bar{x} \pm s$), points].

Group	Diet knowledge		Medication knowledge		Disease knowledge		Sports knowledge		Oxygen therapy knowledge		Total score	
	Before nursing	After nursing	Before nursing	After nursing	Before nursing	After nursing	Before nursing	After nursing	Before nursing	After nursing	Before nursing	After nursing
Control group ($n = 60$)	1.31 ± 0.65	2.05 ± 0.71	2.01 ± 1.04	2.73 ± 1.11	4.19 ± 1.55	5.03 ± 1.59	2.39 ± 1.12	3.14 ± 1.08	1.24 ± 0.48	1.91 ± 0.42	11.14 ± 1.36	14.86 ± 2.57
Study group ($n = 60$)	1.29 ± 0.67	2.39 ± 0.66	2.04 ± 1.02	3.65 ± 1.07	4.16 ± 1.54	6.71 ± 1.46	2.41 ± 1.07	4.11 ± 1.28	1.22 ± 0.46	2.52 ± 0.42	11.12 ± 1.42	19.35 ± 2.96
t	0.166	2.717	0.160	4.622	0.106	6.028	0.100	4.486	0.075	7.955	0.079	8.872
P	0.868	0.008	0.874	0.001	0.915	0.001	0.921	0.001	0.941	0.001	0.937	0.001

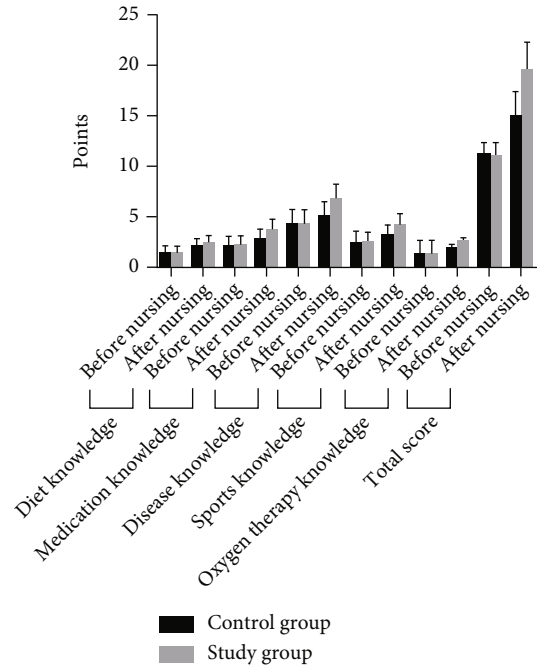

Figure 4: Histogram comparing the knowledge scores of pulmonary rehabilitation between the two groups.

comparison before and after patient care; median and quartile spacing M (Q1, Q3) were applied for those not conforming to the normal distribution, and Wilcoxon's comparison was used between groups. Count data were expressed as n (%), χ^2 test. $P < 0.05$ was considered statistically significant.

3. Results

3.1. Comparison of Pulmonary Function Indexes between the Two Groups. The comparison of pulmonary function between the two groups before care was not significant ($P > 0.05$); after care, the pulmonary function of the two groups was higher than before care, and the increase was more significant in the study group compared with the control group ($P < 0.05$). See Table 3 and Figure 1.

3.2. Comparison of Blood Gas Indicators between the Two Groups. The comparison of blood gases between the two groups before care was not significant ($P > 0.05$); after care, the blood gas indexes of the two groups were higher than before care, and the increase was more significant in the study group compared with the control group ($P < 0.05$). See Table 4 and Figure 2.

3.3. Comparison of SGRQ Scores for Health Impairment between the Two Groups. The comparison of SGRQ scores of health impairment between the two groups before care was not significant ($P > 0.05$); after care, the SGRQ scores of health impairment in both groups were lower than before care, and the reduction was more significant in the study group compared with the control group ($P < 0.05$). See Table 5 and Figure 3.

3.4. Comparison of Knowledge Awareness Scores of Pulmonary Rehabilitation between Two Groups. The comparison of the knowledge scores of the two groups before care was not significant ($P > 0.05$); after care, the knowledge scores of the two groups were higher than before care, and the increase was more significant in the study group compared with the control group ($P < 0.05$). See Table 6 and Figure 4.

3.5. Comparison of Mood and Hope Scores between the Two Groups. The comparison of mood and hope scores between the two groups before care was not significant ($P > 0.05$); after care, the hope scores of the two groups were higher than before care, and the increase was more significant in the study group compared with the control group ($P < 0.05$); after care, the mood scores of the two groups were lower than before care, and the decrease was more significant in the study group compared with the control group ($P < 0.05$). See Table 7 and Figure 5.

3.6. Comparison of the Quality of Survival between the Two Groups. The comparison of the quality of survival scores between the two groups before care was not significant ($P > 0.05$); after care, the quality of survival in both groups was higher than before care, and the increase was more significant in the study group compared with the control group ($P < 0.05$). Table 8, Figure 6.

3.7. Comparison of Prognosis between the Two Groups. The study group had a higher rate of excellent prognosis than the control group ($P < 0.05$). See Table 9.

Table 7: Comparison of emotions and hopes between the two groups [($\bar{x} \pm s$), points].

Group	Hopes											
	Attitude towards reality and the future		Adopt an affirmative action attitude		The attitude of maintaining a close relationship with others		Total score		SAS		SDS	
	Before nursing	After nursing	Before nursing	After nursing	Before nursing	After nursing	Before nursing	After nursing	Before nursing	After nursing	Before nursing	After nursing
Control group ($n = 60$)	10.21 ± 1.96	11.95 ± 1.14	10.24 ± 1.52	12.24 ± 1.05	12.17 ± 0.53	13.38 ± 1.05	33.42 ± 3.62	37.49 ± 3.28	50.13 ± 6.81	39.62 ± 4.62	44.35 ± 6.45	40.43 ± 4.05
Study group ($n = 60$)	10.29 ± 1.82	14.27 ± 1.22	10.31 ± 1.23	14.39 ± 1.19	12.15 ± 0.62	15.31 ± 1.56	33.35 ± 3.12	45.03 ± 4.41	50.64 ± 6.37	35.79 ± 4.14	45.34 ± 6.17	35.71 ± 3.73
t	0.232	10.760	0.277	10.490	0.190	7.950	0.114	10.630	0.424	4.782	0.859	6.640
P	0.817	0.001	0.782	0.001	0.850	0.001	0.910	0.001	0.673	0.001	0.392	0.001

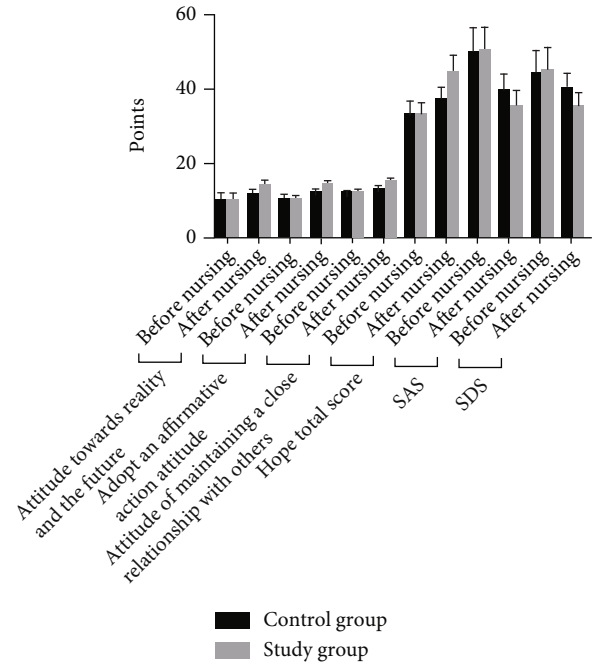

Figure 5: Histogram comparing the mood and hope scores of the two groups.

3.8. Comparison of Nursing Satisfaction between the Two Groups. Nursing satisfaction was higher in the study group than in the control group ($P < 0.05$). See Table 10.

4. Discussion

Currently, the treatment of patients with COPD combined with type II respiratory failure is based on noninvasive ventilation, which is the most commonly used treatment for this disease, and this method has the advantages of easy operation, ready access to the machine, and low trauma to the patient's organism, which can continuously improve the patient's hypoxia and respiratory function after application [1, 4, 5]. However, studies have shown [6] that some patients have varying degrees of psychological negativity in the early stages of treatment, which affects the effect of ventilation and increases the risk of poor prognosis, so appropriate nursing interventions need to be given to patients during treatment to improve the prognosis.

Most of the conventional nursing tools currently used in the clinic are based on the patient's condition in order to maintain treatment, ignoring to some extent the differences in patients' stage needs [7–9]. Stage-based nursing measures are the hotspot studied at present, which was reported [10] that such nursing means can implement targeted measures and interventions at different stages. Duiring the nursing process, the psychological and physiological characteristics of patients are fully considered, which aimed to obtain the rapid disease recovery from early to late stages. Unlike conventional nursing measures, the stage nursing measures have clearer goals and are related to the patient's disease recovery process, and are progressive nursing measures with ideal clinical application value [11, 12]. In this paper, the study group performed targeted noninvasive ventilation care in the early, middle, and late stages of treatment to avoid disease deterioration during the stabilization phase and to focus on postwithdrawal respiratory function training during the late withdrawal process. The improvement in pulmonary function and blood gases was found to be more significant in the study group than in the control group aftercare, a result that may be related to the fact that the study group was more effective in diagnosing the patient's specific disease at multiple stages of care.

It has been reported [13] that some patients develop psychological negativity and lose their level of hope after the onset of the disease due to the fear of not recovering from the disease. The results of this study showed that patients who applied staged care had significantly reduced negative psychological emotions and increased their hope levels, suggesting that staged care may increase hope levels and alleviate negative psychological emotions by promoting patients' recovery from disease. In addition, the clinical evaluation of the effectiveness of treatment is mostly based on the prognosis of the patients [14]. Therefore, this study further analyzed the impact of patient stage care measures on patient prognosis, which showed that patients in the study group had a higher rate of excellent prognosis. This result is consistent with the fact that care measures can improve the prognosis in both physiological and psychological aspects.

In conclusion, staged nursing interventions can significantly improve pulmonary function and blood gases and improve treatment prognosis in patients with COPD combined with type II respiratory failure with ideal results.

Table 8: Comparison of quality of survival scores before and after patient care between the two groups [($\bar{x} \pm s$), points].

Group	Physiological field		Psychological field		Social field		Circumstance field		Total score	
	Before nursing	After nursing	Before nursing	After nursing	Before nursing	After nursing	Before nursing	After nursing	Before nursing	After nursing
Control group ($n = 60$)	9.29 ± 1.03	11.32 ± 1.57	9.18 ± 1.05	12.57 ± 2.18	10.33 ± 1.53	13.52 ± 2.16	11.38 ± 1.08	13.24 ± 1.87	38.79 ± 5.13	48.67 ± 4.37
Study group ($n = 60$)	9.25 ± 1.12	14.68 ± 2.54	9.12 ± 1.03	15.68 ± 2.34	10.24 ± 1.12	16.16 ± 2.48	11.34 ± 1.12	15.63 ± 3.24	38.62 ± 5.22	62.57 ± 8.49
t	0.204	8.716	0.316	7.533	0.368	6.218	0.199	4.949	0.180	11.280
P	0.839	0.001	0.753	0.001	0.714	0.001	0.842	0.001	0.958	0.001

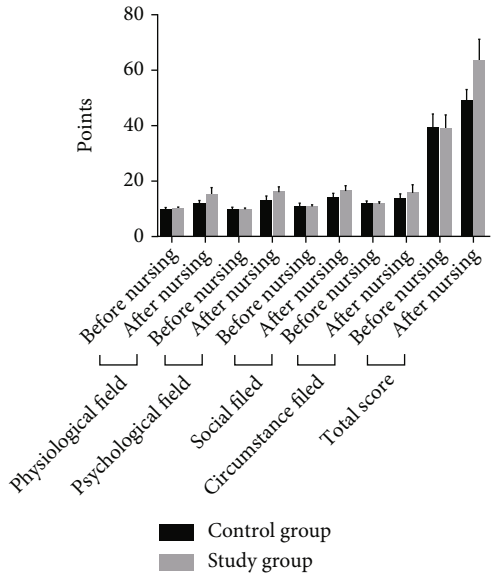

Figure 6: Histogram comparing the quality of survival scores before and after patient care for the two groups.

Table 9: Comparison of prognosis between the two groups (n, %).

Group	Poor prognosis		Good prognosis
Control group ($n = 60$)	11(18.33)		49(81.67)
Study group ($n = 60$)	3(5.00)		57(95.00)
χ^2		5.175	
P		0.023	

Table 10: Comparison of nursing satisfaction between the two groups (n, %).

Group	Very satisfied	Satisfied	Dissatisfied	Very dissatisfied	Nursing satisfaction (%)
Control group ($n = 60$)	35	13	7	5	48(80.00)
Study group ($n = 60$)	40	17	2	1	57(95.00)
χ^2					6.171
P					0.013

Data Availability

The data used to support this study is available from the corresponding author upon request.

Conflicts of Interest

The authors declare that they have no conflicts of interest.

Acknowledgments

This paper was funded by the Chinese Medicine Research Program of Zhejiang Province (2021ZB065, 2022ZB078).

References

[1] S. K. Gadre, A. Duggal, E. Mireles-Cabodevila et al., "Acute respiratory failure requiring mechanical ventilation in severe chronic obstructive pulmonary disease (COPD)," *Medicine (Baltimore)*, vol. 97, no. 17, article e0487, 2018.

[2] J. Sun, Y. Li, B. Ling et al., "High flow nasal cannula oxygen therapy versus non-invasive ventilation for chronic obstructive pulmonary disease with acute-moderate hypercapnic respiratory failure: an observational cohort study," *International Journal of Chronic Obstructive Pulmonary Disease*, vol. 14, no. 1, pp. 1229–1237, 2019.

[3] M. A. Spruit, C. L. Rochester, F. Pitta et al., "Pulmonary rehabilitation, physical activity, respiratory failure and palliative respiratory care," *Thorax*, vol. 74, no. 7, pp. 693–699, 2019.

[4] L. H. Storgaard, H. U. Hockey, B. S. Laursen, and U. M. Weinreich, "Long-term effects of oxygen-enriched high-flow nasal cannula treatment in COPD patients with chronic hypoxemic respiratory failure," *International Journal of Chronic Obstructive Pulmonary Disease*, vol. 13, pp. 1195–1205, 2018.

[5] M. Rutten-van Mölken, B. Roos, and J. A. Van Noord, "An empirical comparison of the St George's respiratory questionnaire (SGRQ) and the chronic respiratory disease questionnaire (CRQ) in a clinical trial setting," *Thorax*, vol. 54, no. 11, pp. 995–1003, 1999.

[6] T. Shi and L. Feng, "Blood biomarkers associated with acute type II respiratory failure in COPD: a meta-analysis," *The Clinical Respiratory Journal*, vol. 16, no. 2, pp. 75–83, 2022.

[7] L. Ai, J. Zhang, and W. Bo, "Respiratory failure in intensive care unit patients with progressive COPD: nursing approaches to patient care," *Alternative Therapies in Health and Medicine*, vol. 28, no. 1, pp. 52–57, 2022.

[8] W. Chou, C. C. Lai, K. C. Cheng, K. S. Yuan, C. M. Chen, and A. C. Cheng, "Effectiveness of early rehabilitation on patients with chronic obstructive lung disease and acute respiratory failure in intensive care units: a case-control study," *Chronic Respiratory Disease*, vol. 16, 2019.

[9] Y. Cui, X. Wang, Q. Wu, J. Huang, and F. Li, "Effect of the establishment of critical care professional nursing team on nursing effect and prognosis of patients with chronic obstructive pulmonary disease with respiratory failure," *Minerva Medica*, vol. 112, no. 6, pp. 840–842, 2021.

[10] V. Sawrikar, E. Stewart, H. M. LaMonica et al., "Using staged care to provide "right care first time" to people with common affective disorders," *Psychiatric Services*, vol. 72, no. 6, pp. 691–703, 2021.

[11] J. H. Shin, "Declining body, institutional life, and making home-are they at odds?," *HEC Forum*, vol. 27, no. 2, pp. 107–125, 2015.

[12] M. Akbarzadeh, A. Nematollahi, M. Farahmand, and S. Amooee, "The effect of Two-Staged Warm compress on the pain duration of first and second labor stages and Apgar score in prim gravida women: a randomized clinical trial," *Journal of Caring Sciences*, vol. 7, no. 1, pp. 21–26, 2018.

[13] J. An, H. Zhou, T. Yang et al., "Relationship of psychological factors with daily activities and quality of life in patients with chronic obstructive pulmonary disease in a Chinese rural population," *Annals of Palliative Medicine*, vol. 10, no. 2, pp. 1675–1684, 2021.

[14] J. Xie and C. Wu, "Ultrasensitive quantification of extracellular vesicles through dual signal amplification for the early diagnosis and prognosis of chronic obstructive pulmonary disease (COPD)," *Analytical Methods*, vol. 13, no. 38, pp. 4437–4441, 2021.

Hindawi
Applied Bionics and Biomechanics
Volume 2022, Article ID 4047845, 10 pages
https://doi.org/10.1155/2022/4047845

Review Article

Effectiveness of Augmented Reality for Lower Limb Rehabilitation: A Systematic Review

Hongbin Chang,[1] Yang Song,[2,3] and Xuanzhen Cen[2,3]

[1]*General Studies Teaching Department, Zhejiang Fashion Institute of Technology, Zhejiang 315211, China*
[2]*Doctoral School on Safety and Security Sciences, Obuda University, Budapest 1034, Hungary*
[3]*Faculty of Engineering, University of Szeged, Szeged 6720, Hungary*

Correspondence should be addressed to Yang Song; yang.song@uni-obuda.hu

Received 5 April 2022; Revised 17 June 2022; Accepted 9 July 2022; Published 18 July 2022

Academic Editor: Wen-Ming Chen

Augmented reality- (AR-) based interventions have shown potential benefits for lower limb rehabilitation. However, current literature has not revealed these benefits as a whole. The main purposes of this systematic review were to determine the efficacy of AR-based interventions on lower limb recovery of the larger population based on the current process that has been made in this regard. Relevant studies were retrieved from five electronic databases (Web of Science, PubMed, ScienceDirect, Scopus, and Cochrane Library) using "augmented reality" OR "AR" AND "lower limb" OR "lower extremity" AND "intervention" OR "treatment". Sixteen studies that met the eligibility criteria were included in this review, and they were further grouped into three categories based on the participant types. Seven studies focused on the elderly adults, six on the stroke patients, and the last three on Parkinson patients. Based on the findings of these trials, the significant effects of AR-based interventions on lower limb rehabilitation (i.e., balance, gait, muscle, physical performance, and fall efficacy) have been initially confirmed. Favorable results were achieved at least the same as the interventions without AR except for the turning and timing in the freezing of gait of Parkinson patients. However, given the infancy of this technology in clinical practices, more robust trials with larger sample sizes and greater homogeneity in terms of devices and treatment settings are warranted for further verification.

1. Introduction

Nowadays, advanced technologies are becoming increasingly common as rehabilitation therapeutic tools in the healthcare setting [1–6]. Among them is virtual reality (VR), which immerses the users into the artificial environment created by the computer simulation [7, 8]. Compared to the conventional retraining techniques, VR technology is considered motivating and engaging, and it offers an artificial environment where the training environment, the difficulty level of tasks, and the feedback types could be relatively effortlessly manipulated [9]. Previous studies have found that participants were more actively engaged in the VR-based rehabilitation training than the conventional one to improve motor ability [10–12]. VR has now been incorporated into varied clinical practices such as poststroke rehabilitation, and it has shown significant effects on improving the motion functions, dynamic balance, and muscle force of both upper and lower limbs among stroke patients [13, 14]. Nevertheless, emerging evidence has concerned the safety of using VR technology in clinical practices, especially for the rehabilitation training of patients with lower limb impairments [9, 15, 16]. For example, the patients may not be able to recognize their body position when using a head-mounted display (HMD) VR device, which would further lead to unexpected physical injuries [9].

Due to the above limitations, the requirement for a safer and automatic rehabilitation training tool has accumulated. In recent years, the introduction of augmented reality (AR) into clinical applications has been proposed and verified [17–19]. AR could be a safer alternative to VR since it does not fully place the users into the simulated environment

but add the fundamental elements of rehabilitation training on a real-world view [20]. In addition, compared to these interactive elements designed by VR in the virtual world, the interactive elements created by AR in the real world could induce much more embodiment to the users [18]. There are emerging studies that reported the benefit of using AR for clinical rehabilitation, and several systematic reviews have further confirmed the promising effects, especially for stroke patients [17–19, 21–23]. Despite that, no review to our knowledge has investigated whether AR-based methods are beneficial for a wide range of adults such as the elderly, stroke patients, and patients with cerebral palsy or multiple sclerosis. Moreover, since the lower limbs are directly involved in most of the daily movement, it is important to further determine if AR-based methods can help to improve the lower limb rehabilitation of these above patients.

As AR technology becomes much more accessible, AR-based treatments could be widely used not only in clinical practices but also in home settings for function rehabilitation. Therefore, this review summarized and analyzed the efficacy of AR-based interventions on lower limb recovery based on the current process that has been made in this regard, aiming to determine whether it could contribute significant benefits to the larger population and further add help to guide future utilization of AR technology.

2. Materials and Methods

2.1. Search Strategy. Five English databases including Web of Science, PubMed, ScienceDirect, Scopus, and Cochrane Library were searched independently by two authors to identify relevant studies published from the very beginning until 1 June 2022. The searching keywords include "augmented reality" OR "AR" AND "lower limb" OR "lower extremity" AND "intervention" OR "treatment". In addition, both the reference lists of the included studies and the retrieved reviews were further searched to identify other relevant articles.

2.2. Eligibility Criteria. In this review, two investigators assessed the retrieved studies independently, and the third investigator would be consulted if any inclusion disagreements happened. The literature exclusion was initially conducted by screening the titles and abstracts, and then, the investigators would screen the full texts of the papers for further confirmation. The eligibility criteria were formed based on participants, experimental design, and outcomes; (1) subjects: studies that reported the effects of AR-based interventions/applications on lower limb rehabilitation of both healthy participants and patients without age limit were included; (2) experimental design: this review focused on the effectiveness of AR for lower limb rehabilitation, and therefore, any randomized controlled trials or observational studies related to this topic were all included; (3) outcomes: the study results should include variables related to lower limb rehabilitation, such as gait kinematics, muscle strength, and balance. In addition, only English original researches published on peer-reviewed journals were included in this study, while reviews, conference proceedings, and study protocols were excluded.

2.3. Data Extraction. The following data from included studies were further extracted and summarized by two investigators and verified by the third one: (1) author, including the name of the first author and published year; (2) study purposes; (3) participant, including the number of participants, age, gender, and physical conditions; (4) intervention, experimental design, and intervention protocols (type, frequency, time, total duration); (5) comparison and comparison protocols (type, frequency, time, total duration); and (6) outcome, the primary findings of these studies. In addition, the Mendeley Desktop Reference Management Software (Mendeley Ltd., Netherlands) was applied for organizing articles and generating citations.

3. Results

3.1. Search Results. The flow chart of the search procedure of this review is presented in Figure 1. A total of 259 papers were initially searched from the five databases. It was reduced to 11 articles after screening according to the eligibility and removing all the duplicates. Five additional papers were identified from the reference lists of these retrieved studies, which makes it in total 16 studies included in this review. Most studies compared the effects of AR interventions with the corresponding control programs, while there are also some studies that evaluated the before-after effects without any control trials. Conventional physical fitness program was normally conducted for control groups; however, some studies also offered insight from other directions, such as Tai Chi, yoga, and functional electrical stimulation. Over half of the studies were performed on elderly adults ($n = 7$), and the rest of the studies were performed on stroke patients ($n = 6$) and Parkinson patients ($n = 3$). The detailed study characteristics are summarized in Table 1, and these included studies were further grouped into three categories based on the types of participants to elaborate the acute or chronic effects of AR interventions on lower limb rehabilitation.

3.2. AR Rehabilitation Systems. Most of the AR rehabilitation systems utilized in the included studies consist of a server computer with a web camera and an optical see-through HMD connected to a personal computer [24, 25, 31–37, 39]. In these systems, patients followed the displayed instruction and performed the corresponding movement. In the meantime, the computer sensed the patients' movement and sent the information to the HMD in order to repeat the task or move to the next level. However, due to the inherent limitations of the HMD devices, unexpected physical side effects (e.g., fatigue and nausea) still cannot be completely avoided. Researchers have already started to look for alternatives. The rest of the included studies developed the 3D interactive augmented reality system using the motion-tracking Kinect sensor (Microsoft Inc., Redmond, WA, USA) [26–30, 38]. A 3D depth map was created by the sensor, and the patients in front of the sensor can be detected as 3D objects on a computer. Patients interacted with the virtual objects on the screen and watch their movement (e.g., gait and posture) at the same time.

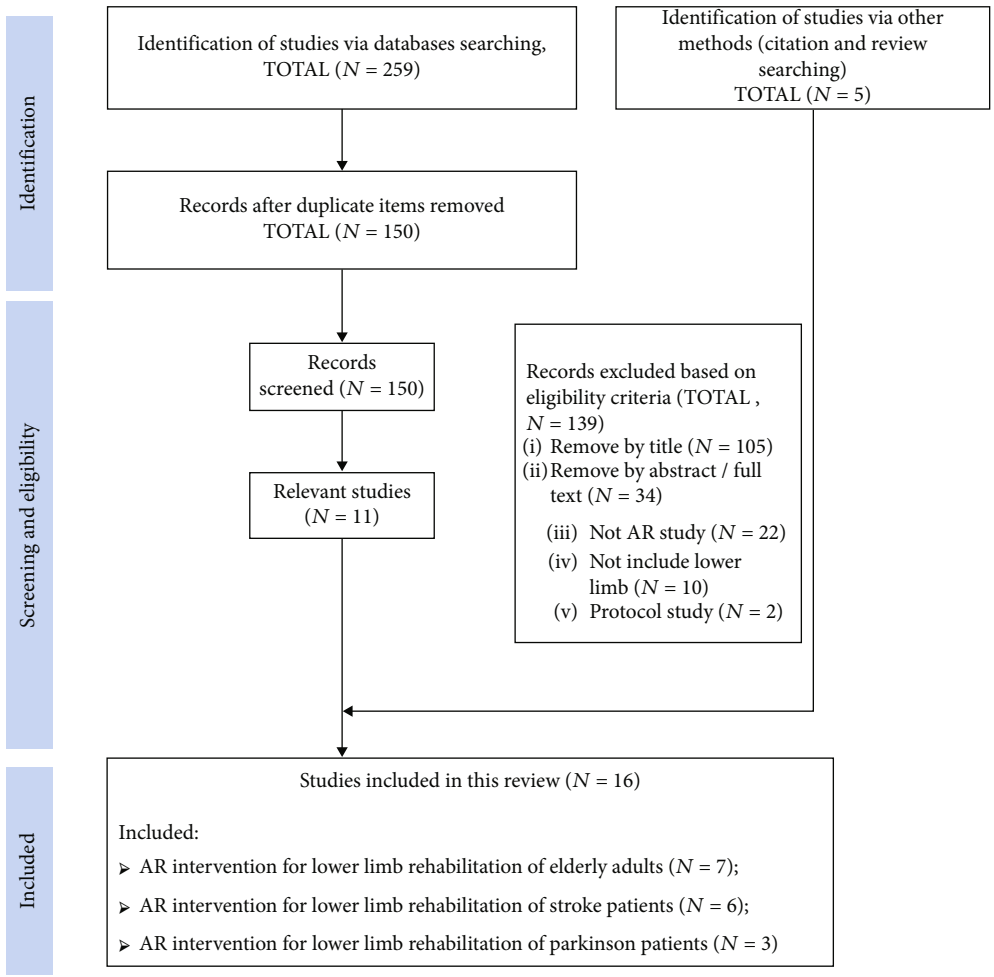

Figure 1: The review flow chart.

3.3. AR Intervention for Lower Limb Rehabilitation of Elderly Adults. The first group of studies investigated the effects of AR interventions for lower limb rehabilitation of healthy elderly adults. Yoo et al. [24] first started AR interventions on elderly women, intending to investigate the effects of AR-based Otago exercise on balance, gait, and fall efficacy. Subjects were asked to perform a 60-minute Otago exercise with or without the AR environment 3 sessions per week for 12 weeks in total. The Otago exercise consists of lower limb muscle strengthening exercises and balance training. The results showed that AR-based Otago exercise significantly improved subjects' lower limb balance, gait velocity, cadence, step length, and stride length, while reduced the fall risk. Similarly, Lee et al. [25] employed the same AR intervention protocol on elderly women. What is more, they further compared the AR-based Otago exercise with yoga or self-exercise programs, and the effects of these interventions on lower limb muscle strength were further investigated. Similar results were found in terms of balance and gait functions, and Lee et al. [25] also confirmed the significant effects of AR-based Otago exercise on knee flexion and ankle dorsiflexion strength.

Two subsequent studies determined the effects of a 3D interactive AR program on the balance and mobility rehabilitation of elderly adults. Im et al. [26] conducted a before-after study, and they required subjects to perform the 30-minute three-dimensional interactive AR program for 10 sessions in 12 weeks. Several tasks that enable specific motions of specific lower limb joints were designed in this program. Specifically, the balloon game for the hip joint, the cave game for the knee joint, and the rhythm game focuses on one-leg standing ability. Both the lower limb balance and mobility were improved after the training, and the success rate and response time for each game also improved gradually across sessions. In Ku et al. [27] study, subjects were randomly divided into two groups, and the control group was asked to perform the 30-minute conventional physical fitness program 3 times per week for 1 month, while the experimental group performed the same 3D interactive AR program 3 times per week for 4 weeks. However, their results only confirmed that the 3D interactive AR program can enhance the balance ability more effectively than the conventional physical fitness program, and they speculated that it is highly associated with motor learning mechanism as the subjects had to make the movement according to the contents in AR environment.

The last three studies were all published in 2020, and they all provided positive results in terms of the effects of AR-based intervention on lower limb rehabilitation of

Table 1: The basic characteristics of the included studies.

Reference	Objective	Participant	Intervention	Intervention frequency	Outcome test
AR intervention for lower limb rehabilitation of elderly adults					
Chen et al. [30]	Investigated the effects of AR-assisted training with selected Tai Chi movements on balance and muscle strength of older adults.	Elderly men ($N = 28$) Experimental group ($N = 14$, age, 72.2 ± 2.8 years) Control group ($N = 14$, age, 75.1 ± 5.5 years)	Experimental group: AR-assisted training with selected Tai Chi movements Control group: 24-form Yang-style Tai Chi movements	30 min per time with 3 sessions per week for 8 weeks	Balance: Berg balance scale test, timed up and go test, functional reach test Muscle strength: lower limb muscle strength test
Yoo et al. [24]	Investigated the effects of AR-based Otago exercise on balance, gait, and fall efficacy of older adults.	Elderly women ($N = 21$) Experimental group ($N = 10$, age, 72.90 ± 3.41 years) Control group ($N = 11$, age, 75.64 ± 5.57 years)	Experimental group: AR-based Otago exercise for muscle strengthening and balance training Control group: Otago exercise for muscle strengthening and balance training	60 minutes per time with 3 sessions per week for 12 weeks	Balance: Berg balance scale test Gait: velocity, cadence, step length, and stride length Fall: fall efficacy test
Lee et al. [25]	Investigated the effects of AR-based Otago exercise on balance, muscle strength, and physical factors in falls of older adults.	Elderly women ($N = 30$) Experimental group ($N = 10$, age, 72.60 ± 2.67 years) Control group 1 ($N = 10$, age, 75.80 ± 5.47 years) Control group 2 ($N = 10$, age, 76.40 ± 5.54 years)	Experimental group: AR-based Otago exercise for muscle strengthening and balance training Control group 1: yoga Control group 2: elastic band exercise program	60 minutes per time with 3 sessions per week for 12 weeks	Balance: foot print test Muscle strength: lower limb muscle strength test Fall: short Morse fall scale test
Im et al. [26]	Investigated the effects of 3D interactive AR system on balance and kinematic function of older adults.	Elderly adults ($N = 18$, age, 64.72 ± 7.27 years)	3D interactive AR system	30 minutes per time for 10 sessions in 12 weeks	Balance: Berg balance scale test; timed up and go test Gait: hip and knee joint angle
Jeon and Kim [29]	Investigated the effects of AR-based muscle reduction prevention exercise program on muscle parameters, physical performance, and exercise self-efficacy of older adults.	Elderly women ($N = 27$) Experimental group ($N = 13$, 72.77 ± 3.79 years) Control group ($N = 14$, 72.71 ± 3.64 years)	Experimental group: AR-based muscle reduction prevention exercise program Control group: NA	30 minutes per time with 5 sessions per week for 12 weeks	Muscle mass: bioelectrical impedance analysis Muscle function: gait speed and hand grip strength Physical performance: senior fitness test Exercise self-efficacy: exercise self-efficacy scale
Chen et al. [28]	Investigated the effects of AR-based exergame system on fall risk of older adults.	Elderly adults ($N = 25$, age, 71.48 ± 4.09 years)	AR-based exergame system	One time	User experience: user experience questionnaire
Ku et al. [27]	Investigated the effects of 3D interactive AR system on the balance and mobility of older adults.	Elderly adults ($N = 36$) Experimental group ($N = 18$, 64.7 ± 7.27 years) Control group ($N = 18$, 65.0 ± 4.77 years)	Experimental group: 3D interactive AR system training Control group: conventional physical fitness program	Conventional physical fitness program: 30 min per time with 3 sessions per week for 1 month 3D interactive AR system training: 30 min per time	Balance and mobility: lower-extremity clinical scale scores, fall index, automatic balance score

Table 1: Continued.

Reference	Objective	Participant	Intervention	Intervention frequency	Outcome test
				with 3 sessions per week for 4 weeks	
AR intervention for lower limb rehabilitation of stroke patients					
Lee et al. [34]	Investigated the effects of AR-based postural control training on balance and gait function of stroke patients.	Stroke patients ($N = 21$) Experimental group ($N = 10$, age, 47.9 ± 12.0 years) Control group ($N = 11$, age, 54.0 ± 11.9 years)	Experimental group: AR-based postural control training+ general physical therapy program Control group: general physical therapy program	General physical therapy program: 30 minutes per time with 5 sessions per week for 4 weeks Additional AR-based postural control training: 30 minutes per time with 3 sessions per week for 4 weeks	Balance: Berg balance scale test, timed up and go test Gait: velocity, cadence, step length, and stride length
Park et al. [35]	Investigated the effects of AR-based postural control training on balance and gait function of stroke patients.	Stroke patients ($N = 20$) Experimental group ($N = 10$, 47.38 ± 13.44 years) Control group ($N = 10$, 53.50 ± 12.43 years)	Experimental group: AR-based postural control training+ conventional physical therapy Control group: conventional physical therapy	Conventional physical therapy: 60 minutes per time with 5 sessions per week for 4 weeks Additional AR-based postural control training: 30 minutes per time with 3 sessions per week for 4 weeks	Balance: Berg balance scale test Gait: 10-meter walk test
Kim et al. [33]	Investigated the effects of AR-based functional electrical stimulation during treadmill gait training on balance, gait, sand muscle trength of stroke patients.	Stroke patients ($N = 28$) Experimental group ($N = 9$, age, 47.44 ± 8.39 years) Control group 1 ($N = 10$, age, 51.50 ± 12.90 years) Control group 2 ($N = 9$, age, 49.11 ± 11.02 years)	Experimental group: AR-based functional electrical stimulation during treadmill gait training Control group 1: functional electrical stimulation during treadmill gait training Control group 2: treadmill gait training	20 minutes per time with 3 sessions per week for 8 weeks	Balance: Berg balance scale test Gait: timed up and go test Muscle strength: lower limb muscle strength test
Jung et al. [32]	Investigated the effects of AR-based EMG-triggered functional electric simulation on the range of motion, muscle activation, and muscle strength of ankle joint of stroke patients.	Stroke patients ($N = 10$) Experimental group ($N = 5$, age, 58.40 ± 8.26 years) Control group ($N = 5$, age, 57.80 ± 10.23 years)	Experimental group: AR-based EMG-triggered functional electric simulation Control group: EMG-triggered functional electric simulation	20 minutes per time with 5 sessions per week for 4 weeks	Muscle activation (ankle) Muscle strength (ankle) Ankle range of motion
Jaffe et al. [31]	Investigated the effects of AR-based walking program on the walking function	Stroke patients ($N = 20$, age, 60.7 ± 2.3 years)	AR-based obstacle training program	60 minutes per time with 6 sessions for 2 weeks	Gait: gait velocity, step length, ability to step over

Table 1: Continued.

Reference	Objective	Participant	Intervention	Intervention frequency	Outcome test
	of patients with poststroke hemiplegia.		Obstacle training program		obstacles, and walking endurance
Held et al. [36]	Investigated the effects of AR for gait impairment after stroke system on overground walking function of a stroke patient.	Stroke patient ($N = 1$, age, 74 years)	Experimental group: AR for gait impairment after stroke system Control group: clinical gait assessments	One time	Gait: hip, knee, and ankle joint angle, position of the center of mass
AR intervention for lower limb rehabilitation of Parkinson patients					
Espay et al. [37]	Investigated the effects of at-home training with a closed-loop AR cueing device on the walking function of Parkinson patients.	Parkinson patients ($N = 13$, age, 73.3 ± 11.7 years)	At-home training with closed-loop AR cueing device	30 minutes per time twice daily for 2 weeks	Gait: gait velocity, stride length, cadence, and freezing of gait questionnaire
Janssen et al. [39]	Investigated the effects of AR visual cues on freezing of gait and turning in place of Parkinson patients experiencing freezing of gait.	Parkinson patients ($N = 16$, age, median 69 years)	AR visual cues	One time	Freezing of gait: percent time frozen, number, and duration Axial kinematics: medial COM deviation and head-pelvis separation Gait: cadence, step height, and stride time
Palacios-Navarro et al. [38]	Investigated the effects of AR-based rehabilitation games on the walking function of Parkinson patients.	Parkinson patients ($N = 7$, age, 67 ± 3 years)	AR-based rehabilitation games	30 min per time with 4 sessions per week for 5 weeks	Gait: 10-meter walk test score

Note: AR: augmented reality; COM: center of mass; NA: not available.

elderly adults. Chen et al. [28] investigated the acute one-time effect of AR-based cognitive-motor intervention training on fall risk of the elderly. Three specific training programs were performed, including the wall dodging game, the fruit picking game, and the rats stomping game. Their results indicated that the AR-based exergame system could help to reduce the fall risk of the elderly in the long run. Jeon and Kim [29] compared the effects of an AR-based muscle reduction prevention exercise program with a control program on muscle parameters, physical performance, and exercise self-efficacy of elderly women. Subjects in the experimental group were required to perform a 30-minute AR-based aerobic and flexibility exercise 5 times a week for 12 weeks, while the exercise for the control group was not specified. They found that the AR-based exercise program is more effective in preventing muscle reduction, improving physical performance, and inducing physical activity in elderly women. The last study conducted by Chen et al. [30] is aimed at determining whether AR-assisted training with selected Tai Chi movements could be as effective as the complete traditional Tai Chi movements in increasing lower limb muscle strength and enhancing balance control. Subjects were asked to perform the selected Tai Chi movements using the AR training system or complete the 24-form Yang-style Tai Chi 30 minutes per time with 3 sessions per week for 8 weeks. The results confirmed their hypothesis that AR-assisted training with selected Tai Chi movements could be at least as effective as the complete sequence for improving muscle strength and balance control. In conclusion, all studies have confirmed the benefit of AR intervention for lower limb rehabilitation of healthy elderly adults, with favorable results found in lower limb balance, muscle strength, gait, physical performance, and fall efficacy. However, whether AR intervention could achieve greater effects on lower limb rehabilitation of healthy elderly adults when compared to the same training protocol without AR requires further investigation.

3.4. AR Intervention for Lower Limb Rehabilitation of Stroke Patients. The second set of identified studies focused on the effects of AR intervention for lower limb rehabilitation of stroke patients. The first research was performed to compare the effects of an obstacle training program with or without an AR environment on gait parameters of stroke patients [31]. Subjects completed six intervention sessions in 2 weeks in which they were asked to step over the virtual obstacle or real foam objects during a 60-minute walking training. The results found that the virtual obstacle walking training showed greater improvement in fast walk velocity, but both training methods exhibited similar effectiveness in self-selected walk velocity, stride length, and walking endurance. The following two studies employed similar AR-based interventions on stroke patients [32, 33]. The functional electrical stimulation was conducted by a functional electrical stimulator which was attached to the proximal and distal part of the tibialis anterior muscle when subjects were asked to perform ankle dorsiflexion or treadmill walking with or without an AR environment. Although the training set is slightly different, both studies found that AR-based functional electrical stimulation was more effective in improving lower limb muscle strength of stroke patients, but Kim and Lee [33] further demonstrated that functional electrical stimulation with and without AR exhibited the same improvement in balance and gait function. Lee et al. [34] and Park et al. [35] also employed similar AR-based interventions on stroke patients. Subjects of the experimental group were asked to further perform the 30-minute AR-based postural control training after the general physical therapy 3 sessions per week for 4 weeks. The AR-based training program incorporated three stages with different body positions (i.e., lying position for stage 1, sitting position for stage 2, and standing position for stage 3). The results of these two studies both demonstrated that AR-based postural control training has greater effects on gait function while no significant difference in balance between groups. The last paper conducted in 2020 is a case report focused on the effects of an AR-based parkour course on the gait function of a stroke patient with chronic minor gait impairment [36]. The subject was required to overstep obstacles during the parkour course. Their results found that the patient changed his gait pattern during the AR-based parkour course compared to the clinical gait assessments, which indicated that the AR-based intervention has the potential to provide gait rehabilitation for stroke patients. To summarize, in patients who had a stroke, AR intervention could help to improve their lower limb balance, muscle strength, and gait. However, similar to the findings of AR intervention on healthy elderly adults, the significant effects of AR training compared to non-AR one need further verification.

3.5. AR Intervention for Lower Limb Rehabilitation of Parkinson Patients. The remaining three studies all investigated the effects of AR-based interventions on gait functions of Parkinson patients. Espay et al. [37] investigated the effects of at-home walking training with a closed-loop AR cueing device on the gait function of Parkinson patients, and they found that the 30-minute training twice daily for 2 weeks enhanced walking velocity and stride length. Palacios-Navarro et al. [38] aimed to determine the effects of an AR-based mole stomping game on the gait function of Parkinson patients, and they also found that the 30-minute game with 4 sessions per week for 5 weeks is effective to improve the completion time score and walk function. However, some conflicting and equivocal results have been proposed by Janssen et al. [39]. In their study, the acute effects of AR-based visual cues on freezing of gait and turning in place of Parkinson patients were assessed, and the results showed that the AR-based visual cues did not reduce freezing of gait and even worsen some gait kinematics and turning in place. They speculated that the insufficient AR-based visual cues, influences of smart glasses, and subjects' unfamiliarity with the training could all be associated with the detrimental effects. According to the results obtained, the benefit of AR intervention for gait function of Parkinson patients is still conflicting, and more studies in this field are warranted.

4. Discussion

This systematic review summarized and analyzed previous studies that explored the effects of AR-based interventions

on lower limb rehabilitation, with the aim to determine whether it could contribute significant benefits to the larger population and further reveal its potential applications to further enhance lower limb rehabilitation.

According to the results of this study, the significant effects of AR-based interventions on lower limb rehabilitation have been initially confirmed. To be specific, the AR-based interventions have currently been conducted for elderly adults, stroke patients, and Parkinson patients. Favorable results were achieved in dynamic balance, gait spatiotemporal variables, gait kinematics, muscle mass, muscle activation, muscle force, physical performance, and fall efficacy. Nevertheless, one study that investigated the effects of an AR-based system on gait function and turning in place of Parkinson patients did not come out with any positive results when compared to the preintervention; they demonstrated that the insufficient cues, influences of AR glasses, and subjects' unfamiliarity with the training could be the main reasons for this controversy [39]. In addition, it is worth mentioning that some studies obtained no significant differences in lower limb rehabilitation after AR treatments when compared to the same interventions only without AR or conventional training programs [27, 30, 33]. In other words, interventions with or without AR seem to provide similar rehabilitation benefits. Chen et al. [30] investigated the effects of AR-assisted training with selected Tai Chi movements on lower limb muscle strength and balance control, and their results found that AR-assisted training with selected Tai Chi movements achieved similar effects with the complete sequence. Ku et al. [27] investigated the effects of a 3D interactive AR program on balance and gait function of the elderly, while only balance was found significant when compared to the conventional physical fitness program, and they speculated that the balance improvement is only because of motor learning mechanism. Overall, this review adds support to previous studies indicating that patients could benefit from AR-based rehabilitation intervention, at least the same as the conventional program. However, given the small sample size included in these studies, more research with a larger sample size is much warranted for further verification.

There is great variability in AR-based training programs evaluated in these included studies, which on one hand makes it hard to determine a general intervention that could contribute benefits to the larger population, while on the other hand, it is supported that AR can provide the opportunities to extend beyond rote rehabilitation training by adding more exercises that is highly related to daily living. Based on the needs and actual motor functions of the patients, an appropriate AR intervention mode could be further designed [18]. In terms of the intervention time setting, it ranged from only one session to 5 sessions per week for 12 weeks, while a thorough examination of these included trials found that 30 or 60 min per session at 3 to 5 times per week for a total of 8 to 12 weeks was the most frequently used setting. The intensity and duration of AR training can be further modified based on the patients' motor condition during the rehabilitation process [18]. Nevertheless, the diverse AR treatments may indicate that this technology is still in the early stage of clinical application, and some drawbacks of AR intervention should be resolved to promote better rehabilitation outcomes. Firstly, although the wearable AR device has a strong sense of immersion and can bring real-time interaction, the induced side effects during and after the intervention (i.e., nausea and fatigue) may reduce the enthusiasm of patients for training. Moreover, some technological or user interface shortcomings may also limit its clinical applications. For example, it is currently impossible to apply the AR system in an unprepared environment since this technology relies on tracking methods in the prepared environment [19].

Two potential limitations that existed should be noted here. Firstly, it is in some cases difficult to compare these findings statistically such as performing a meta-analysis since the homogeneity of instruments, measurement scales, and units applied in these included studies was relatively limited [40, 41]. Moreover, there are limited numbers of studies that were available, while it becomes much fewer after being divided into different categories by the types of participants, which might impact the integration of the results.

5. Conclusions

Based on the results of this literature review, it was found that AR-based interventions have been applied for the lower limb rehabilitation of balance, gait, muscle, physical performance, and fall efficacy of the elderly, stroke, and Parkinson patients. Favorable results were achieved at least the same as the interventions without AR except for the turning and timing in the freezing of gait of Parkinson patients. However, given the infancy of this technology in clinical practices, more robust trials with larger sample sizes and greater homogeneity in terms of devices and treatment settings are warranted for further verification. On the other hand, it is proposed that the future development of AR systems should focus on the following several aspects to make it widespread in the motor rehabilitation field. First, some high technologies such as artificial intelligence should be integrated into the AR rehabilitation systems as they can accurately track patients' progress and intelligently adapt the training programs based on their feedback. Moreover, the development of an AR-based system on mobile devices could contribute to more benefits because it can realize the remote monitoring of patients' recovery and provide real-time attention with lower costs. Finally, more game-based rehabilitation content targeted at different populations would also be of interest for AR systems as it may further improve the users' motivation.

Data Availability

The data used to support the findings of this study are included within the article.

Conflicts of Interest

The authors declare that there is no conflict of interest regarding the publication of this paper.

References

[1] V. Patil, J. Narayan, K. Sandhu, and S. K. Dwivedy, "Integration of virtual reality and augmented reality in physical rehabilitation: a state-of-the-art review," in *Revolutions Prod des Healthc*, K. Subburaj, K. Sandhu, and S. Ćuković, Eds., pp. 177–205, Springer Singapore, 2022.

[2] D. Cooper, R. Kavanagh, J. Bolton, C. Myers, and S. O'Connor, ""Prime time of life", a 12-week home-based online multimodal exercise training and health education programme for middle-aged and older adults in Laois," *Physical Activity and Health*, vol. 5, no. 1, pp. 178–194, 2021.

[3] M. Fiani, A. Dutilloy, M. Ariza, V. Hulot, and M. Gignon, "Effects of a therapeutic patient education network on the glycated hemoglobin and body mass index in 59 patients with type 2 diabetes mellitus: a retrospective study from 2013 to 2018," *Physical Activity and Health*, vol. 5, no. 1, pp. 229–235, 2021.

[4] H. Fan, Y. Song, X. Cen, P. Yu, I. Bíró, and Y. Gu, "The effect of repetitive transcranial magnetic stimulation on lower-limb motor ability in stroke patients: a systematic review," *Frontiers in Human Neuroscience*, vol. 15, article 620573, 2021.

[5] A. S. Nascimento, C. V. Fagundes, F. A. S. dos Mendes, and J. C. Leal, "Effectiveness of virtual reality rehabilitation in persons with multiple sclerosis: a systematic review and meta-analysis of randomized controlled trials," *Multiple Sclerosis and Related Disorders*, vol. 54, p. 103128, 2021.

[6] D. Sun, Y. Song, X. Cen, M. Wang, J. S. Baker, and Y. Gu, "Workflow assessing the effect of Achilles tendon rupture on gait function and metatarsal stress: combined musculoskeletal modeling and finite element analysis," *Journal of Engineering in Medicine*, vol. 236, no. 5, pp. 676–685, 2022.

[7] L. Li, F. Yu, D. Shi et al., "Application of virtual reality technology in clinical medicine," *American Journal of Translational Research*, vol. 9, no. 9, pp. 3867–3880, 2017.

[8] J.-H. Shin, H. Ryu, and S. H. Jang, "A task-specific interactive game-based virtual reality rehabilitation system for patients with stroke: a usability test and two clinical experiments," *Journal of Neuroengineering and Rehabilitation*, vol. 11, no. 1, p. 32, 2014.

[9] Z. Y. S. Chan, A. J. C. MacPhail, I. P. H. Au et al., "Walking with head-mounted virtual and augmented reality devices: effects on position control and gait biomechanics," *PLoS One*, vol. 14, no. 12, article e0225972, 2019.

[10] E. A. Keshner and J. Fung, "The quest to apply VR technology to rehabilitation: tribulations and treasures," *Journal of Vestibular Research*, vol. 27, no. 1, pp. 1–5, 2017.

[11] M. K. Holden, "Virtual environments for motor rehabilitation: review," *Cyberpsychology & Behavior*, vol. 8, no. 3, pp. 187–211, 2005.

[12] H. Pallesen, M. B. Andersen, G. M. Hansen, C. B. Lundquist, and I. Brunner, "Patients' and health professionals' experiences of using virtual reality technology for upper limb training after stroke: a qualitative substudy," *Rehabilitation Research and Practice*, vol. 2018, Article ID 4318678, 2018.

[13] K. E. Laver, B. Lange, S. George, J. E. Deutsch, G. Saposnik, and M. Crotty, "Virtual reality for stroke rehabilitation," *Cochrane Database of Systematic Reviews*, vol. 11, p. CD008349, 2018.

[14] M. C. Howard, "A meta-analysis and systematic literature review of virtual reality rehabilitation programs," *Computers in Human Behavior*, vol. 70, pp. 317–327, 2017.

[15] G. Saposnik, L. G. Cohen, M. Mamdani et al., "Efficacy and safety of non-immersive virtual reality exercising in stroke rehabilitation (EVREST): a randomised, multicentre, single-blind, controlled trial," *Lancet Neurology*, vol. 15, no. 10, pp. 1019–1027, 2016.

[16] N. Norouzi-Gheidari, A. Hernandez, P. S. Archambault, J. Higgins, L. Poissant, and D. Kairy, "Feasibility, safety and efficacy of a virtual reality exergame system to supplement upper extremity rehabilitation post-stroke: a pilot randomized clinical trial and proof of principle," *International Journal of Environmental Research and Public Health*, vol. 17, no. 1, p. 113, 2020.

[17] C. Gorman and L. Gustafsson, "The use of augmented reality for rehabilitation after stroke: a narrative review," *Disability and Rehabilitation. Assistive Technology*, vol. 17, no. 4, pp. 1–9, 2020.

[18] H. L. Phan, T. H. Le, J. M. Lim, C. H. Hwang, and K. I. Koo, "Effectiveness of augmented reality in stroke rehabilitation: a meta-analysis," *Applied Sciences*, vol. 12, no. 4, p. 1848, 2022.

[19] M. J. V. Gil, G. Gonzalez-Medina, D. Lucena-Anton, V. Perez-Cabezas, R.-M. M. Del Carmen, and R. Martín-Valero, "Augmented reality in physical therapy: systematic review and meta-analysis," *JMIR Serious Games*, vol. 9, pp. 1–20, 2021.

[20] H. Mousavi Hondori, M. Khademi, L. Dodakian, S. C. Cramer, and C. V. Lopes, "A spatial augmented reality rehab system for post-stroke hand rehabilitation," *Studies in Health Technology and Informatics*, vol. 184, pp. 279–285, 2013.

[21] J. Negrillo-Cárdenas, J.-R. Jiménez-Pérez, and F. R. Feito, "The role of virtual and augmented reality in orthopedic trauma surgery: from diagnosis to rehabilitation," *Computer Methods and Programs in Biomedicine*, vol. 191, article 105407, 2020.

[22] R. M. Viglialoro, S. Condino, G. Turini, M. Carbone, V. Ferrari, and M. Gesi, "Review of the augmented reality systems for shoulder rehabilitation," *Information*, vol. 10, no. 5, p. 154, 2019.

[23] G. A. de Assis, A. G. D. Corrêa, M. B. R. Martins, W. G. Pedrozo, and R. de Lopes, "An augmented reality system for upper-limb post-stroke motor rehabilitation: a feasibility study," *Disability and Rehabilitation. Assistive Technology*, vol. 11, pp. 521–528, 2016.

[24] H. Yoo, E. Chung, and B. H. Lee, "The effects of augmented reality-based Otago exercise on balance, gait, and falls efficacy of elderly women," *Journal of Physical Therapy Science*, vol. 25, no. 7, pp. 797–801, 2013.

[25] J. Lee, H. N. Yoo, and B. H. Lee, "Effects of augmented reality-based Otago exercise on balance, gait, and physical factors in elderly women to prevent falls: a randomized controlled trial," *Journal of Physical Therapy Science*, vol. 29, no. 9, pp. 1586–1589, 2017.

[26] D. J. Im, J. Ku, Y. J. Kim et al., "Utility of a three-dimensional interactive augmented reality program for balance and mobility rehabilitation in the elderly: a feasibility study," *Annals of Rehabilitation Medicine*, vol. 39, no. 3, pp. 462–472, 2015.

[27] J. Ku, Y. J. Kim, S. Cho, T. Lim, H. S. Lee, and Y. J. Kang, "Three-dimensional augmented reality system for balance and mobility rehabilitation in the elderly: a randomized controlled trial," *Cyberpsychology, Behavior, and Social Networking*, vol. 22, no. 2, pp. 132–141, 2019.

[28] M. Chen, Q. Tang, S. Xu, P. Leng, and Z. Pan, "Design and evaluation of an augmented reality-based exergame system to reduce fall risk in the elderly," *International Journal of*

Environmental Research and Public Health, vol. 17, no. 19, p. 7208, 2020.

[29] S. Jeon and J. Kim, "Effects of augmented-reality-based exercise on muscle parameters, physical performance, and exercise self-efficacy for older adults," *International Journal of Environmental Research and Public Health*, vol. 17, no. 9, p. 3260, 2020.

[30] P. J. Chen, I. W. Penn, S. H. Wei, L. R. Chuang, and W. H. Sung, "Augmented reality-assisted training with selected tai-chi movements improves balance control and increases lower limb muscle strength in older adults: a prospective randomized trial," *Journal of Exercise Science and Fitness*, vol. 18, no. 3, pp. 142–147, 2020.

[31] D. L. Jaffe, D. A. Brown, C. D. Pierson-Carey, E. L. Buckley, and H. L. Lew, "Stepping over obstacles to improve walking in individuals with poststroke hemiplegia," *Journal of Rehabilitation Research and Development*, vol. 41, no. 3, pp. 283–292, 2004.

[32] G. U. Jung, T. H. Moon, G. W. Park, J. Y. Lee, and B. H. Lee, "Use of augmented reality-based training with EMG-triggered functional electric stimulation in stroke rehabilitation," *Journal of Physical Therapy Science*, vol. 25, no. 2, pp. 147–151, 2013.

[33] I. C. Kim and B. H. Lee, "Effects of augmented reality with functional electric stimulation on muscle strength, balance and gait of stroke patients," *Journal of Physical Therapy Science*, vol. 24, no. 8, pp. 755–762, 2012.

[34] C. H. Lee, Y. Kim, and B. H. Lee, "Augmented reality-based postural control training improves gait function in patients with stroke: randomized controlled trial," *Hong Kong Physiotherapy Journal*, vol. 32, no. 2, pp. 51–57, 2014.

[35] Y. H. Park, C. H. Lee, and H. J. Kim, "A pilot study of augmented reality-based postural control training in stroke rehabilitation," *Physical Therapy Rehabilitation Science*, vol. 3, no. 1, pp. 13–19, 2014.

[36] J. P. O. Held, K. Yu, C. Pyles et al., "Augmented reality-based rehabilitation of gait impairments: case report," *JMIR mHealth and uHealth*, vol. 8, no. 5, pp. 1–10, 2020.

[37] A. J. Espay, Y. Baram, A. K. Dwivedi et al., "At-home training with closed-loop augmented-reality cueing device for improving gait in patients with Parkinson disease," *Journal of Rehabilitation Research and Development*, vol. 47, no. 6, pp. 573–581, 2010.

[38] G. Palacios-Navarro, I. García-Magariño, and P. Ramos-Lorente, "A Kinect-based system for lower limb rehabilitation in Parkinson's disease patients: a pilot study," *Journal of Medical Systems*, vol. 39, no. 9, p. 103, 2015.

[39] S. Janssen, J. de Ruyter van Steveninck, H. S. Salim et al., "The effects of augmented reality visual cues on turning in place in Parkinson's disease patients with freezing of gait," *Frontiers in Neurology*, vol. 11, pp. 1–9, 2020.

[40] J. Ying, X. Cen, and P. Yu, "Effects of eccentric exercise on skeletal muscle injury: from an ultrastructure aspect: a review," *Physical Activity and Health*, vol. 5, no. 1, pp. 15–20, 2021.

[41] Y. Song, F. Ren, D. Sun et al., "Benefits of exercise on influenza or pneumonia in older adults: a systematic review," *International Journal of Environmental Research and Public Health*, vol. 17, no. 8, p. 2655, 2020.

Hindawi
Applied Bionics and Biomechanics
Volume 2022, Article ID 9704862, 7 pages
https://doi.org/10.1155/2022/9704862

Research Article

Febuxostat Improves Uric Acid Levels and Renal Function in Patients with Chronic Kidney Disease and Hyperuricemia: A Meta-Analysis

Yanqun Zheng and Jia Sun

Nephrology Department, First People's Hospital of Linping District, Hangzhou, China

Correspondence should be addressed to Yanqun Zheng; 1433301472@qq.com

Received 29 May 2022; Revised 7 June 2022; Accepted 18 June 2022; Published 8 July 2022

Academic Editor: Yaodong Gu

Background. Uric acid nephropathy, also known as hyperuricemia nephropathy or gouty nephropathy, is characterized by uric acid crystal deposition and inflammatory cell infiltration. Herein, we aimed to demonstrate the role of febuxostat on uric acid levels and renal function in patients with chronic kidney disease and hyperuricemia. *Methods*. Eight databases included were searched for clinical randomized controlled trials. Meanwhile, the confidence interval (CI) of either relative risk or mean difference was set to 95%. Besides, the heterogeneity of the research results is tested by I^2. *Results*. Ten studies were ultimately included in this meta-analysis. All of them were considered to be random controlled trials. 10 studies reported the serum uric acid of the test group and the control group, which was significantly lower (SMD: -146.44, 95% Cl: -195.96, -86.93, and $P < 0.01$) than the control group, EGFR (SMD: 3.21, 95% Cl: 1.17, 5.25, and $P < 0.01$), serum creatinine (SMD: -15.27, 95% Cl: -20.75, -9.79, and $P < 0.01$), serum urea nitrogen (SMD: -2.37, 95% Cl: -3.31, -1.61, and $P < 0.01$), and adverse reactions (OR: 0.74, 95% Cl: 0.32, 1.68, and $P = 0.47$). *Conclusion*. The results of this study suggest that febuxostat may be effective in patients with CKD with HUA, as evidenced by serum uric acid, creatinine, urea nitrogen, and EGFR. However, large sample, multicenter, low risk of bias clinical studies, as well as basic medical research, are needed.

1. Introduction

Hyperuricemia (HUA), commonly defined in the literature as serum uric acid (sUA) levels above 6 mg/dl [1], has a prevalence of 21% in the United States [2]. It is associated with a higher risk of high blood pressure, coronary artery disease, and stroke [3]. HUA is associated with the pathophysiology of kidney disease, making clinical research an active research interest [4, 5].

Previous meta-analyses have shown that HUA is a risk factor for the development of chronic kidney disease (CKD) and incidental kidney disease, including end-stage renal disease, albuminuria, or elevated serum creatinine [6]. Rodenbach et al. [7] conducted a 5-year cross-sectional study, and the results showed that the HUA group of CKD children had a worse prognosis than the normal serum uric acid group. It was reported that more than 70% of HUA patients suffered from different degrees of HUA. 36.3% of patients tend to have renal failure [8]. Another study showed that nearly 0.6% to 1.0% of patients with renal failure were caused by gout. A New Zealand report showed that the patients who died due to gouty nephropathy can account for 16% to 27% of the patients who died due to gout complications [9].

Febuxostat is a novel xanthine oxidase-selective inhibitor that inhibits both xanthine oxidase and xanthine dehydrogenase activities and reduces blood urate concentrations [10]. Febuxostat is mainly metabolized by the liver into inactive metabolites, which can be completely excreted from the body. Therefore, the metabolic process is less affected by renal function, and its renal toxicity is also mild. To a certain extent, it can improve renal

function and reduce serum creatinine [11, 12]. Thus, we conducted a meta-analysis to examine the efficacy and safety of febuxostat in patients with CKD with HUA.

2. Materials and Methods

2.1. Eligibility Criteria

2.1.1. Study Design. All randomized controlled trials (RCTs) investigating febuxostat combined with other therapies in the treatment of CKD with HUA were not limited by language or publication status.

2.1.2. Research Object. This includes patients with CKD with HUA, with no recent history of drug therapy such as febuxostat and allopurinol.

2.1.3. Intervention Measures. The experimental group was treated with febuxostat or febuxostat in combination with other therapies for intervention, and the control group was treated with nonfebuxostat, including allopurinol or placebo therapy. In addition, the following exclusion criteria were applied: ① nonrandomized controlled trial research literature, ② literature that did not report febuxostat as an intervention measure, ③ literature without original data or incomplete research data, ④ inconsistent outcome indicators or statistical methods, and ⑤ literature review or animal experiment research.

2.1.4. Outcome Indicators. Through the review of clinical trials published in major databases and academic journals to evaluate CKD with HUA, we found that the commonly used evaluation indicators include the following: ① serum uric acid, ② EGFR, ③ serum creatinine, ④ serum urea nitrogen, and ⑤ adverse reactions.

2.2. Search Strategy. We searched PubMed, Embase, Cochrane Library, Web of Science, Wan-Fang database, China National Knowledge Infrastructure (CNKI), Chinese Scientific Journals Database (VIP), and CBM Libraries for relevant randomized controlled trials in each database from March 2012 up to March 2022. For English databases, we used free text terms such as "febuxostat" or "chronic kidney disease" or "hyperuricemia." For the Chinese databases, it is suggested the search terms could be presented using the Chinese phonetic alphabet.

2.3. Literature Screening and Data Extraction. Two researchers conducted literature screening independently in strict accordance with inclusion and exclusion criteria. Then, they managed and identified the retrieved literature by the NoteExpress software (v.2.7.1). After picking, researchers read the topic and abstract for preliminary screening and then further read the full text for rescreening to determine whether to include and extract valid data, respectively, to establish Excel effective data extraction table. In case of disagreement, a third researcher shall be invited to solve the disagreement through consultation.

2.4. Statistical Analysis. The Stata 15.1 software was used to perform the meta-analysis. If for the binary classification variables using relative risk (RR), said the confidence interval (CI) is set to 95%. Continuity variables were represented by mean difference (MD), and confidence interval (CI) was set at 95%. Heterogeneity of research results was tested by I^2. If $I^2 \leq 50\%$, outcome data of fixed effects model (FE) were selected for analysis; if $I^2 > 50\%$, outcome data of random effects model (RE) were selected for reference analysis. At the same time, sensitivity analysis was used to observe heterogeneous sources and evaluate the stability of meta-analysis results.

3. Results

3.1. Search Results. Based on the search strategy, 631 references were identified. After excluding duplicate studies, 306 studies were scanned based on abstract and title. Then, 12 articles were evaluated in full text. After full text evaluation, 2 records were excluded for the following reasons: data mismatch ($n = 1$) and missing data ($n = 1$). Ultimately, 10 studies [13–16] were included in this meta-analysis (Table 1). The PRISMA statement flow chart shows this process (Figure 1).

3.2. Serum Uric Acid. Six studies reported the serum uric acid of the test group and the control group. Meta-analysis showed that the serum uric acid of the test group was significantly lower (SMD: -146.44, 95% Cl: -195.96, -86.93, and $P < 0.01$, Figure 2) than the control group. The results of all these trials showed high heterogeneity, and thus, a sensitivity analysis was conducted (Figure 3). Compared with the control group, febuxostat significantly reduces the level of uric acid in patients with CKD.

3.3. EGFR. Six studies reported the EGFR of the test group and the control group. Meta-analysis showed that the EGFR of the test group was significantly higher (SMD: 3.21, 95% Cl: 1.17, 5.25, and $P < 0.01$, Figure 4) than the control group. Compared with the control group, febuxostat significantly improves the EGFR level in patients with CKD and HUA.

3.4. Serum Creatinine. Six studies reported the serum creatinine of the test group and the control group. Meta-analysis showed that the serum creatinine of the test group was significantly lower (SMD: -15.27, 95% Cl: -20.75, -9.79, and $P < 0.01$, Figure 5) than the control group.

3.5. Serum Urea Nitrogen. Seven studies reported the serum urea nitrogen of the test group and the control group. Meta-analysis showed that the serum urea nitrogen of the test group was significantly lower (SMD: -2.37, 95% Cl: -3.31, -1.61, and $P < 0.01$, Figure 6) than the control group.

3.6. Adverse Reactions. Seven studies reported the adverse reactions of the test group and the control group. Meta-analysis showed that there was no significant difference in the adverse reactions between the test group and the control group (OR: 0.74, 95% Cl: 0.32, 1.68, and $P = 0.47$, Figure 7).

Table 1: Baseline characteristics.

Study (ref.)	Sample size (*T*/*C*)	Man/woman	Age (years) (mean ± SD) (*T*/*C*)	*T*	*C*	Outcomes
Huang 2018 [14]	42/41	27/14	61.97 ± 3.12	Febuxostat	Placebo	①③④⑤
Sircar 2015 [15]	45/48	66/27	56.22 ± 9.83/61.83 ± 12.00	Febuxostat	Placebo	②⑤
Zhang 2021 (1) [16]	36/30	41/25	80.13 ± 9.67	Febuxostat	Placebo	①②③④⑤
Zhao 2021 [17]	41/41	47/35	68.45 ± 5.20/68.56 ± 5.29	Febuxostat	Placebo	①③④⑤
Sezai 2015 [18]	56/53	85/24	69.4 ± 10.0/69.1 ± 9.2	Febuxostat	Allopurinol	②
Tanaka 2015 [19]	21/19	35/5	70.1 ± 9.5/66.1 ± 7.0	Febuxostat	Allopurinol	②
Zhang 2021 (2) [20]	27/27	31/23	51.58 ± 1.45/51.56 ± 1.44	Febuxostat	Allopurinol	①③④⑤
Zhu 2018 [21]	32/32	NA	NA	Febuxostat	Allopurinol	①③④⑤
Zhang 2021 (3) [22]	67/67	66/68	55.1 ± 9.4/54.2 ± 8.4	Febuxostat	Allopurinol	①②③④⑤
Wang 2022 [23]	69/69	96/42	81.35 ± 2.52/81.40 ± 2.49	Febuxostat	Allopurinol	①②④⑤

①: serum uric acid; ②: EGFR; ③: serum creatinine; ④: serum urea nitrogen; ⑤: adverse reactions.

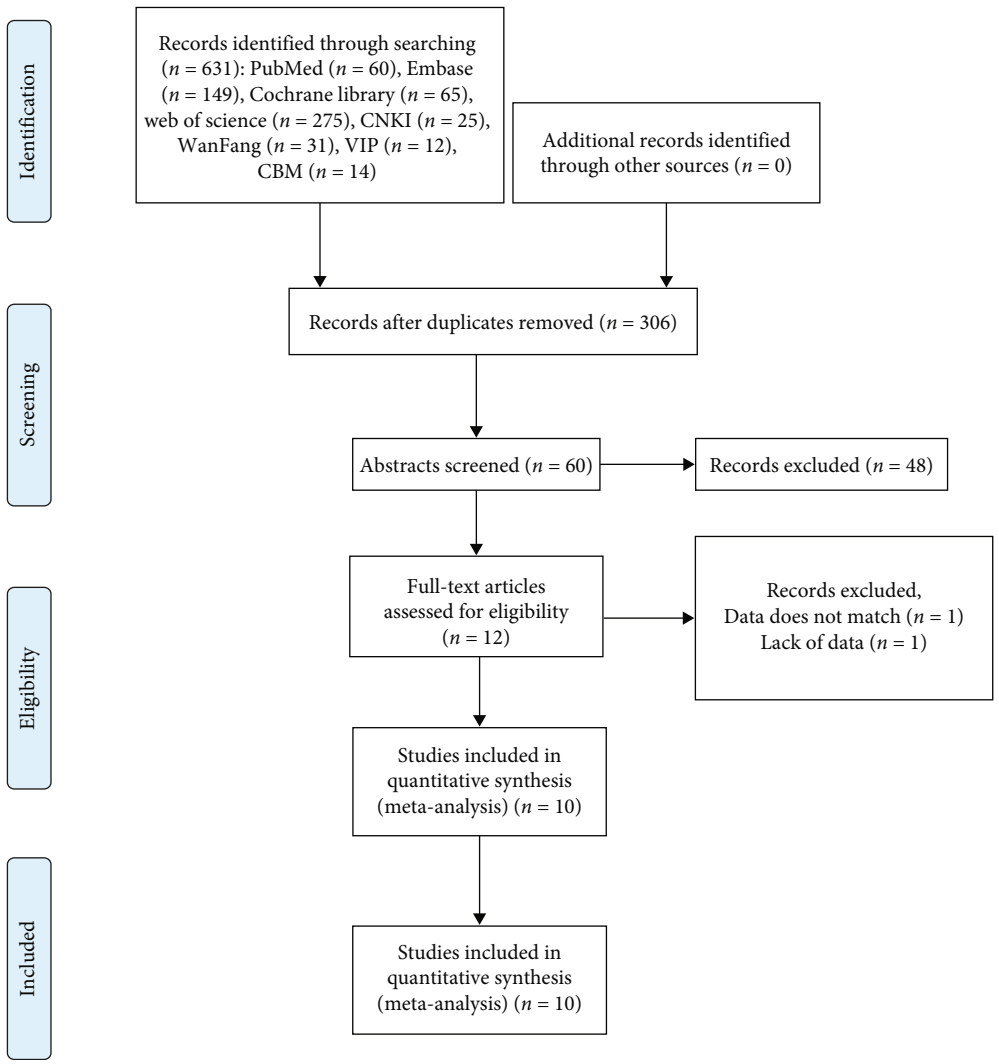

Figure 1: Flow chart.

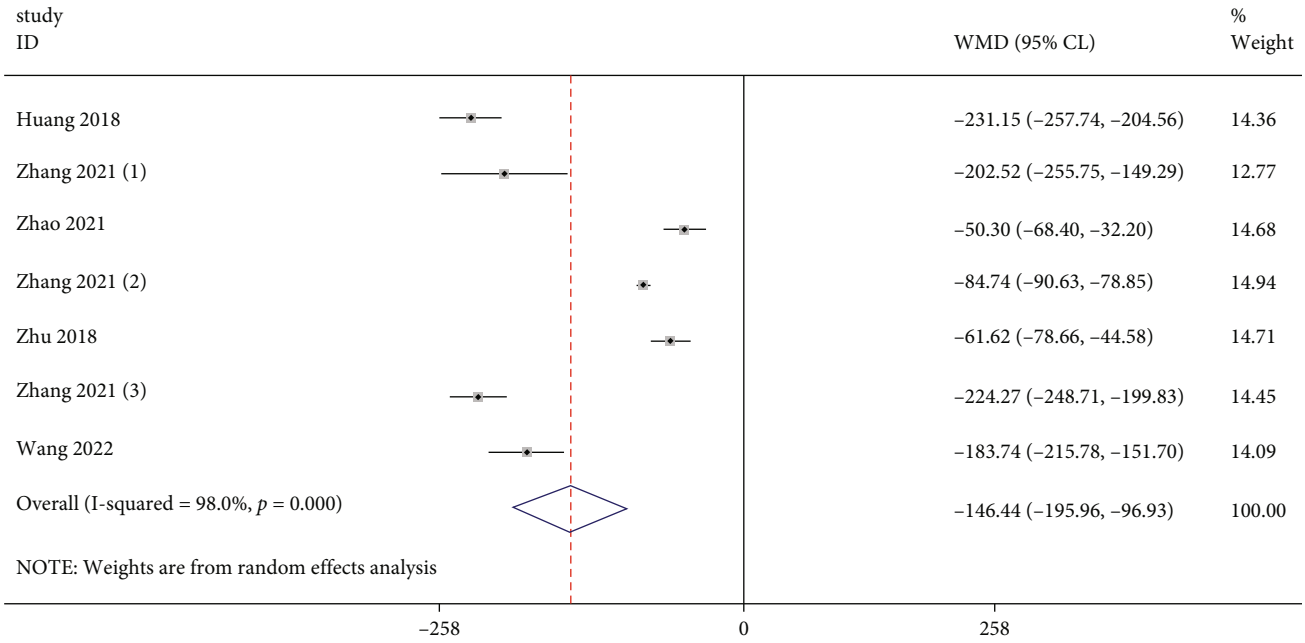

Figure 2: Forest illustration of the serum uric acid.

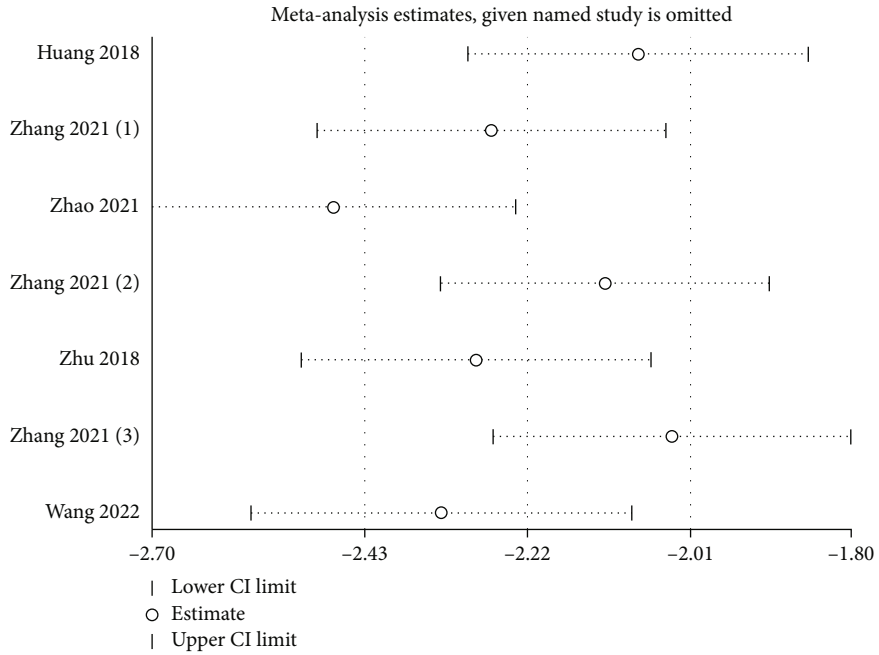

Figure 3: Sensitivity analysis of the serum uric acid.

4. Discussion

Uric acid nephropathy is also known as hyperuricemia nephropathy or gouty nephropathy, and the main pathological changes are the renal pathological changes caused by uric acid crystal deposition and inflammatory cell infiltration are mainly manifested as interstitial nephritis and impaired renal tubular function and structure [17]. According to its pathological changes and clinical manifestations, it is mainly divided into 3 types: chronic uric acid nephropathy, acute uric acid nephropathy, and uric acid nephrolithiasis.

Uric acid is produced by the metabolism of DNA and/or RNA in the body and serves as the final product of purine metabolism. The product is excreted. Since humans lack urate oxidase and cannot decompose it into soluble allantoin, they are prone to hyperuricemia. Uric acid mainly comes from two ways: internal and external, of which endogenous accounts for 80%, which is synthesized by nucleic acid

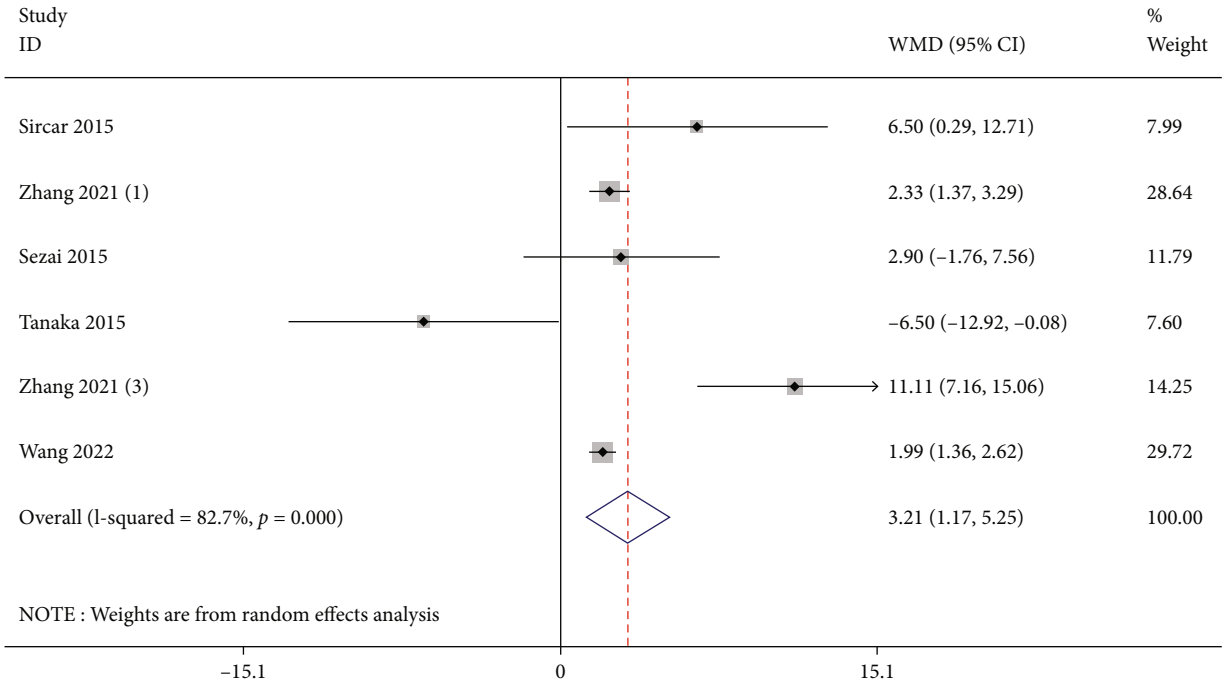

Figure 4: Forest illustration of the EGFR.

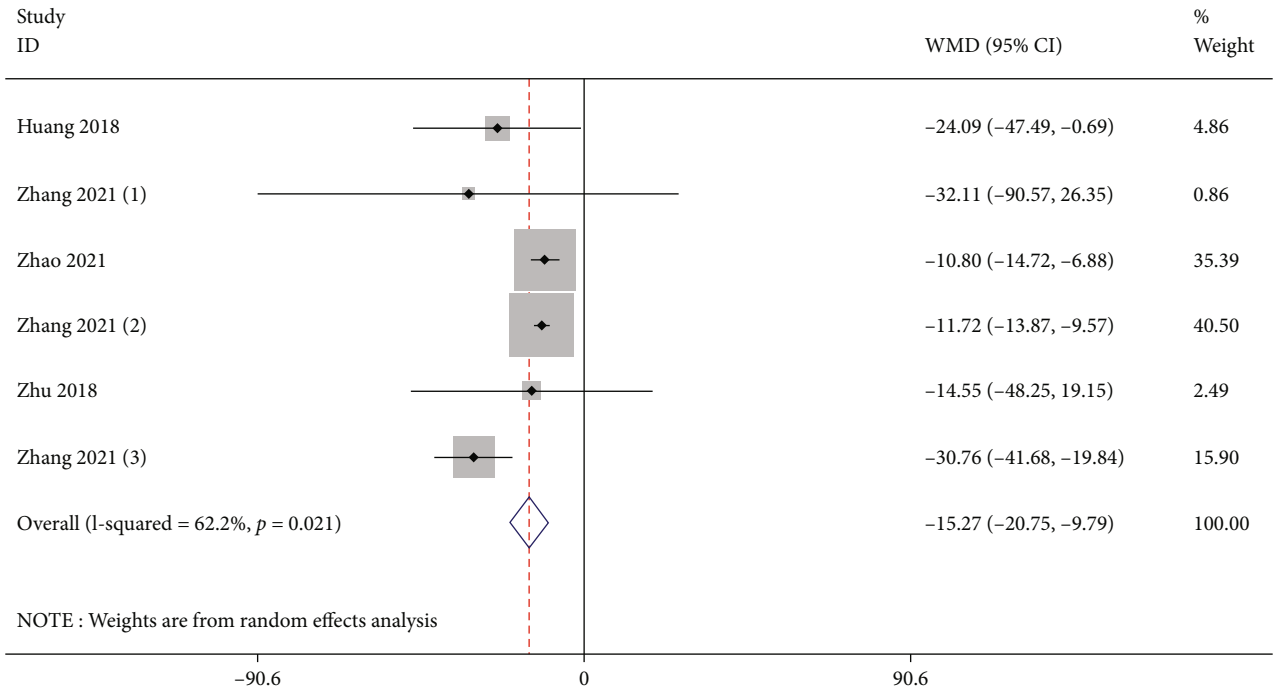

Figure 5: Forest illustration of the serum creatinine.

decomposition and amino acid, phosphoribosyl, etc. Nucleic acid protein food is decomposed. Uric acid is mainly excreted by the kidneys and intestines, of which 75% is excreted through the kidneys, and the rest is excreted after being degraded by microorganisms in the intestines [15, 18–20].

A total of 10 literatures were included in this study, including 436 patients in the experimental group and 427 in the control group. Meta-analysis showed that patients with CKD with HUA who received febuxostat had lower serum uric acid compared with controls. Meta-analysis showed satisfactory serum uric acid level for the experimental group (SMD: -146.44, 95% Cl: -195.96, -86.9, and $P < 0.01$). Based on the results of the meta-analysis of EGFR, compared with the control group, febuxostat significantly

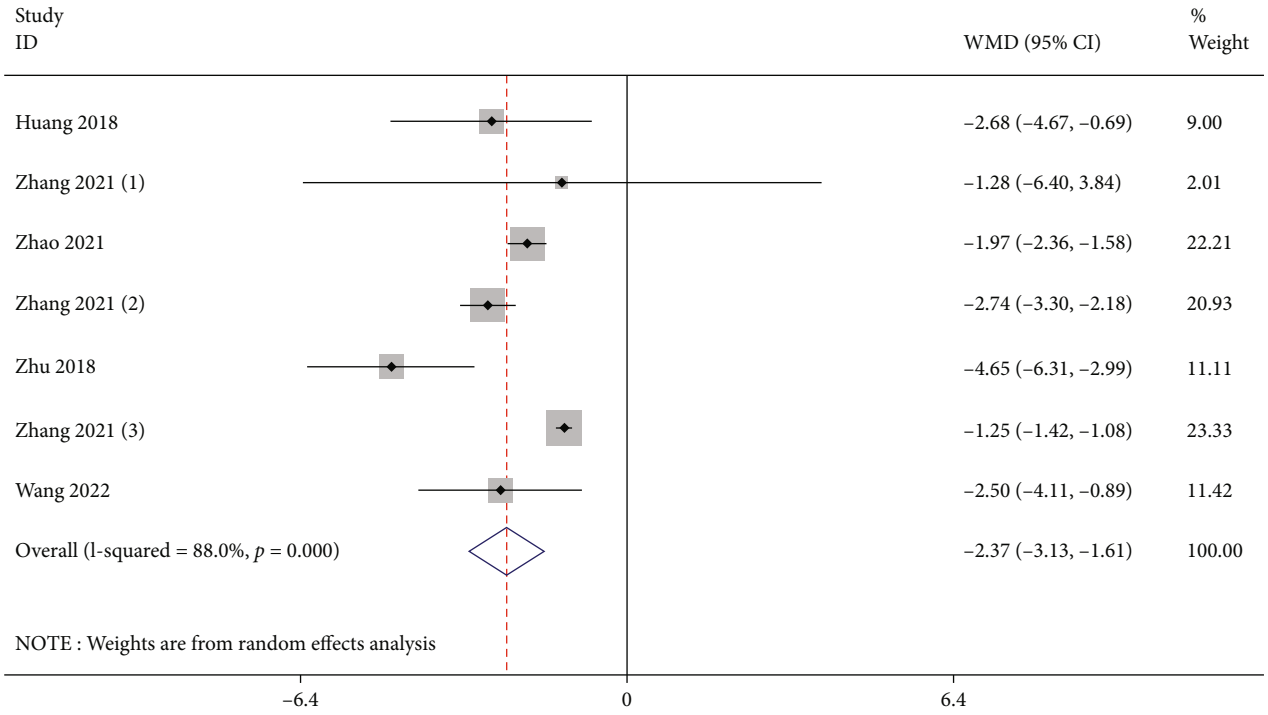

Figure 6: Forest illustration of the serum urea nitrogen.

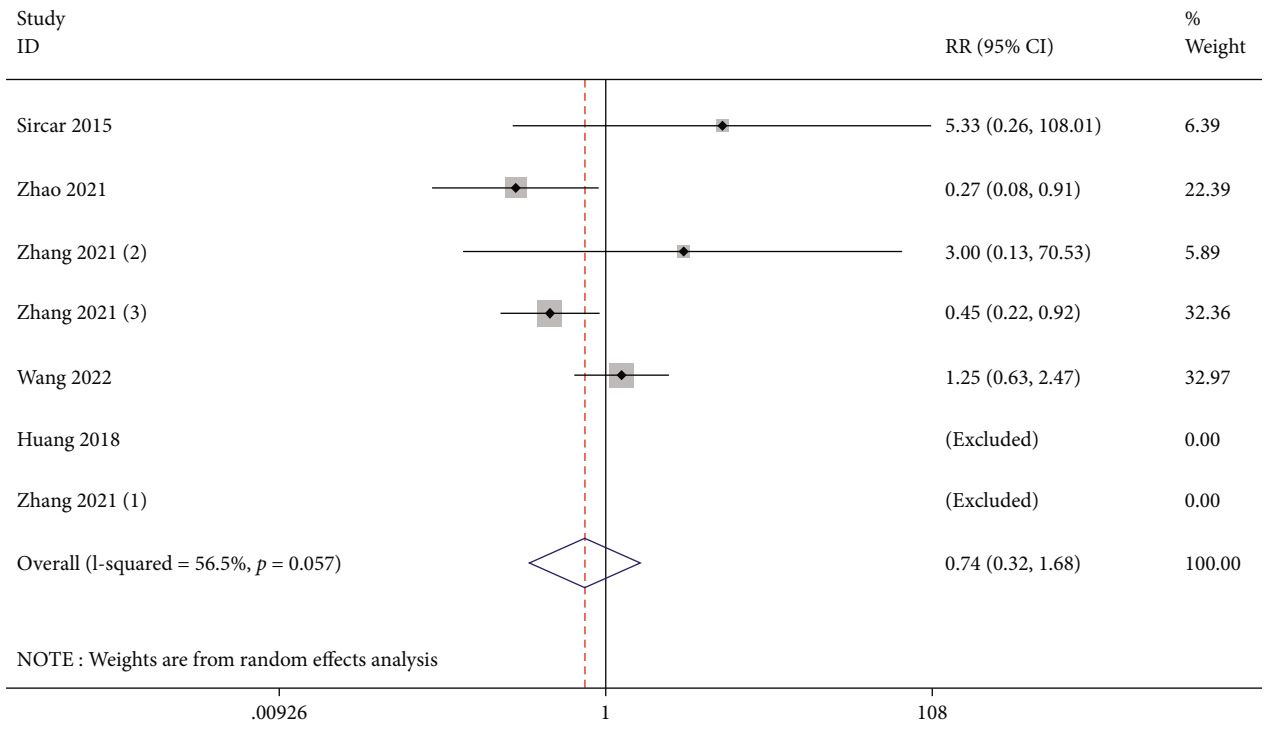

Figure 7: Forest illustration of the adverse reactions.

improves the EGFR level in patients with CKD with HUA (SMD: 3.21, 95% Cl: 1.17, 5.25, and $P < 0.01$). For the results of the meta-analysis of urine creatinine and urea nitrogen, compared with the control group, febuxostat significantly reduces the level of urine creatinine and urea nitrogen in patients with CKD with HUA (SMD: -15.27, 95% Cl: -20.75, -9.79, and $P < 0.01$ and SMD: -2.37, 95% Cl: -3.31, -1.61, and $P < 0.01$). There was no statistical difference in

adverse reactions between the control group and the observation group after treatment (OR: 0.74, 95% Cl: 0.32, 1.68, and $P = 0.47$).

This study also has certain limitations. First, 10 RCTs included 863 patients. The overall sample size is not very large. All RCTs were single-center. The lack of multicenter studies may affect the representativeness of the conclusions to some extent. Second, the small sample size is not sufficient to fully assess the safety of febuxostat or other drugs.

5. Conclusion

The results of this study suggest that febuxostat may be effective in patients with CKD with HUA, as evidenced by serum uric acid, creatinine, urea nitrogen, and EGFR. However, large sample, multicenter, low risk of bias clinical studies, as well as basic medical research, are needed.

Data Availability

The data could be obtained by contacting the corresponding author.

Conflicts of Interest

The authors declare that they have no conflicts of interest.

References

[1] T. Bardin and P. Richette, "Definition of hyperuricemia and gouty conditions," *Current Opinion in Rheumatology*, vol. 26, no. 2, pp. 186–191, 2014.

[2] Y. Zhu, B. J. Pandya, and H. K. Choi, "Comorbidities of gout and hyperuricemia in the US general population: NHANES 2007-2008," *The American journal of medicine*, vol. 125, no. 7, pp. 679–687.e1, 2012.

[3] Y. Zhu, B. J. Pandya, and H. K. Choi, "Prevalence of gout and hyperuricemia in the US general population: the National Health and Nutrition Examination Survey 2007-2008," *Arthritis and Rheumatism*, vol. 63, no. 10, pp. 3136–3141, 2011.

[4] L. G. Sanchez-Lozada, E. Tapia, C. Avila-Casado et al., "Mild hyperuricemia induces glomerular hypertension in normal rats," *American Journal of Physiology. Renal Physiology*, vol. 283, no. 5, pp. F1105–F1110, 2002.

[5] L. G. Sanchez-Lozada, E. Tapia, V. Soto et al., "Treatment with the xanthine oxidase inhibitor febuxostat lowers uric acid and alleviates systemic and glomerular hypertension in experimental hyperuricaemia," *Nephrology, Dialysis, Transplantation*, vol. 23, no. 4, pp. 1179–1185, 2007.

[6] M. T. James, A. S. Levey, M. Tonelli et al., "Incidence and prognosis of acute kidney diseases and disorders using an integrated approach to laboratory measurements in a universal health care system," *JAMA Network Open*, vol. 2, no. 4, p. e191795, 2019.

[7] K. E. Rodenbach, M. F. Schneider, S. L. Furth et al., "Hyperuricemia and progression of CKD in children and adolescents: the chronic kidney disease in children (CKiD) cohort study," *American Journal of Kidney Diseases*, vol. 66, no. 6, pp. 984–992, 2015.

[8] G. H. Zhu, X. P. Sun, J. Li, R. K. Liu, Z. Yang, and Q. Hua, "Association between serum uric acid level and endothelial dysfunction in elderly individuals with untreated mild hypertension," *Journal of Geriatric Cardiology*, vol. 17, no. 5, pp. 264–269, 2020.

[9] J. Yuan, Z. Wang, and Y. P. Wang, "Identification of common key genes associated with Crohn's disease and IgA nephropathy," *European Review for Medical and Pharmacological Sciences*, vol. 26, no. 10, pp. 3607–3620, 2022.

[10] J. E. C. Quilisadio, E. O. Salido, and E. G. Penserga, "Achievement of the target serum urate level among patients with gout treated with allopurinol or febuxostat in an arthritis clinic in the Philippines," *Modern Rheumatology*, vol. 31, no. 3, pp. 755–761, 2021.

[11] S. Kojima, K. Uchiyama, N. Yokota et al., "C-reactive protein levels and cardiovascular outcomes after febuxostat treatment in patients with asymptomatic hyperuricemia: post-hoc analysis of a randomized controlled study," *Cardiovascular Drugs and Therapy*, 2022.

[12] K. Pavelcova, J. Bohata, M. Pavlikova, E. Bubenikova, K. Pavelka, and B. Stiburkova, "Evaluation of the influence of genetic variants of SLC2A9 (GLUT9) and SLC22A12 (URAT1) on the development of hyperuricemia and gout," *Journal of Clinical Medicine*, vol. 9, no. 8, p. 2510, 2020.

[13] Y. Tsuruta, T. Mochizuki, T. Moriyama et al., "Switching from allopurinol to febuxostat for the treatment of hyperuricemia and renal function in patients with chronic kidney disease," *Clinical Rheumatology*, vol. 33, no. 11, pp. 1643–1648, 2014.

[14] A. Sezai, M. Soma, K. I. Nakata et al., "Comparison of febuxostat and allopurinol for hyperuricemia in cardiac surgery patients with chronic kidney disease (NU-FLASH trial for CKD)," *Journal of Cardiology*, vol. 66, no. 4, pp. 298–303, 2015.

[15] A. M. Hu and J. N. Brown, "Comparative effect of allopurinol and febuxostat on long-term renal outcomes in patients with hyperuricemia and chronic kidney disease: a systematic review," *Clinical Rheumatology*, vol. 39, no. 11, pp. 3287–3294, 2020.

[16] X. Zhang, D. Wan, G. Yang, Q. Peng, and X. Wang, "Febuxostat is superior to allopurinol in delaying the progression of renal impairment in patients with chronic kidney disease and hyperuricemia," *International Urology and Nephrology*, vol. 51, no. 12, pp. 2273–2283, 2019.

[17] G. Di Stolfo, S. Mastroianno, D. R. Potenza et al., "Serum uric acid as a prognostic marker in the setting of advanced vascular disease: a prospective study in the elderly," *Journal of Geriatric Cardiology*, vol. 12, no. 5, pp. 515–520, 2015.

[18] J. Maiuolo, F. Oppedisano, S. Gratteri, C. Muscoli, and V. Mollace, "Regulation of uric acid metabolism and excretion," *International Journal of Cardiology*, vol. 213, pp. 8–14, 2016.

[19] W. Hassan, P. Shrestha, K. Sumida et al., "Association of uric acid-lowering therapy with incident chronic kidney disease," *JAMA Network Open*, vol. 5, no. 6, p. e2215878, 2022.

[20] X. Hao, D. Guo, X. Yuan, and B. Xu, "The predictive value of cystatin C combined with lactic acid and uric acid in the occurrence of acute kidney injury in sepsis," *Clinical Nephrology*, vol. 97, no. 1, pp. 60–62, 2022.

Hindawi
Applied Bionics and Biomechanics
Volume 2022, Article ID 1139587, 16 pages
https://doi.org/10.1155/2022/1139587

Research Article

SegChaNet: A Novel Model for Lung Cancer Segmentation in CT Scans

Mehmet Akif Cifci

Dept. of Computer Engineering, Bandirma Onyedi Eylul University, Balikesir, Turkey

Correspondence should be addressed to Mehmet Akif Cifci; mcifci@bandirma.edu.tr

Received 7 April 2022; Accepted 2 May 2022; Published 14 May 2022

Academic Editor: Yaodong Gu

Accurate lung tumor identification is crucial for radiation treatment planning. Due to the low contrast of the lung tumor in computed tomography (CT) images, segmentation of the tumor in CT images is challenging. This paper effectively integrates the U-Net with the channel attention module (CAM) to segment the malignant lung area from the surrounding chest region. The SegChaNet method encodes CT slices of the input lung into feature maps utilizing the trail of encoders. Finally, we explicitly developed a multiscale, dense-feature extraction module to extract multiscale features from the collection of encoded feature maps. We have identified the segmentation map of the lungs by employing the decoders and compared SegChaNet with the state-of-the-art. The model has learned the dense-feature extraction in lung abnormalities, while iterative downsampling followed by iterative upsampling causes the network to remain invariant to the size of the dense abnormality. Experimental results show that the proposed method is accurate and efficient and directly provides explicit lung regions in complex circumstances without postprocessing.

1. Introduction

Lung cancer is the leading cause of cancer-related death globally. According to the World Health Organization (WHO) forecasts for 2019, cancer is the major or second leading cause of death in 112 of 183 nations, and it ranks third or fourth in an additional 23 countries before the age of 70 [1]. The 5-year survival rate is approximately 34% for patients with early-stage, resectable cancer, while the 5-year survival rate is less than 10% for unresectable cancer. Therefore, early identification and diagnosis of lung cancer are essential in enhancing patient treatment results. When images reveal the existence of a tumor, it is critical to histopathologically evaluate diagnostic samples collected by fiber-optic bronchoscopy following National Comprehensive Cancer Network guidelines [2].

The criterion for diagnosing lung cancer is a pathologist's diagnosis of biopsy tissue. On the other hand, diagnostic precision is less than 80% [3]. The four most prevalent malignant lung tumor subtypes are squamous carcinoma, adenocarcinoma, small-cell carcinoma, and undifferentiated carcinoma [4]. To make the optimal treatment decisions, scientists must employ the proper techniques to diagnose distinct cancer subtypes during the biopsy. After the National Lung Screening Trial (NLCT), the leading cancer research and training organization, developed a method to use a low-dose helical computed tomography (CT) to detect lung cancer nationwide in 2015, scientists were finally able to use low-dose CT to diagnose lung cancer nationwide. Furthermore, the Dutch-Belgian lung cancer screening trial, the world's second-largest randomized control trial, confirms the advantages of lung cancer screening [5]. However, implementing the US and prospective lung cancer screening in Europe would likely lead to many whole-slide histopathology images, biopsies, and excised tumors. Researchers have proposed many medical image analysis methods in CT scans to segregate the lung parenchyma region automatically [6]. For example, authors in [7] describe signal thresholding strategies based on contrast information for most methods. Because of their lower densities than the rest of the body, the lung region looks darker when framed by a denser region. The underlying framework of these approaches is straightforward and effective for normal lung segmentation. Still, they fall short when expanding the word "lung" to

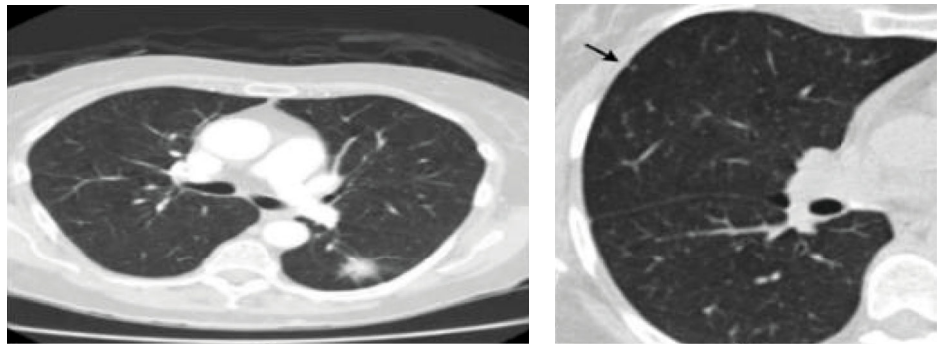

(a) (b)

Figure 1: (a) Lung cancer nodule view. (b) An arrow indicates this 1.25 mm thick CT slice to contain approximately 2 mm long lung nodules.

include aberrant tissues, blood arteries, and normal lung tissues [8]. First, it is crucial to obtain a segmented region using iterative thresholding and then refine the obtained region using an opening-closing morphological operator. Significant success has been found in noninvasive therapy and clinical examination in the health industry, especially when utilizing medical image analysis [9]. Researchers use CT imaging for specific diagnostics, and hence, images such as X-rays, MRIs, and CTs are effective therapeutic methods. Because cancer is the deadliest disease, the value of CT images grows even further, given that 1.61 million individuals die from lung cancer each year, according to the World Health Organization [10]. Despite the progress made in medical imaging technology, including CT scans, lung cancer accounted for 76 million deaths in 2018, and about 13% of those newly diagnosed with lung cancer die from cancer [11]. Most cancer deaths occur in low- and middle-income nations, as over 70% of cancers are found in these regions [12]. The automated identification of lesions and automatic categorization of lung diseases have seen significant advancements in CT scans during the last two decades [13]. Machine learning (ML) systems have played a key role in processing images.

Recently, there has been a significant increase in the attention paid to deep learning (DL) in several domains, including image recognition and biomedical image analysis [14]. After retrieving CT scan features, image processing techniques are applied to the image data to assess whether the patient's cancer is benign or malignant. Figure 1(a) displays a lung cancer nodule view, and Figure 1(b) shows an arrow that indicates a 1.25 mm thick CT slice.

As seen in Figure 1, smaller nodules are in almost any CT scan indicative of problems. For example, the arrow on Figure 1 (b) indicates a tiny nodule to be malignant. Table 1 displays the causes and detection phases of lung cancer.

The objectives and justification of the work are as the following:

This study was aimed at developing a DL-based automated lung cancer tumor segmentation network utilizing CT scans.

Table 1: Lung cancer: causes and prevention.

(i) Detection of lung cancer is generally difficult because specialists cannot find the infected area until it reaches the next stage. As a result, the chance of survival for lung cancer, in 54% of detected cancers, not in the advanced stages, with early intervention, is only 4% [15].
(ii) The probability of increasing lung cancer diagnoses due to the number of cigarettes consumed and sometimes after drinking is proportional. As a result of harmful habits, a minor case of lung cancer may occur even in individuals without disease risk.
(iii) X-ray, CT, or MRI scans are performed to examine lung cancer and differentiate abnormal lung development. The best technique is CT, which experts can overlook when not in ML.

(i) In current procedures, the lung images were taken and subjected to segmentation, to benefit from the support vector machine classifier [16]

(ii) The present framework has a restriction as it could not predict the type, form, or size of the tumor, and it dealt with several pixels, which is not beneficial for the early detection of cancer. Now, when artificial neural network (ANN) develops a testing solution, it does not reveal some information as to why and how. This diminishes trust in the network

(iii) Neural networks (NN) are a black box and have been confined in their capacity to perceive the potential causal links expressively. On the other hand, NN features deep networks with numerous hidden layers and is helpful for modeling complex systems. However, the training process is again more complex and constantly sensitive, creating a few complications

(iv) It is expected that by applying this model, many current data mining and image processing procedures operate jointly in numerous ways. However, the fundamental drawback of the linear discriminant analysis approach is that it only differentiates the images having abnormalities

(v) Because of the issues with classifiers, segmentation performs better in accuracy

The contribution of this work is as below:

(i) This research presents a lung segmentation utilizing 3 traditional and a novel model. This study was aimed at developing a DL-based automated lung cancer tumor segmentation network utilizing CT scans

(ii) Developed a methodology, SegChaNet, that achieves the state-of-the-art performance on numerous segmentation tasks dealing with lung cancer segmentation; of foremost importance is the increase acquired in the precision of tumor segmentation

(iii) Using the channel attention module (CAM) to achieve the goal of managing the feature selection of the bottom-level feature map

(iv) Consequently, this study reveals the capability of early detection of lung cancer, which is known to improve treatment outcomes

The rest of the paper is structured in the following way. The next section contains several examples from the literature and will contrast them with the present study. Next, we explain the methods in Section 3, including methods for the segmentation of lung cancer. Then, we have presented a detailed analysis of the proposed model in Section 4. In addition, the results and a discussion are in this section. Finally, we summarize the full text in Section 5 and present the future work.

2. Literature Scan

Numerous studies on lung segmentation have been conducted using conventional image processing techniques such as thresholding, edge detection, and clustering [17, 18]. When faced with chaotic input images, many image processing algorithms resort to primitive techniques and perform poorly. This project was aimed at developing an automated lung cancer tumor segmentation network based on deep learning using CT images. Researchers are examining lung segmentation using convolutional neural networks (CNNs). The researchers now want to enhance lung segmentation performance through complex image segmentation network topologies and other strategies such as attention modules. It has been demonstrated that the attention mechanism significantly improves performance on many DL-based activities.

As a result, our research focuses on segmentation techniques based on attention. For example, attention U-Net [19] outperforms U-Net by sandwiching an attention module with a fundamental structure between the current U-Net structure's contracting and growing channels. Similarly, the authors of [20–22] enhanced the structure of the corrective adversarial network, which was the first attempt to use adversarial learning for lung segmentation on chest X-rays by incorporating attention U-Net and focal Tversky loss for the generating network and binary cross-entropy, respectively.

Additionally, the researchers in [23, 24] used CC-Net as the backbone network, an image segmentation network based on the criss-cross attention module. Additional learning data were generated using image-to-image translation. XLSor is state-of-the-art software. This project was aimed at developing an automated lung cancer tumor segmentation network based on deep learning using CT images. Numerous lung image segmentation networks use a reference lung segmentation model based on chest X-ray images [25].

In their study, the authors in [26] proposed an algorithm for classifying lung nodules by considering the data learned from tissue, shape, and the D technique. This algorithm utilized a "gray level coformation matrix"-based surface identifier, a Fourier shape identifier, and CNNs to train the properties of nodes to depict the heterogeneity of nodules. However, the authors in [27] focused on computer-aided diagnosis (CAD), which they designed manually, so it is not ideal or sufficient for the solution.

U-Net employs the skip connection, which is symmetrical, to directly supervise and lose back propagate on semantic features instead of using these other procedures. The aspect of scale integration permits the implementation of various features from multiple sizes to support multiscale prediction. Because of this, U-Net is primarily used in the medical imaging industry [28]. The researchers in [29] suggested using a recurrent; the residual convolutional neural network (RRCNN) was introduced in conjunction with a U-Net to train more complex networks and extract deep semantic information. The results obtained using R2U-Net in the vascular, lung, and skin datasets are above expectations. As a result, the depth of the U-Net network varies according to the applications it serves. As a result, Liang et al. designed U-Net, which included smaller-scale U-Net levels in larger-scale U-Net levels, with deep supervision, which allows the network to self-select the appropriate amount of depth via training [30].

On the other hand, the researchers in [31] developed the cellular neural network algorithm to detect lung cancer symptoms. In this study, the authors employed X-ray images and thus the CNN algorithm to diagnose lung cancer. The authors in [32] focused on developing CNNs for lung cancer screening in CT scans. The researchers in [33] used multilayered neurons with independent principal components to diagnose lung cancer.

In their study, the researchers in [34] performed a diagnostic classification of lung nodules using 3D-CNNs. They did not foresee overfitting in their model, so they had to include a retraining phase method to address issues linked to image label imbalance. Chon et al. [35] proposed a method that uses an ANN community chart to differentiate benign from cancerous lung nodules. The experimental results show that the scheme has 78.7% classification accuracy [36]. On the other hand, the authors in [37] utilized an ANN model with a classification accuracy of 92 percent in their study. Zhang et al. [38] presented a methodology with an accuracy rate of 75.01% using the Automatic coder (AC), a DL technique. Table 2 includes the comparison of the literature review in the related field.

Table 2: Comparison to the literature works.

References	Datasets	Method	Result (%)
Chaturvedi et al. 2019 [39]	LUNA 16	3D DL DÖ, V-Net architecture	Sensitivity: 96.5 FP:19.7
Chapaliuk et al., 2019 [40]	ACDC LUNGH	VGG16, ResNet50, and CNN	Sensitivity: 97.9 Accuracy: 93
Petrellis et al., 2018 [41]	UCI	Gaussian blur, Otsu thresholding	Sensitivity: 87 Accuracy: 97
Yuan et al., 2019 [42]	134 BT Shandong hospital	Watershed transform	Sensitivity: 88.8 Accuracy: 90
Cao et al., 2016 [43]	LUNA16	3D and 2D CNN	Precision: 87 Sensitivity: 99.1
Xie et al., 2019 [44]	LUNA16	2D CNN and RCNN	AUC: 95.4
Sun et al., 2017 [45]	LIDC-IDRI	CNN, deep belief network, and Boltzmann machine	Sensitivity: 82.2 AUC: 81.8
Huang et al., 2018 [46]	LIDC-IDRI	CNN, extreme learning machine, and deep transfer	Sensitivity: 91.6 Accuracy: 86.5
Pehrson et al. (2021) [47]	LIDC-IDRI	This study was aimed at developing a DL-based automated lung cancer tumor segmentation network utilizing CT scans	Sensitivity: 91.7 Accuracy: 93.8
Sharma et al., 2011 [48]	LIDC-IDRI	Diagnostic indicators	Accuracy: 80.1
Akram et al., 2012 [49]	LIDC-IDRI	Neurofuzzy	Accuracy: 95.5
Paulin et al. 2011 [50]	LIDC-IDRI	For MLP SVM training, the back propagation technique is employed	Accuracy: 83.6
JIA et al. 2007 [51]	NCA	For MLP SVM training, the back propagation technique is employed	Accuracy: 92.4

3. Methodology

3.1. Data Acquisition. Images of 46,698 CT scans, both with and without tumors, from the Cancer Imaging Archive (https://wiki.cancerimagingarchive.net/display/Public/RIDER+Lung+CT) were made available. 80% of the data were used for training and 10% for validation to obtain a reliable and accurate network, while the remaining 10% of the data were for testing. We have used different parameters for training segmentation models. We have applied the data augmentation steps to the data. On each patient's scan, we employed intensity normalization based on the mean and standard deviation of the intensities. We implemented our models on a machine with an NVIDIA GeForce RTX 2080 8 GB and Intel Core i9-9980hk processor configuration. We utilized Python (3.8.12), the major programming language, for constructing the framework's subsequent phases. The proposed architecture is implemented using the libraries Anaconda3 (64-bit), Jupyter Notebook, TensorFlow, and Keras.

As seen in Table 3, the dataset is split into train, test, and validation. The CT scan slices are as with tumors and without tumors.

Table 3: Some distinct sorts of CT scan slices in the dataset.

Data	Number of patients	Tumor	Without tumor	Notes
Train	370	14,848	20,840	35,688
Test	90	4520	4740	9260
Validation	50	850	900	1750
Total	510	20,218	26,480	46,698

3.2. Preprocessing CT Scans. Preprocessing CT scans dealing with high variation in data is a typical job performed during preprocessing. The first step was to truncate all the Hounsfield unit (HU) values between −1000 and 400 [52]. The HU is a metric that measures the density of materials where the air has a value of −1000 HU and bone has a value of 1000 HU; values outside the range of −1000–400 is not considered necessary for lobar segmentation [18]. We then normalized the CT scans to a zero mean with unit variance. To fit the images into a 3D model, we resized all the images and made them the same size, satisfying the memory constraints of the GPU. Two main approaches to this task achieve similar performance: downsampling CT images or applying a patch-based method by partitioning the images into overlapping patches. Since we needed to incorporate tracheal and bronchial segmentation as an auxiliary task into the segmentation, we opted for the downsampling technique, ensuring that the trachea and bronchi were present in each image. The size should be the same on all three axes to downsample the image [53]. If one axis is of better resolution than another, the performance along lower resolution axes is worse, as they contain less information than the other axes. All the CT scans, with their masks, were resized to $128 \times 128 \times 128$ using linear and neighbor interpolation, respectively, as it was the most significant cube size shape we could fit into memory. What makes SegChaNet different from U-Net is that U-Net was initially designed for medical image

interpretation and segmentation, while we developed SegChaNet for lung image segmentation.

U-Net has a wide variety of industrial applications and has played an important part in the development of the image automation society. The architecture of SegChaNet is defined by its appealing and expansive components. The contracting path comprises several convolutional patches with 3×3 filters and unity strides in both directions, which are preceded by ReLU layers. This path takes the input and extracts the key features, yielding a feature vector of a certain length. The second path uses information from the contractive path to creating an output segmentation map by copying and cropping the feature vector using upconvolutions. The exploit that connects the first and second channels is vital for this system. This connection enables the network to get very precise information from the contractive route, developing a segmentation mask close to the desired output. SegChaNet benefits from extremely asymmetric datasets because of its composition of big chunks of lung images. Due to the lungs' different geometries and image density distributions, it is difficult to distinguish them in clinical ultrasound images automatically.

SegChaNet resembles U-Net but as explained above, combining two different paths, and utilizing Binary cross Entropy, integrated with the Channel Attention Module, differs it from the rest. The encoder layers are similar to the convolutional layers of the U-Net.

For SegChaNet, nine distinct hyperparameters are used in training to determine the optimal configuration. These training hyperparameters are listed in Table 4. For training purposes, all trials were done in 500 epochs for training purposes. Training time variation was small across networks, with an average of 18 minutes.

3.3. U-Net Model. U-Net is a technique for automatically segmenting images. U-Net is a pixel-based image segmentation algorithm for various architectural and convolutional neural network layers. It outperforms traditional models in terms of success. It also performed well on datasets with a minimal number of photos. The term "U-Net" comes from its U-shaped design. U-Net is made up of encoding and decoding components. The content of the images is recorded in the code section. It is made up of top pooling layers. On the other hand, the decoding portion is the symmetric expansion route utilized to obtain exact localization via the use of delegated convolutions. The U-Net model is shown in Figure 2. Each of the $32 \times 128 \times 128$ voxels included inside the input layer corresponds to a single channel. We did 1D convolution on the input by applying a $1 \times 3 \times 3$, $2 \times 3 \times 3$, and $1 \times 1 \times 1$ filter. Using max pooling, we perform one-dimensional max pooling. By using 1D upsampling, the voxel size was raised from 2 2 to 4 4. To model U-Nets, we use the rectified linear unit (ReLU) as the input and the sigmoid function as the output layer's activation function. Data augmentation is a strategy that may assist avoid overfitting and increase performance by increasing the quantity of data points. The left-to-right inversion and white-to-black inversion methods were used in this work to provide data augmentation. We used Adam as an optimizer because of its adaptive moment estimation. To arrive at the ideal learning rate, various values were tried, including those between 0.3 and 0.1, with every successive change made along with the range. To optimize a solution, we must minimize the loss function, the difference between the projected result, and the correct answer. We calculated these equations to get the following:

Table 4: Hyperparameters used for training SegChaNet.

Exp.	SegChaNet	
	ILR	Minibatch
1	1e−4	2
2	1e−4	8
3	1e−4	12
4	1e−3	2
5	1e−3	4
6	1e−3	8
7	3e−3	4
8	3e−3	12
9	3e−3	8

$$\begin{aligned} &\text{Loss function} = 2 - \{\text{IOU}(A, B) + \text{DSC}(A, B)\}, \\ &\text{IOU}(A, B) = \frac{|A \cap B|}{|A \cup B|}, \\ &DSC(A, B) = \frac{2|A \cap B|}{|A| + |B|}. \end{aligned} \tag{1}$$

In this case, the estimated value, B, is an estimation and the actual value, A, is accurate. The intersection over union (IOU) and dice similarity coefficient (DSC) are represented as the Jaccard Index (JI). The JI and the DSC are both methods of measuring class similarity. To determine the accuracy of contour demarcation, we use DSC. The ensemble learning for five inference results comprises 5-fold cross-validation; afterward, we obtained DSC for U-Net. The following example illustrates this principle in ensemble learning, for which we have found a pixel value of 1 for three inferences but a value of zero for two inferences. In this case, we selected a majority value of 1.

In Figure 2, the path has two distinctive sections: a contracting section and an expansive one. A typical convolutional architecture often features a contracting path. It is a 2×2 max pooling with stride 2 and a ReLU followed by two unpadded convolutions such as 3×3 convolutions. We have increased the amount of feature channels by a factor of two each time while performing downsampling. The enlarging path has upsampling, followed by 2×2 convolutions.

3.4. V-Net Model. We applied the V-Net architecture using the TensorFlow and Keras frameworks in Anaconda, as stated in Data Acquisition. We have employed the V-Net, an autoencoder, for 3D image segmentation. Its residual connections aid networks to converge and perform well on small datasets. Figure 3 shows the model's architecture,

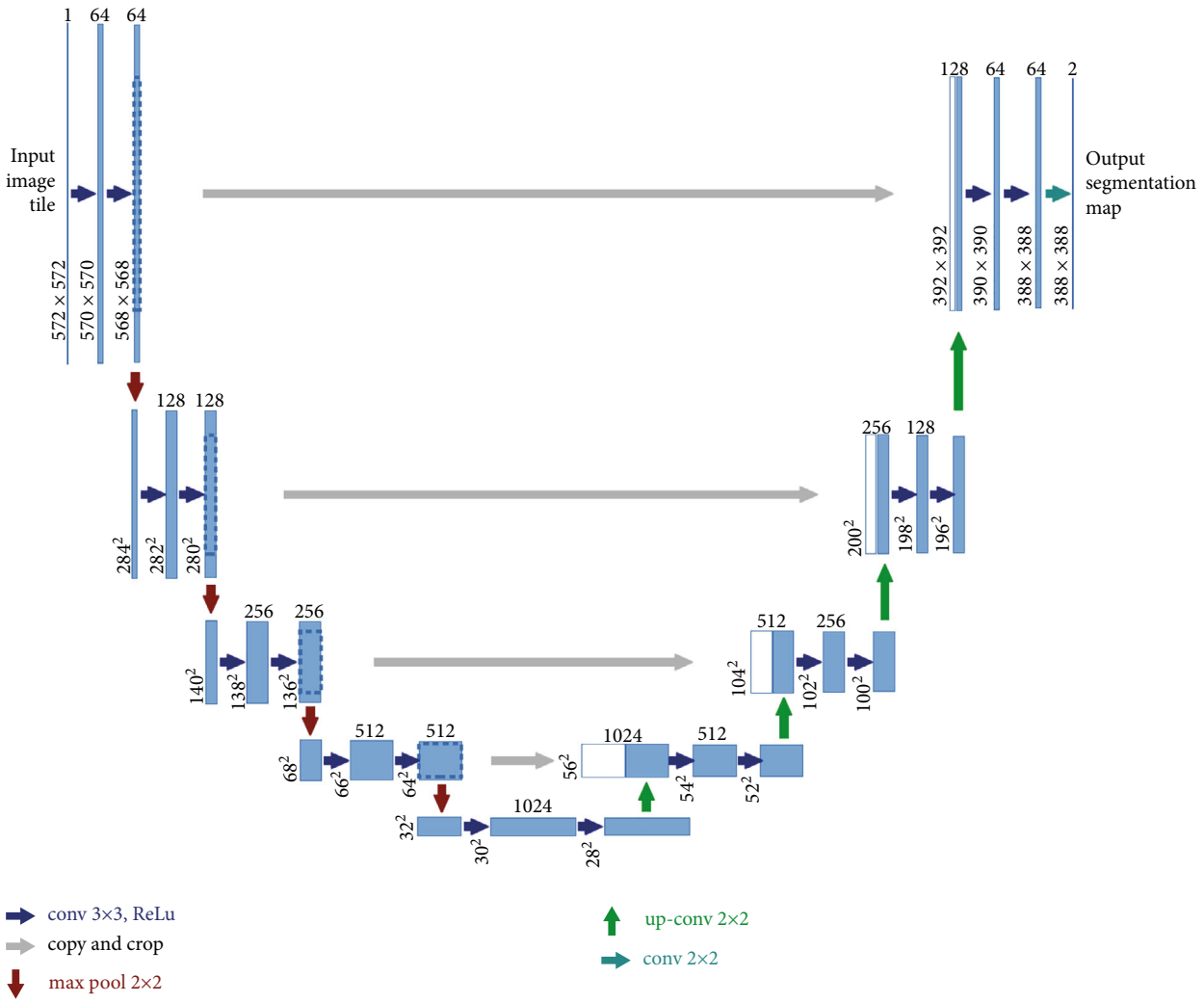

Figure 2: U-Net architecture.

where the input image is $128 \times 128 \times 128 \times 1$ (height, width, depth, and channels) and passes through six encoder layers. As seen from Figure 3, V-Net, we used convolutional layers with a stride of $2 \times 2 \times 2$ instead of the max pooling operation. The last layer before each output was a $1 \times 1 \times 1$ convolution with a softmax activation function that gives us the probability that each voxel belongs to one of the classes. Various regularization techniques enhanced the model's generalizability, including dropout and batch normalization. Training the model on distinct but relevant tasks has been shown to increase a model's performance. The model's performance is measured using the DSC, a function of sensitivity and specificity typically used in segmentation studies, permitting a comparison of our model's performance to others. We compared our model to other models by researchers who released the original dataset. A p value obtained using a t-test, more diminutive than 0.05 between the models, was considered statistically significant for independent comparisons. Figure 3 shows V-Net architecture.

We illustrate our CNN using the schematic in Figure 3. To both find features in the data, we use convolutions, as well as to reduce the resolution after each stage by employing stride suitable to the level. In the left portion of the network, we used a compression path to reduce the file size, and in the right portion, we decompressed the file until we reached its original size. We employed all of the convolutions with the proper amount of padding.

3.5. SegChaNet Model. Segmentation tasks generally concentrate on learning multiscale features and the integration of local and global contexts. However, computationally demanding training segmentation networks including these qualities and implementing these directly on volumetric data is difficult. To help promote multiscale learning, we integrate CAM convolutions into the network and place these convolutions at the very end of the feature extraction process. They work together with the output of the decoder layers to promote the learning of multiscale features. We use this connection to assist the training of network gradients as well. We maintained residual links between the decoding component and the alteration when we adjusted. The proposed network consists of four blocks of encoders and

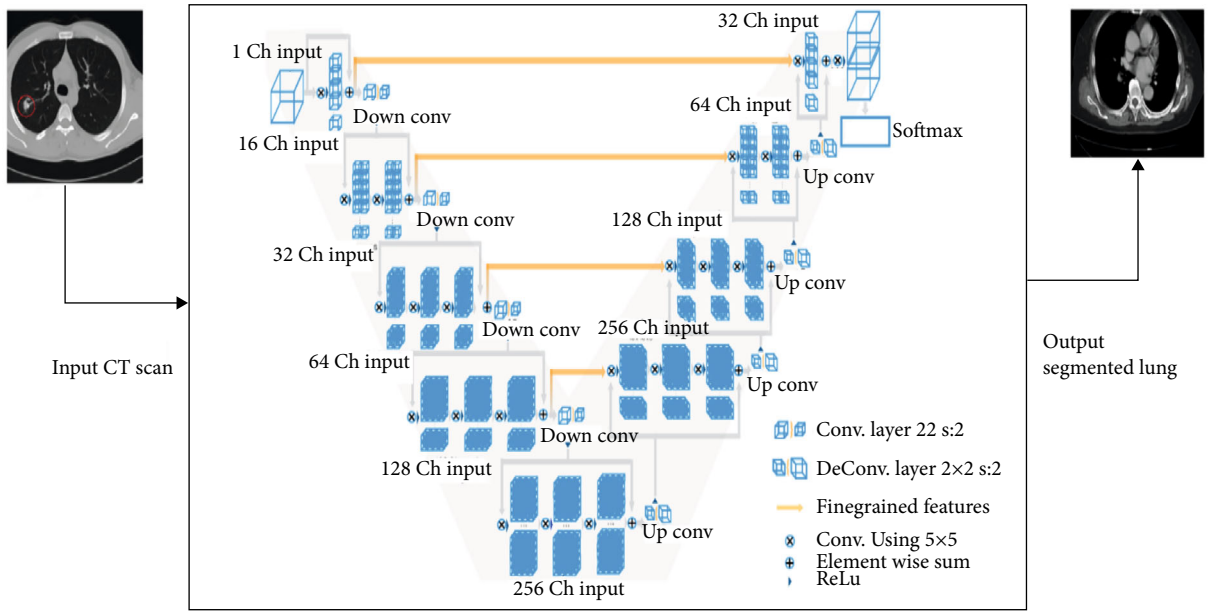

Figure 3: V-Net architecture.

decoders each using two 3D convolution layers with a $3 \times 3 \times 3$ kernel size and a batch normalization and leaky ReLU activation function.

However similar it may seem, SegChaNet varies from U-Net. For example, we use the maximum linked component detection to extract the whole region, and SegChaNet additionally takes use of CAM. Besides, preprocessing steps have been applied before the SegChaNet model is applied. So, it necessarily comprises a preprocessing phase. Figure 4 displays the main novel architecture.

As seen in Figure 4, this decoder uses a 2× upsampling method. We proposed the convolution of the augmentation module's CAM convolution layers such that the first layer utilizes a dilation rate of one, and each subsequent layer doubles the dilation rate. It is upsampled to scale each decoder's output, followed by all concatenated outputs.

3.5.1. Channel Attention Module. This section delves further into SegChaNet's model architecture (illustrated in Figure 4). Because of its higher performance, the pixel-level classification strategy is employed in medical image segmentation tasks based on the U-Net model. We included the cross-level feature fusion module (CFFM) in our end-to-end network architecture, SegChaNet, to create a merged network with two primary components and CAM. The CFFM enables the fusion of features from the top-level feature map into the feature map of the bottom layer, allowing the CAM to regulate feature selection in the bottom-level feature map. The second component is the U-Net, a two-part encoder-decoder architecture in which the first half is used to extract features and the second half is upsampled. Special caution is required when using a skip connection topology between the encoder and the decoder. Additionally, a skip link was used to connect the downsampled and upsampled feature maps. The CAM and architecture used are shown in Figure 4. Because the high level includes much semantic information, it may help guide the low-level choices. Several studies have shown that attentiveness is vital in human perception. Recently, attention processes have been included in complicated sequences and transformation models for various activities. Channel attention modules, in particular, have been utilized to boost deep learning performance in a variety of computer vision applications. DL methods for image classification and semantic segmentation rely on continuous fundamental convolutional processes. Consequently, deep learning networks can only manage the local components of an image, resulting in the loss of global information.

A sophisticated method must be used to estimate the parameters. The parameters of the investigation were determined in three steps. Attenuation coefficients can be derived from the attenuation profile using a single-path model and a least squares estimator. The number, position, and amplitude of key pathways may be calculated from the impulse response using a basic peak detection approach. In simpler cases, this phase usually gives enough precision. To expand the number of pathways, parameters must be developed using either impulse response or amplitude and phase responses. To estimate parameters, complex procedures must be applied. The parameters of the investigation were determined in three steps. An initial estimate of the attenuation coefficients can be generated from the attenuation profile using least squares estimators. The number, position, and amplitude of key pathways may be calculated from the impulse response using a basic peak detection approach. In most cases, this is all that is required. To increase the number of pathways, the parameters must be further changed through an evolutionary process employing quality criteria such as impulse response or amplitude and phase response.

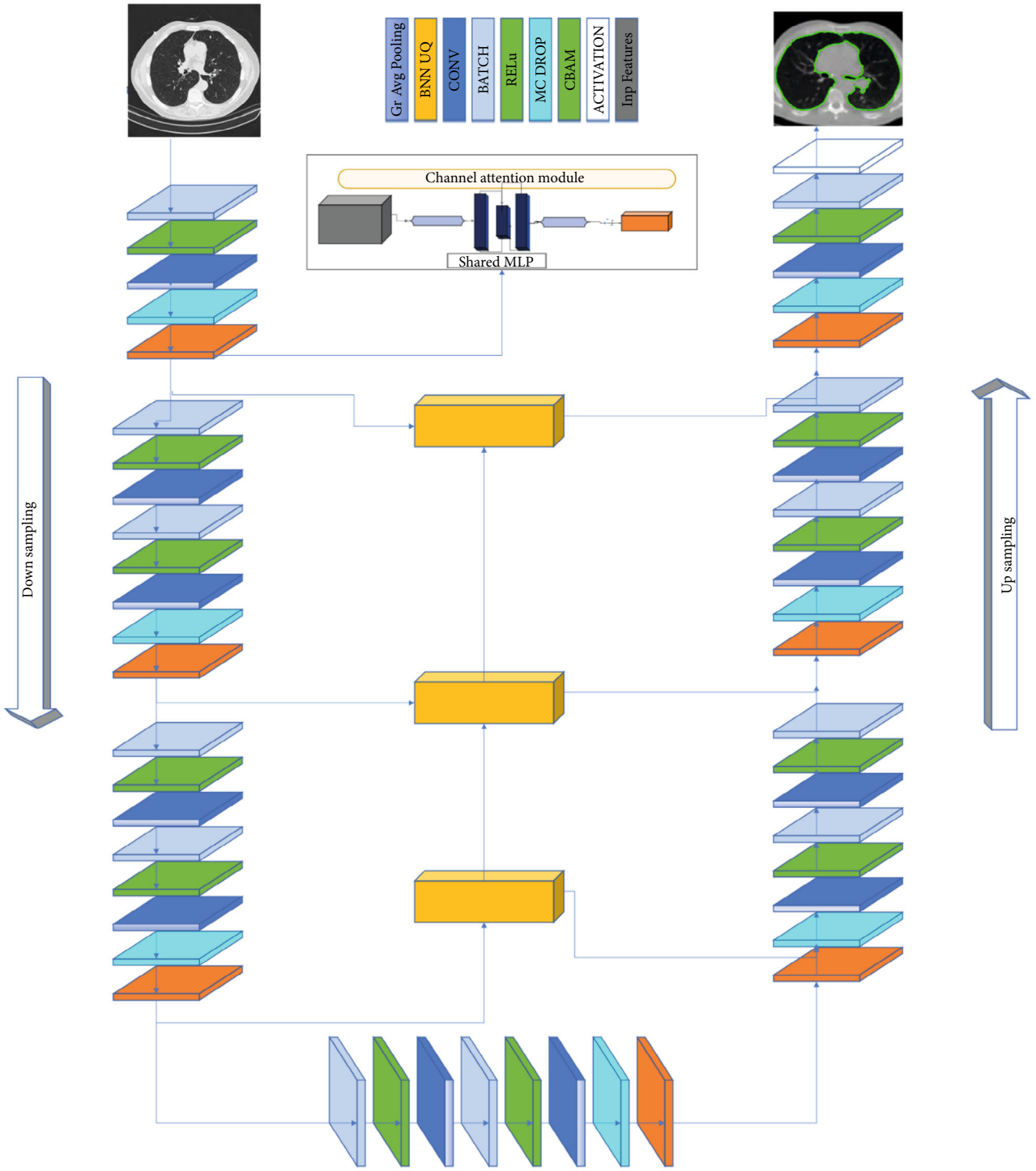

Figure 4: An encoder-stage-to-decoder stage residual connection network architecture. The encoder uses residual connections and 3D max pooling operations.

We have provided a more specific resolution information option. Furthermore, the SegChaNet model may learn the weight of each channel via CAM, resulting in attention in the channel domain. The CAM procedure is as follows:

$$X_{\text{cam}} = \text{CAM}(X_L, X_H), \tag{2}$$

where X_{cam} represents the output of the CAM module and X_L and X_H represent the low-level feature map and high-level feature map, respectively.

$$x_{\text{cam}}^{i,j,k} = x_{gL}^{i,j,k} + \text{up}\left(x_H^{i,j,k}\right), \tag{3}$$

Table 5: U-Net method with/out CAM performance.

U-Net method	Dice (%)	Sensitivity	Specificity	Precision	*F*-measure	Accuracy (%)
Without CAM	88.61	97.45	93.12	93.01	93.21	93.21
With CAM	95.94	97.62	90.43	89.87	95.56	95.14

Table 6: The V-Net method with/out CAM performance.

V-Net method	Dice (%)	Sensitivity	Specificity	Precision	*F*-measure	Accuracy (%)
Without CAM	87.35	88.29	84.74	86.51	91.14	91.63
With CAM	95.75	96.96	89.77	89.21	94.91	94.48

Table 7: SegChaNet method with/out CAM performance.

SegChaNet	Dice (%)	Sensitivity	Specificity	Precision	*F*-measure	Accuracy (%)
Without CAM	96.81	93.79	90.19	92.15	96.89	96.47
With CAM	98.48	92.82	94.08	96.66	98.49	98.90

where $x_{\text{cam}}^{i,j,k}$ represents the pixel value of the ith row, jth column, and kth channel in the output feature map of the CAM.

In addition, $x_H^{i,j,k}$ H is the pixel value of the ith row, jth column, and kth channel of the high-level feature map. up $(.)$ means the bilinear interpolation.

$$X_{gL} = \text{Conv1}\left(\left[X_L' k \times g\left(X_H^k\right)\right]_{k=0}^{k=c-1}\right). \tag{4}$$

Global pooling transforms the feature map X_{gL} and low-level feature map X_L. The 3×3 convolution operation adjusts the feature map size and merges the channel features. Still, because the low-level and high-level features' feature map size and channel number are different, the low-level feature needs a 3×3 convolution operation.

$$X_L' = \text{Conv3}(X_L). \tag{5}$$

Global pooling, convolution with a 3×3 convolution kernel, and convolution with a 1×1 convolution kernel which are known as $g(.)$, conv3$(.)$, and conv1$(.)$, respectively. The letter "c" denotes the total number of channels [54].

When global pooling is used, CAM gives an initial global context that serves as a guide for recognizing low-level features. To decrease the number of feature mappings in the encoder, we first apply three convolution filters to the low-level features. A global context is created by multiplying the low-level features by the high-level features using a 1×1 convolution process. Finally, we have combined low-level and high-level features. Thus, the CAM module uses scale feature maps more effectively while delivering information to lower-level feature maps.

When it comes to the model's performance, as seen, Table 5 shows the performance of the U-Net method with and without CAM.

As seen in Table 5, accuracy of the U-Net method without CAM is 88.61.21 while with CAM is 95.94. Table 6 displays the methods and performance of the V-Net method with and without CAM.

From Table 6, the accuracy of the V-Net method without CAM is 87.35 while with CAM is 95.75. Table 7 shows the methods and performance of the novel method SegChaNet with and without CAM.

From Table 7, it is evident that the accuracy of the SegChaNet method without CAM is 96.81% while with CAM is 98.48. Figure 5 shows the performance of SegChaNet, illustrating the comparison of the novel model with the state-of-art ROC performance. Table 8 compares models' accuracy evaluated in DSC, JI.

Table 8 displays the results with CAM. As seen, SegChaNet is far better when compared with the other methods.

From Figure 5, it is evident that the AUC of V-Net, U-Net, and SegChaNet without CAM is lower when compared with used models plus CAM.

3.6. Training Procedures. We are creating a new model from scratch and will use the DSC, JI, and normalized surface distance to test it. We computed normalized surface distance as a combination of the model-predicted segmentations that overlap with the ground truth. In the segmentation process, we utilized these variables to determine segmentation accuracy. Segmentation networks' segmentation binary cross-entropy is commonly employed. As proposed, we employed binary cross-entropy and DSC loss functions to train the networks in this investigation. The loss value applied on SegChaNet is in Equation (2), proving that the overall loss is less sensitive to class imbalance. Our tests found greater segmentation accuracy when utilizing the binary cross-entropy over the individual loss. The equation in [55] is as follows:

$$\zeta(y, \hat{y}) = \zeta_{dc}(y, \hat{y}) + \zeta_{bce}(y, \hat{y}). \tag{6}$$

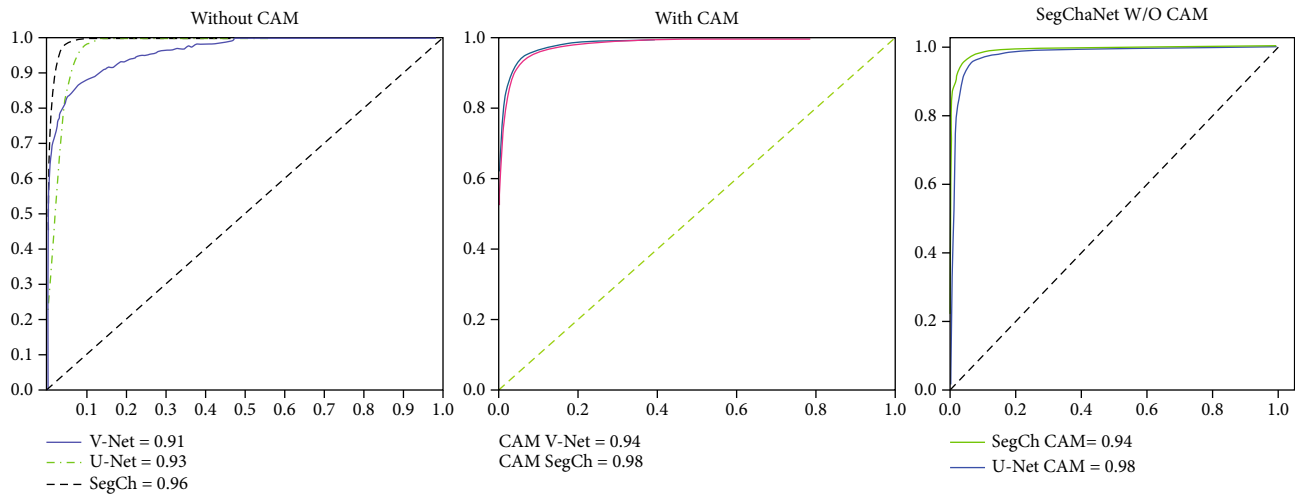

Figure 5: SegChaNet, U-Net, and V-Net model with and without CAM.

Table 8: Evaluation of segmentation accuracy in DSC, JI for 3 models.

Models	Training DSC	Val DSC	Testing DSC	JI
V-Net	0.953	0.907	0.893	0.949
U-Net	0.955	0.893	0.911	0.956
SegChaNet	0.989	0.947	0.937	0.957

In Equation (6), $\hat{y}$ denotes the model's output, and the ground truth labels are denoted by y. We use the two-class version of the DSC loss $\zeta(y, \hat{y})$ proposed in [56], a fully connected DL model trained on 500 epochs with an Adam optimization learning rate of 0.0005. If the validation binary cross-entropy did not improve after 15 epochs, we would reduce the learning rate by 0.1 per ten epochs. We updated the dataset with additional random rotations and flipping to help minimize overfitting and improve the resilience of our technique to varied hippocampus shapes. Our research noticed that the segmentation masks became poorer during additional large rotation angles. So, to remain consistent, we reduced the rotation angles to fall within roughly 10 degrees.

3.7. Evaluation Metrics. The precision of segmentation directly affects the success or failure of the segmentation process. Therefore, three measurement variables, DSC, sensitivity, and specificity, are utilized to assess the accuracy of the suggested techniques. In addition, true positives (TP), false positives (FP), true negatives (TN), and false negatives (FN) are also crucial in the assessment [57].

Dice: designed to evaluate the overlap rate of prediction results and ground truth. DSC ranges from 0 to 1, and the better-predicted result will have a more considerable DSC value.

$$\text{DSC} = \frac{2\text{TP}}{2\text{TP} + \text{FP} + \text{FN}}. \tag{7}$$

Sensitivity (also known as the true positive rate or the recall) indicates the percentage of genuine positives that are accurately detected.

$$\text{Sensitivity} = \frac{\text{TP}}{\text{TP} + \text{FN}}. \tag{8}$$

Specificity (also called the true negative rate) measures the proportion of correctly identified actual negatives.

$$\text{Specificity} = \frac{\text{TN}}{\text{TN} + \text{FP}}, \tag{9}$$

where TP denotes the true positive voxels, TN denotes the true negative voxels, FP denotes the false positive voxels, and FN denotes the false negative voxels. We use the 4-union (IOU), DSC value, and Hausdorff distance [58]. Here, we defined IOU as

$$\text{IOU} = \frac{\text{TP}}{\text{FN} + \text{FP} + \text{TP}} \tag{10}$$

To understand what this output means, think of a medical test proposed target capture, in which a group of clinicians manually label the target region, and the network prediction shows the areas around it.

The intersection and union of two sets are equivalent when defined as the IOU ratio [59]. Researchers use the IOU score widely to quantify pixel-level image segmentation performance in image recognition algorithms. IOU can have a value from 0 to 1. As the IOU increases, the overlap between the two zones will decrease and vice versa.

4. Results and Discussion

As demonstrated in Figures 2 and 3, we enhanced lung cancer segmentation in the proposed model SegChaNet by comparing it to two state-of-the-art models. Despite having almost identical encoder and decoder designs, U-Net

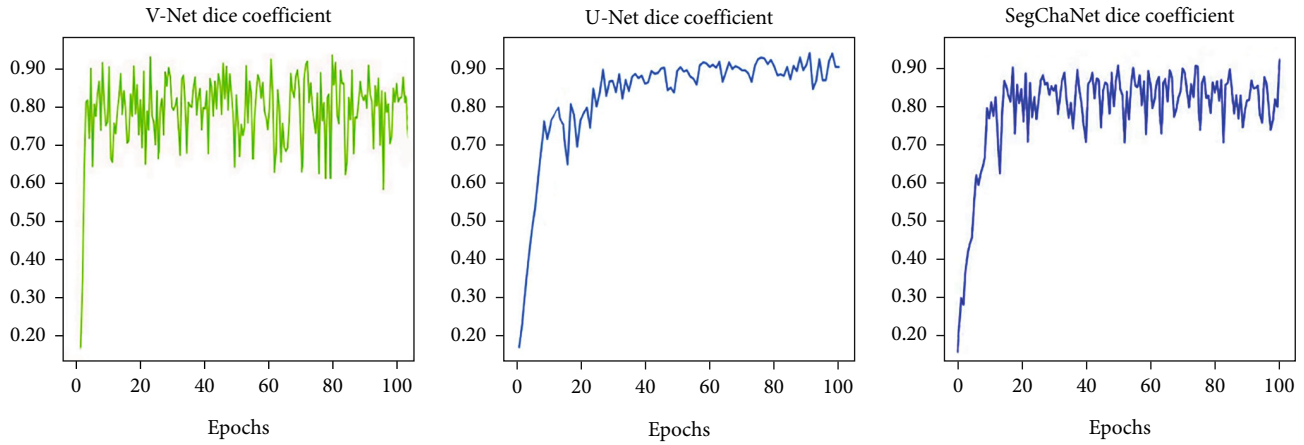

Figure 6: Applied model dice coefficient.

structures and their variants outperform non-U-Net structures. While decoders on other networks employ the addition operation, the skip connector and upsampling set of inputs are concatenated in the decoder. We lowered the data dimension to compensate for the value lost during the addition procedure. In addition, to impact the behavior of other network features, we paired SegChaNet's encoder and decoder with a large number of recurrent, residual convolutions. As a result, when we utilized SegChaNet to evaluate the CT scan dataset, we found that it was prone to overfitting. That is why we used CAM, which performs a function by correctly utilizing all of the feature information on each level. Unlike attention U-Net, which segments the esophagus with an air hole, the SegChaNet considers the air hole a boundary when segmenting. Furthermore, U-Net cannot identify small airways [60], required for esophageal analysis. This is due to the underutilization of complex features. However, neither can they use the features of several layers to guide feature selection, nor can they combine low-level and high-level features with driving feature selection at a lower level. On the other hand, CAM uses the channel to combine the features of many stages.

In contrast, CFFM selects low-level, fine-grained features based on high-level semantic features, resulting in the network producing features on the shape and border of the esophagus. As a result, we achieved our primary goal of enhancing segmentation effects and generalization capacities. Figure 6 depicts a comparison of the DSC coefficient performance of the employed models.

When compared to other works in the literature, such as segmentation techniques in [61], we can observe that, while they have profited from alpha attribute maximization, the result is not as expected, with an IOU of 74.18 percent and 84.80 percent. Furthermore, compared to 3D-U-Net neural in [62], they used 3D U-Net, and their DSC performance reached 95.30 percent. Speaking of which, the SegChaNet approach performs significantly better.

As seen from Figure 6, V-Net shows a good performance, but it fails in the final part, while the best performance is from the SegChaNet model. For the first 20 epochs, U-Net shows the worst performance. Figure 7 displays marked images using grad cam.

As seen in Figure 7, we have marked images using grad cam. Also, we utilized the DSC, JI, and normalized surface distance (NSD) with 4 mm performance to test various networks. As illustrated in Figure 8, we examined the segmentation performance of V-Net, U-Net, and U-Net and V-Net with CAM convolutions. The V-Net attained mean DSC scores of 95.75% without CAM, 87.35% for the training, validation, and test sets. At the same time, the U-Net results match the V-Net scores relatively well. CAM convolutions allowed U-Net to improve the scores to 88.61% and 95.94%. The proposed technique demonstrated 96.81% without CAM and 98.48% with CAM for the training, validation, and test sets.

Furthermore, our method outperformed other cutting-edge networks for both the JI and NSD metrics. This is highlighted clearly. Figure 7 shows the segmentation quality of the proposed method next to other methods so that it can be compared visually. When used to color coordinate ground truth with predictions, red represents the ground truth, while yellow, green, and cyan represent the V-Net, U-Net, and method provided in this article predictions. The top-right area of the mask in Figure 7 comprises small discontinuous portions; we demonstrated the advantage of CAM convolutions by effectively segmenting such small sections. However, when the learned qualities become more prevalent worldwide, the U-Net and the suggested method might effectively gather the regions. Figure 8 depicts the three-dimensional surface meshes of two different patients. We can observe how the SegChaNet model influences our conclusions in the method provided in columns 3 and 4. The bottom boundary of the red component of the hippocampus is about one hundred millimeters below the ground's surface. Figure 8 depicts SegChaNet's top and worst performance ratings.

Figure 8 displays the SegChaNet model's best and worst performance. As seen, the best score is about 95 while the worst one is 51.47.

For the segmentation of lung nodules using low-dose CT imaging, we investigated the imaging features of lung

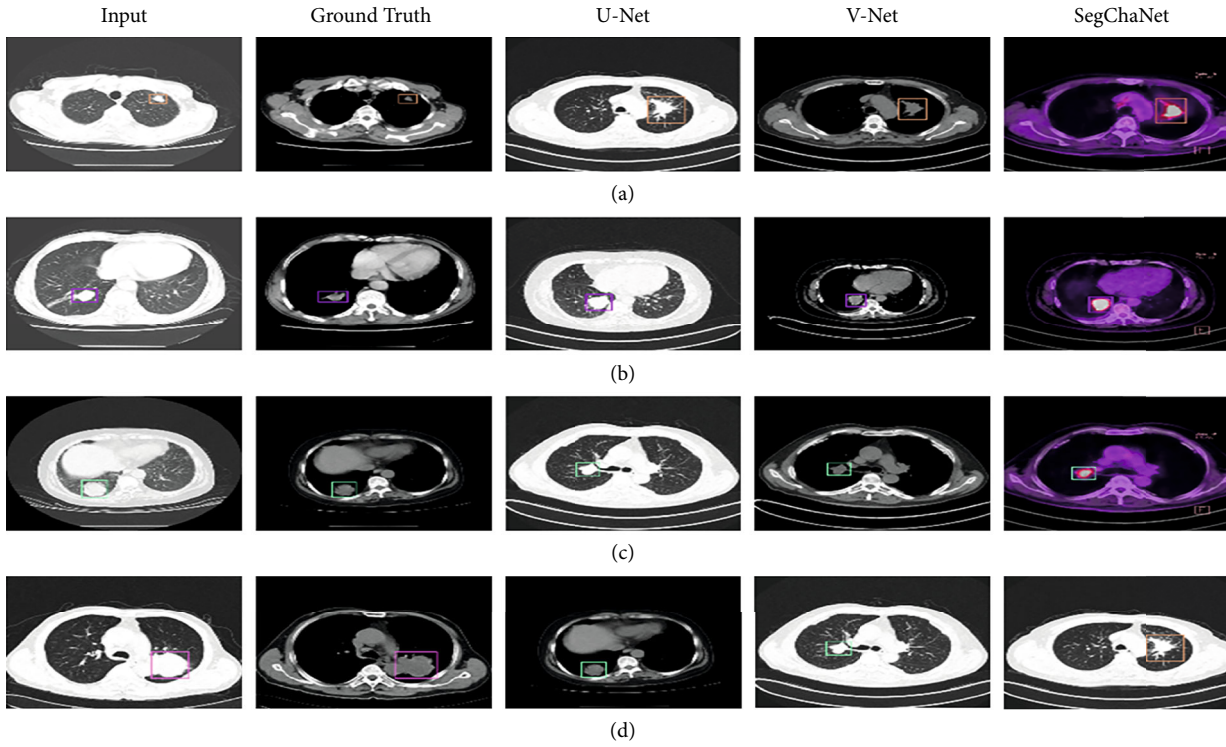

Figure 7: Marked images using grad cam.

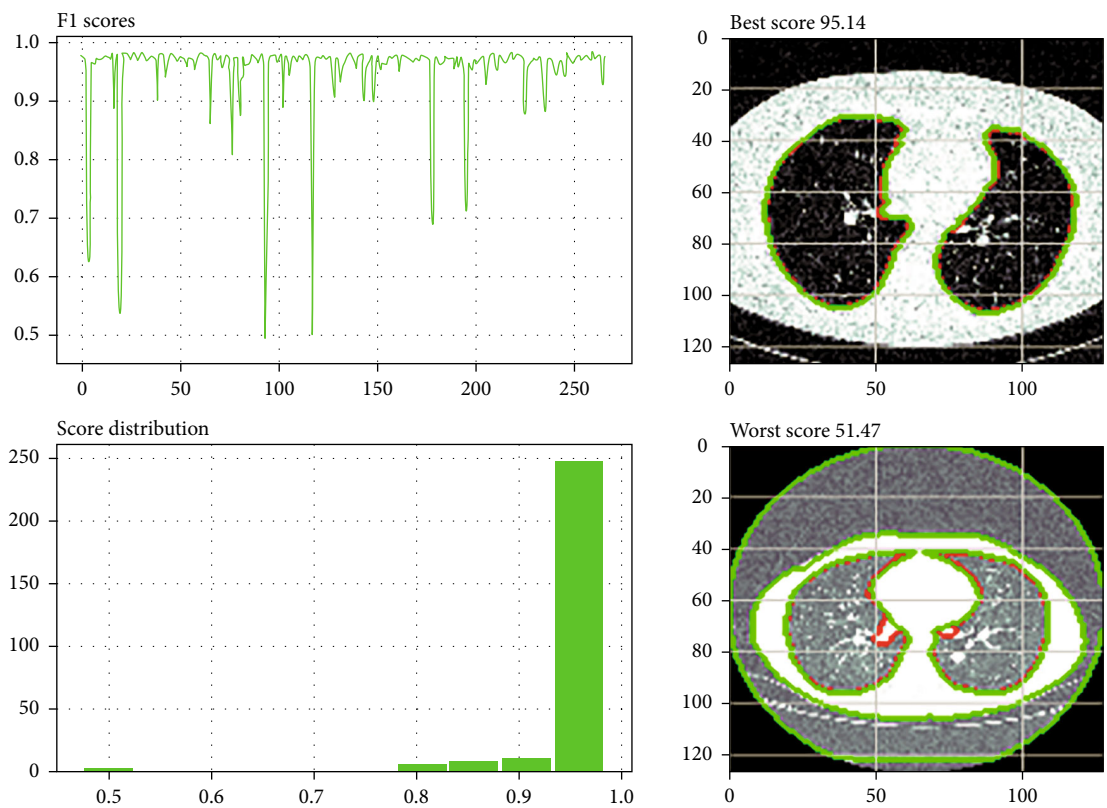

Figure 8: SegChaNet's best and worst performance scores.

Table 9: Comparison of the performance of the SegChaNet segmentation model with other state-of-the-art works.

Author (year) [reference]	Dataset	Accuracy	Qualitative analysis	Conclusion
Skourt, BA, et al. (2018)	MV, MI, and ME (union) auto: MV phase	0.95	The number of patients with nDSC 1 (within 1-millimeter uncertainty): 7. There are no discernible differences between b-spline and demons	With autocontouring, one may get sharp edges and corners.
Wouter R. P. H., et al. (2021)	All processes are done manually. Auto: dependent on the amount of artifacts, either ME or MI	0.76	NA	In the main breathing phase, there is good agreement between ITV and GTV with manual contours.
Mingjie X., et al. (2019)	Manuel: every stage auto: inherited from the MI phase	0.95	The number of patients that need manual adjustment	Good agreement between auto and manual contours.
Xu, M, et al. (2019)	Manual: all phases Auto: propagate from MI phase	0.92	Minimal. NA	Although autocontouring is precise, it produces bigger shapes.
Qinhua, H., et al. (2020)	Manual: every stage auto: propagated from ME phase	0.94	NA	Deformed contours agree well with physician-drawn contours.
Chiu, T. W., et al. (2021)	Manual: every stage auto: propagated from ME phase	0.63	The propagated IGTVs were mostly within the mIGTVs	The rigid body propagation method generates ITV within a 1 mm margin of error.
Jiang, J. et al. (2018)	Manual: ME (expert) and MI phase auto: ME phase	0.74	NA	The algorithm utilized generated more precise results. Results of segmentation differ from those in previously published papers.
SegChaNet (the proposed network)	Images of 46,698 CT scans both with and without tumors from the cancer imaging archive auto: ME phase	98.90	The applied preprocessing steps	A combined network with two primary components with many CAM has been utilized. We do not employ any manual contours.

nodules ranging in size from 5 to 32 mm in diameter in cancer patients undergoing low and normal voltage CT scans. This study was aimed at developing a DL-based automated lung cancer tumor segmentation network utilizing CT scan segmentation approaches combined with the assessment of segmentation uncertainty. Additionally, we investigated the influence of two widely used cost functions, dice and JI, on the model output's uncertainty measures. All three segmentation models perform well on the segmentation challenge, with dice-trained models marginally outperforming JI-trained models. The most precise methods for predicting nodule volumes were not the most repeatable, emphasizing the need to evaluate their precision and accuracy. Significant variations in algorithm performance were seen, especially in a sample of heterogeneous nodules, highlighting the need to use the same software throughout a longitudinal study.

In contrast to some recently proposed methods, we aimed to increase segmentation prediction variability by producing segmentation hypotheses with our novel method. Importantly, SegChaNet encompasses the entire space of possible segmentations rather than providing information about the models' uncertainty [63]. As is well known, manual, automated, and semiautomatic segmentation pose difficulties in terms of repeatability. The ability to accurately and consistently target lung cancer regions from surrounding tissues using CT images is critical for the clinical assessment of disease progression. The obtained features contribute to SegChaNet throughput and are subsequently decoded to provide an automatic network segmentation. In addition, these features are expected to encapsulate some of the intratumorally and peritumoral area's complex structural and functional geometry, some of which may be related to cancer survival. Overall, we show that SegChaNet, when combined with UQ, shows the best accuracy in lung cancer segmentation. When the existing V-Net models' results are studied, a novel SegChaNet model is proposed that capitalizes on the SegChaNet's superior qualities over the V-Net and U-Net models. On this dataset, three models were run, including the SegChaNet model, and the organ and tumor segmentation procedures were carried out independently. It has been shown that V-Net models can efficiently segregate organs and tumors using computerized images and that by handling the coding and decoding phases separately, more successful models may be developed than present V-Net models. Using medical imaging may be possible to develop more accurate models for multiorgan segmentation. The study may potentially be utilized as a reference for future SegChaNet models due to the success of the original SegChaNet model implementation and the beneficial contribution of the CAM architecture. Since the CAM design was applied solely to the output layer, tiny segmentation characteristics may be recorded. This is crucial for model design since each parameter is only effective when introduced to the appropriate model blocks. Table 9 compares the SegChaNet segmentation model's performance to that of other leading-edge studies.

Table 9 shows the performance of the SegChaNet segmentation model compared with other state-of-the-art works. Because of utilizing preprocessing stages and UQ methods, SegChaNet demonstrates the highest accuracy and dice outcomes.

5. Conclusions

The primary goal of this work is to offer a practical approach to lung segmentation. This paper describes a novel method, SegChaNet, that compared two traditional models (V-Net and U-Net) for lung cancer segmentation in CT scan images. SegChaNet achieves its top performance by utilizing a U-Net framework with CAM convolutions in the network's deepest layer and substantial supervision in its decoder layer. The proposed architecture surpasses state-of-the-art methods in segmentation accuracy and demonstrates initial feasibility in autosegmentation of the lung. Furthermore, it is likely to perform with various datasets and apply to other segmentation challenges in medical imaging. Overall, the SegChaNet method without CAM is 96.81% while with CAM is 98.48%.

Future studies will focus on whether the segmentation results help clinicians in the clinical setting while treating cancer. Additionally, we believe SegChaNet still has potential for improvement in terms of computing costs.

Data Availability

Data sharing is not applicable to this article as no datasets were generated during the current study.

Conflicts of Interest

The author declares that there is no conflict of interest.

References

[1] H. Sung, J. Ferlay, R. L. Siegel et al., "Global cancer statistics 2020: GLOBOCAN estimates of incidence and mortality worldwide for 36 cancers in 185 countries," *CA: a Cancer Journal for Clinicians*, vol. 71, no. 3, pp. 209–249, 2021.

[2] R. Adam, "Chemotherapy and surgery: new perspectives on the treatment of unresectable liver metastases," *Annals of Oncology*, vol. 14, p. ii13-ii16, 2003.

[3] M. Ilie, C. Butori, S. Lassalle et al., "Optimization of EGFR mutation detection by the fully-automated qPCR-based Idylla system on tumor tissue from patients with non-small cell lung cancer," *Oncotarget*, vol. 8, no. 61, pp. 103055–103062, 2017.

[4] X. Fan, X. Zhang, Z. Zhang, and Y. Jiang, "Deep learning-based identification of spinal metastasis in lung cancer using spectral CT images," *Scientific Programming*, vol. 2021, 7 pages, 2021.

[5] V. Donati, G. Fontanini, M. Dell'Omodarme et al., "WWOX expression in different histologic types and subtypes of non–small cell lung cancer," *Clinical Cancer Research*, vol. 13, no. 3, pp. 884–891, 2007.

[6] F. Shariaty, M. Orooji, E. N. Velichko, and S. V. Zavjalov, "Texture appearance model, a new model-based segmentation paradigm, application on the segmentation of lung nodule in the CT scan of the chest," *Computers in Biology and Medicine*, vol. 140, article 105086, 2022.

[7] N. S. Punn and S. Agarwal, "Modality specific U-Net variants for biomedical image segmentation: a survey," *Artificial Intelligence Review*, pp. 1–45, 2022.

[8] Y. Yang and C. Yu, "Advances in silica based nanoparticles for targeted cancer therapy," *Nanomedicine: Nanotechnology, Biology and Medicine*, vol. 12, no. 2, pp. 317–332, 2016.

[9] P. Savadjiev, J. Chong, A. Dohan et al., "Image-based biomarkers for solid tumor quantification," *European Radiology*, vol. 29, no. 10, pp. 5431–5440, 2019.

[10] V. Bhavsar, S. Zhang, and D. Bhugra, "Globalization, migration, and mental health," *Oxford Textbook of Public Mental Health*, vol. 281, 2018.

[11] S. Kumar, A. Srinivasan, and F. Nikolajeff, "Role of infrared spectroscopy and imaging in cancer diagnosis," *Current Medicinal Chemistry*, vol. 25, no. 9, pp. 1055–1072, 2018.

[12] R. Osuala, K. Kushibar, L. Garrucho et al., "A review of generative adversarial networks in cancer imaging: new applications, new solutions," 2021, arXiv preprint arXiv:2107.09543.

[13] A. González Rodríguez, *Early Detection of Lung Cancer through Nodule Characterization by Deep Learning (Bachelor's Thesis)*, Universidad Autónoma de Madrid, Spain, 2019.

[14] S. Wang, J. Cao, and P. Yu, "Deep learning for spatio-temporal data mining: a survey," *IEEE transactions on knowledge and data engineering*, p. 1, 2020.

[15] W. Fullick, *Human Infectious Disease and Public Health*, Oxford University Press, USA, 2019.

[16] S. M. B. Netto, A. C. Silva, R. A. Nunes, and M. Gattass, "Automatic segmentation of lung nodules with growing neural gas and support vector machine," *Computers in Biology and Medicine*, vol. 42, no. 11, pp. 1110–1121, 2012.

[17] A. Zotin, Y. Hamad, K. Simonov, and M. Kurako, "Lung boundary detection for chest X-ray images classification based on GLCM and probabilistic neural networks," *Procedia Computer Science*, vol. 159, pp. 1439–1448, 2019.

[18] M. N. Saad, Z. Muda, N. S. Ashaari, and H. A. Hamid, "Image segmentation for lung region in chest X-ray images using edge detection and morphology," in *In 2014 IEEE International Conference on Control System, Computing and Engineering (ICCSCE 2014)*, pp. 46–51, IEEE, 2014, November.

[19] X. Li, Y. Yang, Q. Zhao, T. Shen, Z. Lin, and H. Liu, "Spatial pyramid-based graph reasoning for semantic segmentation," in *In Proceedings of the IEEE/CVF Conference on Computer Vision and Pattern Recognition*, pp. 8950–8959, Seattle, WA, USA, June 2020.

[20] M. Kim and B. D. Lee, "Automatic lung segmentation on chest X-rays using self-attention deep neural network," *Sensors*, vol. 21, no. 2, p. 369, 2021.

[21] B. Maga, "Chest X-ray lung and heart segmentation based on minimal training sets. arXiv preprint arXiv:2101.08309," 2021.

[22] S. Jadon, "A Survey of Loss Functions for Semantic Segmentation," in *In 2020 IEEE Conference on Computational Intelligence in Bioinformatics and Computational Biology (CIBCB)*, pp. 1–7, IEEE, 2020, October.

[23] S. Minaee, Y. Y. Boykov, F. Porikli, A. J. Plaza, N. Kehtarnavaz, and D. Terzopoulos, "Image segmentation using deep learning: a survey," *IEEE Transactions on Pattern Analysis and Machine Intelligence*, p. 1, 2021.

[24] G. Zhang, G. Kang, Y. Wei, and Y. Yang, "Few-shot segmentation via cycle-consistent transformer," 2021, arXiv preprint arXiv:2106.02320.

[25] H. Tang, X. Qi, D. Xu, P. H. Torr, and N. Sebe, "Edge guided GANs with semantic preserving for semantic image synthesis," 2020, arXiv preprint arXiv:2003.13898.

[26] S. M. Naqi, M. Sharif, and A. Jaffar, "Lung nodule detection and classification based on geometric fit in parametric form and deep learning," *Neural Computing and Applications*, vol. 32, no. 9, pp. 4629–4647, 2020.

[27] G. Savitha and P. Jidesh, "A holistic deep learning approach for identification and classification of sub-solid lung nodules in computed tomographic scans," in *Computers & Electrical Engineering*, vol. 84, article 106626, Elsevier, New York, United States, 2020.

[28] Y. Han and J. C. Ye, "Framing U-net via deep convolutional framelets: application to sparse-view CT," *IEEE Transactions on Medical Imaging*, vol. 37, no. 6, pp. 1418–1429, 2018.

[29] M. Z. Alom, M. Hasan, C. Yakopcic, T. M. Taha, and V. K. Asari, *Recurrent Residual Convolutional Neural Network Based on U-Net (R2U-Net) for Medical Image Segmentation*, 2018.

[30] L. Liang, I. Zharkov, F. Amjadi, H. R. V. Joze, and V. Pradeep, "Guidance network with staged learning for image enhancement," in *In Proceedings of the IEEE/CVF Conference on Computer Vision and Pattern Recognition*, pp. 836–845, Nashville, TN, USA, June 2021.

[31] I. M. Nasser and S. S. Abu-Naser, "Lung cancer detection using artificial neural network," *International Journal of Engineering and Information Systems (IJEAIS)*, vol. 3, no. 3, pp. 17–23, 2019.

[32] P. Kale and D. S. Yadav, "Lung cancer prognosis by implementing various evolutionary Image processing steps," *By the International journal of analytical and experimental modal analysis*, vol. 12, no. 9, pp. 1103–1117, 2020.

[33] A. M. Mesleh, "Lung cancer detection using multi-layer neural networks with independent component analysis: a comparative study of training algorithms," *Jordan Journal of Biological Sciences*, vol. 10, no. 4, pp. 239–249, 2017.

[34] Y. Gu, X. Lu, L. Yang et al., "Automatic lung nodule detection using a 3D deep convolutional neural network combined with a multi-scale prediction strategy in chest CTs," *Computers in Biology and Medicine*, vol. 103, pp. 220–231, 2018.

[35] A. Chon, N. Balachandar, and P. Lu, *Deep Convolutional Neural Networks for Lung Cancer Detection*, Standford University, 2017.

[36] M. A. Khan, S. Rubab, A. Kashif et al., "Lungs cancer classification from CT images: an integrated design of contrast-based classical features fusion and selection," *Pattern Recognition Letters*, vol. 129, pp. 77–85, 2020.

[37] V. Inturi, N. Shreyas, K. Chetti, and G. R. Sabareesh, "Comprehensive fault diagnostics of wind turbine gearbox through adaptive condition monitoring scheme," *Applied Acoustics*, vol. 174, p. 107738, 2021.

[38] X. Zhang, L. Ning, Y. Hu et al., "Prognostic factors for primary localized gastrointestinal stromal tumors after radical resection: Shandong Gastrointestinal Surgery Study Group, Study 1201," *Annals of Surgical Oncology*, vol. 27, no. 8, pp. 2812–2821, 2020.

[39] P. Chaturvedi, A. Jhamb, M. Vanani, and V. Nemade, "Prediction and classification of lung cancer using machine learning techniques," in *In IOP Conference Series: Materials Science and Engineering*, vol. 1099no. 1, p. 012059, IOP Publishing, 2021, March.

[40] B. Chapaliuk and Y. Zaychenko, "Deep Learning Approach in Computer-Aided Detection System for Lung Cancer," in *In 2018 IEEE First International Conference on System*

Analysis & Intelligent Computing (SAIC), pp. 1–4, IEEE, 2018, October.

[41] N. Petrellis, "A review of image processing techniques common in human and plant disease diagnosis," *Symmetry*, vol. 10, no. 7, p. 270, 2018.

[42] Q. Yuan, M. Sui, C. Qin et al., "Migration, Transformation and Removal of Macrolide Antibiotics in the Environment: A Review," *Environmental Science and Pollution Research*, vol. 29, no. 18, pp. 26045–26062, 2022.

[43] H. Cao, H. Liu, E. Song et al., "Multi-branch ensemble learning architecture based on 3D CNN for false positive reduction in lung nodule detection," *IEEE access*, vol. 7, pp. 67380–67391, 2019.

[44] H. Xie, D. Yang, N. Sun, Z. Chen, and Y. Zhang, "Automated pulmonary nodule detection in CT images using deep convolutional neural networks," *Pattern Recognition*, vol. 85, pp. 109–119, 2019.

[45] W. Sun, B. Zheng, and W. Qian, "Automatic feature learning using multichannel ROI based on deep structured algorithms for computerized lung cancer diagnosis," *Computers in Biology and Medicine*, vol. 89, pp. 530–539, 2017.

[46] X. Huang, Q. Lei, T. Xie, Y. Zhang, Z. Hu, and Q. Zhou, "Deep transfer convolutional neural network and extreme learning machine for lung nodule diagnosis on CT images," *Knowledge-Based Systems*, vol. 204, article 106230, 2020.

[47] L. M. Pehrson, M. B. Nielsen, and C. Ammitzbøl Lauridsen, "Automatic pulmonary nodule detection applying deep learning or machine learning algorithms to the LIDC-IDRI database: a systematic review," *Diagnostics*, vol. 9, no. 1, p. 29, 2019.

[48] D. Sharma and G. Jindal, "Identifying lung cancer using image processing techniques," *In International Conference on Computational Techniques and Artificial Intelligence (ICCTAI'2011)*, vol. 17, pp. , 2011872–880, 2011.

[49] M. U. Akram, S. Khalid, A. Tariq, and M. Y. Javed, "Detection of neovascularization in retinal images using multivariate m-Mediods based classifier," *Computerized Medical Imaging and Graphics*, vol. 37, no. 5-6, pp. 346–357, 2013.

[50] F. Paulin and A. Santhakumaran, "Classification of breast cancer by comparing back propagation training algorithms," *International Journal on Computer Science and Engineering*, vol. 3, no. 1, pp. 327–332, 2011.

[51] T. Jia, D. Z. Zhao, J. Z. Yang, and X. Wang, "Automated detection of pulmonary nodules in HRCT images," in *In 2007 1st International Conference on Bioinformatics and Biomedical Engineering*, pp. 833–836, IEEE, 2007, July.

[52] T. Javaheri, M. Homayounfar, Z. Amoozgar et al., "CovidCT-Net: an open-source deep learning approach to diagnose covid-19 using small cohort of CT images," *NPJ digital medicine*, vol. 4, no. 1, pp. 1–10, 2021.

[53] M. B. Martell, M. Chen, K. Linton-Reid, J. M. Posma, S. J. Copley, and E. O. Aboagye, "Development of a multi-task learning V-Net for pulmonary lobar segmentation on computed tomography and application to diseased lungs," 2021, arXiv preprint arXiv:2105.05204.

[54] Q. Zheng, M. Yang, X. Tian, N. Jiang, and D. Wang, "A full stage data augmentation method in deep convolutional neural network for natural image classification," *Discrete Dynamics in Nature and Society*, vol. 2020, 11 pages, 2020.

[55] L. Qian, *Augmented Reality Assistance for Surgical Interventions Using Optical See-Through Head-Mounted Displays(Doctoral dissertation)*, The Johns Hopkins University, United States, 2020.

[56] J. Ma, J. Chen, M. Ng et al., "Loss odyssey in medical image segmentation," *Medical Image Analysis*, vol. 71, p. 102035, 2021.

[57] H. G. Lee and S. C. Lee, "Morphological multi-cell discrimination for robust cell segmentation," *IEEE Access*, vol. 8, pp. 49837–49847, 2020.

[58] M. Hashemi, M. Akhbari, and C. Jutten, "Delve into multiple sclerosis (MS) lesion exploration: a modified attention U-net for MS lesion segmentation in brain MRI," *Computers in Biology and Medicine*, vol. 145, p. 105402, 2022.

[59] M. A. Rahman and Y. Wang, "Optimizing Intersection-over-Union in Deep Neural Networks for Image Segmentation," in *In International symposium on visual computing*, pp. 234–244, Springer, Cham, 2016, December.

[60] T. Pang, S. Guo, X. Zhang, and L. Zhao, "Automatic lung segmentation based on texture and deep features of HRCT images with interstitial lung disease," *BioMed Research International*, vol. 2019, 8 pages, 2019.

[61] J. Cai, L. Lu, Y. Xie, F. Xing, and L. Yang, "Improving deep pancreas segmentation in CT and MRI images via recurrent neural contextual learning and direct loss function," 2017, arXiv preprint arXiv: 1707.04912.

[62] A. C. F. D. Oliveira, *Segmentation of Lungs on CT: Tools to Aid Radiotherapy Planning(Doctoral dissertation)*, Universidade de Coimbra, Portugal, 2019.

[63] Z. Xiao, B. Liu, L. Geng, F. Zhang, and Y. Liu, "Segmentation of lung nodules using improved 3D-UNet neural network," *Symmetry*, vol. 12, no. 11, p. 1787, 2020.

Hindawi
Applied Bionics and Biomechanics
Volume 2022, Article ID 9279638, 14 pages
https://doi.org/10.1155/2022/9279638

Research Article

A Biomechanical Study on Failed Snatch Based on the Human and Bar Combination Barycenter

Gongju Liu,[1,2] Houwei Zhu,[3] Jing Ma,[1] Huiju Pan,[3] Xu Pan,[1] Yingyue Zhang,[1] Ting Hu,[1] Gusztáv Fekete,[2] Haiying Guo ,[1] and Minjun Liang [4,5]

[1]*Scientific Research Department, Zhejiang College of Sports, China*
[2]*Faculty of Engineering, University of Pannonia, Hungary*
[3]*College of Physical Education and Health Sciences, Zhejiang Normal University, China*
[4]*Research Academy of Grand Health, Ningbo University, China*
[5]*Department of Physical and Health Education, Udon Thani Rajabhat University, Thailand*

Correspondence should be addressed to Haiying Guo; 71766420@qq.com and Minjun Liang; liangminjun@nbu.edu.cn

Received 20 February 2022; Accepted 19 April 2022; Published 10 May 2022

Academic Editor: Justin Fernandez

Objective. The purpose of this research was to use a new method the human and bar combination barycenter to exposit the differences between successful and failed characteristics of snatch attempts in competition. Try to establish an effective biomechanical method that can uncover the main factors for the failed snatch. The obtained results will provide valuable information for weightlifters to improve the success rate in snatch by altering their technical issues accordingly. *Methods*. A 3-D video analysis method was used to compare the characteristics of the heaviest successful and failed attempts of ten elite weightlifters in the men's 73 kg category. The video was captured under competitive conditions at the 2019 World Weightlifting Championships, the 2019 Asian Weightlifting Championships, and the 2020 China Olympic Trial. The video data were digitized using the SIMI°Motion7.50 3-D system (Germany). *Results*. Significant difference ($P > 0.05$) was not found between the successful and failed attempts in the parameters, such as the maximal vertical rising velocity, the maximal vertical height, and the vertical displacement of the barbell. The maximal descending acceleration of the human body, the time duration, the angles of the hip, and knee joints were no significant difference. However, significant differences were found in the variation of the human and bar combination barycenter on the X -axis in the inertial ascent stage and the squat support stage ($t = 2.862, P < 0.05$; $t = 3.376, P < 0.05$). *Conclusions*. A probable cause of the failed snatch is that the displacement of human and bar combination barycenter on the X -axis is not enough to reach the position for supporting barbell during the inertial ascent stage and the squat support stage. The reason is that the strength of reclining of torso at the end of the force phase is insufficient. Insufficient knee flexion in the knee flexion phase ($M2$), which leads to a lower maximum vertical velocity of barbell, may be an indirect factor leading to the failed snatch. The cumulative variation of human and bar combination barycenter on the X -axis can effectively determine the technical characteristics between the success and failure in snatch.

1. Introduction

The technical principle of the snatch shows that weightlifters need to follow the three principles of "Near," "Fast," and "Low" during the snatch process [1, 2]. "Near" means that the barbell is required to be as close to the body as possible during the lifting, which is determined by the horizontal distance (L_H) between the center of gravity (COG) of barbell and human body [3]. "Fast" means that pulling the barbell and action force should be fast, which is determined by the maximal velocity at the end of the force phase ($V_{\max}$) [3]. "Low" refers to requiring lifters to reduce the *COG* of body at the fastest speed to facilitate the support to the barbell, which is determined by the biggest falling acceleration (a_f) of *COG* of body during the squat support stage [3].

With the application of 3-D technology, the parameters which were used to determine the three principles are more diverse and precise. The maximal height (H_{bmax}) and the fall

distance of the barbell (H_{bd}) are the key parameters to evaluate the support technique [4, 5]. The trajectory of *COG* of barbell and body are used as an overall analysis of snatch technical characteristics [6–8]. Spatial-temporal characteristics and angle of joints of human body are parameters for evaluating the structure of the snatch after the division of snatch movement [9, 10]. Phases of snatch reveal that the snatch technique must not only conform to the mechanics principle but also adapt to the body structure and physiological characteristics. "Phases" of snatch is an important supplement to the three principles, which can be called the fourth principle.

In recent years, there are many studies on the technical characteristics of elite weightlifters in terms of snatch structure evaluation, *COG* of barbell, and *COG* of human body. Wang et al. and Li et al. used 3-D kinematics method to analyze the time structure, the changes of barbell space structure, and joints angle characteristics of different phases of Chinese female elite weightlifters [9, 10]. Yang et al. and Erbil compared the technical differences between male and female lifters in a series parameters such as time structure, barbell spatial structure, work ratio, and joints angle [11, 12]. Ikeda et al. and Musser et al. analyzed the technical differences among different categories [13, 14]. Some studies compared the successful and unsuccessful snatch technique of elite lifters in temporal structure, spatial structure, and characteristics of *COG* of barbell in phases [15–17].

Wang et al. reported that the failed snatch of most elite lifters occurred during the support completion phase [18]. Therefore, it is speculated that the main reason for failure of forward or backward is that the position of the *COG* of human body and barbell on the sagittal plan exceeds the lifters' control limit. Since the trajectory of the *COG* of barbell will be different of every attempt of each lifter, there is a certain relationship between the trajectories of the *COG* of barbell and human body. Therefore, it is difficult to find the difference between successful and failed attempts only from the trajectory of the *COG* of human body or barbell. In this case, the human and bar combination barycenter may be a good choice. The concept of human and bar combination barycenter was first coined by Wang in 1984 [19], due to the technical limitations, the characteristics and the roles of human and bar combination barycenter were not explained in their research at that time. Although there are some studies that try to compare successful and failed attempts, this is insufficient and the factors of failed snatch are still unclear.

In the snatch competition, each athlete only has 3 attempts to lift the barbell, so the success rate is the guarantee for the best results. The present study proposes to use the human and bar combination barycenter as the parameter to compare the successful and failed snatch attempts. The purpose of the present research is to analyze the three principles of "Near," "Fast," and "Low," the phased principle, and the human and bar combination barycenter, to exposit the differences between successful and failed characteristics of snatch in competition, and to explore the biomechanical factors that cause the snatch failure.

Table 1: Information of subjects ($n = 10$).

Subjects	Body mass (kg)	Height (m)	Heaviest successful weight (kg)	Heaviest unsuccessful weight (kg)
1	72.88	1.70	155	150
2	72.56	1.71	155	146
3	73.00	1.68	158	154
4	72.79	1.70	146	140
5	72.90	1.68	146	144
6	72.55	1.71	161	156
7	73.00	1.74	148	145
8	72.39	1.69	156	151
9	72.92	1.70	150	148
10	72.63	1.65	144	140

2. Subjects and Methods

2.1. Subjects. The data were captured in the final A of World Weightlifting Championships (2019), the Asian Weightlifting Championships (2019), and the China Olympic Trial (2020). The weightlifters in the men's 73 kg category of snatch competition were selected, and the attempts of their maximum weights for success and failure were selected for analysis. The selection criteria for the unsuccessful performances are that the moment of failure must occur in the support completion phase, and all the unsuccessful performances are forward falling to facilitate the data analysis. Data on height, body mass, and maximum successful and failed results are shown in Table 1. The present study was authorized by the Ethics Committee of General Administration of Sport of China. All video data are from public competitions, and the video collection method used will not affect the athletes' performance in any way.

2.2. Experimental Design

2.2.1. Camera System and Coordinate System

(1) Camera System. In order to acquire kinematic indexes of human body and barbell, according to the on-site surroundings, we used two professional cameras, which were set approximately 15 meters from the center of the platform. The optical axis of the two cameras formed an angle of about 45° with the middle line of frontal plane (Figure 1(a)). The focal length and position of the two cameras kept unchanged during the whole competition. The raw data were smoothed using a low-pass digital filter with the 4 Hz of cut-off frequency [11, 20].

(2) Coordinate System. One hour before the snatch competition starts, we used the PEAK 3-D framework to calibrate the space of weightlifting platform (Figure 1(b)). At the beginning of snatch, the coordinates of the *COG* of barbell are set to (0, 0, and 22.5) in cm, and the coordinates of position of human body and barbell correspond to it during the movement. The setting of coordinate system is that the positive direction of X -axis is directly behind the lifter, the

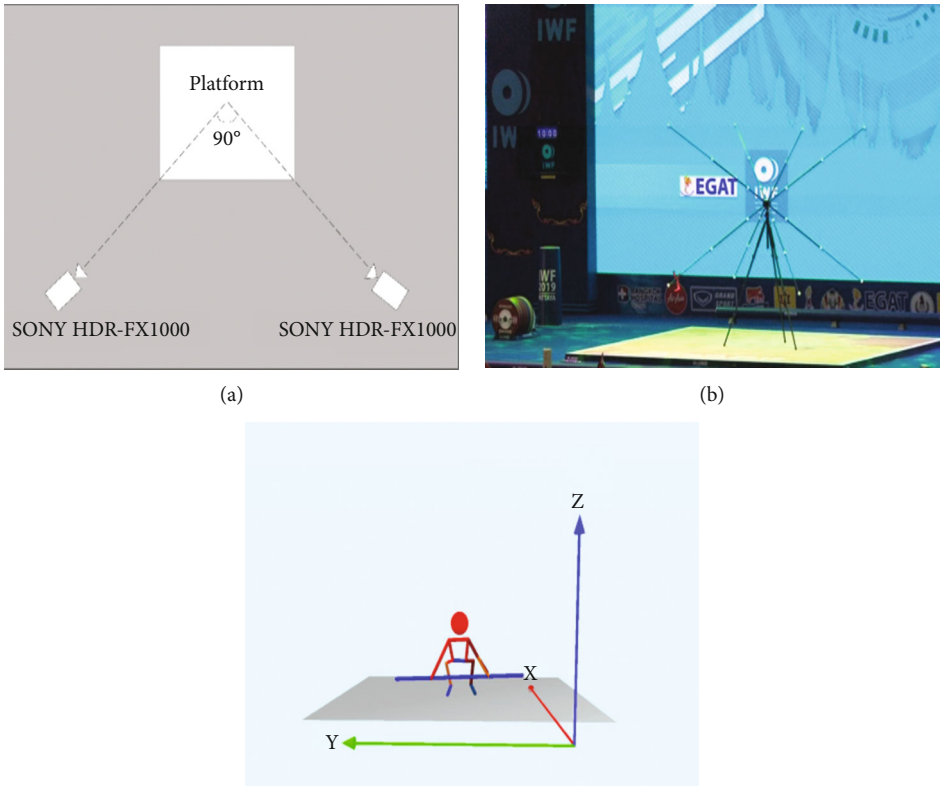

Figure 1: Experimental design and 3-D coordinate system.

positive direction of y-axis is on the right side, and the positive direction of Z -axis is vertically upward (Figure 1(c)).

2.2.2. Data Collection and Calculation

(1) Phases Division of Snatch. The snatch process was divided into six phases in most previous studies; they are the first pull phase, the transition phase, the second pull phase, the turnover phase, the catch phase, and fully stand phase [11, 21–24]. And they reported that the phases before the full stand were the most important in snatch [20, 22, 25, 26]. In the present study, the snatch action from start to end of squat position, which is consistent with literature, was divided as the knee extension phase, the knee flexion phase, the force phase, the inertial ascent phase, the squat support phase, and the support completion phase, which were abbreviated as $M1$-$M6$ [27]. The characteristics of each phase are shown in Figure 2; each picture represents the beginning and end of the phase.

(2) Data Collection. In order to calculate the kinematic indexes of human body and barbell, seventeen key points were manually digitized in the SIMI°Motion7.50 3-D system (Figure 3). These key points include the head, bilateral shoulder, bilateral elbow, bilateral wrist, bilateral hip, bilateral knee, bilateral ankle bone, bilateral tiptoe, and two endpoints of barbell [28]. The *COG* position of barbell was calculated form the geometric center of the two endpoints of barbell, and the *COG* position of human body was obtained by Hanavan Body Mathematical Model; they were obtained in the SIMI°Motion system automatically.

In the present study, several variables were selected to assess the three principles of "Near," "Fast," and "Low" and the characteristics of phases. The minimum horizontal distance between the *COG* of barbell and human body when the barbell was rising (L_{Hmin}) was selected for assessing the "Near" principle. The maximal vertical rising velocity (V_{max}) and the maximal vertical height of barbell (H_{bmax}) were selected to assess the "Fast" principle [16]. At the end of $M3$, the lifter's body begins to squat down quickly, at which time the maximum falling acceleration of the *COG* of body (a_f), the vertical distance between the *COG* of barbell and human body at the end of $M4$ (L_{Hz1}) and $M5$ (L_{Hz2}), and the vertical height of human body (H_{bd5}) and barbell (H_{b5}) at the end of $M5$ were selected for assessing the "Low" principle. The vertical displacement of barbell and the time duration of each phase and the angles of hip and knee joints at the end of each phase were chosen to assess the characteristics of phases.

(3) Human and Bar Combination Barycenter Calculation. The original coordinate data of *COG* of barbell and human body were exported by the SIMI°Motion system, and the position of human and bar combination barycenter was calculated by the following formulas.

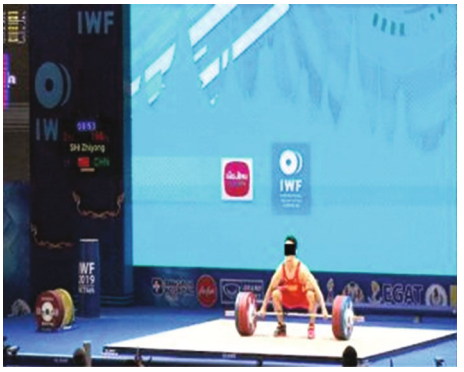

Start position

(a)

1st maximum knee extension

(b)

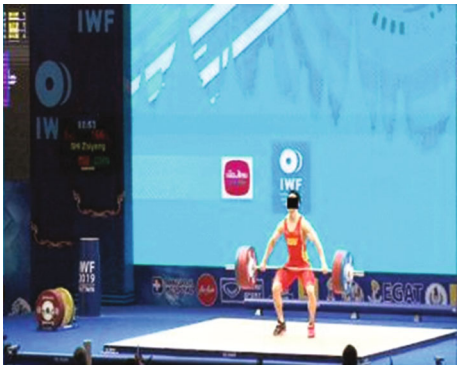

Maximum knee flexion

(c)

Maximum vertical rising velocity of barbell

(d)

Maximum vertical height of barbell

(e)

Maximum vertical falling velocity of barbell

(f)

Figure 2: Continued.

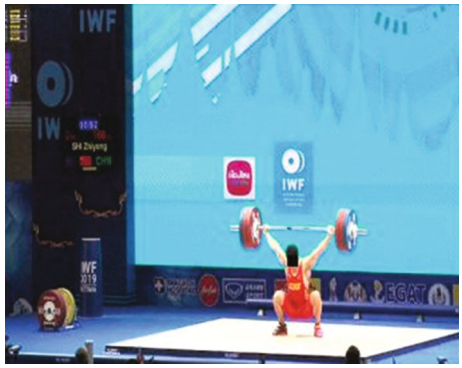

Squat position

(g)

Fully recover

(h)

Figure 2: The feature pictures of each phase of snatch.

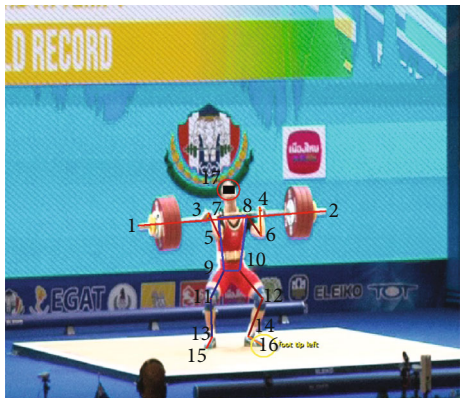

Figure 3: Seventeen key points on the human body and barbell manually digitized.

(4) Calculation of X-Axis Coordinates of Human and Bar Combination Barycenter (X_c). The *COG* of human body position on the X -axis is $X1$, the *COG* of barbell position on the X -axis is $X2$, the weight of lifter is $M1$, and the weight of barbell is $M2$.

$$X_c = \frac{(X1 \times M1 + X2 \times M2)}{(M1 + M2)}. \quad (1)$$

(5) Calculation of Y-Axis Coordinates of Human and Bar Combination Barycenter (Y_c). The *COG* of human body position on the Y -axis is $Y1$, the *COG* of barbell position on the Y -axis is $Y2$, the weight of lifter is $M1$, and the weight of barbell is $M2$.

$$Y_c = \frac{(Y1 \times M1 + Y2 \times M2)}{(M1 + M2)}. \quad (2)$$

(6) Calculation of Z-Axis Coordinates of Human and Bar Combination Barycenter (Z_c). The *COG* of human body position on the Z -axis is $Z1$, the *COG* of barbell position on the Z -axis is $Z2$, the weight of lifter is $M1$, and the weight of barbell is $M2$.

$$Z_c = \frac{(Z1 \times M1 + Z2 \times M2)}{(M1 + M2)}. \quad (3)$$

2.3. Statistical Analyses. The homogeneity of variance and normal distribution assumptions were analyzed by Levene's tests and Kolmogorov-Smirnov, respectively. Using Box-whisker plot to test outliers in variables. The data comparison was analyzed by a paired-sample t test and calculated the linear variation with time of human and bar combination barycenter on X -axis using a linear regression equation. $P < 0.05$ indicates a significant difference between successful and failed snatch. The results of statistical analysis were obtained using the IBM SPSS 20.0 (SPSS Inc., Chicago, IL, USA).

3. Results

3.1. Comparison of the Characteristics of "Near," "Fast," and "Low" Principles. Comparison the successful and failed snatch of the ten lifters, the characteristics of "Near," "Fast," and "Low" principles are shown in Table 2. There were no significant differences between success and failure in the minimum horizontal distance between the *COG* of barbell and human body during the barbell rising (L_{Hmin}), in the maximal vertical rising velocity (V_{max}), in the maximal vertical height (H_{bmax}), in the vertical height of human body (H_{bd5}) and barbell (H_{b5}) at the end of $M5$, and in the vertical distance between the *COG* of barbell and human body at the end of $M5$ (L_{Hz2}). Furthermore, there was no significant difference between success and failure in the maximum falling acceleration of the *COG* of human body (a_f) ($t = -1.189$, $P = 0.265$). In the successful attempts, the a_f is 0.3938 m/s^2 greater than that in unsuccessful attempts. However, it is worth noting that the a_f of eight lifters in successful and unsuccessful actions are greater than the acceleration of gravity ($g = 9.8$ m/s^2), and the a_f of other two lifters are less than the acceleration of gravity. In addition, significant

Table 2: Comparative analysis of the parameters of "Near," "Fast," and "Low" principles.

	Successful	Unsuccessful
L_{Hmin} (m)	0.04192 ± 0.0158	0.0431 ± 0.0163
$V_{\max}$ (m/s)	1.6984 ± 0.1421	1.6137 ± 0.16342
H_{bmax} (m)	1.1791 ± 0.03618	1.1840 ± 0.11316
a_f (m/s^2)	−13.0760 ± 4.6054	−12.6822 ± 4.4197
L_{Hz1} (m)	0.5152 ± 0.0354	0.4957 ± 0.0386*
H_{b5} (m)	1.1193 ± 0.0421	1.1083 ± 0.0349
H_{bd5} (m)	0.5236 ± 0.0232	0.5180 ± 0.0321
L_{Hz2} (m)	0.5912 ± 0.0467	0.5914 ± 0.0164

*Statistically significant difference ($P < 0.05$).

difference ($t = 4.043, P = 0.01$) could be found between success and failure in the vertical distance between the *COG* of barbell and human body at the end of $M4$ (L_{Hz1}). The L_{Hz1} in successful attempts is 1.95 cm larger than that in unsuccessful actions.

3.2. Comparison of the Characteristics of Phases. In order to analyze the characteristics of snatch in more details, the snatch process is usually divided into several phases. In the present study, the snatch from start to the squat position was divided as six phases (Figure 2). Since the unsuccessful attempts all occur in the $M6$, the comparison of phase characteristics does not include the $M6$. The vertical displacement of each phase of barbell, the duration time, and the angles of the hip and knee joints at the end of each phase is chosen for analyzing. The comparison of the characteristics of phases between the successful and unsuccessful attempts is shown in Tables 3 and 4. In the present study, there was no significant difference between success and failure of the ten weightlifters in the vertical displacement and duration time of each phase, the angle of hip, and knee joints at the end of the six phases.

3.3. Comparison of Human and Bar Combination Barycenter. The "combination barycenter" is derived from the calculation of the *COG* of combined objects in physics. The human and bar combination barycenter is to view the human body and barbell as a whole, the combination barycenter of the *COG* of body and barbell. Before calculating the human and bar combination barycenter, the data are unified firstly, and the 3-D coordinates are defined as X-, Y-, and Z-axis. Set the 3-D coordinates of the *COG* of barbell before the snatch to (0, 0, 0.225), and the corresponding 3-D coordinates of the *COG* of body are processed accordingly, so that the 3-D coordinates at the beginning of all attempts are consistent. The comparison of the human & bar combination barycenter between the successful and unsuccessful attempts on the X-, Y-, and Z-axis are shown in Figures 4–6.

The trajectory changes of the human and bar combination barycenter of the successful and unsuccessful attempts on the X -axis are shown in Figure 4. The displacement of human and bar combination barycenter of ten lifters all increase with time, and the slopes of successful snatch of all lifters are higher than that of unsuccessful snatch. Figure 5 shows the trajectory changes of human and bar combination barycenter of successful and unsuccessful attempts on the Y -axis. The offsets of all lifters on the Y -axis are very small, and there is no obvious regular pattern. Figure 6 shows the trajectory changes of the human and bar combination barycenter on the Z -axis. The trajectories of human and bar combination barycenter of successful and unsuccessful on the Z -axis show a trend of rising first and then decreasing, and the trajectories show a high degree of consistency.

In order to further study the characteristics of human and bar combination barycenter of successful and failed attempts, the present study intercepted the values of the human and bar combination barycenter on the X -axis at the characteristic pictures of each phase and calculated the variation of each phase and compared the difference of human and bar combination barycenter between successful and failed attempts on the X -axis. Secondly, this study used the method of calculating the cumulative variation to analyze the difference of the human and bar combination barycenter between the successful and unsuccessful actions on the Y - and Z -axis.

Table 5 shows the results of displacement of the human and bar combination barycenter at the characteristic pictures of each phase and displacement change of each phase of successful and failed snatch on the X -axis. There are significant differences in the displacement of human and bar combination barycenter on the X -axis between successful and failed snatch at the end of $M1, M2, M4$, and $M5$ ($t = 2.480, P < 0.05$; $t = 2.493, P < 0.05$; $t = 3.584, P < 0.05$; $t = 4.104, P < 0.05$). There was no statistical difference at the beginning of $M1$ and the end of $M3$ ($t = 1.429, P = 0.187$; $t = 2.152, P = 0.060$). Since the change of the human and bar combination barycenter on the X -axis shows an upward trend, the change values were used to represent the variation of each phase. Significant differences were found in the variation of human and bar combination barycenter between successful and unsuccessful on the X -axis in the phase of $M4$ and $M5$ ($t = 2.862, P < 0.05$; $t = 3.376, P < 0.05$). In the other three phases, there was no significant difference between success and failure ($t = 0.176, P = 0.864$; $t = 1.383$, $P = 0.200$; $t = 1.824, P = 0.102$).

Since the change of human and bar combination barycenter fluctuates on the Y -axis and Z -axis, the cumulative variation in phase is used to analyze the characteristics of the successful and failed attempts (Table 6). Assuming that there n frames in each phase, the calculation formula of the cumulative variation (Y_{cn}) of the human and bar combination barycenter on the Y -axis in this phase is as follows (the calculation of Z_{cn} and Y_{cn} is the same):

$$Y_{cn} = |Yc2 - Yc1| + |Yc3 - Yc2| \cdots + |Ycn - Yc(n-1)|. \quad (4)$$

There is no significant difference (Table 6) in the cumulative variation of the human and bar combination barycenter on the y-axis at each phase between success and failure

Table 3: Vertical displacement of barbell and time duration of each phase of the successful and unsuccessful snatch.

	Vertical displacement of each phase (m)		Duration of each phase (s)	
	Successful	Unsuccessful	Successful	Unsuccessful
*M*1	0.5584 ± 0.0839	0.5533 ± 0.0674	0.454 ± 0.049	0.458 ± 0.0537
*M*2	0.1271 ± 0.0389	0.1312 ± 0.0508	0.290 ± 0.2354	0.300 ± 0.2400
*M*3	0.2610 ± 0.0541	0.2566 ± 0.0516	0.416 ± 0.2819	0.409 ± 0.2837
*M*4	0.2889 ± 0.0278	0.2784 ± 0.0189	0.552 ± 0.3821	0.546 ± 0.3737
*M*5	0.0593 ± 0.0054	0.0648 ± 0.0117	0.532 ± 0.4896	0.536 ± 0.4903

Table 4: Angles of hip and knee joints at the end of each phase of successful and unsuccessful snatch.

	Knee angel (degree)		Hip angle (degree)	
	Successful	Unsuccessful	Successful	Unsuccessful
*M*1	121.85 ± 11.42	124.24 ± 9.93	85.02 ± 5.63	88.87 ± 14.27
*M*2	111.9 ± 6.47	118.89 ± 9.22	111.18 ± 7.75	112.22 ± 7.39
*M*3	153.13 ± 9.22	151.84 ± 7.88	144.68 ± 19.58	152.64 ± 6.54
*M*4	68.47 ± 8.38	68.72 ± 9.37	99.08 ± 20.43	101.67 ± 18.78
*M*5	44.71 ± 6.2	45.29 ± 10.34	52.38 ± 11.62	58.72 ± 16.45

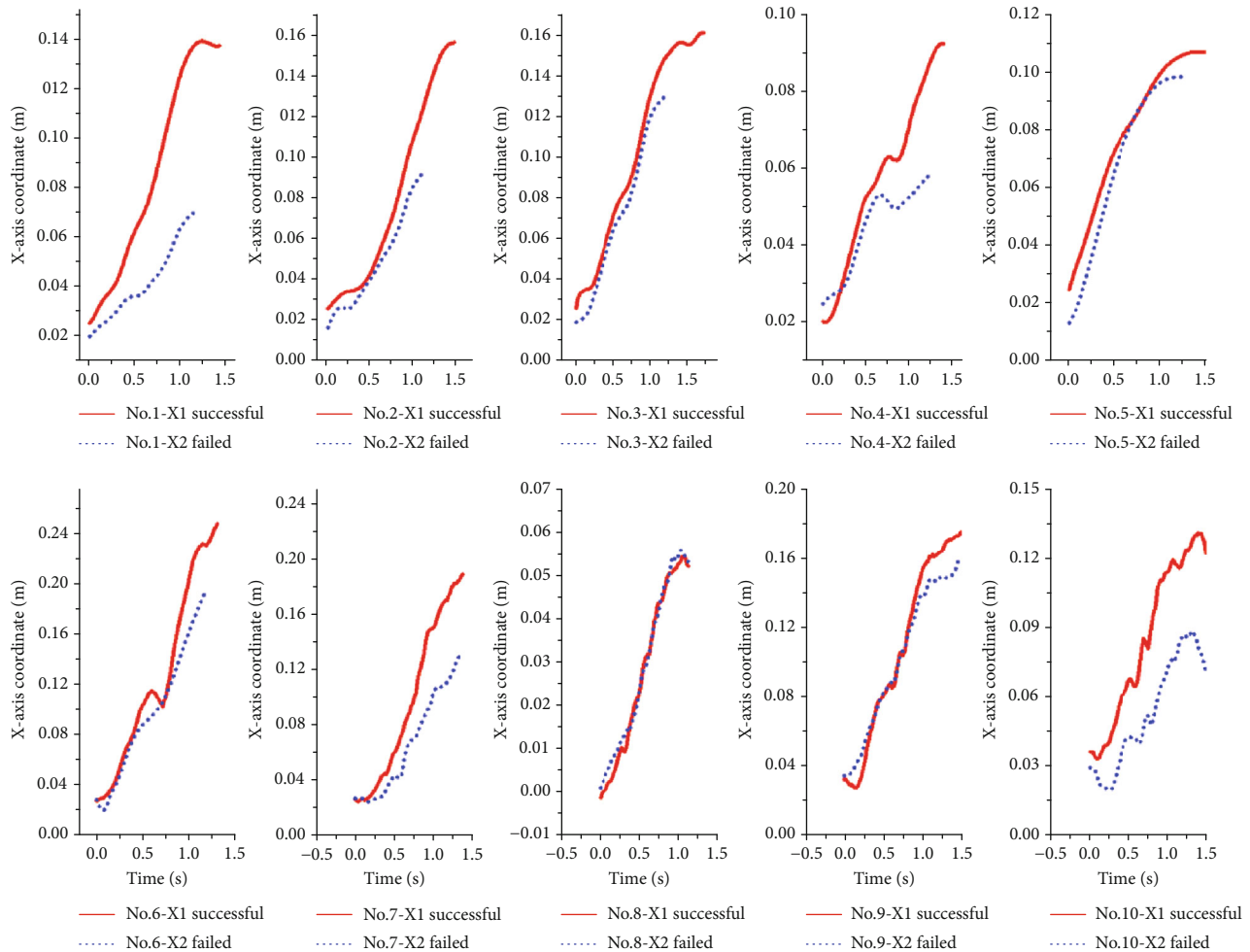

Figure 4: The trajectories of the human and bar combination barycenter of successful and unsuccessful snatch on the *X* -axis.

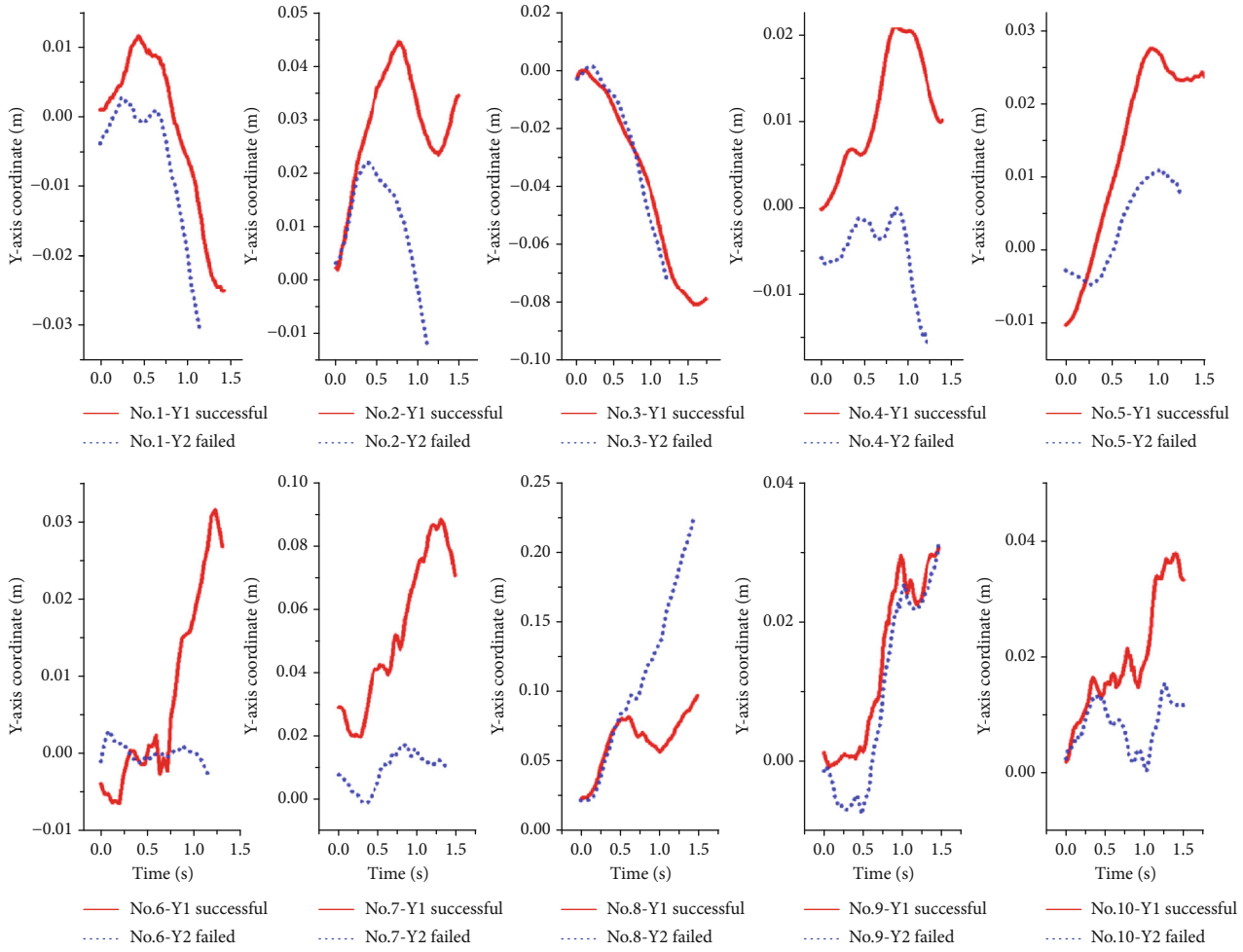

Figure 5: The trajectories of the human and bar combination barycenter of successful and unsuccessful snatch on the Y -axis.

($t = 1.025, P = 0.332$; $t = -1.326, P = 0.217$; $t = 1.012, P = 0.338$; $t = -0.319, P = 0.757$; $t = -0.931, P = 0.376$). And there is no significant difference in the cumulative variation of the human and bar combination barycenter on the Z -axis at each phase between success and failure ($t = -0.496, P = 0.632$; $t = -1.556, P = 0.154$; $t = 1.275, P = 0.234$; $t = 1.433, P = 0.186$; $t = -1.112, P = 0.295$).

3.4. Analysis of the Regression Equation of the Human and Bar Combination Barycenter on the X -Axis during the Phases of M4 and M5. Given that the differences of human and bar combination barycenter on the X -axis between successful and failed attempts mainly occur in the $M4$ and $M5$ phases, the present study established the regression equations of the displacement change of the human and bar combination barycenter on the X -axis with time in these two phases. Take time as the independent variable (χ) and the value of human & bar combination barycenter on the X -axis as the dependent variable (y). The regression equation model was used to establish a linear unitary regression equation for the success and failure in the phases of $M4$ and $M5$ (Table 7). The fitting degree of each linear regression equation model is represented by the R^2 value (Table 8), and the R^2 values of all regression equation models are greater than 0.85, indicating that the data is well fitted and linear. The t-test of all independent variables of the regression equation is less than 0.001, and the sample regression coefficient (the slope of the regression line) of successful linear regression equation of each athlete is greater than the failure.

4. Discussion

4.1. Analysis of the "Near," "Fast," and "Low" Principles and the Parameters in Phases. In the present study, the snatch can be divided into two parts: the first part is from the moment of snatch start to the barbell's maximum vertical velocity; the second part is from the beginning of the barbell's inertial rise to the athlete's squatting and receiving the barbell. The first part can be divided into three phases: knee extension phase ($M1$), knee flexion phase ($M2$), and force phase ($M3$). This part is mainly for athletes to lift the barbell, give the barbell an upward force, so that the barbell can gain a certain speed and height and obtain the most appropriate initial velocity (V_{max}) at the end of this part. The 2nd part can be divided into three stages: the inertial ascent stage ($M4$), the squat support stage ($M5$), and the support completion stage ($M6$). The second part mainly uses the speed obtained in the first part to make the barbell

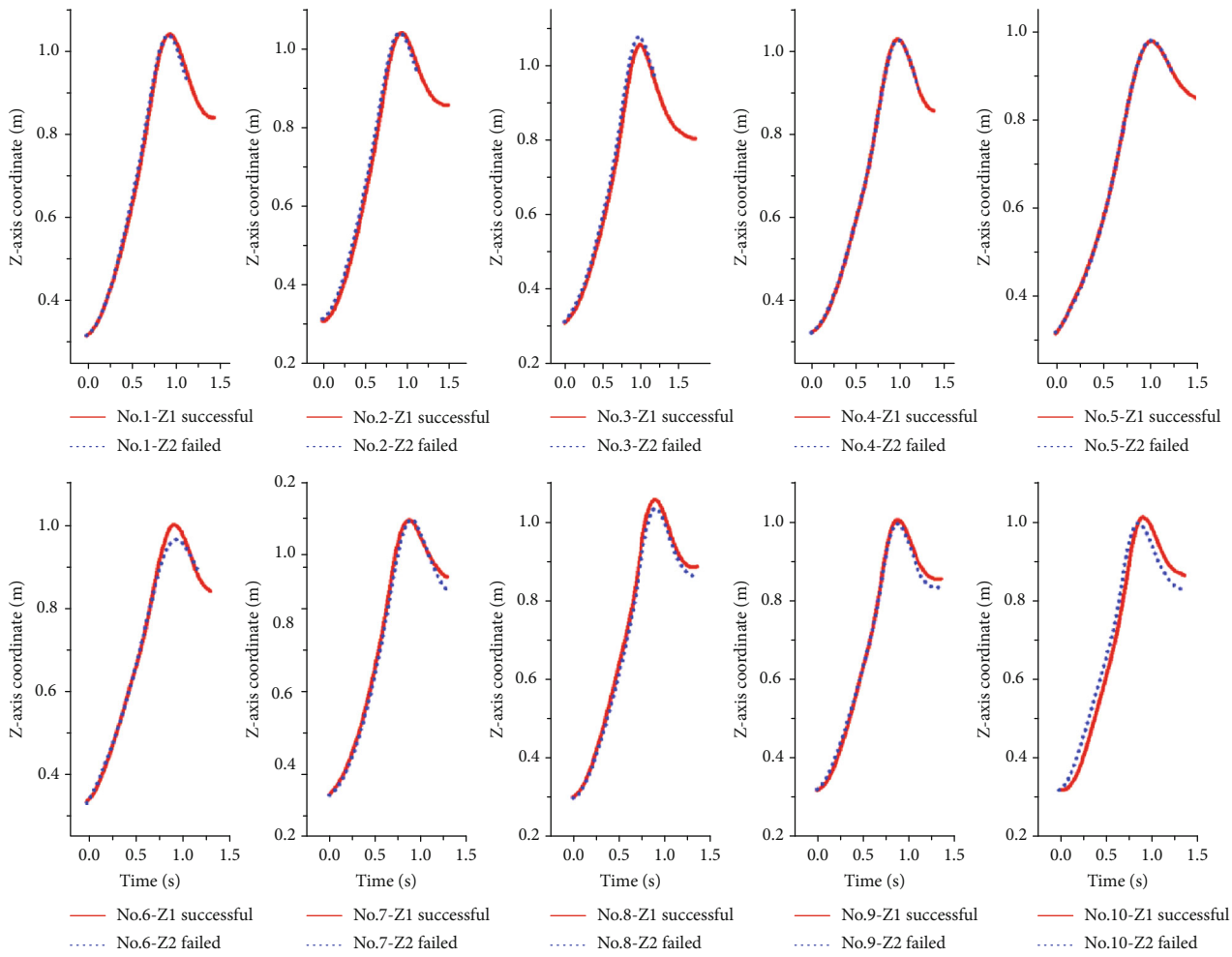

Figure 6: The trajectories of the human and bar combination barycenter of successful and unsuccessful snatch on the Z -axis.

Table 5: The displacement of the human and bar combination barycenter at the characteristic pictures and the variation of each phase of successful and failed snatch on the X -axis (cm).

	Value of characteristic pictures			Variation of phases	
	Successful	Unsuccessful		Successful	Unsuccessful
a	1.7431 ± 1.1772	1.5077 ± 1.1016			
b	4.5164 ± 2.6399	4.0348 ± 2.6847*	$M1$	2.9789 ± 1.4836	2.9305 ± 1.9815
c	5.498 ± 3.2521	4.6025 ± 2.9853*	$M2$	1.8293 ± 2.5905	0.716 ± 0.3614
d	6.7040 ± 3.1200	5.7138 ± 3.4461	$M3$	1.5435 ± 0.4132	1.2525 ± 0.6647
e	9.9856 ± 5.6563	7.6494 ± 4.7551*	$M4$	3.3174 ± 2.5498	2.0456 ± 1.2762*
f	10.9535 ± 6.2216	8.2245 ± 5.4097*	$M5$	1.3129 ± 1.1732	0.8453 ± 0.9844*

*Statistically significant difference ($P < 0.05$).

continue to rise inertially, while relying on "swing arms and turning wrists" [29] which make the barbell continue to gain a certain speed during the inertial ascent. At the same time, the reaction force of the barbell acts on the human body to make lifter obtain greater downward acceleration, so as to quickly squat to support and receive barbell [30, 31].

Previous studies [10, 32–35] pointed out that insufficient knee flexion in the knee flexion phase is one of the important factors leading to the failure of snatch. At the knee flexion phase, athletes need to actively extend the hip joint and fully flex the knee joint. On the contrary, that is, knee joint is not fully flexed, and the extension of the hip joint is limited. The present study compared the characteristics of the successful and failed attempts of ten athletes. In the first part, the minimum horizontal distance between the *COG* of the human body and barbell, the barbell's maximum vertical velocity, the time parameters, space parameters, and the joints angle are all compared. There is no statistical difference, which

Table 6: The cumulative change of the human and bar combination barycenter of successful and failed snatch on the Y -axis and Z -axis.

	Y -axis		Z -axis	
	Successful	Unsuccessful	Successful	Unsuccessful
$M1$	2.3924 ± 1.7699	2.119 ± 1.6302	25.7886 ± 4.0861	26.2975 ± 3.642
$M2$	0.3357 ± 0.1692	0.5692 ± 0.5474	8.7441 ± 4.8083	11.4343 ± 4.0532
$M3$	1.2283 ± 0.7987	1.0141 ± 0.8591	23.0791 ± 5.1511	20.8446 ± 4.0949
$M4$	1.6672 ± 1.3182	1.7646 ± 1.1674	14.9653 ± 2.5195	13.9429 ± 2.1093
$M5$	0.7373 ± 0.3157	0.9771 ± 0.8159	7.5426 ± 1.8076	8.1324 ± 1.3437

Table 7: Linear regression equation of variation trend of the human and bar combination barycenter on the X -axis.

Subjects	Successful	Unsuccessful
1	$y = -0.006 + 0.138\chi$	$y = -0.009 + 0.71\chi$
2	$y = -0.042 + 0.153\chi$	$y = -0.017 + 0.098\chi$
3	$y = -0.078 + 0.133\chi$	$y = -0.012 + 0.099\chi$
4	$y = 0.005 + 0.066\chi$	$y = 0.029 + 0.019\chi$
5	$y = 0.056 + 0.041\chi$	$y = 0.071 + 0.021\chi$
6	$y = -0.119 + 0.322\chi$	$y = -0.034 + 0.186\chi$
7	$y = -0.050 + 0.205\chi$	$y = -0.019 + 0.118\chi$
8	$y = 0.022 + 0.038\chi$	$y = 0.025 + 0.028\chi$
9	$y = 0.001 + 0.042\chi$	$y = -0.018 + 0.0272\chi$
10	$y = 0.015 + 0.037\chi$	$y = -0.013 + 0.010\chi$

Table 8: R^2 value of linear regression equation of variation trend of the human and bar combination barycenter on the X-axis.

Subjects	Successful		Unsuccessful	
	R^2	P value	R^2	P value
1	0.972	≤0.001	0.983	≤0.001
2	0.987	≤0.001	0.952	≤0.001
3	0.969	≤0.001	0.976	≤0.001
4	0.956	≤0.001	0.958	≤0.001
5	0.942	≤0.001	0.891	≤0.001
6	0.941	≤0.001	0.968	≤0.001
7	0.934	≤0.001	0.978	≤0.001
8	0.892	≤0.001	0.877	≤0.001
9	0.883	≤0.001	0.852	≤0.001
10	0.855	≤0.001	0.857	≤0.001

showed that there was no obvious difference between the success and failure in the first part, which is consistent with related research [4, 15]. Although all parameters were not statistically different, some parameters are still worthy of our attention because they are very important for technical actions [36, 37]. For instance, the average value of the knee angle of the successful attempts is 6.99° smaller than that of failed attempts at the end of the knee flexion phase, and the maximum vertical velocity of successful attempts is 0.0847 m/s greater than that of failure. Insufficient knee flexion will affect the secondary force and will inevitably affect the maximum velocity of the barbell. It may be a potential factor for snatch failure. However, in this study, due to research limitations, it cannot be confirmed that the direct cause of snatch failure is insufficient knee flexion.

The study of Wang and Liu [18] showed that the maximum vertical distance between the *COG* of body and barbell is not enough to form a favorable support posture, which may be the main reason for the failed snatch. The studies of Gourgoulis et al. [4, 15] pointed out that there is no significant difference in the temporal and spatial characteristics between successful and failed snatch. In our study, the successful and failed attempts of ten athletes were compared. In addition to the significant difference in the vertical distance between the *COG* of barbell and human body at the end of the inertial ascent stage ($M4$) in the second part, there are no significant differences in the vertical acceleration of body, time parameters, spatial parameters, and joints angle. Since there is no significant difference in the barbell's maximal vertical height at the end of the inertial ascent stage ($M4$) between the successful and failed attempts, the average difference is only 0.049 cm. However, the vertical distance between the *COG* of body and barbell is different at the end of the inertial ascent stage ($M4$), the L_{Hz1} of successful snatch is 1.95 cm larger than that of failed snatch, which indicates that the falling velocity of the *COG* of body of successful attempts is higher than that of failed attempts in the inertial ascent stage ($M4$). At the same time, the average hip and knee angles of the successful attempts are less than those of the failed attempts at the end of the squat support stage ($M5$). There is no significant difference in the vertical height of *COG* of human body, the vertical height of barbell, and the vertical distance between the *COG* of human body and barbell at the end of the squat support stage ($M5$). Based on these, the insufficient support space may be one of the reasons for failure which pointed out in related study [18], and the conclusion lack sufficient evidence. The results of the present study are basically consistent with the results of previous studies [4, 15].

4.2. Analysis of the Human and Bar Combination Barycenter. The human and bar combination barycenter is the *COG* formed by the combination of the *COG* of barbell and *COG* of human body. The changes of the human and bar combination barycenter is affected by the change of the *COG* of barbell and/or *COG* of human body. The change of the human and bar combination barycenter on the Y -axis

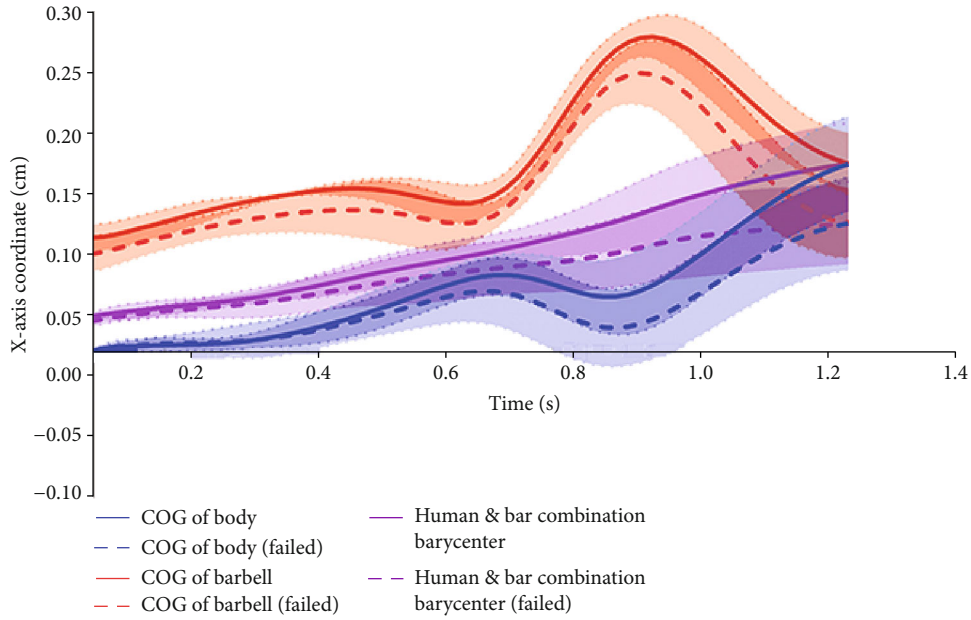

Figure 7: Successful and unsuccessful trajectories of the *COG* of barbell and body and human and bar combination barycenter on the *X* -axis.

indicates that the left and right deviation of the *COG* of barbell and human body in the snatch. The smaller the cumulative change in each phase, the smaller offset of the *COG* of barbell and human body in this stage, and more stable snatch technique. The results of the present study showed that the human and bar combination barycenter on the *Y* -axis of successful attempts is greater than the failure in *M* 1 and *M*3, but there is no significant difference (Table 6). There is no significant difference in the cumulative change of the human and bar combination barycenter on the *Z* -axis, and Figure 6 shows that the change of the human and bar combination barycenter for successful and failed snatches tends to be consistent.

Compared the changes of the human and bar combination barycenter on the *X* -axis between the successful and failed attempts, it was found that the values of the end of knee extension phase (*M*1), the knee flexion phase (*M*2), the inertial ascent stage (*M*4), and the squat support stage (*M*5) are statistically different. And the changes in the inertial ascent stage (*M*4) and in the squat support stage (*M*5) are also statistically different, all the successful attempts are greater than the failed attempts. The average value of human and bar combination barycenter at the end of knee extension phase (*M*1) of successful attempts is 0.4816 cm larger than the failed attempts. The average value of human and bar combination barycenter at the end of knee flexion phase (*M*2) of successful attempts is 0.8955 cm larger than the failed attempts. The average value of human and bar combination barycenter at the end of the inertial ascent stage (*M*4) of successful attempts is 2.3362 cm larger than the failed attempts. The average value of human and bar combination barycenter at the end of the squat support stage (*M*5) of successful attempts is 2.729 cm larger than the failed attempts. The variation of human and bar combination barycenter in the inertial ascent stage (*M*4) of successful attempts is 1.2718 cm larger than the failed attempts. And the variation of human and bar combination barycenter in the squat support stage (*M*5) of successful attempts is 0.4676 cm larger than the failed attempts. These indicate that the key problems of failed snatch are caused by the insufficient increase of human and bar combination barycenter on the *X* -axis during the inertial ascent stage (*M*4) and the squat support stage (*M*5).

In the present study, the unitary regression equations were established from the beginning of the inertial ascent stage (*M*4) to the end of the squat support stage (*M*5) of the success and failure of ten athletes. It can be seen from Table 7 that the slope of the regression line for success is greater than that for failure. Figure 7 shows the changes of *COG* of barbell, *COG* of body, and human and bar combination barycenter on the *X* -axis during the entire snatch process. It is easy to find that the gap of the human and bar combination barycenter between successful and failed attempts is getting bigger and bigger over time; especially, after the beginning of the inertial ascent stage, the slope of the human and bar combination barycenter of successful is obviously higher than that of the failure. The trajectory of the *COG* of barbell shows a trend of falling first and then rising from this stage, while the trajectory of *COG* of body shows the opposite trend of rising first and then failing. If weightlifters want to maintain the continuous growth of the human and bar combination barycenter, they need to reduce the downward trend of the *COG* of barbell and increase the growth trend of the *COG* of body.

From the perspective of technical performance, the barbell obtained the maximum vertical velocity after the force phase (*M*3) is over. By now, the *COG* of body drops rapidly, with the elbow joint as the center of the circle, and the forearm as the radius to swing the barbell to continue rising. Previous research [29] pointed out that since the barbell moves in an arc form during the inertial ascent stage, the force on the barbell can be decomposed into a vertical

upward force $F1$ and a positive X -axis force $F2$. $F1$ raises the barbell to the maximum height, and $F2$ brings the barbell close to the body and reaches the support position. If $F2$ is too large, the COG of barbell will move backward and cause the barbell to fall behind, and if $F2$ is too small, it will cause the COG of barbell to move forward and cause the barbell to fall forward. The power of $F1$ mainly comes from the "swing arms and turning wrists", while the power of $F2$ comes from the proper upper body reclining at the end the force phase ($M3$). At this stage, the COG of human body relies on the reaction force of the barbell and hip and knee flexion to actively descend. It is worth noting that some studies have pointed out that the falling acceleration of human body of elite weightlifters should be greater than the acceleration of gravity ($g = 9.8\,\mathrm{m/s^2}$). In the present study, the maximum acceleration of human body in eight weightlifters is greater than the acceleration of gravity, which shows that the squatting and supporting technique of the two other lifters still need to be improved.

The present study believes that a probable cause of the failure is that the human and bar combination barycenter does not reach the specified position, and the reason is insufficient backward leaning of torso at the end of the force phase ($M3$). The research of Gourgoulis et al. [4, 15] showed that the difference of the resultant acceleration on the vector direction and the instability of the force direction during the knee extension phase ($M1$) are the main reasons for the failure of snatch. The probable reasons for the difference may be that multiple categories of lifters (69 kg, 77 kg, and 85 kg) were selected in literatures, and individuals are quite different. Furthermore, they did not distinguish the type of failure (the barbell falls forward or backward). In the present study, all the unsuccessful attempts are forward falling.

In summary, compared the characteristics of successful and failed snatch, it is concluded that the probable cause of the failure is that the position of the human and bar combination barycenter on the X -axis is more forward than the position of the successful attempts at the end of the inertial ascent stage ($M4$) and the squat support stage ($M5$). The reasons are that the upper body does not lean back properly at the end of the force phase ($M3$) and the shoulder, waist, and back muscles are not used to give proper force to barbell, which leads to the growth of the human and bar combination barycenter on the X -axis is insufficient during the inertial ascent stage ($M4$) and the squat support stage ($M5$), and result in failure of COG of barbell to reach the proper position and finally causing the snatch failure. In addition, insufficient knee flexion in the knee flexion phase ($M2$) leads to insufficient secondary force, which causes the maximum vertical velocity of barbell to be too low, and it may also be an indirect factor that causes the snatch failure, because the insufficient maximum vertical velocity may cause the lifters to use more power for barbell rising and reduce the force on the positive direction of the X -axis during inertial ascent stage ($M4$), which indirectly leads to the failure of the snatch. Therefore, in the present study, the effectiveness of human and bar combination barycenter in judging the successful and failed attempts of elite weightlifters has been verified.

4.3. Limitations. In order to avoid the influence of technical differences between weightlifting categories, the present study only selected the men's 73 kg category snatch competition in recent years. The relatively small number of research samples is one of the limitations of this study. In addition, the present study only discussed the factors for the failure of the barbell to fall forward, and whether it is also effective for the backward drop still needs further verification. Furthermore, the video was obtained under competitive conditions only using two cameras. It is inevitable that the body joints, such as the knee joint, are hidden by local limbs or not visible on side camera when video digitizing. Under this circumstance, the method of zooming in the local joints we used makes the joints of human body more clearly, which is helpful for the accuracy of the data. However, there are still some limitations compared with the multicamera method.

5. Conclusions

The present study compared the successful and failed techniques of snatch of elite lifters and analyzed the characteristics of "Near," "Fast," and "Low" principles, the parameters in phases, and the parameters of human and bar combination barycenter. And we established the regression equation of the human and bar combination barycenter on the X -axis during the inertial ascent stage ($M4$) and the squat support stage ($M5$). And we found the effectiveness of the human and bar combination barycenter in judging success and failure snatch. The main conclusions are as follows:

(1) A probable cause of the failed snatch is that the displacement of human and bar combination barycenter on the X -axis is not enough to reach the position for supporting barbell during the inertial ascent stage ($M4$) and the squat support stage ($M5$). The reason is that the strength of reclining of t torso at the end of the force phase ($M3$) is insufficient, so it is reminded that weightlifters who often fall forward in snatch should strengthen reclining exercises

(2) Insufficient knee flexion during the knee flexion stage ($M2$) leads to a lower maximal vertical velocity of barbell and difference of vertical distance between the COG of human body and barbell at the end of the inertial ascent stage ($M4$), which may be an indirect factor leading to the failure of snatch

(3) The cumulative variation of human and bar combination barycenter on the X -axis can effectively determine the technical characteristics between the success and failure of elite weightlifters in snatch

Data Availability

The data of the present study that support the findings are available from the corresponding author upon reasonable request.

Conflicts of Interest

The authors declare that they have no conflicts of interest.

Acknowledgments

The present study was part of the Sports Scientific Research Projects of the General Administration of Sport of China and Science Technology Department of Zhejiang Province (2021C03128).

References

[1] M. Wang, *Biomechanical Study of Weightlifting Technology*, China National Sports Administration, BeiJing China, 1987.

[2] Y. Zhang, G. Cai, Q. Lu, Y. Wang, and D. Lu, "A 3-D video analysis of he Zhuoqiang's record-setting performance," *China Sport Science*, vol. 9, pp. 70–74, 1989.

[3] X. Qin, "Explain the three principles of "near", "fast" and "low" in snatch from the perspective of mechanics," *Journal of Sport Science*, vol. 19, pp. 34–36, 1998.

[4] Z. Bi and L. Zhang, "Kangwei Ai, a comparative study on the snatch technique of Lu Haojie and Lv Xiaojun," *Shandong Sports Science & Technology*, vol. 37, pp. 40–43, 2015.

[5] G. Hadi, H. Akkuş, and E. Harbili, "Three-dimensional kinematic analysis of the snatch technique for lifting different barbell weights," *The Journal of Strength and Conditioning Research*, vol. 26, no. 6, pp. 1568–1576, 2012.

[6] K. Ai, F. Li, W. Hao, and T. Yuan, "Kinematical comparison and analysis between snatch and clean in weightlifting," *China Sport Science*, vol. 25, pp. 39–42, 2005.

[7] P. Chang, J. Liu, H. Zhu, and G. Liu, "Huiju Pan, a study on the snatch technique of Lv Xiaojun in trials for the Rio Olympic Games," *Journal Zhejiang Normal University*, vol. 41, pp. 115–120, 2018.

[8] X. Wang, *The biomechanics study of females's snatch technique and identifying of the center of the barbell during weightlifting*, Beijing Sport University, 2006.

[9] J. Li and J. Wang, "Analysis on kinematic parameters of OUYANG Xiao-fang breaking snatch National Record 122 kilograms in the 11th National Games of the People' s Republic of China," *China Sport Science and Technology*, vol. 46, pp. 70–73, 2010.

[10] X. Wang, M. Liu, and W. Xu, "Biomechanical analysis on snatch technique of elite women weightlifters," *China Sport Science and Technology*, vol. 44, pp. 93–95, 2008.

[11] E. Harbili, "A gender-based kinematic and kinetic analysis of the snatch lift in elite weightlifters in 69-kg category," *Journal of Sports Science & Medicine*, vol. 11, no. 1, pp. 162–169, 2012.

[12] J. Yang, M. Liu, and X. Wang, "Analysis of the sensitive indicators of the snatch technique of the elite weightlifters," *Sport Science Research*, vol. 31, pp. 21–23, 2010.

[13] L. J. Musser, J. Garhammer, R. Rozenek, J. A. Crussemeyer, and E. M. Vargas, "Anthropometry and barbell trajectory in the snatch lift for elite women weightlifters," *Journal of Strength and Conditioning Research*, vol. 28, no. 6, pp. 1636–1648, 2014.

[14] Y. Ikeda, T. Jinji, T. Matsubayashi et al., "Comparison of the snatch technique for female weightlifters at the 2008 Asian championships," *Journal of Strength and Conditioning Research*, vol. 26, no. 5, pp. 1281–1295, 2012.

[15] V. Gourgoulis, N. Aggeloussis, A. Garas, and G. Mavromatis, "Unsuccessful vs. successful performance in snatch lifts: a kinematic approach," *Journal of Strength and Conditioning Research*, vol. 23, no. 2, pp. 486–494, 2009.

[16] Z. Bi, K. Ai, L. Zhang, Z. Wen, and X. Han, "Comparative study on the successful and unsuccessful performance of the elit male weightlifters' snatch technique," *Sport Science Research*, vol. 36, pp. 18–22, 2015.

[17] H. Nagao, Y. Kubo, T. Tsuno, S. Kurosaka, and M. Muto, "A biomechanical comparison of successful and unsuccessful snatch attempts among elite male weightlifters," *Sports*, vol. 7, no. 6, 2019.

[18] M. Wang and W. Liu, "Biomechanics analysis in failing snatches," *Journal of Sports Science*, vol. 22, pp. 32-33, 2001.

[19] Y. Wang, D. Lu, K. Ai, and Y. Li, "Biomechanical characteristics of weightlifting technology," *China Sport Science*, vol. 4, pp. 63–67, 1984.

[20] V. Gourgoulis, N. Aggeloussis, P. Antoniou, C. Christoforidis, G. Mavromatis, and A. Garas, "Comparative 3-dimensional kinematic analysis of the snatch technique in elite male and female Greek weightlifters," *Journal of Strength and Conditioning Research*, vol. 16, no. 3, pp. 359–366, 2002.

[21] W. Baumann, V. Gross, K. Quade, P. Galbierz, and A. Schwirtz, "The snatch technique of world class weightlifters at the 1985 world championships," *Journal of Applied Biomechanics*, vol. 4, no. 1, pp. 68–89, 1988.

[22] V. Gourgoulis, N. Aggelousis, G. Mavromatis, and A. Garas, "Three-dimensional kinematic analysis of the snatch of elite Greek weightlifters," *Journal of Sports Sciences*, vol. 18, no. 8, pp. 643–652, 2000.

[23] E. Harbili and A. Alptekin, "Comparative kinematic analysis of the snatch lifts in elite male adolescent weightlifters," *Journal of Sports Science & Medicine*, vol. 13, no. 2, pp. 417–422, 2014.

[24] S. M. A. Rahmati and M. Mallakzadeh, "Prediction of weightlifter's motor behavior to evaluate snatch weightlifting techniques based on a new method of investigation of consumed energy," *Human Movement Science*, vol. 38, pp. 58–73, 2014.

[25] V. Gourgoulis, N. Aggeloussis, V. Kalivas, P. Antoniou, and G. Mavromatis, "Snatch lift kinematics and bar energetics in male adolescent and adult weightlifters," *The Journal of Sports Medicine and Physical Fitness*, vol. 44, no. 2, pp. 126–131, 2004.

[26] J. T. Mierzwicki, "Weighted Vest Training in Community-Dwelling Older Adults: A Randomized, Controlled Pilot Study," *Physical Activity and Health*, vol. 3, no. 1, pp. 108–116, 2019.

[27] L. Gongju, G. Fekete, H. Yang et al., "Comparative 3-dimensional kinematic analysis of snatch technique between top-elite and sub-elite male weightlifters in 69-kg category," *Heliyon*, vol. 4, pp. 1–17, 2018.

[28] A. Lu, *Sports Biomechanics*, Peoples Sports Publishing House, BeiJing China, 1st ed. edition, 2010.

[29] Q. Wu, "Discussion on "Arm swing" in snatch," *China Sport Science and Technology*, vol. 4, pp. 22–25, 1981.

[30] X. Shan, Z. Yan, and Y. Zhang, "Analysis of Cui Wenhua's snatch technique-200.5kg, exceeding the world record," *Journal of Beijing University of Physical Edvcation*, vol. 22, pp. 48–51, 1999.

[31] A. Lu, J. Pang, and X. Wu, "Biomechanical characteristics of men's snatch movement under different weight of barbell," *Shanghai University of Sport*, vol. 24, pp. 58–61, 2000.

[32] S. Afaq, M. Loh, J. Kooner, and J. Chambers, "Evaluation of Three Accelerometer Devices for Physical Activity Measurement Amongst South Asians and Europeans," *Physical Activity and Health*, vol. 4, no. 1, pp. 1–10, 2020.

[33] X. Hu, "Study on snatch technique of elite women weightlifters in China," *Shanghai University of Sport.*, vol. 31, pp. 37–39, 1989.

[34] P. Liu, G. Zhang, Y. Tong, and J. Liu, "Research on snatch technical structure of our male elite weightlifters," *China Sport Science*, vol. 25, pp. 46–49, 2005.

[35] H. Zhu, J. Liu, P. Chang, J. Ma, and H. Pan, "A comparative study on the snatch technique of Olympic Champions Shi Zhiyong and Liao Hui, China Sport," *Science and Technology*, vol. 53, pp. 127–133, 2017.

[36] X. Liu and S. Li, "Some errors of the application to statistic concepts in sports scientific research," *China Sport Science*, vol. 22, pp. 117–119, 2002.

[37] Z. Shi and D. Sun, "Conflict between weightlifting and health," *The Importance of Injury Prevention and Technology Assistance. Physical Activity and Health*, vol. 6, pp. 1–4, 2022.

Hindawi
Applied Bionics and Biomechanics
Volume 2022, Article ID 7452229, 8 pages
https://doi.org/10.1155/2022/7452229

Research Article

Effects of Patellofemoral Pain Syndrome on Changes in Dynamic Postural Stability during Landing in Adult Women

Chanki Kim,[1,2] **Seunghyeok Yeom**,[2] **Seji Ahn**,[2,3,4] **Nyeonju Kang**,[3,4,5] **Kiwon Park**,[6] **and Kyoungkyu Jeon**[2,3,4,5]

[1]*Department of Human Movement Science, Incheon National University, Incheon, Republic of Korea*
[2]*Functional Rehabilitation Biomechanics Laboratory, Incheon National University, Incheon, Republic of Korea*
[3]*Division of Sport Science, Incheon National University, Incheon, Republic of Korea*
[4]*Sport Science Institute, Incheon National University, Incheon, Republic of Korea*
[5]*Health Promotion Center, Incheon National University, Incheon, Republic of Korea*
[6]*The Department of Mechatronics Engineering, Incheon National University, Incheon, Republic of Korea*

Correspondence should be addressed to Kyoungkyu Jeon; jeonkay@inu.ac.kr

Received 18 March 2022; Revised 7 April 2022; Accepted 15 April 2022; Published 10 May 2022

Academic Editor: Yaodong Gu

Background. This study investigated the effects of lower limb movements on dynamic postural stability (DPS) during drop landing in adult women with patellofemoral pain syndrome (PFPS). *Methods*. Thirty-eight adult women were recruited and divided into two groups, the PFPS group and the control group. The study participants performed a single-leg drop landing from a 30 cm box, and their lower limb movements and DPS were measured. Differences between groups were examined using independent sample *t* -tests. In addition, stepwise multiple linear regression was used to examine the kinematic parameters that contribute to the DPS. *Results*. The PFPS group had significantly lower hip flexion, internal rotation, knee flexion, ankle external rotation, pelvic oblique, tilt, rotation, and higher hip abduction, knee valgus, and ankle plantarflexion. In terms of DPS, the PFPS group had a significantly higher anteroposterior and a lower mediolateral than that of the control group. In the control group, regression analysis revealed a controlled anteroposterior using knee flexion, while the PFPS group controlled mediolateral through ankle plantarflexion. *Conclusions*. Patients with PFPS experienced more shock on their knee joint during landing than patients in the control group with greater anteroposterior instability and lower mediolateral instability.

1. Introduction

The patellofemoral pain syndrome (PFPS) is a disease that is characterized by continuous pain around the anterior knee. It is caused by several factors, such as excessive use of the knee joint, cartilage injury, increased *Q*-angle, vastus medialis weakness, and patellar misalignment and instability [1–3]. PFPS are reported to affect one out of every six physically active individuals, and affected individuals tend to engage in less physical activity due to the pain [4]. A study that followed up patients diagnosed with PFPS as teenagers for 10 years discovered that 91% of the patients suffered functional impairment, local tenderness, patellar femoral friction, and faced difficulty bending the knees due to continuous knee pain [5].

Because women have a wider pelvis in relation to their femoral length, they are twice as likely as men to develop PFPS [6]. Consequently, knee and hip flexion causes excessive adduction and internal rotation, reducing the patellofemoral joint contact area [7]. Furthermore, women have a weaker quadriceps femoris, with a larger *Q*-angle than men, which delays the activation of the vastus medialis in a dynamic situation while increasing the lateral glide of the patella and knee joint pressure, resulting in pain [3, 8].

Women are reported to experience more patellofemoral stress while running, jumping, landing, and climbing stairs due to the increased load during knee flexion as a result of these structural features [1, 9]. Landing, a common task performed in daily life and sports, generates shock that is 2–3

times greater than body weight [10], and the knee joints play an important role in shock absorption during landing, absorbing approximately 41% of the total shock [11]. However, small hip flexion and large internal rotation during landing direct substantial shock onto the knee joints, and the consequently greater patellofemoral stress increases the risk of an injury [12] Women with PFPS put more strain on the patellofemoral joint during single-leg squats and landing, due to excessive knee abduction, increasing their risk of anterior cruciate ligament (ACL) injury and arthritis [13–16].

As described here, the assessment of lower limb movement and balance during a dynamic task, such as a single-leg squat or landing, is a valid method for predicting the risk of potential knee injuries [17, 18]. Patients with PFPS have been reported to have unstable landing patterns during double-leg landing, compared to their healthy counterparts [19]. These patients try to reduce knee pain by increasing hip flexion. However, they have a greater tibial internal rotation moment and an anteriorly displaced center of pressure (COP) [19]. Among the various methods for assessing dynamic postural stability [20, 21], dynamic posture stability (DPS) can be used as an indicator of the ability to maintain balance during the transition from a dynamic to a static state upon landing [22].

Landing motion is a common activity in daily life, and previous research has primarily focused on the knee joint during landing. Because women with PFPS may experience changes in the movement patterns of their entire lower limbs during landing due to structural differences, not only the knee joint but also the ankle joint and hip joint must be examined [13, 23, 24]. Furthermore, studies comparing the factors of dynamic stability during landing between patients with PFPS and healthy individuals, as well as identifying the specific dynamic factors that affect the DPS, are lacking. This study is aimed at comparing the kinematic features of major lower limb joints during single-leg landing between adult women with PFPS and their healthy counterparts, as well as to identify the specific kinematic parameters that contribute to the DPS via regression analysis, to present foundational data for developing desirable landing strategies for patients with PFPS. The hypotheses of this study are as follows. First, during single-leg drop landing, the PFPS group will have a significant difference in the angles of the hip and knee joints in the frontal plane compared to the control group. Second, the kinematic parameters affecting DPS will also appear differently.

2. Materials and Methods

2.1. Study Participants. Thirty-eight women aged 20–29, with no history of lower limb joint injuries in the previous 6 months, other than PFPS, were enrolled. The participants were divided into two groups based on their orthopedic diagnosis of PFPS: the PFPS group ($n = 19$) and the control group ($n = 19$). This study was approved by the Institutional Review Board of the Incheon National University (INUIRB No. 7007971-201801-001). This experiment was conducted according to the Declaration of Helsinki (1964). The participants provided informed consent after receiving sufficient explanations regarding the study contents and procedures. Table 1 presents the physical characteristics of the participants.

Table 1: Characteristic of participants.

Variables	PFPS group ($n = 19$)	Normal group ($n = 19$)	p
Age (years)	23.11 ± 2.56	23.32 ± 2.24	.789
Height (cm)	163.42 ± 4.65	164.00 ± 4.78	.707
Weight (kg)	58.68 ± 7.61	55.08 ± 7.06	.139

Note: data are mean ± standard deviation. Abbreviations: PFPS: patellofemoral pain syndrome.

2.2. Procedures. Drop landing is based on a study by Orishimo et al. [25], participants were instructed to perform a drop landing from a 30 cm box by slowly shifting their body weight anteriorly and landing in a free fall. Landing outside the ground force plate or stumbling on landing were considered failed attempts, and measurements were repeated in such cases. Because the left side was affected in the PFPS group, both groups were instructed to land on their left leg. To prevent injury, the participants performed 10 minutes of warm-up and practiced drop landing for 15 minutes before beginning the measurement. To ensure accurate measurements, all participants performed a single-leg drop landing and maintained balance for at least 5 seconds after landing. To improve accuracy, the analysis used the average values of three repeated measurements of successful attempts.

2.3. Data Analysis

2.3.1. Motion Analysis. During a drop landing, eight video analysis cameras (6 Eagle & 2 Raptor Camera System, Motion Analysis Corp., Santa Rosa, CA, USA) and one ground force plate (OR6-5-2000, AMTI Inc., Watertown, MA, USA) were used to collect kinematic and kinetic data from lower limb joints. The video analysis cameras were installed around the participant (anteroposterior and mediolateral), such that the entire range of motion with reference to the reference coordinates could be captured. Segment axis systems were established with the x-axis designated as the mediolateral direction of drop landing, the y-axis as the anteroposterior direction, and the z-axis as the vertical direction off the ground. The equipment was calibrated to establish spatial coordinates. To measure the anatomical static posture, 19 reflective markers were attached around the major lower limb joints using Helen Hayes Marker Set [26]. The remaining 15 markers were used to take measurements during the drop landing task after four markers attached to the knee joints and the medial aspect of the ankle joints were removed (Figure 1).

Using Cortex 5 (Motion Analysis Corp., Santa Rosa, CA, USA), we processed all kinematics and kinetic data. The data was sampled at 120 frames per second. For data processing, it was smoothed using digital filtering (Butterworth Low-Pass Digital Filtering) method to remove noise errors, the point of peak vertical GRF was analyzed, and a rigid body

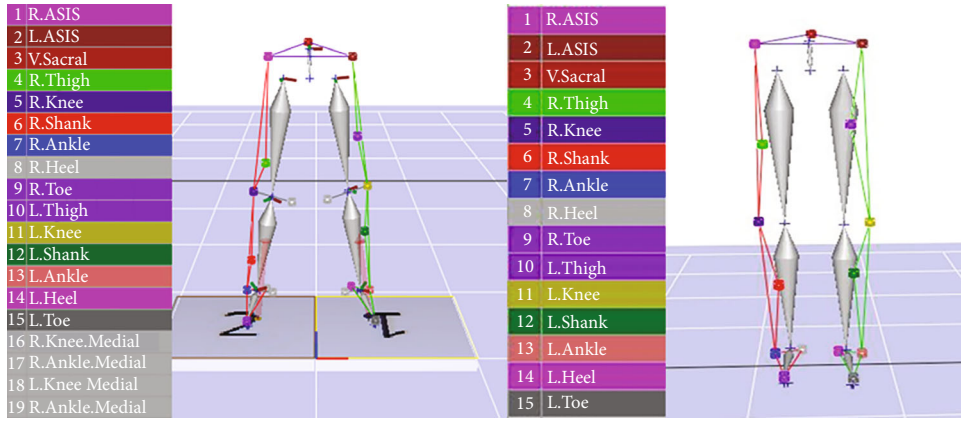

(a) (b)

Figure 1: Reflective marker attachment. (a) Static posture marker. (b) The four medial markers for movement have been removed.

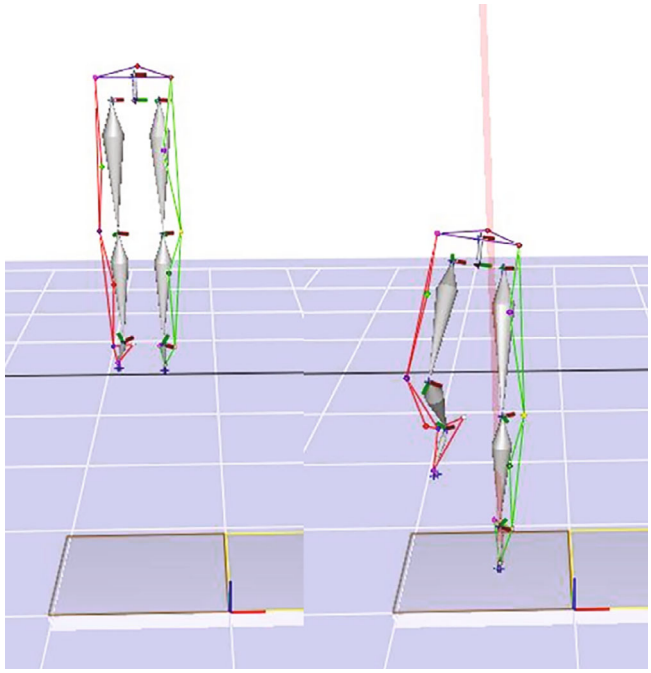

Figure 2: Point of maximum ground reaction force during single-leg drop landing.

system was used for the analysis (Figure 2). The cut-off frequency was set at 10 Hz to minimize error during data processing. We synchronized the data using an analog-digital converter (A/D convertor, NI-USB 6218, National Instruments, Hungary) for measurement and analysis to align the time points for all data.

2.3.2. Dynamic Postural Stability Index (DPSI). GRF values were established with the xGRF designated as the mediolateral direction of drop landing, the yGRF as the anteroposterior direction, and the zGRF as the vertical direction off the ground. DPSI was computed based on the study by Wikstrom et al. [22]. The stability was calculated with reference to three directions (anteroposterior, mediolateral, and vertical). The stability is a mean square deviation that assesses variation around zero rather than a standard deviation that assesses variation around the mean. The medial-lateral stability index (MLSI) and anterior-posterior stability index (APSI) assess variation around zero along the mediolateral and anteroposterior axes of the force plate, and the vertical stability index (VSI) assesses the variation in vertical GRF along the vertical axis of the force plate standardized with the participant's body weight. To ensure the accuracy of the DPSI analysis, data was collected for 3 seconds from the point of initial contact with the ground for the calculation [22, 27].

$$\text{MLSI} = \sqrt{\left[\frac{\sum(0-x)^2}{\text{number of datapoints}}\right]} \quad (1)$$

$$\text{APSI} = \sqrt{\left[\frac{\sum(0-y)^2}{\text{number of datapoints}}\right]} \quad (2)$$

$$\text{VSI} = \sqrt{\left[\frac{\sum(\text{bodyweight}-z)^2}{\text{number of datapoints}}\right]} \quad (3)$$

$$\text{DPSI} = \sqrt{\left[\frac{\sum(0-x)^2+\sum(0-y)^2+\sum(\text{bodyweight}-z)^2}{\text{number of datapoints}}\right]} \quad (4)$$

2.3.3. Statistical Analysis. All outcome variables calculated in this study were presented as mean and standard deviation using the SPSS 26.0 (IBM, Chicago, IL USA) software for Windows. Normality assumption was first checked with the Shapiro–Wilk test ($p > 0.05$). The differences in kinematic and kinetics variables between the groups were analyzed using independent sample t-tests, and the kinematic variables influencing DPS were identified using stepwise multiple linear regression. Goodness of fit of the model is presented as the adjusted multiple coefficients of determination (R^2). Coefficients (R^2) were interpreted as weak (0.00–0.40), moderate (0.41–0.69), or strong

Table 2: Results of kinematics and kinetics at maximum ground reaction force.

Variables			PFPS group	Control group	t	p
Kinematics (°)	Hip	Flexion	11.262 ± 10.058	32.314 ± 9.786	-6.539	≤.001***
		Abduction	14.802 ± 5.319	5.219 ± 4.283	6.117	≤.001***
		Internal rotation	−7.459 ± 17.379	6.909 ± 9.787	-3.140	.003**
	Knee	Flexion	18.775 ± 8.986	28.846 ± 8.634	-3.523	.001**
		Valgus	−2.674 ± 5.939	−7.986 ± 5.219	2.929	.006**
		Internal rotation	−10.944 ± 13.740	−11.547 ± 13.067	.139	.891
	Ankle	Plantarflexion	19.771 ± 6.974	8.725 ± 5.021	5.602	≤.001***
		Internal rotation	6.129 ± 7.214	−1.788 ± 7.389	-3.342	.002**
		Eversion	−13.808 ± 8.495	−11.016 ± 10.067	-.924	.362
Kinetics		mGRF	2.742 ± 0.817	4.432 ± 0.470	-7.815	≤.001***
		Leg stiffness	27.680 ± 8.968	33.118 ± 8.993	-1.866	.070

Note: data are mean ± standard deviation. **$p < .01$, ***$p < .001$; abbreviations: PFPS: patellofemoral pain syndrome; mGRF: max ground reaction force; "+" is the movement on the table, and "–"is the opposite movement (+: flexion, abduction, internal rotation, valgus, plantarflexion, and eversion; -: extension, adduction, external rotation, varus, dorsiflexion, and inversion).

Table 3: Results of dynamic stability index.

Variables	PFPS group ($n = 19$)	Normal group ($n = 19$)	t	p
APSI	.007 ± .002	.005 ± .001	3.240	.003**
MLSI	.012 ± .002	.013 ± .002	-2.956	.005**
VSI	.017 ± .009	.019 ± .010	-.956	.345
DPSI	.035 ± .011	.037 ± .010	-.713	.480

Note: data are mean ± standard deviation. **$p < .01$; abbreviations: PFPS: patellofemoral pain syndrome; APSI: anteroposterior stability index; MLSI: mediolateral stability index; VSI: vertical stability index; DPSI: dynamic postural stability index.

(0.70–1.00). An α level is for all analyses was set at .05. Statistical significance level was set at $p < .05$.

3. Results

3.1. Kinematics and Kinetics Variables. The kinematic results of lower extremity joint angles and the kinetics results were compared at the time of mGRF. Except for knee internal rotation and ankle eversion, the two groups differed significantly across all variables. When compared with the control group, the PFPS group had significantly less hip flexion, internal rotation, knee flexion, and ankle external rotation and significantly more hip abduction, knee valgus, and ankle plantarflexion. There was a significant difference in mGRF, and there was no significant difference in leg stiffness. Compared with the control group, the mGRF of the PFPS group was significantly smaller (Table 2).

3.2. DPSI Results. DPSI was compared between the groups. The PFPS group had significantly greater APSI but significantly lower MLSI compared to the control group (Table 3).

3.3. Linear Regression Analysis of DPSI. Stepwise linear regression analysis was used to examine the effects of the landing motion on DPSI changes. In the control group, has been explained as having a negative effect on APSI ($R^2_{(abj)} = .198$, $y = 0.007 - 7.422^{-5}x$, Figure 3(a)), while knee internal rotation has been explained as having a positive effect on MLSI ($R^2_{(abj)} = .186$, $y = 0.014 + 5.927^{-5}x$, Figure 3(b)). In the PFPS group, ankle plantar flexion was explained to have a positive effect on MLSI ($R^2_{(abj)} = .302$, $y = 0.009 + 0.0001x$, Figure 4).

4. Discussion

This study compared kinematics and kinetics variables and DPS during single-leg landing between the PFPS and control groups and used regression analysis to examine the effects of landing movement on DPS. We aimed to understand the kinetic features of lower limb joints and joint coordination during single-leg landing, as well as the influence of each lower limb joint on the DPS during single-leg landing in adult women with PFPS, to present foundational data for developing education about correct landing posture in patients with PFPS. As a result, the joint angle of the lower extremities and mGRF showed a significant difference between the PFPS group and the control group. In terms of DPS, the anteroposterior and mediolateral angles of the PFPS group were significantly higher than the control group, and the variables affecting the DPS were also different.

During single-leg landing, the PFPS group had less hip flexion and internal rotation and a larger abduction angle than the control group. According to studies, women with PFPS overstrain their knee joints due to valgus and hip adduction and internal rotation during knee flexion, when flexing the knee joints, and have a weaker hip abduction due to hip abductor muscle weakness [28, 29]. Pollard et al. [30] reported that people who exhibit a small hip flexion during drop landing place a greater load on the frontal

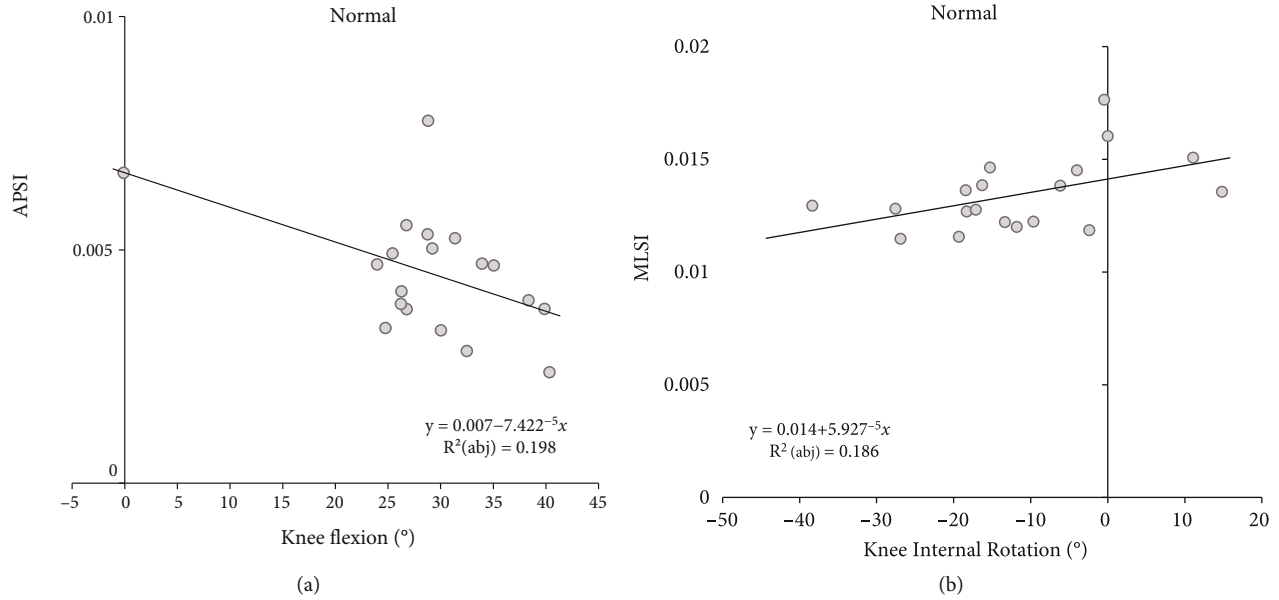

Figure 3: Results of linear regression analysis to normal group. (a) Results of linear regression analysis to normal group APSI. (b) Results of linear regression analysis to normal group MLSI. Abbreviations: APSI: anteroposterior stability index; MLSI: mediolateral stability index; adj: adjusted.

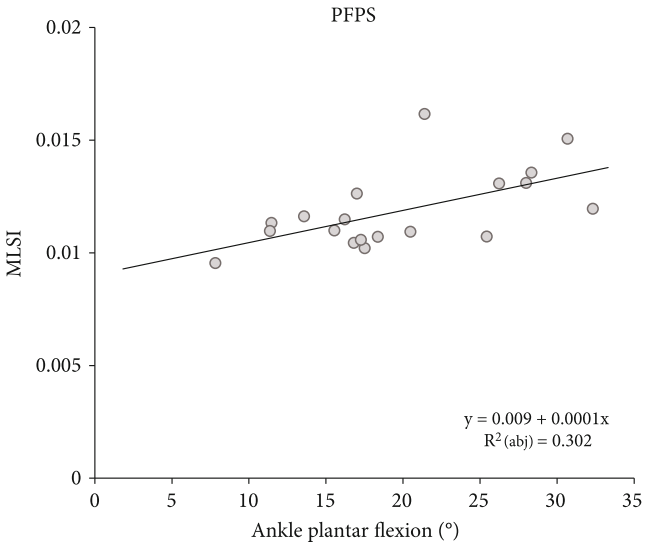

Figure 4: Results of linear regression analysis to PFPS group; results of linear regression analysis to PFPS group MLSI. Abbreviations: PFPS: patellofemoral pain syndrome; MLSI: mediolateral stability index; abj: adjusted.

plane of the knee joint, which is consistent with our findings. Participants with a small hip flexion angle use a strategy involving the knee extensor muscle, rather than the hip extensor muscle, to alleviate the shock, implying that using the hip extensor muscle is necessary to effectively use hip flexion during landing [30]. Furthermore, patients with PFPS have a weakening of the hip abduction and external rotation force [31]. Activating the hip external rotator and extensor muscles may help prevent the exacerbation of PFPS.

According to Pollard et al. [30], women with a small knee flexion angle during landing have more knee valgus than the control group. These women are thought to have compensated for the shock inflicted during single-leg drop landing through the knee valgus, similar to the PFPS group in our study who showed small knee flexion patterns during landing. Furthermore, the PFPS group's knee valgus pattern during landing may impair the ability to maintain knee alignment due to increased internal patellofemoral pressure, which intensifies the load in a smaller contact area and potentially escalates the pressure on the patellofemoral joint [13, 32]. Additionally, individuals also have an abnormal joint position sense [33], emphasizing the importance of joint repositioning training.

To absorb the GRF produced during landing, the ankle joints must shift from plantarflexion to dorsiflexion, and such an elevation of dorsiflexion may promote the stability of landing [34, 35]. In this study, the PFPS group was found to use an unstable and limited landing strategy, with significantly greater plantarflexion and internal rotation angle during single-leg landing than the control group. This is consistent with previous findings that a small dorsiflexion angle is related to knee flexion during landing [36, 37]. Furthermore, the PFPS group in previous study appears to have had impaired shock absorption control, which is consistent with previous studies that attributed the significant reduction in sagittal plane angle during landing in women with PFPS compared to their healthy counterparts to an impairment in shock absorption control [38]. In this study, the mGRF of the PFPS group was smaller than control group, and there was no difference in leg stiffness. It is thought that the PFPS group adopted a landing strategy differently from the control group, such as knee valgus. Rather than that, shock absorption was not properly controlled.

In terms of DPSI, the PFPS group had a higher APSI than the control group. PFPS causes quadriceps femoris and hamstring weakness, which results in an anterior displacement of the COP at peak GRF during landing [19, 39]. Patients with PFPS have severe anteroposterior instability, and inducing knee extensor fatigue increases anteroposterior instability [40]. Furthermore, the PFPS group had a low MLSI, which may be related to decreased control over knee movement due to knee valgus and pain [13]. A previous study found that the PFPS group had less COP displacement during a single-leg squat, and that a 9-week physical therapy intervention reduced pain while increasing COP displacement [41]. However, because it is unclear whether DPS is associated with knee movement and the motion characteristics may differ depending on the experimental task, further research on DPS is required [42, 43].

In this study, we used stepwise multiple regression to determine which kinematic variables best predict DPS. Knee flexion predicted APSI negatively while knee internal rotation predicted MLSI positively in the control group. A small amount of maximal knee flexion during landing may increase the shock to the lower limbs, and studies have shown that this is a poor landing strategy [44, 45]. Previous studies have found that stronger knee flexor and extensor muscles, as well as better proprioception, result in a greater knee flexion angle at initial grounding [46]. In another study, four weeks of plyometric and core training resulted in increased knee flexion and decreased internal rotation, which were attributed to lower knee joint loads [47]. Our findings suggest that increasing knee flexion while decreasing internal rotation is a strategy that promotes stability.

In the PFPS group, ankle plantarflexion was a positive predictor of MLSI, with MLSI increasing as ankle plantarflexion increased. Fong et al. [48] found that a small passive ankle dorsiflexion range of motion (ROM) can lead to large plantarflexion at landing, statistically significant high GRF and knee valgus, and small knee flexion, in a study on the correlation between passive ankle dorsiflexion ROM and landing. Furthermore, single-leg landing with a fatigued leg increases ankle plantarflexion and knee flexion, which is a compensatory strategy for fatigue-induced balance impairment and muscle weakness [34]. The PFPS group had large ankle plantarflexion and small knee flexion at peak GRF in this study, which can be attributed to the use of an ankle strategy during landing due to impaired knee motor control.

5. Limitation

The limitations of this study are as follows. Practicing single-leg drop landings for 15 minutes prior to the experiment may have affected the individual's pain level in this experiment. The control group may not have been affected, but the PFPS group may have been affected by the pain and landed with strategy to minimize the impact on the knee. In this study, the patellofemoral joint compression force was not measured directly, but was implied by the knee joint flexion angle. Further investigation in this area is needed in future studies. As a way to improve the landing strategy of the PFPS group, it may be helpful to practice the landing motion itself, which not only improves muscles strength but also improves coordination of the lower extremities.

6. Conclusions

This study observed that the PFPS group sustained more shock on their knees during landing compared to the control group. Also, while the control group used the knee and hip joint in the landing strategy, the PFPS group used the ankle strategy to compensate for the small flexion angle of the knee and hip joint. Individuals with PFPS use an unstable landing strategy, which causes an imbalance among the lower limb joints and raises knee pressure. To avoid this, the hip abductor, external rotator, and extensor muscles must be strengthened to allow for hip flexion. Furthermore, strategies for strengthening ankle dorsiflexion and activating the knee and hip flexors are required to correct the ankle-based landing strategy, and joint repositioning training should be performed to prevent pressure build-up due to abnormal joint position. In summary, it will be helpful to selectively classify the occurrence of PFPS through the analysis of the landing motion of adult women in this study and to develop rehabilitation training focusing on PFPS.

Data Availability

The experiment data used to support the findings of this study are available from the corresponding authors upon request.

Conflicts of Interest

The authors declare that there is no conflict of interest regarding the publication of this paper.

Acknowledgments

The authors would like to thank the participants for their time and commitment to this research. This work was supported by Incheon National University Research Grant (2019-0100).

References

[1] D. Sisk and M. Fredericson, "Update of risk factors, diagnosis, and management of patellofemoral pain," *Current Reviews in Musculoskeletal Medicine*, vol. 12, no. 4, pp. 534–541, 2019.

[2] W. Al-Hakim, P. K. Jaiswal, W. Khan, and D. Johnstone, "The non-operative treatment of anterior knee pain," *The Open Orthopaedics Journal*, vol. 6, no. 1, pp. 320–326, 2012.

[3] W. Petersen, A. Ellermann, A. Gösele-Koppenburg et al., "Patellofemoral pain syndrome," *Knee Surgery, Sports Traumatology, Arthroscopy*, vol. 22, no. 10, pp. 2264–2274, 2014.

[4] B. E. Smith, P. Hendrick, and P. Logan, "Patellofemoral pain: challenging current practice - a case report," *Manual Therapy*, vol. 22, pp. 216–219, 2016.

[5] E. Stathopulu and E. Baildam, "Anterior knee pain: a long-term follow-up," *Rheumatology*, vol. 42, no. 2, pp. 380–382, 2003.

[6] B. Noehren, M. B. Pohl, Z. Sanchez, T. Cunningham, and C. Lattermann, "Proximal and distal kinematics in female runners with patellofemoral pain," *Clinical biomechanics*, vol. 27, no. 4, pp. 366–371, 2012.

[7] T. G. Almonroeder and L. C. Benson, "Sex differences in lower extremity kinematics and patellofemoral kinetics during running," *Journal of Sports Sciences*, vol. 35, no. 16, pp. 1575–1581, 2017.

[8] J. Stephen, A. Alva, P. Lumpaopong, A. Williams, and A. A. Amis, "A cadaveric model to evaluate the effect of unloading the medial quadriceps on patellar tracking and patellofemoral joint pressure and stability," *Journal of Experimental Orthopaedics*, vol. 5, no. 1, pp. 1–10, 2018.

[9] L. Zavala, V. Flores, J. A. Cotter, and J. Becker, "Patellofemoral joint kinetics in females when using different depths and loads during the barbell back squat," *European Journal of Sport Science*, vol. 21, no. 7, pp. 976–984, 2021.

[10] K. Jeon, K. Kim, and N. Kang, "Leg stiffness control during drop landing movement in individuals with mechanical and functional ankle disabilities," *Sports Biomechanics*, pp. 1–4, 2020.

[11] M. J. Decker, M. R. Torry, D. J. Wyland, W. I. Sterett, and J. R. Steadman, "Gender differences in lower extremity kinematics, kinetics and energy absorption during landing," *Clinical biomechanics*, vol. 18, no. 7, pp. 662–669, 2003.

[12] C. M. Powers, "The influence of abnormal hip mechanics on knee injury: a biomechanical perspective," *Journal of Orthopaedic & Sports Physical Therapy*, vol. 40, no. 2, pp. 42–51, 2010.

[13] L. Herrington, "Knee valgus angle during single leg squat and landing in patellofemoral pain patients and controls," *The Knee*, vol. 21, no. 2, pp. 514–517, 2014.

[14] E. Magalhães, T. Y. Fukuda, S. N. Sacramento, A. Forgas, M. Cohen, and R. J. Abdalla, "A comparison of hip strength between sedentary females with and without patellofemoral pain syndrome," *Journal of Orthopaedic & Sports Physical Therapy*, vol. 40, no. 10, pp. 641–647, 2010.

[15] H. Numata, J. Nakase, K. Kitaoka et al., "Two-dimensional motion analysis of dynamic knee valgus identifies female high school athletes at risk of non-contact anterior cruciate ligament injury," *Knee Surgery, Sports Traumatology, Arthroscopy*, vol. 26, no. 2, pp. 442–447, 2018.

[16] K. A. Russell, R. M. Palmieri, S. M. Zinder, and C. D. Ingersoll, "Sex differences in valgus knee angle during a single-leg drop jump," *Journal of Athletic Training*, vol. 41, no. 2, pp. 166–171, 2006.

[17] M. K. Chevidikunnan, A. Al Saif, R. A. Gaowgzeh, and K. A. Mamdouh, "Effectiveness of core muscle strengthening for improving pain and dynamic balance among female patients with patellofemoral pain syndrome," *Journal of Physical Therapy Science*, vol. 28, no. 5, pp. 1518–1523, 2016.

[18] V. Ugalde, C. Brockman, Z. Bailowitz, and C. D. Pollard, "Single leg squat test and its relationship to dynamic knee valgus and injury risk screening," *Pm&r*, vol. 7, no. 3, pp. 229–235, 2015.

[19] K. Jeon and S. Yeom, "Effects of kinematics and kinetics of the lower extremities joint during drop landing in adult women with patellofemoral pain syndrome," *Korean Journal of Sport Biomechanics*, vol. 31, no. 1, pp. 64–71, 2021.

[20] L. Kanko, T. Birmingham, D. Bryant et al., "The star excursion balance test is a reliable and valid outcome measure for patients with knee osteoarthritis," *Osteoarthritis and Cartilage*, vol. 27, no. 4, pp. 580–585, 2019.

[21] E. A. Wikstrom, M. E. Powers, and M. D. Tillman, "Dynamic stabilization time after isokinetic and functional fatigue," *Journal of Athletic Training*, vol. 39, no. 3, pp. 247–253, 2004.

[22] E. A. Wikstrom, M. D. Tillman, A. N. Smith, and P. A. Borsa, "A new force-plate technology measure of dynamic postural stability: the dynamic postural stability index," *Journal of Aathletic Training*, vol. 40, no. 4, p. 305, 2005.

[23] J. Park, W. M. Denning, J. D. Pitt, D. Francom, J. T. Hopkins, and M. K. Seeley, "Effects of experimental anterior knee pain on muscle activation during landing and jumping performed at various intensities," *Journal of Sport Rehabilitation*, vol. 26, no. 1, pp. 78–93, 2017.

[24] L. C. Schmitt, M. V. Paterno, K. R. Ford, G. D. Myer, and T. E. Hewett, "Strength asymmetry and landing mechanics at return to sport after anterior cruciate ligament reconstruction," *Medicine and Science in Sports and Exercise*, vol. 47, no. 7, pp. 1426–1434, 2015.

[25] K. F. Orishimo, M. Liederbach, I. J. Kremenic, M. Hagins, and E. Pappas, "Comparison of landing biomechanics between male and female dancers and athletes, part 1: influence of sex on risk of anterior cruciate ligament injury," *The American Journal of Sports Medicine*, vol. 42, no. 5, pp. 1082–1088, 2014.

[26] M. Kadaba, H. Ramakrishnan, M. Wootten, J. Gainey, G. Gorton, and G. Cochran, "Repeatability of kinematic, kinetic, and electromyographic data in normal adult gait," *Journal of Orthopaedic Research*, vol. 7, no. 6, pp. 849–860, 1989.

[27] E. Wikstrom, M. Tillman, T. Chmielewski, J. Cauraugh, K. Naugle, and P. Borsa, "Dynamic postural control but not mechanical stability differs among those with and without chronic ankle instability," *Scandinavian Journal of Medicine & Science in Sports*, vol. 20, no. 1, pp. e137–e144, 2010.

[28] J. Van Cant, C. Pineux, L. Pitance, and V. Feipel, "Hip muscle strength and endurance in females with patellofemoral pain: a systematic review with meta-analysis," *International Journal of Sports Physical Therapy*, vol. 9, no. 5, pp. 564–582, 2014.

[29] M. R. Prins and P. Van der Wurff, "Females with patellofemoral pain syndrome have weak hip muscles: a systematic review," *The Australian Journal of Physiotherapy*, vol. 55, no. 1, pp. 9–15, 2009.

[30] C. K. Pollard, S. M. Sigward, and C. M. Powers, "Limited hip and knee flexion during landing is associated with increased frontal plane knee motion and moments," *Clinical biomechanics*, vol. 25, no. 2, pp. 142–146, 2010.

[31] R. J. van Arkel, L. Modenese, A. T. Phillips, and J. R. Jeffers, "Hip abduction can prevent posterior edge loading of hip replacements," *Journal of Orthopaedic Research*, vol. 31, no. 8, pp. 1172–1179, 2013.

[32] T. Q. Lee, G. Morris, and R. P. Csintalan, "The influence of tibial and femoral rotation on patellofemoral contact area and pressure," *Journal of Orthopaedic & Sports Physical Therapy*, vol. 33, no. 11, pp. 686–693, 2003.

[33] V. Baker, K. Bennell, B. Stillman, S. Cowan, and K. Crossley, "Abnormal knee joint position sense in individuals with patellofemoral pain syndrome," *Journal of Orthopaedic Research*, vol. 20, no. 2, pp. 208–214, 2002.

[34] D. M. Brazen, M. K. Todd, J. P. Ambegaonkar, R. Wunderlich, and C. Peterson, "The effect of fatigue on landing biomechanics in single-leg drop landings," *Clinical Journal of Sport Medicine*, vol. 20, no. 4, pp. 286–292, 2010.

[35] K. Kim and K. Jeon, "Comparisons of knee and ankle joint angles and ground reaction force according to functional

differences during single-leg drop landing," *Journal of Physical Therapy Science*, vol. 28, no. 4, pp. 1150–1154, 2016.

[36] M. C. Hoch, K. E. Farwell, S. L. Gaven, and J. T. Weinhandl, "Weight-bearing dorsiflexion range of motion and landing biomechanics in individuals with chronic ankle instability," *Journal of Athletic Training*, vol. 50, no. 8, pp. 833–839, 2015.

[37] P. Malloy, A. Morgan, C. Meinerz, C. Geiser, and K. Kipp, "The association of dorsiflexion flexibility on knee kinematics and kinetics during a drop vertical jump in healthy female athletes," *Knee Surgery, Sports Traumatology, Arthroscopy*, vol. 23, no. 12, pp. 3550–3555, 2015.

[38] G. S. Nunes, C. J. Barton, and F. V. Serrao, "Females with patellofemoral pain have impaired impact absorption during a single-legged drop vertical jump," *Gait & Posture*, vol. 68, pp. 346–351, 2019.

[39] H. Guney, I. Yuksel, D. Kaya, and M. N. Doral, "Correlation between quadriceps to hamstring ratio and functional outcomes in patellofemoral pain," *The Knee*, vol. 23, no. 4, pp. 610–615, 2016.

[40] H. Negahban, M. Etemadi, S. Naghibi et al., "The effects of muscle fatigue on dynamic standing balance in people with and without patellofemoral pain syndrome," *Gait & Posture*, vol. 37, no. 3, pp. 336–339, 2013.

[41] P. M. Carry, R. Gala, K. Worster et al., "Postural stability and kinetic change in subjects with patellofemoral pain after a nine-week hip and core strengthening intervention," *International Journal of Sports Physical Therapy*, vol. 12, no. 3, pp. 314–323, 2017.

[42] J. E. Willson and I. S. Davis, "Lower extremity mechanics of females with and without patellofemoral pain across activities with progressively greater task demands," *Clinical biomechanics*, vol. 23, no. 2, pp. 203–211, 2008.

[43] N. R. Heebner, D. M. Rafferty, M. F. Wohleber et al., "Landing kinematics and kinetics at the knee during different landing tasks," *Journal of Athletic Training*, vol. 52, no. 12, pp. 1101–1108, 2017.

[44] J. T. Podraza and S. C. White, "Effect of knee flexion angle on ground reaction forces, knee moments and muscle co-contraction during an impact-like deceleration landing: implications for the non-contact mechanism of ACL injury," *The Knee*, vol. 17, no. 4, pp. 291–295, 2010.

[45] M. Walsh, M. C. Boling, M. McGrath, J. T. Blackburn, and D. A. Padua, "Lower extremity muscle activation and knee flexion during a jump-landing task," *Journal of Athletic Training*, vol. 47, no. 4, pp. 406–413, 2012.

[46] T. Nagai, T. C. Sell, A. J. House, J. P. Abt, and S. M. Lephart, "Knee proprioception and strength and landing kinematics during a single-leg stop-jump task," *Journal of Athletic Training*, vol. 48, no. 1, pp. 31–38, 2013.

[47] K. R. Pfile, J. M. Hart, D. C. Herman, J. Hertel, D. C. Kerrigan, and C. D. Ingersoll, "Different exercise training interventions and drop-landing biomechanics in high school female athletes," *Journal of Athletic Training*, vol. 48, no. 4, pp. 450–462, 2013.

[48] C. -M. Fong, J. T. Blackburn, M. F. Norcross, M. McGrath, and D. A. Padua, "Ankle-dorsiflexion range of motion and landing biomechanics," *Journal of Athletic Training*, vol. 46, no. 1, pp. 5–10, 2011.